

INFORMATION TO USERS

This manuscript has been reproduced from the microfilm master. UMI films the text directly from the original or copy submitted. Thus, some thesis and dissertation copies are in typewriter face, while others may be from any type of computer printer.

The quality of this reproduction is dependent upon the quality of the copy submitted. Broken or indistinct print, colored or poor quality illustrations and photographs, print bleedthrough, substandard margins, and improper alignment can adversely affect reproduction.

In the unlikely event that the author did not send UMI a complete manuscript and there are missing pages, these will be noted. Also, if unauthorized copyright material had to be removed, a note will indicate the deletion.

Oversize materials (e.g., maps, drawings, charts) are reproduced by sectioning the original, beginning at the upper left-hand corner and continuing from left to right in equal sections with small overlaps.

Photographs included in the original manuscript have been reproduced xerographically in this copy. Higher quality 6" x 9" black and white photographic prints are available for any photographs or illustrations appearing in this copy for an additional charge. Contact UMI directly to order.

**Bell & Howell Information and Learning
300 North Zeeb Road, Ann Arbor, MI 48106-1346 USA**

UMI[®]
800-521-0600

**The Evolution of Carbonatite Melts and their Aqueous
Fluids: Evidence from Amba Dongar, India,
and Phalaborwa, South Africa**

by
David A. S. Palmer

**A thesis submitted to the Faculty of Graduate Studies and Research
in partial fulfilment of the requirements of the degree of
Doctor of Philosophy**

**Department of Earth and Planetary Sciences
McGill University
Montreal, Quebec
Canada**

© David Palmer, MCMXCVIII



**National Library
of Canada**

**Acquisitions and
Bibliographic Services**

**395 Wellington Street
Ottawa ON K1A 0N4
Canada**

**Bibliothèque nationale
du Canada**

**Acquisitions et
services bibliographiques**

**395, rue Wellington
Ottawa ON K1A 0N4
Canada**

Your file Votre référence

Our file Notre référence

The author has granted a non-exclusive licence allowing the National Library of Canada to reproduce, loan, distribute or sell copies of this thesis in microform, paper or electronic formats.

The author retains ownership of the copyright in this thesis. Neither the thesis nor substantial extracts from it may be printed or otherwise reproduced without the author's permission.

L'auteur a accordé une licence non exclusive permettant à la Bibliothèque nationale du Canada de reproduire, prêter, distribuer ou vendre des copies de cette thèse sous la forme de microfiche/film, de reproduction sur papier ou sur format électronique.

L'auteur conserve la propriété du droit d'auteur qui protège cette thèse. Ni la thèse ni des extraits substantiels de celle-ci ne doivent être imprimés ou autrement reproduits sans son autorisation.

0-612-50232-5

Canada

Abstract

The Amba Dongar complex, India, consists of calciocarbonatite, ankerite-dominated ferrocarnatite and numerous nephelinitic bodies intruded into Late Cretaceous quartz sandstones and Deccan basalts.

Ankeritic (mottled) and calcite \pm barite \pm ankerite (multiphase) melt inclusions were observed in apatite hosted by calciocarbonatite. Mottled inclusions start melting at temperatures of 610°C and are completely molten at temperatures >800°C. The onset of melting, of multiphase inclusions, is at 680°C, and final melting occurs above 1100°C. Based on the coexistence of mottled (ankeritic) and multiphase (calcitic) inclusions, a model is proposed for the genesis of calciocarbonatite and ferrocarnatite that calls upon separation of immiscible ankeritic and calcitic liquids from a parent carbonate melt.

Primary fluid inclusions, in apatite hosted by calciocarbonatite, and in quartz of the surrounding fenitized sandstones, record a complex evolution of aqueous fluids. The fluids (orthomagmatic) were trapped at temperatures between 1000 and 260°C, at pressures ranging from 12.5 kbars to 500 bars, respectively, while fenitizing fluids ranged in temperature from 260 to 120°C, and were trapped at <500 bars pressure. The low temperature phase behaviour of all inclusions indicates that the fluids are NaCl-, KCl-bearing brines with salinities between 15 and 15 wt.%. The compositions of decrepitate residues indicate that early fluids were dominated by SO_4^{2-} and HCO_3^- , and had low Na/(Na+K) ratios (<0.5). More evolved fluids display an increasing dependence on Cl^- , over SO_4^{2-} and HCO_3^- , and are increasingly depleted in K relative to Na.

The replacement of quartz by potassium feldspar in fenites was accompanied by significant losses of Si and additions of K, Al, Ca, Ba, Fe, La, Ce, F, Rb, Sr, Y and HREE. The water-rock ratio during fenitization was ≈ 722 .

The Phalaborwa complex, South Africa (2060 Ma) consists of a large intrusion of pyroxenite which was later cored by phoscorite and subsequently intruded by banded (early) and transgressive (late) carbonatites. The carbonate rocks are host to 400 Mt of early bornite and late chalcopyrite ores.

Solid-vapour and solid-liquid-vapour melt inclusions are present in phoscorite and transgressive carbonatite. The solids comprise calcite, a magnesian silicate and magnetite \pm Cu-Fe sulphide, while the fluid is a saline Mg-, Fe- and S-bearing NaCl-KCl brine (≈ 22 wt.% NaCl eq.). Solid-vapour inclusions in phoscorite produce immiscible carbonate and silicate liquids between 680 and 800°C. Melt inclusions in transgressive carbonatites produce only one liquid between 550°C to 670°C and homogenize above 750°C. Liquid immiscibility was important in removing Si from the carbonate-rich melt, however, silicate and carbonate rocks are not related by liquid immiscibility. Fractionation is considered to have been the dominant process in forming the complex.

Two episodes of fenitization were discerned in surrounding granites and gneisses, from chemical and mineralogical changes, and were associated with emplacement of pyroxenite and carbonatite. Both events were accompanied by significant gains in K, Ca, Ba, Mg, Fe, Sr, Th and LREE, and losses in Si and Na.

The presence of Cu-bearing sulphides in solid-vapour inclusions hosted by phoscorite indicates that Phalaborwa magmas were enriched in Cu before emplacement. Solid-liquid-vapour inclusions provide the first evidence of a separate magmatic aqueous fluid phase at Phalaborwa and support interpretation of a hydrothermal origin for copper mineralization in transgressive carbonatite.

Sommaire

Le complexe d'Amba Dongar de L'Inde se compose de calcicarbonatite, de ferrocarbonatite dominé par l'ankérite, et de plusieurs intrusions néphelénitique injectés dans des grès de quartz et des basaltes du Deccan.

Des inclusions de fonte contenant l'ankérite (mouchetés) et calcite \pm barite \pm ankérite (multiphase) ont été observées dans l'apatite du calciocarbonatite. Les inclusions mouchetées commencement à fondre à une température de 610°C, et elles deviennent complètement fondues au-delà de 800°C. Le début de la fusion des inclusions multiphase est à 680°C, et le processus achève à plus de 1100°C. Du à la co-existence des inclusions mouchetées (ankéritiques) et multiphase (calcitiques), un modèle est proposé pour la genèse ces calciocarbonatite et ferrocarbonatite ou des liquides ankéritique et calcitiques immiscible se sont séparés de la fonte carbonatique originelle.

Des inclusions fluides primaires, dans l'apatite du calciocarbonatite et dans le quartz des grès environnants, enregistrent une évolution complexe de fluide aqueux. Les fluides (orthomagmatiques) ont été piégés à des températures de 1000 à 260°C, et sous des pressions de 12.5 kbars à 500 bars, respectivement, tandis que les fluides causant l'altération fénitique ont eu des températures de 260 à 120°C, et ils ont été capturés sous des pressions de moins que 500 bars. La caractérisation à base température de toutes les inclusions indique que les fluides sont des saumures de NaCl et KCl avec des salinités de 15 à 1.5 wt.%. Les compositions des résidus de décrepitation indiquent que les fluides précoces ont été dominés par SO_4^{2-} et HCO_3^- , et mais des rapports peu élevés de Na/Na+K. Les fluides plus évolués montrent une dépendance de Cl^- plus important que des SO_4^{2-} et HCO_3^- , et deviennent s'appauvrissent en K relatif à Na.

Le remplacement du quartz par le feldspath potassique dans les roches fénitiques se coïncide avec des pertes importantes de Si et l'addition de K, Al, Ca, Ba, Fe, La, Ce, F, Rb, Sr, Y et les terres rares lourdes. La proportion de fluide/roche durant la fénitisation à été ≈ 722 .

Le complexe Phalaborwa de l'Afrique Sud (2060 Ma) se compose d'une grande intrusion de pyroxénite qui a ensuite été envahie au centre par une phoscorite; le tout ayant finalement été coupé par des carbonatites laminés (précoces) et transgressifs (tardifs). Les roches carbonatées contiennent 400 Mt de minerais riches en bornite (précoce) et en chalcopryrite (tardif).

Les inclusions de fonte de deux types (solide-vapeur et solide-liquide-vapeur) sont présent dans le phoscorite et le carbonatite transgressif. Les solides comprennent le calcite, l'olivine, et le magnétite \pm sulfures de Cu-Fe, tandis que le fluide est une saumure de NaCl-KCl (≈ 22 wt.% NaCl) contenant du Mg, Fe et du S. Les inclusions de type solide-vapeur dans le phoscorite produisent des liquides immiscibles carbonatés et silicates entre les températures de 680 et 800°C. Les inclusions de fontes dans les carbonatites transgressifs produisent un seul liquide entre 550 et 670°C, et se homogénéisent au delà de 750°C. L'immiscibilité liquide était important pour l'enlèvement de Si de la fonte riche en carbonates. Cependant les roches silicatées et carbonatées ne sont pas reliés génétiquement par l'immiscibilité liquide. Le fractionnement est considéré comme le processus dominant dans la formation du complexe.

Deux épisodes de fénitization ont été enregistrés par de changements chimiques et minéralogiques dans les granites et les gneisses entourant le complexe, et ces changements ont été associés aux emplacements du pyroxénite et du carbonatite. Les deux événements ont été accompagnés par des gains de K, Ca, Ba, Mg, Fe, Sr, Th et des terres rares légères, et par des pertes de Si et Na.

La présence de sulfures de Cu-Fe dans les inclusions de type solide-vapeur du phoscorite indique que les magmas de Phalaborwa se sont enrichis en Cu avant leur emplacement. Les inclusions solide-liquide-vapeur fournissent la première évidence de la séparation de fluide aqueux magmatique à Phalaborwa, et ceci soutient l'interprétation d'une origine hydrothermale pour la minéralisation cuprifère dans le carbonatite transgressif.

Acknowledgments

The most important part of University is the students and I would like to thank those who made my time at McGill memorable.

Table of Contents

Abstract	i
Sommaire	ii
Acknowledgments	iv
Table of Contents	v
List of Figures	x
List of Tables	xii
Preface	xiv
Chapter 1: General Introduction	1
Introduction	2
Carbonatite Genesis	3
Carbonatite Evolution	4
Theoretical and Experimental Evidence	4
Melt Inclusions	5
Aqueous Fluids	7
Fenitization	7
Fenitization associated with Carbonatites	10
Fluid inclusions	11
Previous Work – Amba Dongar	12
Previous Work - Phalaborwa	13
Thesis Organization	14
References	17
Chapter 2: Geology of the Amba Dongar Complex	24
Location	25
Regional Geology	25
Country Rock Geology	27
Deccan Basalt	27
Bagh Sandstone	28
Bagh Limestone	28
The Carbonatite Complex	29
General Geology	29
Carbonatite Geology	29
Fenitization	31
References	33
Chapter 3: Geology of The Phalaborwa Complex	35
Location	36

History of Mining	36
Regional Geology	36
Geology of the Complex	38
Pyroxenite	39
Massive and micaceous pyroxenite	39
Feldspathic pyroxenite	40
Pegmatitic pyroxenite	41
Phoscorite	41
Carbonatite	43
Satellite Bodies	44
Carbonatite-hosted Copper Mineralization	45
Fenitization	48
Dykes	48
References	50
<i>Chapter 4: Carbonate-Carbonate Liquid Immiscibility and the Formation of Ferrocarbonatite: Evidence from Melt Inclusions in the Amba Dongar Carbonatite Complex, India (Manuscript)</i>	52
Abstract	53
Introduction	53
Geology of Amba Dongar	55
Methodology	57
Solid Inclusions	58
Mottled inclusions	58
Petrography	58
Chemistry	60
Multiphase Inclusions	60
Petrography	60
Chemistry	63
Mixed Inclusions	63
Monomineralic Inclusions	67
Petrography	67
Chemistry	67
High Temperature Phase Relations	67
Monomineralic Inclusions	67
Mottled Inclusions	67
Multiphase Inclusions	69
Discussion	69
Melt versus Trapped Solid	69
Carbonatite Evolution	75
Model	78
Conclusions	82
References	84
<i>Bridge to Chapter 5</i>	88
<i>Chapter 5: Fluid Evolution of the Amba Dongar Carbonatite Complex, India (Manuscript)</i>	89

Abstract	90
Introduction	91
Geology	92
Carbonatites	92
Fenites	94
Fluid Inclusions	95
Fluid Inclusions in Apatite	95
Solids	98
Fluid Inclusions in Calcite	98
Fluid Inclusions in Quartz and Feldspar	100
Microthermometry	100
Results from Apatite	104
Results for calcite	106
Results for Quartz and Feldspar	107
Decrepitates	107
Results	108
Apatite	108
Calcite	110
Quartz	110
Discussion	113
Fluid Types	113
Fluid compositions	114
Fluid Evolution	118
Pressure and Temperature	122
Fluid Model	123
Conclusions	126
References	128
<i>Bridge to Chapter 6</i>	<i>131</i>
<i>Chapter 6: Fenitization Associated with the Amba Dongar Carbonatite Complex, India (Manuscript)</i>	<i>132</i>
Abstract	133
Introduction	133
Geology	134
Carbonatites	136
Bagh Formation	136
Fenites	137
Potassic Fenites	137
Sodic Fenites	137
Alteration Chemistry	138
Mass Balance	143
Mass losses	147
Mass Gains	147
Discussion	149
Mass Changes During Fenitization	149
Water-Rock Ratios	150
Calculated Fluid Composition	151

Conclusions	154
References	155
Bridge to Chapter 7	158
Chapter 7: Solid Inclusions from the Phalaborwa complex, South Africa: Evidence of silicate-carbonate immiscibility (Manuscript)	159
Abstract	160
Introduction	161
Geology	162
Pyroxenite	164
Phoscorite	164
Carbonatite	166
Apatite	167
Solid inclusions	167
Solid-Vapour Inclusions in Phoscorite	167
Solid-Vapour Inclusions in Transgressive Carbonatite	169
Solid-Liquid-Vapour -Bearing Inclusions in Transgressive Carbonatite	169
Composition of Solid Inclusions	169
Solid-Vapour Inclusions from Phoscorite	174
Solid-Vapour Inclusions from Transgressive Carbonatite	174
Microthermometric Results	177
Solid-Vapour Inclusions in Phoscorite	177
Solid-Vapour Inclusions in Transgressive Carbonatite	180
Solid-liquid-vapour Inclusions in Transgressive Carbonatite	180
Discussion	183
Crystallization History	184
Copper Mineralization	186
Conclusions	186
References	188
Bridge to Chapter 8	191
Chapter 8: Fenitization Associated with the Phalaborwa Complex, South Africa (Manuscript)	192
Abstract	193
Introduction	193
Geology	195
Pyroxenite	195
Phoscorite	197
Carbonatite	197
Copper mineralization	199
Fenitization	199
Methodology	204
Chemistry	204
Fenite Chemistry	204
Whole Rock Chemistry	207

Mineral Chemistry	212
Mass Changes	218
Whole rock	218
Mass Transfers	221
Mineral Mass Transfers	224
Pyroxene-Amphibole	224
Potassium Feldspar	224
Calcite-Dolomite	226
Discussion	230
Fluid Compositions from Fenitization Studies	232
Implications for copper mineralization	232
Conclusions	233
References	235
Chapter 9: Conclusions	237
Conclusions	238
Contributions to Knowledge	242
Recommendations for Future Work	243
References	244
Appendix I: Calculation of Fluid Composition from Decrepitate Residues and Fluid Inclusion Salinity	245
Example for Sulphur	246
Appendix II: Melt Inclusion Microthermometric Data (Amba Dongar, India)	249
Appendix III: Fluid Inclusion Microthermometric Data (Amba Dongar, India)	252
Appendix IV: Melt Inclusion Microthermometric Data (Phalaborwa, South Africa)	262
Appendix V: Electron Microprobe Mineral Analyses	265

List of Figures

Figure 2-1 The geology of the Amba Dongar complex, India and surrounding area	26
Figure 3-1 The geology of the Phalaborwa complex, South Africa	37
Figure 3-2 Geology of the Palabora Mining Company's open pit	42
Figure 3-3 Photomicrographs showing copper mineralization	47
Figure 4-1 The geology of the Amba Dongar complex and surrounding area	56
Figure 4-2 SEM photomicrographs of solid inclusions hosted by apatite in calciocarbonatite	59
Figure 4-3 Compositions of multiphase and mottled inclusions and calciocarbonatites and ferrocarnatites	62
Figure 4-4 Melting behaviour of mottled inclusions	70
Figure 4-5 Melting behaviour of a multiphase inclusion	71
Figure 4-6 Melting behaviour of a multiphase inclusion	72
Figure 4-7 The formation of two liquids in a multiphase inclusion at high temperature	79
Figure 4-8 Backscattered electron image of a homogenised multiphase melt inclusion	80
Figure 4-9 Backscattered electron image of a homogenised multiphase melt inclusion	81
Figure 5-1 The geology of the Amba Dongar complex and surrounding area	93
Figure 5-2 Fluid inclusions in apatite (calciocarbonatite) and quartz (fenite) at Amba Dongar	96
Figure 5-3 Photomicrographs of fluid inclusion-bearing apatite crystals in calciocarbonatite	97
Figure 5-4 Photomicrograph of secondary quartz overgrown on quartz grain in fenitised sandstone	101
Figure 5-5 Histograms showing fluid inclusion data	103
Figure 5-6 Photomicrographs of LVMS inclusion in apatite showing phase changes during heating	105
Figure 5-7 Salinity versus temperature diagrams	115
Figure 5-8 Na/Na+K versus S/Cl diagram showing compositions of decrepitate residues from LVS, LVMS, LV (ap) and LV (qtz) inclusions	116
Figure 5-9 Ternary diagrams showing compositional trends of apatite- and quartz-hosted fluid inclusions in calciocarbonatite and fenite	120
Figure 5-10 Temperature versus salinity diagram for apatite- and quartz-hosted fluid inclusions	121

Figure 5-11 Isochoric projection of LVS, LVMS, LV (ap) and LV (qtz) fluid inclusions	124
Figure 6-1 The geology of the Amba Dongar complex and surrounding area	135
Figure 6-2 Major element compositions of progressively fenitised Bagh sandstone	140
Figure 6-3 Minor element compositions of progressively fenitised Bagh sandstone	141
Figure 6-4 Normative mineralogy of progressively fenitised Bagh sandstone.	142
Figure 6-5 Chondrite-normalized rare earth element (REE) profiles for unaltered and altered Bagh sandstone	144
Figure 6-6 Isocon digrams for six progressively fenitized Bagh sandstones	146
Figure 7-1 The geology of the Phalaborwa complex, South Africa	163
Figure 7-2 The geology of Palabora Mining Company's open pit.	165
Figure 7-3 Solid inclusions in apatite from phoscorite and transgressive carbonatite	168
Figure 7-4 SEM photomicrographs of melt inclusions	175
Figure 7-5 Melting behaviour of melt inclusions in phoscorite-hosted apatite	179
Figure 7-6 Melting behaviour of melt inclusions in phoscorite-hosted apatite	181
Figure 7-7 Dissolution and melting behaviour of aqueous liquid-vapour-bearing melt inclusions in transgressive carbonatite.	182
Figure 8-1 The geology of the Phalaborwa complex, South Africa	196
Figure 8-2 The geology of the Phalaborwa open pit	198
Figure 8-3 Features of transgressive carbonatite mineralization	200
Figure 8-4 Normative mineral plots for fenitized granite and gneiss	202
Figure 8-5 Photomicrographs showing fenitization	203
Figure 8-6 Major element plots for progressively fenitized granite	208
Figure 8-7 Minor element plots for progressively fenitized granite	209
Figure 8-8 Major element plots for progressively fenitized granitic gneiss	210
Figure 8-9 Minor element plots for progressively fenitized granitic gneiss	211
Figure 8-10 Ternary diagrams of A) Ca-Al-Na; B) Ca-Mg+Fe-Na+K; and C) Ca-Mg-Fe for pyroxenes and amphiboles of fenitised granites and granitic gneisses	216
Figure 8-11 Isocon diagrams for progressively fenitised granites	219
Figure 8-12 Isocon diagrams for progressively fenitised granitic gneisses	220
Figure 8-13 Isocon diagrams for the replacement of calcite by Mg-calcite and dolomite	229

List of Tables

Table 1-1	Fenitization associated with carbonatite occurrences _____	8
Table 4-1	Compositions of mottled inclusions _____	61
Table 4-2	Compositions of homogenised multiphase inclusions _____	64
Table 4-3	Compositions of phases in multiphase inclusions _____	65
Table 4-4	Compositions of crystals in multiphase inclusions _____	66
Table 4-5	EDS analyses of monomineralic inclusions _____	68
Table 4-6	Representative analyses of calciocarbonatites and ferrocarbonatites. _____	74
Table 5-1	EDS analyses of fluid inclusion solids _____	99
Table 5-2	Microthermometric data from fluid inclusions in apatite, calcite and quartz _____	102
Table 5-3	EDS analyses of decrepitates from apatite-hosted fluid inclusions (calciocarbonatites) _____	109
Table 5-4	EDS analyses of decrepitates from calcite-hosted fluid inclusions (calciocarbonatites) _____	111
Table 5-5	EDS analyses of decrepitates from quartz-hosted fluid inclusions (fenites) _____	112
Table 6-1	Fenite analyses _____	139
Table 6-2	Mass transfers associated with fenitization of Bagh sandstone. _____	148
Table 6-3	Concentration of trace elements in fenitizing solutions _____	153
Table 7-1	EDS analyses of calcite and dolomite from melt inclusions in _____ Phoscorite _____	170 170
Table 7-2	EDS analyses of olivine from phoscorite melt Inclusions _____	171
Table 7-3	EDS analyses of magnetite and CPY from phoscorite melt inclusions _____	172
Table 7-4	EDS analyses of melt leakage on apatite _____	173
Table 7-5	Compositions of melt leaks _____	176
Table 7-6	Decrepitate analyses _____	178
Table 8-1	Chemical analyses of granite fenites _____	205
Table 8-2	Chemical analyses of granitic gneiss fenites _____	206
Table 8-3	Composition of pyroxenes and amphiboles in contact fenites (PF-5c and d) _____	213

Table 8-4	Composition of pyroxenes and amphiboles in regional fenites (PF-7)	215
Table 8-5	Mass transfers associated with dolomitization of calcite	217
Table 8-6	Mass transfers associated with fenitization of granite	222
Table 8-7	Mass transfers for fenitized granitic gneisses	223
Table 8-8	Mass transfers associated with replacement of diopside by richterite	225
Table 8-9	Mass transfers associated with feldspar alteration around pyroxenite veinlets in contact fenitized granitic rocks.	227
Table 8-10	Mass transfers associated with feldspar alteration around pyroxenite veinlets in regional fenitized granitic rocks	228

Preface

This study is a continuation of research into the evolution of carbonatite-derived aqueous fluids and carbonatite melts by the author. The thesis is divided into nine chapters, five of which are manuscripts, two are detailed reviews of the geology of the field areas and the remaining chapter comprises general conclusions. Chapters 4, 5, 6, 7 and 8 are co-authored by Dr. Williams-Jones, who critically reviewed the text. Fieldwork at Phalaborwa, South Africa was accomplished with the help of Dr. Williams-Jones and Dr. R. E. Harmer. Drs. S. J. Viladkar and A.E. Williams-Jones and J. Roelofsen assisted in field work during mapping and sampling of the Amba Dongar complex, India. Melt and fluid inclusion experiments, petrography and SEM analyses were carried out by the author. Electron microprobe analyses were conducted by the author with the assistance of G. Poirier. Major and trace element compositions of whole rocks were established using X-ray fluorescence by T. Ahmedali at the Department of Earth and Planetary Sciences, McGill University, while other trace elements and REE were obtained by Dr. E. Hoffmann at Activation Laboratories, Ancaster, Ontario.

The following is an excerpt from the "Guidelines Concerning Thesis Preparation" as required by the Faculty of Graduate Studies and Research at McGill University:

"Candidates have the option of including, as part of their thesis, the text of one or more papers submitted, or to be submitted, for publication, or the clearly-duplicated text of one, or more, published papers. These texts must be bound as an integral part of the thesis. If this option is chosen, connecting texts, providing logical bridges between the different papers, are mandatory"

"The thesis must still conform to all other requirements of the Guidelines Concerning Thesis Preparation and should be in a literary form that is more than a mere collection of manuscripts published or to be published. The thesis must include, as separate chapters or sections: (1) a Table of Contents, (2) a general abstract in English

and French, (3) an introduction which clearly states the rationale and objectives of the study, (4) a comprehensive general review of the background literature to the subject of the thesis, when this review is appropriate, and (5) a final overall conclusion and/or summary."

"Additional material must be provided where appropriate (e.g. in appendices) and in sufficient detail to allow a clear and precise judgement to be made of the importance and originality of the research reported in the thesis."

"In the case of manuscripts co-authored by the candidate and others, the candidate is required to make an explicit statement in the thesis as to who contributed to such work and to what extent. Supervisors must attest to the accuracy of such statements at the doctoral oral defense. Since the task of the examiners is made more difficult in these cases, it is in the candidate's interest to make perfectly clear the responsibilities of all authors of the co-authored papers."

Contributions of Authors

The thesis author, D. A. S. Palmer, is responsible for all of the new scientific knowledge which is presented in this thesis. Dr. A.E. Williams-Jones is a co-author of Chapters 4, 5, 6, 7 and 8, and only acted in an advisory capacity with respect to organization and editing.

Chapter 1: General Introduction

Introduction

Although tremendous progress has been made in the field of carbonatite petrology, during the past thirty years most of the research has focussed on the genesis of the magmas (Wyllie and Tuttle, 1960; Cooper *et al.*, 1975; Freestone and Hamilton, 1980; Gittins, 1988; Wallace and Green, 1988; Wyllie, 1989; Harmer and Gittins, 1997; Lee and Wyllie, 1998). These studies have revealed that silicate-carbonate liquid immiscibility and partial melting of a carbonated mantle are the two most plausible hypotheses for producing carbonatite magmas.

Two important aspects of carbonatite petrology that have received comparatively little attention are the subsequent evolution of the melts, and the role of aqueous fluids in this evolution. Most researchers ascribe the evolution of carbonatites to fractionation of a parental melt (Gittins, 1988; Le Bas, 1989; Harmer and Gittins, 1997; Lee and Wyllie, 1998). However, there has been growing support for the idea that carbonatite melts also evolve through unmixing of a carbonate liquid (Brooker and Hamilton, 1990; Mitchell, 1997; Nielsen *et al.*, 1997).

The presence of metasomatically altered rocks, i.e., fenites, surrounding carbonatite complexes, and the abundance of fluid inclusions in carbonatite minerals, indicate that aqueous fluids are an integral part of carbonatite magmas and may play a fundamental role in their evolution. In many cases, it is the fluids, exsolved during carbonatite evolution, which are responsible for the ore deposits associated with carbonatite complexes (Deans, 1966; Mariano, 1989; Palmer and Williams-Jones, 1996). The most common hydrothermal ore deposits associated with carbonatites are those of REE, niobium and fluorite, although copper, barium and thorium deposits are known to occur (Mariano, 1989).

This thesis examines the melt and aqueous fluid evolution in two economically interesting carbonatite complexes at Amba Dongar, India and Phalaborwa, South Africa. Amba Dongar hosts a large fluorite deposit and contains zones of significant (up to 10 wt.%; S. Viladkar, pers. comm.) REE enrichment. The Phalaborwa carbonatite contains the only economic concentrations of copper known in carbonatites (400 Mt @ 0.69% Cu) (Mariano, 1989).

The presence of melt and fluid inclusions in primary minerals of carbonatites in both complexes, allows for detailed physico-chemical characterization of the melts and aqueous fluids which were present during the emplacement of the carbonatite. Studies of fenitization associated with the emplacement of both complexes are used to provide further compositional data on the fluids associated with carbonatite magmatism.

Carbonatite Genesis

The addition of silica to synthetic carbonate systems, and the recognition of silicate-carbonate liquid immiscibility (Koster van Groos and Wyllie, 1973), created a major division in the opinions on the origin of carbonatites which continues today (Kjarsgaard and Hamilton, 1989; Gittins, 1989). The hypothesis that carbonatite magmas are generated by carbonate-silicate liquid immiscibility has received considerable support owing to the close association of alkaline silicate rocks and carbonatites in alkaline complexes (Heinrich, 1966; Barker, 1989). Results of experimental work by Freestone and Hamilton (1980) have shown that natrocarbonatite, similar to that observed at Oldoinyo Lengai, can be produced by exsolution from phonolitic magmas. Kjarsgaard and Hamilton (1988) extended the compositional range of this immiscibility to include alkali-poor carbonatites, and concluded that calciocarbonatite could also be generated by silicate-carbonate immiscibility. These researchers subsequently reported producing a conjugate carbonate liquid, containing at least 90 wt.% CaCO_3 , from a peralkaline parental silicate melt (Hamilton and Kjarsgaard, 1993). This claim was later challenged by Lee and Wyllie (1996, 1998), who concluded, from experimental studies of the systems $\text{NaAlSi}_3\text{O}_8\text{-CaCO}_3$ and $\text{CaO-(MgO+FeO)-(Na}_2\text{O+K}_2\text{O)-(SiO}_2\text{+Al}_2\text{O}_3\text{+TiO}_2\text{)-CO}_2$, that carbonate liquids produced by immiscibility can never exceed 80 wt.% CaCO_3 and must contain at least 5 wt.% Na_2CO_3 . These authors also concluded that calciocarbonatites and natrocarbonatites cannot form directly from primary, mantle-derived magmas, and magnesiocarbonatite cannot be produced by liquid immiscibility (Lee and Wyllie, 1998).

The origin of carbonatites as primary melts generated by partial melting of the mantle is also supported by experimental studies (Wallace and Green, 1988; Dalton and

Wood, 1993; Sweeney, 1994; Lee and Wyllie, 1998). Compositions of primary melts, however, are all magnesian and favour the formation of magnesiocarbonatite over other types of carbonatite. Wallace and Green (1988) found that melting of amphibole-bearing lherzolite could produce a Na-, Mg-, Ca- and Fe-rich carbonate liquid which would crystallize dolomite and Na-Mg carbonates. This was confirmed by Sweeney's (1994) repetition of the experiments. Carbonate liquids in equilibrium with spinel wehrlite and harzburgite were also found to be dolomitic (Dalton and Wood, 1993).

Carbonatite Evolution

Theoretical and Experimental Evidence

The three most common types of carbonatite, listed in decreasing order of importance, are calciocarbonatite, magnesiocarbonatites and ferrocarbonatite. This is also the order in which they are generally emplaced, i.e., calciocarbonatite \Rightarrow magnesiocarbonatite \Rightarrow ferrocarbonatite (Barker, 1989). Calciocarbonatites are dominated by calcite, magnesiocarbonatites by dolomite, and ferrocarbonatite by dolomite and Fe-oxides. In rare cases, the iron in ferrocarbonatites occurs predominantly as ankerite (Gittins and Harmer, 1997).

The most widely accepted process for the evolution of carbonatites, from Ca to Mg- and Fe-enriched varieties, is through fractionation of a parental carbonate melt (Lee and Wyllie, 1998; Harmer and Gittins, 1997). Harmer and Gittins (1997) have proposed that fractionation of a primary mantle-derived, magnesian, carbonatitic melt could produce magnesiocarbonatites and calciocarbonatites. The reaction of an ascending Mg-rich carbonatite melt with wehrlitic wall rocks would drive the melt to more calcic compositions, producing calciocarbonatite at early stages and, after armouring of the conduit, subsequent emplacement of more magnesian melts. However, experimental investigations in the system $\text{CaO}-(\text{MgO} + \text{FeO})-(\text{Na}_2\text{O} + \text{K}_2\text{O})-(\text{SiO}_2 + \text{Al}_2\text{O}_3 + \text{TiO}_2)-\text{CO}_2$ by Lee and Wyllie (1998) show that calciocarbonatites can only originate from carbonate melts exsolved from silicate magmas, not primary, mantle-derived melts, and

magnesiocarbonatite cannot be produced by immiscibility. The formation of magnesiocarbonatite can only be achieved from a primary melt or, contrary to Gittins and Harmer (1997), through fractionation of a calciocarbonatite melt (Lee and Wyllie, 1998). Neither of these studies or, to my knowledge, any other, have demonstrated how fractionation leads to the formation of late-stage ferrocarbonatite.

Another mechanism that has been proposed to explain the evolution of carbonatite magmas is that of carbonate-carbonate liquid immiscibility (Brooker and Hamilton, 1990; Mitchell, 1997; Nielsen *et al.*, 1997). Experimental studies by Brooker and Hamilton (1990) in the system $\text{SiO}_2\text{-Al}_2\text{O}_3\text{-CaO-Na}_2\text{O-CO}_2$ have produced three immiscible liquids, at temperatures of approximately 1225°C, of nephelinitic (Na-rich), Ca-rich carbonate and Ca-Na carbonate compositions. Three-liquid immiscibility is supported by studies of melt inclusions by Nielsen *et al.* (1997) who reported melt inclusion evidence for the presence of three coexisting liquids, of melilitite, Ca-carbonate and Ca-Na carbonate compositions, in the formation of the Gardiner Complex, Greenland. The homogenization temperatures of the three melt inclusions were similar, ranging between 900 and 1060°C. Further support for carbonate-carbonate liquid immiscibility was found by Mitchell (1997) from the Oldoinyo Lengai lavas, Tanzania. Evidence of two coexisting liquids was found in the groundmass of natrocarbonatite lava, that consisted of a carbothermal brine, which crystallized gregoryite, sodian sylvite, potassium neighborite and a Ba-rich carbonate, and a Na-rich carbonate liquid. Although carbonate-carbonate immiscibility has only been documented for natrocarbonatite, the lack of data for Fe-bearing carbonate systems makes it difficult to evaluate its role in the evolution of ferrocarbonatite. Carbonate-carbonate immiscibility needs to be reconsidered for other carbonatite compositions, particularly that of ferrocarbonatite.

Melt Inclusions

Melt inclusions trapped by minerals crystallizing in carbonatite magmas provide a direct window into the evolution of natural carbonatite magmas. If closed system conditions were maintained following trapping, both composition and phase relationships can, in principle, be determined for these carbonate and carbonate-silicate melts.

Although only a small volume of research has been undertaken on melt inclusions, what is available indicates a diversity in the processes of carbonatite formation, from fractionation (Andersen, 1986; Ting *et al.*, 1994; Morogan and Lindblom, 1995) to silicate-carbonate liquid immiscibility (Rankin and Le Bas, 1974) and even carbonate-carbonate liquid immiscibility (Nielsen *et al.*, 1997).

Andersen (1986) reported two types of solid inclusion in apatite from the Fen complex, Norway, one consisting of calcite and the other of dolomite. Although no thermometric studies of these inclusions were undertaken, they were interpreted to represent the evolution, at mid-crustal levels, through fractionation, of a Ca-rich liquid to one of more magnesian composition. Ting *et al.* (1994) observed similar inclusions in apatite of the Sukulu carbonatite, Uganda, consisting of calcite \pm dolomite and magnesian calcite. Some of the latter inclusions melted at temperatures between 740 to 1052°C, and were interpreted to represent droplets of Mg-enriched liquid within the Ca-carbonate melt. Ijolites and carbonatites of the Alnö alkaline complex, Sweden, contain numerous trapped solids consisting of dolomite and Mg-calcite, respectively (Morogan and Lindblom, 1995). Heating of dolomite inclusions from calciocarbonatite produced no changes in the temperature range 800 to 900°C, and they are thus thought to represent the fractionation of dolomite crystals from the carbonate melt, i.e., they are trapped solids.

Rankin and Le Bas (1974) and Nielsen *et al.* (1997) have documented the only occurrences of silicate-carbonate liquid immiscibility prior to this study. Solid inclusions were identified by Rankin and Le Bas (1974) in ijolite-hosted apatite from the Usaki complex, Kenya comprising silicate- and carbonate-rich and mixed silicate-carbonate types. Heating of the carbonate-rich inclusions produced incipient melting at approximately 500°C, and complete melting at temperatures between 640 and 700°C. Mixed carbonate-silicate inclusions, with <20 vol.% silicate, began melting between 575 and 640°C. The first phase to melt was carbonate, followed by the silicate phase between 820 and 900°C, and homogenization of the inclusions between 950 and 1100°C. Mixed inclusions, in which silicate makes up over 20 vol.% of the inclusion, produced two immiscible liquids in the temperature range 950 and 1100°C, with silicate and carbonate compositions. Evidence of both silicate-carbonate and carbonate-carbonate liquid immiscibility was reported by Nielsen *et al.* (1997). They observed carbonate-silicate,

Ca-carbonate and Ca-, Na-carbonate solid inclusions in melilitite of the Gardiner complex, Greenland, which homogenized at 1060°C, 1030-1060°C and 900-1030°C, respectively. These inclusions are interpreted to represent a three-phase immiscibility system involving two carbonate liquids and one silicate liquid.

Aqueous Fluids

The presence of dissolved H₂O in carbonatite melts has long been accepted by researchers. Field evidence of large metasomatic halos surrounding carbonatite complexes (McKie, 1966; Woolley, 1982; Kresten and Morogan, 1986; Morogan, 1994), and experimental studies (Wyllie, 1989; Gittins *et al.*, 1990) show volatiles to be an important constituent of carbonatite melts. However, relatively little research has been focussed on this aspect of carbonatite formation and evolution.

Fenitization

Most of our information on the nature of the aqueous fluids exsolved from carbonatites comes from the study of fenitization. Fenitization, the metasomatic alteration of country rock surrounding alkaline intrusions, is typically divided into three classes: sodic; potassic; and sodic-potassic. At one time, sodic fenitization was generally attributed to fluids exsolved from alkaline silicate intrusions, while potassic fenitization was considered to be wholly a result of carbonatite-derived fluids (Le Bas, 1981). However, an increasing body of field evidence has shown that both sodic and potassic fenitization can accompany carbonatite magmatism, and this is true for both calcian and magnesian carbonatites (Currie and Ferguson, 1971; Kapustin, 1982; Mian and Le Bas, 1986; Viladkar, 1986; Morogan, 1994; Ferguson *et al.*, 1975). Table 1-1 summarizes some of the features of fenites and conditions of fenitization for a selection of carbonatite intrusions in various parts of the world.

Table 1-1 Fenitization associated with carbonatite occurrences

Locality	Source	Host lithology	Fenite Style	Fenite Type	Mineralogical Changes		Temperature	Reference
					Gain	Loss		
Fen, Norway	Carbonatite	Granitic Gneiss	sodi-potassic	N.A.	Ab, Or, Micr, Rieb, Fe-Rch, Aeg, Aeg-Aug, Phl, Cc, Ap	Qtz	<500-700 °C	Morogan (1994) Kresten and Morogan (1986) Kresten (1988)
	ljolite		sodi-potassic		Ab, Or, Perth, Mg Arf, Aeg, Aeg-Aug	Qtz	500-600 °C	
Alno, Sweden	Carbonatite	Migmatitic gneiss (Qtz, Micr, Olig, Bt)	sodi-potassic	N.A.	Ab, Or, Pth, Mg-Arf, Bt, Aeg-Aug Rch, Cc, Titn, Ap, Fl	N.A.	650-700°C	Morogan (1994)
	ljolite		sodi-potassic	N.A.	Ab, Or, Pth, Mg-Arf, Bt, Aeg-Aug	N.A.	500-650°C	Morogan and Wooley (1988)
Amethyst Carbonatites Colorado	Carbonatite	granite	sodi-potassic	N.A.	Micr, Ht, minor Na-Amph and Pyrx chl, Cc	Qtz, Bt	N.A.	Heinrich and Shappirio (1966)
Callander Bay, Ontario	Carbonatite	granitic gneiss	sodi-potassic	inner	Micr, Aeg, Na-Amph, Ht, Cc	Qtz, Plag, Hbld, Bt	450-700°C	Currie and Ferguson (1971)
	Carbonatite	granitic gneiss	sodic	middle	Ab, Aeg, Na-Amph	Qtz, Plag, Hbld, Bt		
	Carbonatite	granitic gneiss	hematization	outer	Ht, Cc veinlets, chl	Qtz		
Amba Dongar, India	Carbonatite	quartzite	sodic	deep	Ab, Aeg-Aug	Qtz	High - T	Viladkar (1986)
	Carbonatite	quartzite	sodi-potassic	N.A.	Or, Aeg	Qtz	Low - T	Roelofsen (1997)
	Carbonatite	quartzite	potassic	shallow	Or	Qtz	Low - T	
	ljolite	quartzite	sodi-potassic	deep	Microph, Aeg-Aug	Qtz	High - T	

Plag - plagioclase, Ab - albite, And - andesine, Olig - oligoclase, K-fsp - potassium feldspar, Micr - microcline, Or - orthoclase, Perth - perthite, Aeg - Aegirine, Aug - augite, Rieb - riebeckite, Rch - richterite, Arf - arfvedsonite, Amph, amphibole, Phl - phlogopite, Bt - biotite, chl - chlorite, Musc - muscovite, Ap - apatite, Cc - calcite, Ht - hematite, Titn - titanite, Fl - fluorite, Canc - cancrinite, Ox - oxides, Qtz - quartz

N.A. Not Available

Table 1-1 *con't*

Locality	Source	Host lithology	Fenite Style	Fenite Type	Mineralogical Changes		Temperature	Reference
					Gain	Loss		
Epembe, South West Africa	Carbonatite	granitoid	sodic	high-grade	Ab, Canc	Micr, Plag, Qtz	450-680°C	Ferguson et al. (1975)
			sodi-potassic [*]	low-grade	Musc, Ab	Micr, Plag, Qtz	N.A.	
		Amphibolite	sodi-potassic [*]	high-grade	Bt, Ab	Chl, Musc, Plag	N.A.	
			hematization	low-grade	Chl, Ep, Zois, Ht	Bt	N.A.	
Novopolitava, Azov	Carbonatite	granitic gneiss	sodi-potassic	inner	Micr, Ab, Ap, Cc	Aeg-Aug	N.A.	Kapustin (1982)
			sodic	middle	Pth, Ab, Aeg-Aug	Qtz, Micr, Bt	N.A.	
			sodic	outer	Ab	Qtz, Micr	N.A.	
		plagioclase gneiss	sodic	inner	Aeg-Aug,			
			sodic	middle	Aeg-Aug, Olig, Cc, Ap, Zirc			
			sodic	outer	Aeg-Aug, Olig, Pth	Hbld, Bt, Plag, Micr	N.A.	
Great Glenn Fault Area Scotland	Carbonatite	Biotite granite	sodic	inner	Ab, Aeg	K-fsp, Bt, Qtz	N.A.	Garson et al. (1984)
			sodi-potassic	middle	Or-Microph, Ab, Aeg, Titn	Qtz, K-fsp, Olig	N.A.	
			sodic	middle	Aeg-Cc-Ab veinlets	N.A.	N.A.	
			hematization	outer	Ht	N.A.	N.A.	
Lemitar carbonatites New Mexico	Carbonatite	granite	potassic	N.A.	Fe-ox, Cc, K-fsp	Qtz	N.A.	McLemore and Modreski (1990)
		diorite/gabbro	sodic-potassic	N.A.	And-Ab, K-fsp	Qtz, Lab	N.A.	
		amphibolite	carbonatization	N.A.	Cc, K-fsp	Qtz	N.A.	
Chipman Lake, Ontario	Carbonatites	granite	sodic-potassic	N.A.	Ab, Micr, Mg-Arf, Aeg, Phl, Cc	Qtz, mafic minerals	N.A.	Garth-Platt and Wooley (1990)

Plag - plagioclase, Ab - albite, And - andesine, Olig - oligoclase, K-fsp - potassium feldspar, Micr - microcline, Or - orthoclase, Perth - perthite, Aeg - Aegirine, Aug - augite, Rie - riebeckite, Rch - richterite, Arf - arfvedsonite, Amph, amphibole, Phl - phlogopite, Bt - biotite, chl - chlorite, Musc - muscovite, Ap - apatite, Cc - calcite, Ht - hematite, Titn - titanite, Fl - fluorite, Canc - cancrinite, Ox - oxides, Qtz - quartz
N.A. Not Available

Fenitization associated with Carbonatites

Mineralogical changes associated with sodic fenitization are remarkably similar among complexes and invariably involve additions of aegirine and albite, and less commonly sodic amphibole, to the host rock. Mafic minerals typically grow at the expense of the original mafic minerals and quartz, while potassium feldspar and plagioclase either undergo ion exchange reactions to form albite or simply replace quartz.

Potassic fenitization is typically manifested by the addition and recrystallization of orthoclase, microcline and rarely sanidine and the loss of sodic minerals such as aegirine and albite. The more common sodic-potassic style of fenitization also shows marked similarities among different complexes. As suggested by the description, these fenites show elements of both sodic and potassic fenitization with additions of some or all of the following minerals: aegirine, aegirine-augite, albite, orthoclase, microcline and sodic amphibole, typically as a result of replacement, or recrystallization, of earlier mafic minerals, feldspars and quartz.

Accessory minerals are present in all three fenite types, and consist, in decreasing order of importance, of calcite, apatite, phlogopite, titanite and magnetite. Although these minerals are found in all three fenite types, they appear to be more common in the sodic-potassic fenites.

Mineralogical, as well as chemical, changes of altered host rocks, caused by fluid disequilibrium, are an excellent means by which to obtain information on the composition of the fenitizing fluid. Unfortunately, few studies of fenitization have been used for this purpose. The fenite type, i.e, sodic, potassic or sodic potassic, has generally been attributed to differences in the Na/K ratios of the fluids exsolved from carbonatites, with high Na/K values causing sodic fenitization and low values causing potassic fenitization (McKie, 1966; Heinrich, 1966; Kresten and Morogan, 1986; Morogan, 1994). However, Rubie and Gunter (1983) have found that other variables such as temperature, pressure and CO₂ content have a much more pronounced effect on fenitization than the Na/K ratio. They showed that both sodic and potassic fenites can be generated by a fluid with constant Na/K under different PTX_{CO₂} conditions, with higher temperature and lower X_{CO₂} conditions favouring the formation of sodic fenites.

Most studies of fenitization conclude that fenitizing fluids must have contained high concentrations of Na, K, Fe, Mg, Ca and CO₂ and been deficient in Si. However, few authors have attempted to determine the temperatures under which fenitization takes place. The data that are available suggest that the lower and upper limits of fenitization are 450 and 700°C, respectively (Currie and Ferguson, 1971; Ferguson *et al.*, 1975; Kresten and Morogan, 1986; Morogan and Woolley, 1988; Morogan, 1994). However, the data apply only to sodic-potassic fenites, whereas data presented in this thesis suggests significantly lower temperatures for the formation of potassic fenites (<300°C).

Fluid inclusions

The most reliable source of information on aqueous fluids from carbonatites comes from the fluids themselves. Although a comparatively small number of researchers have investigated fluid inclusions in carbonatites, what has been accomplished provides valuable insight into the nature of primary fluids in equilibrium with carbonatite melts (Rankin 1975; Nesbitt and Kelly, 1977; Haapala, 1980; Andersen, 1986. Ting *et al.* 1994; Morogan and Lindblom, 1995; Poutiainen, 1995; Samson *et al.*, 1995a)

Primary carbonatite-derived aqueous fluids are typically CO₂-bearing, moderate-salinity NaCl-KCl brines with high Na/K ratios (Rubie and Gunter, 1983; Rankin, 1975). Fluid inclusions typically record an evolutionary split in this primary fluid, into a low salinity carbonic fluid and a high salinity, dominantly aqueous, fluid (Andersen, 1986; Ting *et al.*, 1994; Poutiainen, 1995; Morogan and Lindblom, 1995). Studies have shown that there is a wide diversity in the composition of inclusion fluids, and this is well illustrated by the variety of carbonate, sulphate, halide and oxide and sulphide opaque solids which fluid inclusions can contain. In some cases, up to 80% of the volume of a carbonatite-hosted fluid inclusion can be made up of solids (Roedder, 1973; Haapala, 1980). The most common daughter minerals are nahcolite and halite (Rankin, 1975, 1977; Nesbitt and Kelly, 1977; Ting *et al.*, 1994; Samson *et al.*, 1995b), although a myriad of solids have been reported including calcite, sylvite, magnetite, arcanite (K₂SO₄), thenardite (Na₂SO₄), hydrophyllite (CaCl₂), gypsum, phlogopite, glauberite

($\text{Na}_2\text{Ca}(\text{SO}_4)_2$), celestite, syngenite ($\text{K}_2\text{Ca}(\text{SO}_4)_2 \cdot \text{H}_2\text{O}$), barite, strontianite, LREE carbonates and occasionally apatite (Rankin, 1975, 1977; Nesbitt and Kelly, 1977; Aspden, 1980; Samson *et al.*, 1995b). Homogenization temperatures usually range between 200 and 550°C for most complexes (Rankin 1975; Nesbitt and Kelly, 1977; Andersen, 1986; Jaireth *et al.*, 1991; Ting *et al.*, 1994; Morogan and Lindblom, 1995; Poutiainen, 1995; Samson *et al.*, 1995a), however, temperatures greater than 550°C have been reported (Rankin, 1975; Puzanov, 1977; Haapala, 1980).

Previous Work – Amba Dongar

The geology of the Amba Dongar complex has been documented by a number of researchers (Sukheswala and Udas, 1963; Deans and Powell, 1968; Deans *et al.*, 1972; Viladkar, 1981; Srivastava, 1989; Gwalani *et al.*, 1993). In all studies the authors conclude that the complex formed as a ring-structured intrusion of calciocarbonatite and ferrocarbonatite, which was coeval with formation of the surrounding nephelinite intrusives, during mid to late Deccan volcanism.

Extensive work has been carried out on the fluid inclusions in fluorite from the late stage fluorite deposit (Roedder, 1973; Lahiry, 1976; Kaul *et al.*, 1988; Palmer, 1994; Palmer and Williams-Jones, 1996). Palmer and Williams-Jones (1996) concluded that the interaction of primary magmatic fluids, containing significant Al, S and F, with Ca-bearing meteoric waters was responsible for fluorite mineralization. Roedder (1973) observed several types of primary fluid inclusions in apatite from carbonatite, although no microthermometry was undertaken. These comprise H_2O - or CO_2 rich types and a high density aqueous type which contains up to 50 vol.% solids (Roedder, 1973).

Although fenitization is well developed at Amba Dongar, it has received comparatively little attention. Only three studies have focussed on the fenites (Deans *et al.*, 1972; Viladkar, 1986, Roelofsen, 1997). Deans *et al.* (1972) were the first to demonstrate that the potassium feldspar rocks associated with the Amba Dongar carbonatites were in fact fenites. They noted that the feldspar (microcline, orthoclase and minor plagioclase) content increases dramatically from unaltered Bagh sandstone to its contact with the carbonatite. A follow-up study by Viladkar (1986) divided fenites into

potassic and sodic varieties based on surface outcrop and diamond drill core. He observed that sodic fenite assemblages (albite and aegirine) occurred in the deeper, unexposed parts of the complex and that potassic fenites were restricted to the upper levels (Viladkar, 1986). Roelofsen (1997) extended this work at Amba Dongar by characterizing the fenite mineralogy, and demonstrating its hydrothermal nature.

Previous Work - Phalaborwa

A considerable amount of research has been carried out on the Phalaborwa complex (Lombaard *et al.*, 1964; Hanekom *et al.*, 1965; Palabora Mining Company, 1976; Eriksson, 1989), including three Ph.D. theses by Van Rensburg (1965), Aldous (1980) and Eriksson (1982), which focussed on the geology, the copper mineralization and the geochemistry and origins of Phalaborwa, respectively. All these authors agree that the formation of the complex was initiated by intrusion of a large lobe of pyroxenite which was subsequently cored by phoscorite, banded carbonatite and transgressive carbonatite melts. However, the origins of copper mineralization in carbonatite remain unresolved.

It was thought initially that copper mineralization was produced by late stage hydrothermal fluids circulating within the carbonatite (Hanekom *et al.*, 1965; Palabora Mining Company, 1976), however, large scale sulphide zonation and melt inclusion studies have thrown some doubt on this as the primary mode of formation. Aldous (1980) showed that sulphides were present in both silicate and carbonatite melts early in their histories and concluded that early copper mineralization may have been a primary magmatic feature. However, he interpreted late-stage copper mineralization in transgressive carbonatite to be the result of remobilisation of primary copper sulphides by orthomagmatic fluids.

A generally accepted model for the formation of Phalaborwa has been developed by Eriksson (1982). Based on a comprehensive mineralogical and Sr isotopic study of the complex she concluded that isotopic heterogeneity between silicate and carbonatite rocks ruled out liquid immiscibility as a mechanism for carbonatite formation. She proposed, instead, that the Phalaborwa complex formed as a result of multiple injections

of silicate- and carbonate-rich magmas (Eriksson, 1982). In a subsequent radiogenic and stable isotopic study Eriksson (1989) also concluded that the carbonatites could not have formed by crystal fractionation or liquid immiscibility processes alone, but noted that there were similarities between silicate and carbonatite members.

Fenitization is not well developed at Phalaborwa. According to Frick (1975), it is manifested by the growth of orthoclase at orthoclase-quartz and plagioclase-quartz boundaries, and by an increase in orthoclase content and the appearance of alkali amphibole. The precursor to fenite is a pink granite or a white, biotitic granitic gneiss (Eriksson, 1982). Evidence of desilication and an increase in the potassium feldspar content with increasing fenitization are common features in both precursors (Eriksson, 1982).

Organization of this Thesis

The original intent of this thesis was twofold, firstly, to characterize hydrothermal fluids associated with carbonatite magmatism, a topic which has received very little attention, and secondly, to discover the role of these fluids in the development of economic ore bodies hosted by carbonatites. However, the discovery of melt inclusions in apatite hosted by carbonatites of both complexes prompted a change in the direction of the thesis, resulting in a study that investigated the evolution of both carbonatite melts and aqueous fluids.

The chapters dealing with Amba Dongar in this thesis are a continuation of a M.Sc. project by the author, which determined the nature of late-stage fluids responsible for fluorite mineralization. The presence of REE mineralization and the abundant evidence of early aqueous fluids, i.e., fenitization, fluid inclusions, encouraged the author to undertake further studies to characterize the entire fluid evolution of the complex. The discovery of primary melt inclusions in apatite proved useful in determining the evolution of carbonatite melts during the emplacement of the complex and provided the first evidence that ferrocarbonatites can form by the separation of an immiscible Fe-rich melt from calciocarbonatite.

The Phalaborwa complex was chosen for study in order to characterize orthomagmatic fluids associated with the carbonatites and determine their role in the development of Phalaborwa's economic copper deposit. Solid and solid-liquid inclusions discovered during the course of the study were used to explain the formation of carbonate-bearing lithologies

Chapters 2 and 3 of this thesis provide detailed descriptions of the geology of the Amba Dongar and Phalaborwa complexes, respectively. They are intended to give the reader a detailed understanding of the regional and local geology of the complexes that is not possible in the journal manuscripts.

Melt inclusions identified in apatite of calciocarbonatite from the Amba Dongar complex are dealt with in Chapter 4. The compositions and high temperature phase relationships of solid inclusions are discussed with reference to the origins of calciocarbonatite and ferrocarbonatite. The results indicate that fractionation was not responsible for ferrocarbonatite formation and suggest that carbonate-carbonate liquid immiscibility occurred to produce both calciocarbonatite and ferrocarbonatite.

Chapter 5 characterizes the chemical and pressure-temperature evolution of orthomagmatic fluids associated with carbonatite emplacement in the Amba Dongar complex. A combination of destructive and nondestructive fluid inclusion techniques were used to establish the pressure-temperature conditions and bulk compositions of aqueous fluids exsolved from calciocarbonatite.

Calculations of mass changes which occurred between unaltered sandstones, that host the Amba Dongar complex, and carbonatite-derived fluids are presented in Chapter 6. The mass balance methods of Gresens (1967) and Grant (1986) were used to achieve unprecedented accuracy in determining the mass change, owing to the almost monomineralic (quartz) nature of the sandstones. This allowed even further characterization of aqueous fluid compositions, in particular trace element concentrations, which could not be analysed by fluid inclusion techniques.

Apatite-hosted melt inclusions in carbonate-bearing rocks, i.e., phoscorite and carbonatites, of the Phalaborwa complex are discussed in Chapter 7. Their compositions and behaviour during high temperature microthermometric experiments suggest that silicate-carbonate liquid immiscibility was an important process in the evolution of the

complex and played a major role in the formation of phoscorite and carbonatite. Another important conclusion of the chapter is that carbonatite lithologies were related to one another through later fractionation. Melt inclusion compositions suggest that early copper mineralization was a primary magmatic process associated with the crystallization of early carbonatite, while aqueous fluid-bearing melt inclusions in late stage carbonatites suggest that late copper mineralization resulted from hydrothermal remobilisation of primary sulphides.

Chapter 8 details the fluid evolution of the Phalaborwa complex during its emplacement. Fluid compositions are inferred from chemical changes which attended metasomatic alteration, i.e., fenitization, of the surrounding host rocks. Two fluid events were discerned, corresponding to pyroxenite- and carbonatite-emplacement, and both resulting in potassic fenitization. However, mass balance calculations based on mineralogical changes indicate that carbonatite-derived fluids contained more Na, Mg and S, and were responsible for deposition of late copper mineralization.

References

- Aldous, R.T., 1980, Ore genesis in copper-bearing carbonatites; a geochemical, fluid inclusion and mineralogical study: Unpublished Ph.D. thesis, Imperial College, London, 365p..
- Andersen, T., 1986, Magmatic fluids in the Fen carbonatite complex, S.E. Norway: *Contrib. Mineral. Petrol.*, v. 93, p. 491-503.
- Aspden, J. A., 1980, The mineralogy of primary inclusions in apatite crystals extracted from Alnö ijolite: *Lithos*, v. 13, p. 263-268.
- Barker, D.S., 1989, Field relations of carbonatites: *in* K. Bell (ed.), *Carbonatites: genesis and evolution*: London, Unwin Hyman, p. 38-69.
- Brooker, R.A. and Hamilton, D.L., 1990, Three-liquid immiscibility and the origin of carbonatites: *nature*, v. 346, p. 459-462.
- Cooper, A.F., Gittins, J., and Tuttle, O.F., 1975, The system $\text{Na}_2\text{CO}_3\text{-K}_2\text{CO}_3\text{-CaCO}_3$ at 1 kilobar and its significance in carbonatite petrogenesis: *American Journal of Science*, v. 275, p. 534-560.
- Currie, K.L. and Ferguson, J., 1971, A study of fenitization around the alkaline complex at Callander Bay, Ontario, Canada: *Canadian Journal of Earth Sciences*, v. 8, p. 498-517.
- Dalton, J.A., and Wood, B.J., 1993, The compositions of primary carbonate melts and their evolution through wallrock reaction in the mantle: *Earth and Planetary Science Letters*, v. 119, p. 511-525.
- Deans, T., 1966, Economic mineralogy of African carbonatites, *in* Tuttle, O.F., and Gittins, J., eds., *Carbonatites*: London, Wiley & Sons, p. 385-416.
- Deans, T., and Powell, J.L., 1968, Trace elements and strontium isotopes in carbonatites, fluorites and limestones from India and Pakistan: *Nature*, v. 218, p. 750-752.
- Deans, T., Sukheswala, R.N., Sethna, S.F. and Viladkar, S.G., 1972, Metasomatic feldspar rocks (potash fenites) associated with the fluorite deposits and carbonatites of Amba Dongar, Gujarat, India: *Trans. Inst. Min. Metall. (sect. B: earth sci.)*, v. 81, p. B1-B9.
- Eriksson, S.C., 1982, Aspects of the petrochemistry of the Phalaborwa Complex, northeastern Transvaal, South Africa: Unpublished Ph.D. thesis, University of the Witwatersrand, Johannesburg.

- Eriksson, S.C., 1989, Phalaborwa, a saga of magmatism, metasomatism and miscibility: in K. Bell (ed.), Carbonatites: genesis and evolution: London, Unwin Hyman, p. 221-254.
- Ferguson, J., McIver, J.R., and Danchin, R.V., 1975, Fenitization associated with the alkaline-carbonatite complex of Epembe, South West Africa: Trans. Geol. Soc. S. Afr., v. 78, p. 111-121.
- Freestone, I.C., and Hamilton, D.L., 1980, The role of liquid immiscibility in the genesis of carbonatites – an experimental study: Contrib. Mineral. Petrol., v. 73, p. 105-117.
- Frick, C., 1975, The Phalaborwa syenite intrusions: Trans. Geol. Soc. S. Afr., v. 78, p. 201-213.
- Garson, M.S., Coats, J.S., Rock, N.M.S., and Deans, T., 1984, Fenites, breccia dykes, albitites, and carbonatitic veins near the Great Glen Fault, Inverness, Scotland: J. geol. Soc. London, v. 141, p. 711-732.
- Garth-Platt, P., and Woolley, A.R., 1990, The carbonatites and fenites of Chipman Lake, Ontario: Canadian Mineralogist, v. 28, p. 241-250.
- Gittins, J., 1988, The origin of carbonatites: Nature, v. 335, p. 295-296.
- Gittins, J., 1989, Carbonatite origin and diversity – Reply: Nature, v. 338, p. 548.
- Gittins, J., Beckett, M.F., and Jago, 1990, Composition of the fluid accompanying carbonatite magma: A critical examination, American Mineralogist, v. 75, p. 1106-1109.
- Gittins, J., and Harmer, R.E., 1997, What is ferrocarbonatite? A revised classification: Journal of African Earth Sciences, v. 25, p. 159-168.
- Grant, J.A., 1986, The isocon diagram-A simple solution to Gresens' equation for metasomatic alteration: Economic Geology, v. 81, p. 1976-1982.
- Gresens, R.L., 1967, Composition-volume relationships of metasomatism: Chem. Geol. v. 2, p. 47-65.
- Gwalani, L.G., Rock, N.M.S., Chang, W.J., and Fernandez, S., 1993, Alkaline rocks and carbonatites of Amba Dongar and adjacent areas, Deccan Igneous Province, Gujarat, India: 1. Geology, Petrography and Petrochemistry: Mineralogy and Petrology, v. 47, p. 219-253.
- Haapala, I., 1980, Fluid Inclusions in the apatite of the Sokli carbonatite, Finland: A preliminary report: Geologi, v.32 (7), p. 83-87.

- Hamilton, D.L., and Kjarsgaard, B.A., 1993, The immiscibility of silicate and carbonate liquids: *S.Afr. J. Geol.*, v. 96, p. 139-142.
- Hanekom, H.J., van Staden, C.M., Smit, P.J., and Pike, D.R., 1965, The geology of the Palabora Igneous Complex: *South Africa Geological Survey Handbook, memoir 54*.
- Harmer, R.E., and Gittins, J., 1997, The origin of dolomitic carbonatites: field and experimental constraints: *Journal of African Earth Sciences*, v. 25, p. 5-28.
- Heinrich, E.Wm., 1966, *The Geology of Carbonatites*: Rand McNally & Company, Chicago, 553p.
- Heinrich, E.Wm. and Shappirio, J.R., 1966, Alkaline rocks and carbonatites of the Arkansas River Canyon, Fremont County, Colorado. 3. The amethyst carbonatites: *American Mineralogist*, v. 51, p. 1088-1106.
- Jaireth, S., Sen, A. K., and Varma, O. P., 1991, Fluid inclusion studies in apatite of the Sung Valley Carbonatite Complex, N. E. India: Evidence of melt-fluid immiscibility: *Journal Geological Society of India*, v. 37, p. 547-559.
- Kapustin, Yu.L., 1982, Features of fenitization around carbonatite bodies: *AN SSR Izvestiya, ser. Geol.*, no. 9, p. 48-60.
- Kaul, K., Rao, C.N., Sanyal, T., and Akhtar, S.H., 1988, Fluorite crystallization temperatures: evidence from thermoluminescence characteristics and fluid inclusion studies: *Indian Journal of Geology*, v. 60, (4), p. 258-265.
- Kjarsgaard, B.E., and Hamilton, D.L., 1988, Liquid immiscibility and the origin of alkali-poor carbonatites: *Mineralogical Magazine*, v. 52, p. 43-55.
- Kjarsgaard, B.E., and Hamilton, D.L., 1989, Carbonatite origin and diversity: *Nature*, v. 338, p. 547-548.
- Koster Van Groos, A.F., and Wyllie, P.J., 1973, Liquid Immiscibility in the join $\text{NaAlSi}_3\text{O}_8\text{-CaAl}_2\text{Si}_2\text{O}_8\text{-Na}_2\text{CO}_3\text{-H}_2\text{O}$: *American Journal of Science*, v. 273, p. 465-487.
- Kresten, P., 1988, The chemistry of fenitization: examples from Fen, Norway: *Chemical Geology*, v. 68, p. 329-349.
- Kresten, P., and Morogan, V., 1986, Fenitization at the Fen complex, southern Norway: *Lithos*, v. 19, p. 27-42.
- Lahiry, A., 1976, Observations on fluor spar mineralization at Amba Dongar, Gujarat based on fluid inclusion data: *Indian Journal of Earth Sciences*, v. 3, (1), p. 37-43.

- Le Bas, M.J., 1981, Carbonatite Magmas, *Mineralogical Magazine*, v. 44, p. 133-140.
- Le Bas, M.J., 1989, Diversification of Carbonatites: *in* K. Bell (ed.), *Carbonatites: genesis and evolution*: Unwin Hyman, Boston, p. 428-447.
- Lee, W.-J., and Wyllie, P.J., 1996, Liquid immiscibility in the join $\text{NaAlSi}_3\text{O}_8\text{-CaCO}_3$ at 2.5 GPa and the origin of calciocarbonatite Magmas : *Journal of Petrology*, v. 38, p. 1113-1135.
- Lee, W.-J., and Wyllie, P.J., 1998, Petrogenesis of carbonatite magmas from mantle to crust, constrained by the system $\text{CaO-(MgO + FeO}^*\text{)-(Na}_2\text{O + K}_2\text{O)-(SiO}_2\text{ + Al}_2\text{O}_3\text{ + TiO}_2\text{)-CO}_2$: *Journal of Petrology*, v. 39, p. 495-517.
- Lombaard, A.F., Ward-Able, N.M., and Bruce, R.W., 1964, The exploration and main geological features of the copper deposit in carbonatite at Looilekop, Palabora Complex: *In* Haughton, S.H., ed., *The geology of some ore deposits in Southern Africa*, The geological society of South Africa, Johannesburg, p. 315-337.
- Mariano, A.N., 1989, Nature of economic mineralization in carbonatites and related rocks: *in* Bell, K., ed., *Carbonatites: genesis and evolution*: London, Unwin Hyman, p. 149-176.
- McKie, D., 1966, Fenitization: *in* Tuttle, O.F., and Gittins, J., eds., *Carbonatites*: London, Wiley & Sons, p. 261-294.
- McLemore, V.T., and Modreski, P.J., 1990, Mineralogy and geochemistry of altered rocks associated with Lematir carbonatites, central New Mexico, U.S.A.: *Lithos*, v. 26, p. 99-113.
- Mian, I., and Le Bas, M.J., 1986, Sodic amphiboles in fenites from the Loe Shilman carbonatite complex, NW Pakistan: *Mineralogical Magazine*, v. 50, p. 187-197.
- Mitchell, R.H., 1997, Carbonate-carbonate immiscibility, neighborite and potassium iron sulphide from Oldoinyo Lengai natrocarbonatite: *GAC/MAC Annual Meeting May 19-21: Abstract Volume*, p. A104.
- Morogan, V., 1994, Ijolite versus carbonatite as sources of fenitization: *Terra Nova*, v. 6, p. 166-176.
- Morogan, V. and Lindblom, S. 1995, Volatiles Associated with the alkaline – carbonatite magmatism at Alnö, Sweden: a study of fluid and solid inclusions in minerals from the Långersholmen ring complex: *Contrib. Mineral. Petrol.* V 122, p. 262-274.

- Morogan, V., and Woolley, A.R., 1988, Fentitzation at the Alnö carbonatite complex, Sweden; distribution, mineralogy and genesis: *Contrib. Mineral. Petrol.*, v. 100, p. 169-182.
- Nesbitt, B.E., and Kelly, W.C., 1977, Magmatic and Hydrothermal inclusions in carbonatite of the Magnet Cove Complex, Arkansas: *Contrib. Mineral. Petrol.*, v. 63, p. 271-294.
- Nielson, T. F. D., Solovova, I. P., and Veksler, I. V., 1997, Parental melts of melilitolite and origin of alkaline carbonatite: evidence from crystallized melt inclusions, Gardiner complex: *Contrib. Mineral. Petrol.*, v. 126, p. 331-344.
- Palabora Mining Company, 1976, The geology and the economic deposits of copper, iron and vermiculite in the Palabora Igneous Complex: a brief review: *Economic Geology*, v. 71, p. 177-192.
- Palmer, D.A.S., 1994, Geology and geochemistry of the Amba Dongar carbonatite-hosted fluorite deposit, India: Unpublished M.Sc. thesis, McGill University, Montreal, 110p..
- Palmer, D.A.S., and Williams-Jones, A.E., 1996, Genesis of the carbonatite-hosted fluorite deposit at Amba Dongar, India: Evidence from fluid inclusions, stable isotopes and whole rock-mineral geochemistry: *Economic Geology*, v. 91, p. 934-950.
- Poutiainen, M., 1995, Fluids in the Siilinjärvi carbonatite complex, eastern Finland: Fluid inclusion evidence for the formation conditions of zircon and apatite: *Bull. Geol. Soc. Finland*, v. 67, part 1, p. 3-18.
- Puzanov, L.S., 1977, Origin of fluorite mineralization in carbonatite of the Bol'shaya Tagna pluton, Eastern Sayan: *Doklady Akademii Nauk SSSR*, v. 233, (3), p. 463-466.
- Rankin, A.H., 1975, Fluid inclusion studies in apatite from carbonatites of the Wasaki area of western Kenya: *Lithos*, v. 8, p. 123-136.
- Rankin, A.H., 1977, Fluid-inclusion evidence for the formation conditions of apatite from the Tororo carbonatite complex of eastern Uganda: *Mineralogical Magazine*, v. 41, p. 155-164.
- Rankin, A.H. and Le Bas, M.J., 1974, Liquid Immiscibility between silicate and carbonate melts in naturally occurring ijolite magma: *Nature*, v 250, p. 206-209.
- Roedder, E., 1973, Fluid inclusions from the fluorite deposits associated with carbonatite at Amba Dongar, India, and Okorusu, South West Africa: Metasomatic feldspar rocks (potash fenites) associated with the fluorite deposits and carbonatites of Amba Dongar, Gujarat, India: Discussion and contributions: *Trans. Inst. Min. Metall. (sect. B: earth sci.)*, v. 82, p. B35-B39.

- Roelofsen, J.N., 1997, The primary and secondary mafic silicates of two alkaline anorogenic complexes: Strange Lake (Quebec-Labrador) and Amba Dongar (Gujarat, India): Unpublished Ph.D. thesis, McGill University, Montreal, 489p..
- Rubie, D.C., and Gunter, W.D., 1983, The role of speciation in alkaline igneous fluids during fenite metasomatism: *Contrib. Mineral. Petrol.*, v. 82, p. 165-175.
- Samson, I.M., Weining, L., and Williams-Jones, A.E., 1995a, The nature of orthomagmatic hydrothermal fluids in the Oka carbonatite, Quebec: evidence from fluid inclusions: *Geochim. Cosmochim. Acta*, v. 59, p. 1963-1977.
- Samson, I.M., Williams-Jones, A.E., and Weining, L., 1995b, The chemistry of hydrothermal fluids in carbonatites: Evidence from leachate and SEM-decrepitate analysis of fluid inclusions from Oka, Quebec, Canada: *Geochim. Cosmochim. Acta*, v. 59, p. 1979-1989.
- Srivastava, R.K., 1989, Evolution of alkaline carbonatitic complex of Ambadungar, District Baroda, Gujarat:: *Indian Journal of Geochemistry*, v. 4, (1), p. 1-38.
- Sukheswala, R.N. and Udas, G.R., 1963, Note on the carbonatite of Amba Dongar (Gujarat State) and its economic potentialities: *Science and Culture*, v. 29, p. 563-568.
- Sweeney, R.J., 1994, Carbonatite melt compositions in the earth's mantle: *Earth and Planetary Science Letters*, v. 128, p. 259-270.
- Ting, W., Rankin, A. H. and Woolley, A. R., 1994, Petrogenetic significance of solid carbonate inclusions in apatite of the Sukulu carbonatite, Uganda: *Lithos*, v. 31, p. 177-187.
- Van Rensburg, W.C., 1965, Copper mineralization in the carbonate members and phoscorite, Phalaborwa, South Africa: Unpublished Ph.D. thesis, University of Wisconsin, Madison.
- Viladkar, S.G., 1981, The carbonatites of Amba Dongar, Gujarat, India: *Bulletin of the Geological Society of Finland*, v. 53, p. 17-28.
- Viladkar, S.G., 1986, Fenitization at the Amba Dongar Carbonatite alkalic complex, India: *in* M. Gabriel (ed), *Symposium New Mineral Raw Materials: Proceedings*, p. 170-189.
- Wallace, M.E., and Green, D.H., 1988, An experimental determination of primary carbonatite magma composition: *Nature*, v. 335, p. 343-346.

Woolley, A.R., 1982, A discussion of carbonatite evolution and nomenclature, and the generation of sodic and potassic fenites: *Mineralogical Magazine*, v. 46, p. 13-17.

Wyllie, P.J., 1989, Origin of carbonatites: evidence from phase equilibrium studies: *in* K. Bell (ed.), *Carbonatites: genesis and evolution*: London, Unwin Hyman, p.149-176.

Wyllie, P.J. and Tuttle, O.F., 1960, The system $\text{CaO-CO}_2\text{-H}_2\text{O}$ and the origin of carbonatites: *Journal of Petrology*, v. 1, p. 1-46.

Chapter 2: Geology of the Amba Dongar Complex

Location

The Amba Dongar complex is situated approximately 400 km northeast of Bombay, India in the Baroda district of Gujarat State (Fig. 2-1). It outcrops over an area of approximately 3.5 km and lies at a minimum elevation of 380 meters above sea level with a maximum relief of 61 meters.

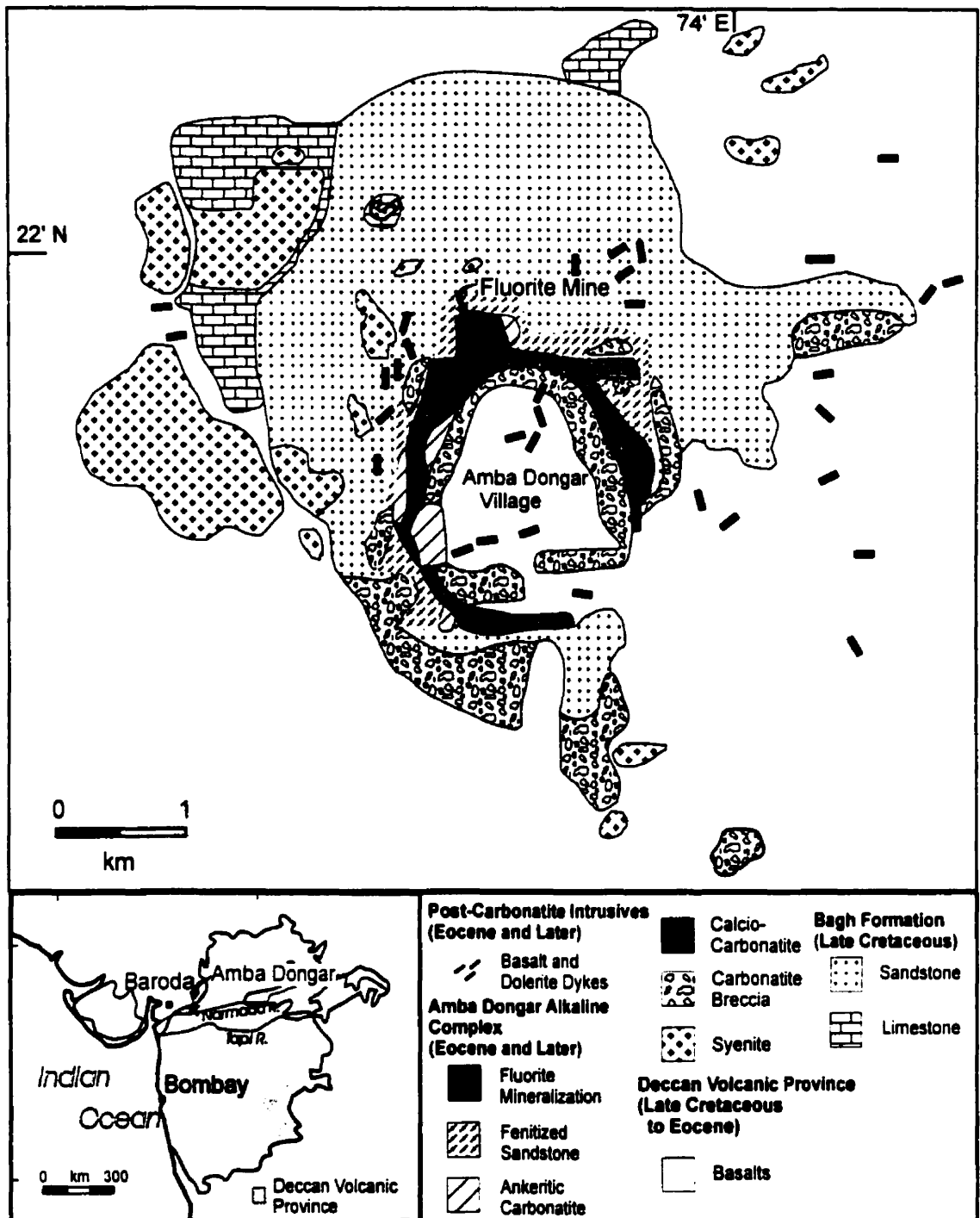
Regional Geology

The carbonatite complex of Amba Dongar was emplaced into the northern part of the Deccan Volcanic Province which covers an area of approximately 500,000 km² of West-Central India, and forms one of the largest geological formations of the country (Krishnan, 1982) (Fig. 2-1). The extrusion of basalt is thought to have occurred during rifting, along reactivated lineaments, as a result of the upwelling of tholeiitic magma when India passed over a mantle thermal center at around 65 Ma (Dietz and Holden, 1970; Gupta and Gaur, 1984; Srivastava, 1989; Karkare and Srivastava, 1990). A general chronology for the area is: 1) eruption and extrusion of voluminous flood basalts; 2) intrusion of alkaline silicate and carbonatitic bodies; and 3) emplacement of late picritic and basaltic dykes (Gwalani *et al.*, 1993; Srivastava, 1989; Sukheswala *et al.*, 1976).

The complex lies within a major zone of structural weakness represented by the ENE trending Narmada rift, which is located nine kilometers to the south (Fig. 2-1 inset). To the north of the complex, is a sympathetic set of faults related to the Narmada rift (Viladkar, 1981). The rift system is thought to be the arm of a failed triple junction that originated along the older Vindhayan fault (Karkare and Srivastava, 1990; Deans *et al.* 1972; Courtillot *et al.*, 1988). Structural expressions of this zone of weakness consist of numerous parallel (to the rift), mafic dyke swarms and NE trending strike-slip faults (Srivastava, 1989).

Intrusion of the carbonatite caused updoming of the country rock which is reflected in dips of 35 to 60 degrees outwards from the body. These structural features

Figure 2-1 The geology of the Amba Dongar complex, India and surrounding area
(Modified from Deans *et al.*, 1972).



are evident up to 5 km away from the ring. Numerous faults are distributed radially around from the complex and have given rise to steep valleys and scarps.

The carbonatite ring structure was intruded into Deccan basalts, which comprise its southern and southwestern boundaries, and a small inlier of Late Cretaceous Bagh sandstones and limestones (Viladkar, 1981), which flank the intrusion on all other sides (Fig. 2-1). Deccan basalts are also present inside the ring structure, and are interpreted by Deans and Powell (1968) to represent a roof over the intrusive site which collapsed during emplacement of the carbonatite. Viladkar (1981), however, has suggested that the basaltic core may represent a later igneous event following carbonatite emplacement. The underlying basement rocks consist of Precambrian granitic gneisses which are poorly exposed and do not outcrop in the area (Srivastava and Karkare, 1991; Deans *et al.*, 1972).

Country Rock Geology

Deccan Basalt

By far the most common rock type in the surrounding area is the flood basalt of the Deccan Traps. The latter consist predominantly of tholeiitic flows and yield whole rock K-Ar dates of 65 Ma to 50 Ma which place them in the Late Paleocene to Early Eocene period (Wellman and McElhinny, 1970). The area surrounding the Narmada Rift belongs to one of a number of alkali olivine basalt subprovinces which occur within the Deccan province (Chatterjee, 1964; Srivastava, 1989; Gwalani, 1981).

The dominant lithologies of the Trappean beds are basaltic lavas and agglomerates. Dykes of glassy basalt and diabase are also common, and trend parallel to the Narmada lineament (Srivastava, 1989). Basalt is typically porphyritic and locally glomerophytic. Phenocrysts, as well as the groundmass, consist of augite and labradorite which, modally, make up 70 to 80 % of the rock. Accessory minerals include olivine, calcite, zeolites and apatite. Evidence of vesiculation is common in the basalts, typically in the form of amygdules. Diabase forms dark gray dykes which range in width from 0.5 to 15 m and can be followed for distances of up to 1.5 km (Srivastava, 1989). Modally,

plagioclase is more important in the diabase than in the basalt, and the percentage of plagioclase plus augite is, at least, 80%. The texture is commonly ophitic to sub-ophitic and locally porphyritic with labradorite occurring as the micro-phenocrysts (Srivastava, 1989). Accessory minerals include olivine and iron oxides.

Bagh Sandstone

The only other rock type which borders the complex is the Late Cretaceous Bagh sandstone (Fig. 2-1). The sandstone belongs to a wave-dominated shelf sequence, which has been divided into five main facies: 1) a conglomeratic lag deposit; 2) coarse-grained sandstone; 3) sandstone; 4) mudstone; and 5) limestone (Bose and Das, 1986). Chiplonkar *et al.* (1977) have interpreted the sequence as being between Upper Albian and Turonian in age (100 Ma - 88.5 Ma), based on paleontological observations. The Bagh sandstone consists of an almost pure quartz sandstone (>96% quartz) which, in outcrop, appears white to light gray. The grain size varies from medium to coarse, and there are local concentrations of small quartz pebbles. The sandstones are generally well sorted comprising spherical quartz grains which commonly show evidence of recrystallization, possibly due to pressure solution. Sedimentary features observed in outcrop include cross-bedding, normal grading and asymmetric ripple marks, indicating a moderate velocity, shallow fluvial environment. In some areas adjacent to the ring complex, the Bagh sandstone has been intensely fenitized, which is evident as K-feldspar pseudomorphs after quartz. In these areas, the sandstone takes on a reddish hue.

Bagh Limestone

To the west of the complex, and separated from it by the sandstones, is a unit of limestone that was deposited after the quartz-rich sediments (Viladkar, pers. comm.). The limestone is a thinly to moderately thickly bedded, fine-grained, tan-colored unit which displays gentle folding in outcrops nearest the complex.

The Carbonatite Complex

General Geology

The carbonatite complex of Amba Dongar is a ring structured intrusion with a diameter of approximately two kilometers, and consists mainly of a prominent ridge of calciocarbonatite, which forms the principal topographical feature of the ring, and an inner lining of calciocarbonatite breccia (Fig. 2-1). Breccias also occur around the circumference of the ring as variably sized, isolated plugs, parallel to the ring's border. Along both margins of the calciocarbonatite ring are numerous small plugs of ankeritic carbonatite. Small dykes (<1 m) of ankeritic carbonatite and calciocarbonatite cut the above lithological units. In the calciocarbonatite, intense fracturing, manifested by numerous jasper and quartz-fluorite veins, may have provided the pathway for fluids which deposited large quantities of fluorite in open space-filled veins and vugs. In a number of areas the calciocarbonatite shows evidence of intense silicification surrounding barren quartz veins. Formation of the complex also included the intrusion of a number of moderately sized (200m - 1500m in diameter) syenitic plugs in the surrounding country rock.

Deans *et al.* (1972) and Viladkar (1981) have developed a chronological sequence for intrusion of the ring. Formation of the structure is interpreted to have begun with the emplacement of the calciocarbonatite breccia followed by intrusion of the calciocarbonatite and finally the plugs of ankeritic carbonatite. Silicification and fluorite deposition are thought to have post-dated all igneous activity.

Carbonatite Geology

The calciocarbonatite breccia consists mainly of fragments of calciocarbonatite and minor metamorphic rocks, sandstone, basalt and nephelinite all set in a matrix of calcitic or ankeritic material. Differential weathering of the fragments and the harder matrix give the breccia a very rough, irregular appearance.

Calciocarbonatite, which forms the main component of the ring system, shows a large variation in grain size, texture and color. Early calciocarbonatite tends to be coarser-grained, occurring as xenoliths in the later, fine-grained calciocarbonatite. The most frequently observed texture consists of interlocking, equigranular calcite crystals. A porphyritic texture is well developed locally, with larger calcite phenocrysts set in a matrix of finer grained calcite. The proportions of other minerals in calciocarbonatite vary greatly, comprising from 1% to over 30% of the rock by volume. In decreasing order of importance, martite (hematite after magnetite), apatite, fluorite, barite, galena, pyrochlore, zircon, phlogopite and aegirine are the most commonly found of these other minerals. Color variations of the calciocarbonatite are numerous, ranging from white to red, brown or a mottled white and black. This range in color is due mainly to the nature of the dominant accessory minerals.

Ankeritic carbonatite is generally a dark red, highly oxidized, fine-grained rock. Accessory minerals, the most important of which is martite (hematite after magnetite), are abundant in this unit in some samples martite can comprise over 50% of the volume of the rock. Other accessory constituents include fluorite, barite, apatite, bastnaesite, pyrochlore, monazite, thorite, pyrite, galena and chalcopryite (Viladkar and Wimmenauer, 1992). Calciocarbonatite dykes as well as small jasper veins are found within the ankeritic carbonatite. Following carbonatite intrusion, a hydrothermal event caused silicification of large volumes of calciocarbonatite surrounding zones of intense quartz veining. Hydrothermal activity also caused the formation of numerous fluorite deposits scattered throughout the calciocarbonatite. The fluorite mineralization occurs as vein and replacement deposits. Deposition of fluorite occurred in two stages; an early stage characterized by a blue to purple variety and a later stage characterized by yellow to colorless fluorite. Fluorite occurs as large, euhedral cubic crystals in the larger veins and vugs, and as anhedral groups of interlocking crystals in smaller veins. Minor proportions of quartz can also be found in the veins and vugs along with small quantities of barite, hematite, galena, pyrite and chalcopryite.

Surrounding the ring complex are a number of plug-like intrusions which are expressed as topographic highs. The plugs vary in diameter from 200m to 1.5 km, and are hosted by Bagh sandstones and limestones, and Deccan volcanics. These intrusive

rocks are of two types; nepheline syenite and phonolite (Viladkar, 1984). They are generally brown to dark green in color and consist of a fine-grained, glassy matrix with phenocrysts of nepheline, alkali feldspar, pyroxene and melanite garnet. Magnetite occurs as a minor phase in some samples. The rocks tend to be highly weathered, and are commonly pink to red in color.

Fenitization

A distinctive feature of the Amba Dongar complex is the occurrence of a well developed zone of fenitization in the sandstone surrounding the carbonatite. Xenoliths of nephelinite in the carbonatite also show the effects of fenitization, typically as intense phlogopitization of pyroxene. Fenitization of sandstones, associated with the carbonatites, was of two types, with some gradation between the two. The first, potassic fenitization, is evident at higher levels of the complex; whereas the second, sodic fenitization, is only recorded in deeper sections (Viladkar, 1986; Roelofsen, 1997). Potassic fenites are the most common of the altered rocks, occurring within the carbonatite and around its periphery. The intensity of metasomatism is variable, with sandstone xenoliths within the carbonatite typically showing complete replacement of quartz by potassium feldspar, and fenite outside the ring containing as little as 5% potassium feldspar. Proximal sandstones may show up to 70% replacement of quartz by feldspar and at distances of between 100 m to 150 m away from the ring, sandstones will contain only 5-10% feldspar. Further out they are essentially unaltered.

In outcrop, potassium-fenitized sandstone varies in color from white to light pink with various degrees of mottling depending on the extent of fenitization. Megascopically, quartz retains many of the characteristics of quartz in unaltered samples, although there appears to have been some recrystallization. Within potassic fenites, feldspar consists of both lath-like orthoclase crystals and small irregular grains which appear to be pseudomorphs after quartz. The color of the feldspar ranges from white to pink.

Sodic metasomatized rocks are relatively uncommon except where they have been uncovered during mining operations. These rocks have been divided into two types:

sodic fenites, consisting of albitized, aegirine-augite bearing rocks; and ultrasodic fenites, or albitites, which are composed only of albite (Viladkar, 1986). The precursor rocks in both cases are reported to be the Bagh sandstone (Viladkar, 1986), however, Roelefsen (1997) has evidence that at least some sodic fenitized rocks were derived from ijolite. Albitites consist of a monomineralic groundmass of small anhedral to subhedral albite. Accessory minerals include rare aegirine-augite and relict quartz grains (Viladkar, 1986). Sodic fenites are the rarest of the metasomatized rocks, occurring in only one outcrop in the northwestern section of the complex (Viladkar, 1986). The rock is made up of over 50% albite intergrown with pale green aegirine-augite and small proportions of relict quartz grains (Viladkar, 1986).

References

- Bose, P.K. and Das, N.G., 1986, A transgressive storm- and fair-weather wave dominated shelf sequence: Cretaceous Nimar Formation, Chakrud, Madhya, Pradesh, India: *Sedimentary Geology*, V. 46, p. 147-167.
- Chiplonkar, G.W., Ghare, M.A. and Badve, R.M., 1977, Bagh Beds - their fauna, age and affinities: A retrospect and prospect: *Biovigyanam*, v. 3, p. 33-60.
- Chatterjee, S.C., 1964, An alkaline-olivine basalt sub-province in the Deccan Traps: In: *Proceedings of the 22nd International Geological Congress*, New Delhi, Pt. 7, p. 35-41.
- Courtillot, V.F., Maluski, H., Vandamme, D., Moreau, M.G. and Besse, J., 1988, Deccan flood basalts and the Cretaceous-Tertiary boundary: *Nature*, v. 333, p. 843-846.
- Deans, T., and Powell, J.L., 1968, Trace elements and strontium isotopes in carbonatites, fluorites and limestones from India and Pakistan: *Nature*, v. 218, p. 750-752.
- Deans, T., Sukheswala, R.N., Sethna, S.F. and Viladkar, S.G., 1972, Metasomatic feldspar rocks (potash fenites) associated with the fluorite deposits and carbonatites of Amba Dongar, Gujarat, India: *Trans. Inst. Min. Metall. (sect. B: earth sci.)*, v. 81, p. B1-B9.
- Dietz, R.S. and Holden, J.C., 1970, Reconstruction of Pangaea: breakup and dispersion of continents, Permian to Present: *J. Geophys. Res.*, v. 75 (26), p. 4939-4956.
- Gupta, M.L. and Gaur, V.K., 1984, Surface heat flow and probable evolution of Deccan volcanism: *Tectonophysics*, v. 105, p. 309-318.
- Gwalani, M.L., 1981, *Petrology of Deccan Traps and Bagh beds of Dugdha-Naswadi, Gujarat*: Somaiya Publications, Bombay, 107p..
- Gwalani, L.G., Rock, N.M.S., Chang, W.J., and Fernandez, S., 1993, Alkaline rocks and carbonatites of Amba Dongar and adjacent areas, Deccan Igneous Province, Gujarat, India: 1. *Geology, Petrography and Petrochemistry: Mineralogy and Petrology*, v. 47, p. 219-253.
- Karkare, S.G. and Srivistava, R.K., 1990, Regional dyke swarms related to the Deccan Trap Alkaline province, India: in A.J. Parker, P.C. Rickwood and D.H. Tucker (eds.), *Mafic Dykes and Emplacement Mechanisms, Proceedings of the Second International Dyke Conference, Adelaide, South Australia, September, 1990*, p. 335-347.
- Krishnan, M.S., 1982, *Geology of India and Burma*: CBS Publishers and Distributors, 536p.

- Roelofsen, J.N., 1997, The primary and secondary mafic silicates of two alkaline anorogenic complexes: Strange Lake (Quebec-Labrador) and Amba Dongar (Gujarat, India): Unpublished Ph.D. thesis, McGill University, Montreal, 489p..
- Srivastava, R.K., 1989, Evolution of alkaline carbonatitic complex of Ambadungar, District Baroda, Gujarat:: Indian Journal of Geochemistry, v. 4, (1), p. 1-38.
- Srivastava, R.K., and Karkare, S.G., 1991, Economic potential of the alkaline carbonatitic complex of Ambadungar, District Baroda, Gujarat:: The Mining, Geological and Metallurgical Institute of India, v. 88, (2), p. 94-112.
- Sukheswala, R.N., Sirivastava, A.N., Mahambre, S.J. and Gwalani, L.G., 1976, Geology of Bakhatgarh-Phulmahal and Dugdha-Naswadi sectors in the Malwa region of the lower Narmada valley: In: Report on the geology of the Deccan Trap in southern part of Malwa Region, University Grants Commission, India, 19p..
- Viladkar, S.G., 1981, The carbonatites of Amba Dongar, Gujarat, India: Bulletin of the Geological Society of Finland, v. 53, p. 17-28.
- Viladkar, S.G., 1984, Alkaline rocks associated with the carbonatites of Amba Dongar, Chhota Udaipur, Gujarat, India: The Indian Mineralogist, p. 130-135.
- Viladkar, S.G., 1986, Fenitization at the Amba Dongar Carbonatite alkalic complex, India: in M. Gabriel (ed), Symposium New Mineral Raw Materials: Proceedings, p. 170-189.
- Viladkar, S.G. and Wimmenauer, W., 1992, Geochemical and Petrological Studies on the Amba Dongar Carbonatites (Gujarat, India): Chem Erde, v. 52, p. 277-291.
- Wellman, P. and McElhinny, M.W., 1970, K-Ar age of the Deccan Trap, India: Nature, v. 227, p. 595-596.

Chapter 3: Geology of The Phalaborwa Complex

Location

The Phalaborwa complex is located in the Eastern Transvaal region of South Africa, approximately 50 km west of the Moçambique border (Fig 3-1). The complex covers an area of approximately 16 sq. km and originally lay at an elevation of around 400m above sea level. The current production level is at approximately 100m below sea level.

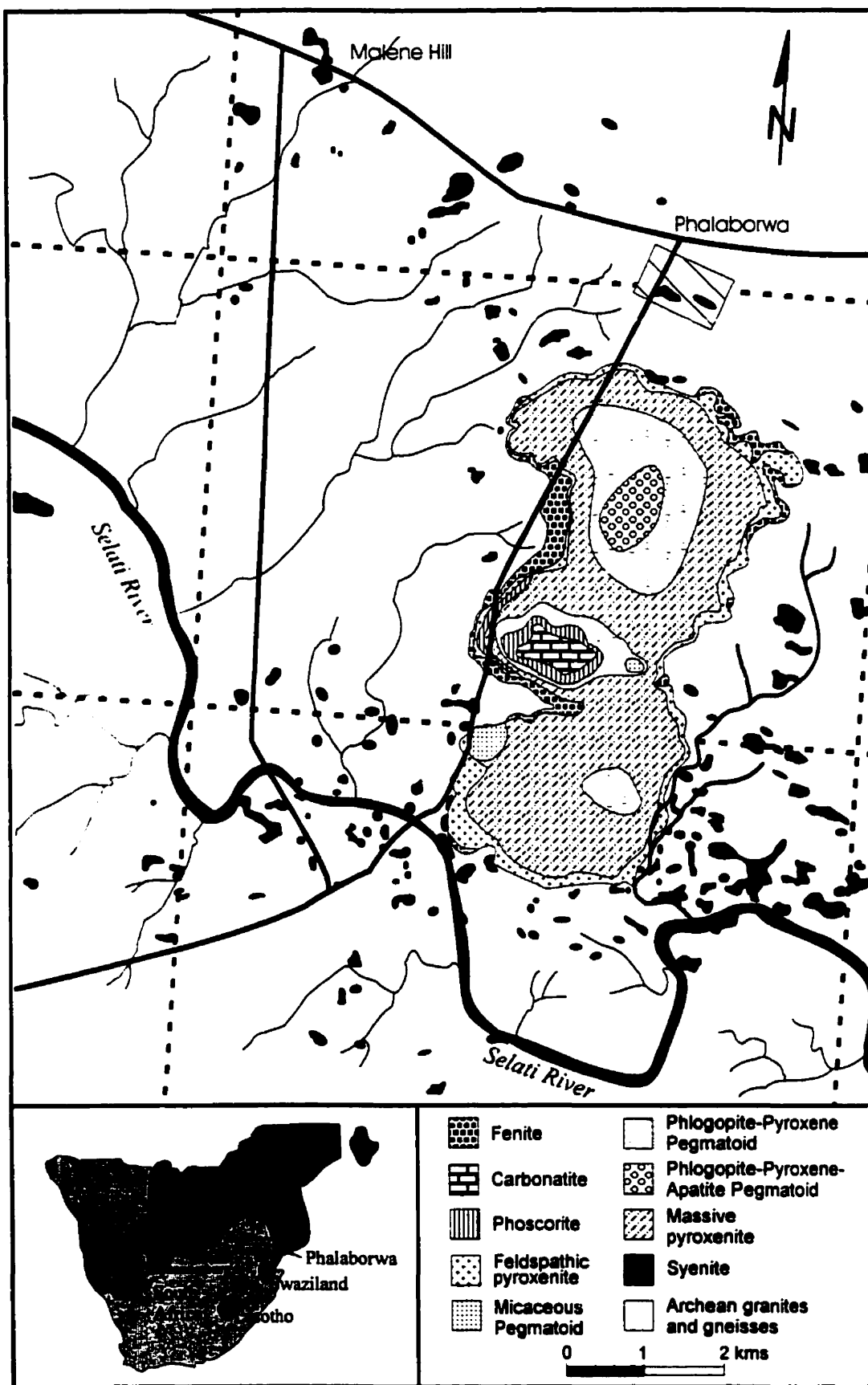
History of Mining

The first exploitation of mineral resources at Phalaborwa occurred during the eight century A.D. when iron and copper were extracted by smelting chalcopyrite and bornite collected from outcrop as evidenced by charcoal fragments and primitive furnaces uncovered in the area. Major exploitation of these metals, however, only began in the mid-sixteenth century with the Bantu people, and continued until the arrival of the Portugese in the mid-nineteenth century. Apatite was the first commodity exploited by modern mining methods, first briefly in 1934 by South African Phosphates Ltd., and then on a permanent basis by Foskor in 1955. Production of vermiculite began in 1946. During 1955 and 1956 Newmont Mining Corporation and Rio Tinto Zinc explored the possibility of developing the copper occurrences into an economic deposit. Following identification of at least 400 Mt of carbonatite-hosted ore, grading an average of 0.69% Cu, production began at Phalaborwa during 1965 using open cast mining techniques. After approximately 30 years of open pit mining it was decided that continued production of the Phalaborwa ore body would take place through underground mining methods (Palabora Mining Company, pers. comm.).

Regional Geology

The host rocks of the Phalaborwa complex consist of an Archean complex of granites and granitic gneisses which cover a wide area of the north and northeastern

Figure 3-1 The geology of the Phalaborwa complex, South Africa (Modified from Hanekom *et al.*, 1965; Frick, 1975).



Transvaal and a large portion of Swaziland (Hanekom *et al.*, 1965). In the vicinity of Phalaborwa, the Archean complex consists of two dominant lithologies. Surrounding the southern half of Phalaborwa is a white, medium- to coarse-grained, granitic gneiss, composed of feldspar, quartz and biotite (Hanekom *et al.*, 1965; Eriksson, 1982). In the northern area of Phalaborwa the country rock consists of a pink, equigranular granite which is intrusive into earlier gneiss (Hanekom *et al.*, 1965). The granite contains no micas, and in some areas is pegmatitic in texture (Hanekom *et al.*, 1965). Younger granitic veins and dykes, in turn, cut both granites and granitic gneisses (Hanekom *et al.*, 1965). The Archean complex also includes serpentine-talc and amphibole schists, but there is no report of these units in the vicinity of the Phalaborwa complex. Foliation in the granitic gneiss trends predominantly east-west and dips steeply to the south, or vertically (Hanekom *et al.*, 1965).

Geology of the Complex

The Phalaborwa complex belongs to a group of intrusions which contain both silicate and carbonate rocks. This early Proterozoic complex was intruded into granites and granitic gneisses of the Archean complex (Hanekom *et al.*, 1965) and consists of a large body of pyroxenite which is cored by later intrusions of phoscorite and carbonatite (Fig.3-1). Surrounding the pyroxenite are a number of smaller syenite and feldspathic pyroxenite bodies which were intruded during and after emplacement of the main complex (Hanekom *et al.*, 1965; Eriksson, 1982).

Based on several U/Pb age determinations, the carbonatites are interpreted to have been emplaced between 2047 and 2060 Ma. Holmes and Cahen (1956) obtained an age of 2060 Ma from thorianite, while an age of 2047 ± 19 Ma was obtained by Eriksson (1982) from uranthorianite and badellyite. More recent U/Pb analyses of phoscorite by Reischmann (1995) yielded a precise age of 2060 ± 0.5 Ma. These ages are similar to those of the layered rocks of the Bushveld complex, 2061 ± 27 Ma for mafic rocks (Walraven *et al.*, 1990), 120 km to the west, and the Schiel complex, $2059 +36/-35$ Ma (Walraven *et al.*, 1992), which is petrologically similar to Phalaborwa (Reischmann, 1995; Walraven *et al.*, 1990). Little work has been done on dating of the silicate rocks.

Rb-Sr analyses of phlogopite from clinopyroxenites yield an isochron of 2012 ± 19 Ma, while one U-Pb analysis of zircon in glimmerite yielded an age of 2050 Ma (Eriksson, 1989). Paleomagnetic analyses of satellites surrounding the main complex indicate that syenite magmatism may have spanned a 200 Ma period with initial intrusion coinciding with emplacement of the main clinopyroxenites (Morgan and Briden, 1984)

The most striking feature of the Phalaborwa igneous complex is the variety of mineralization types. The pyroxenite is host to economic deposits of vermiculite, thought to have been formed as a result of fluid infiltration of massive phlogopite pods found within pyroxenite (Eriksson, 1982) and phosphate. Surrounding the carbonatite is a rim of phoscorite containing economic concentrations of phosphorous, as apatite, while the carbonatites host a 400 Mt deposit of Cu with an average grade of 0.69% Cu. A satellite body of feldspathic pyroxenite hosts a much smaller copper deposit which was only briefly mined (Aldous, 1986). By-products from copper and phosphate mining include Au and Pt and Zr, respectively (Palabora Mining Company (PMC), 1976; Aldous, 1980).

Pyroxenite

The first phase of formation of the Phalaborwa complex was intrusion of a large, kidney shaped lobe of pyroxenite into the Archean Complex. Pyroxenite, which makes up approximately 70% of the complex (Eriksson, 1989), can be broadly subdivided into four dominant lithologies: a massive textured, diopside pyroxenite; a phlogopite-bearing pyroxenite, which can grade into phlogopite-rich glimmerite; pegmatitic varieties of pyroxenite; and feldspathic pyroxenite (Hanekom *et al.*; 1965; Eriksson, 1982). Massive and micaceous varieties predominate, and are roughly equal in proportion (Hanekom *et al.*, 1965).

Massive and micaceous pyroxenite

Massive pyroxenites are found throughout the complex and show sharp contacts with country rocks and other varieties of pyroxenite. Mineralogically they are homogeneous, invariably consisting of prismatic crystals of diopside with minor

concentrations of interstitial apatite and phlogopite (Hanekom *et al.*, 1965). Apatite crystals commonly exhibit a sub-parallel orientation with respect to diopside, indicative of flow texturing (Eriksson, 1982). Phlogopite also shows a preferred orientation, with bands developing an almost schistose texture, parallel to pyroxenite contacts (Hanekom *et al.*, 1965). Micaceous pyroxenite differs from massive varieties only in phlogopite content and represents a continuum between phlogopite-bearing massive pyroxenite and phlogopite-rich glimmerite.

Studies of the pyroxenites by Eriksson (1982) and Eriksson *et al.* (1985) concluded that phlogopite formed as a result of metasomatic alteration of diopside. Evidence of recrystallization was observed in areas of concentrated phlogopite (Eriksson, 1982). Eriksson (1989) and Eriksson *et al.* (1985) considered massive and micaceous pyroxenites to be crystal cumulates, with phlogopite concentration resulting from flow differentiation. Diopside, phlogopite and apatite all show evidence of having crystallized directly from the primary magma (Eriksson, 1989).

On the western edge of the complex, Foskor mining operations have uncovered a centimeter-scaled, monotonously and concentrically banded phlogopite-diopside rock. Moore (1984) ascribed this "orbicular layering" to episodic precipitation of the two minerals due to different growth rates caused by contrasting diffusion rates of mineral constituents

Feldspathic pyroxenite

Feldspathic pyroxenite is typically restricted to the margins of the pyroxenite body and is commonly associated with syenite intrusions (Hanekom *et al.*, 1965). Contact relationships between massive and feldspathic pyroxenite vary from graded to sharp, with sharp contacts suggesting intrusion of massive pyroxenite into the feldspathic variety (Eriksson, 1982).

Mineralogically, feldspathic pyroxenite is composed of microcline and diopside with accessory apatite and rare phlogopite (Eriksson, 1982). Microcline is generally anhedral and can be on the order of centimetres in diameter. Pyroxene can either be poikilitically enclosed within microcline, where the feldspar content of the rock is high,

or occur as massive clusters in less feldspathic material (Hanekom *et al.*, 1965; Eriksson, 1982). Apatite, which occurs in trace to major proportions, forms small crystals which can be found within and interstitial to microcline and pyroxene (Eriksson, 1982).

Ideas on the origins of feldspathic pyroxene have ranged from fractionation (Hall, 1912) to contamination of the pyroxenite magma, by granite or syenite (Hanekom *et al.*, 1965). Based on Sr isotopic data, Eriksson (1982) concluded that feldspathic pyroxenites are cumulate in origin and could not have resulted from crustal contamination.

Pegmatitic pyroxenite

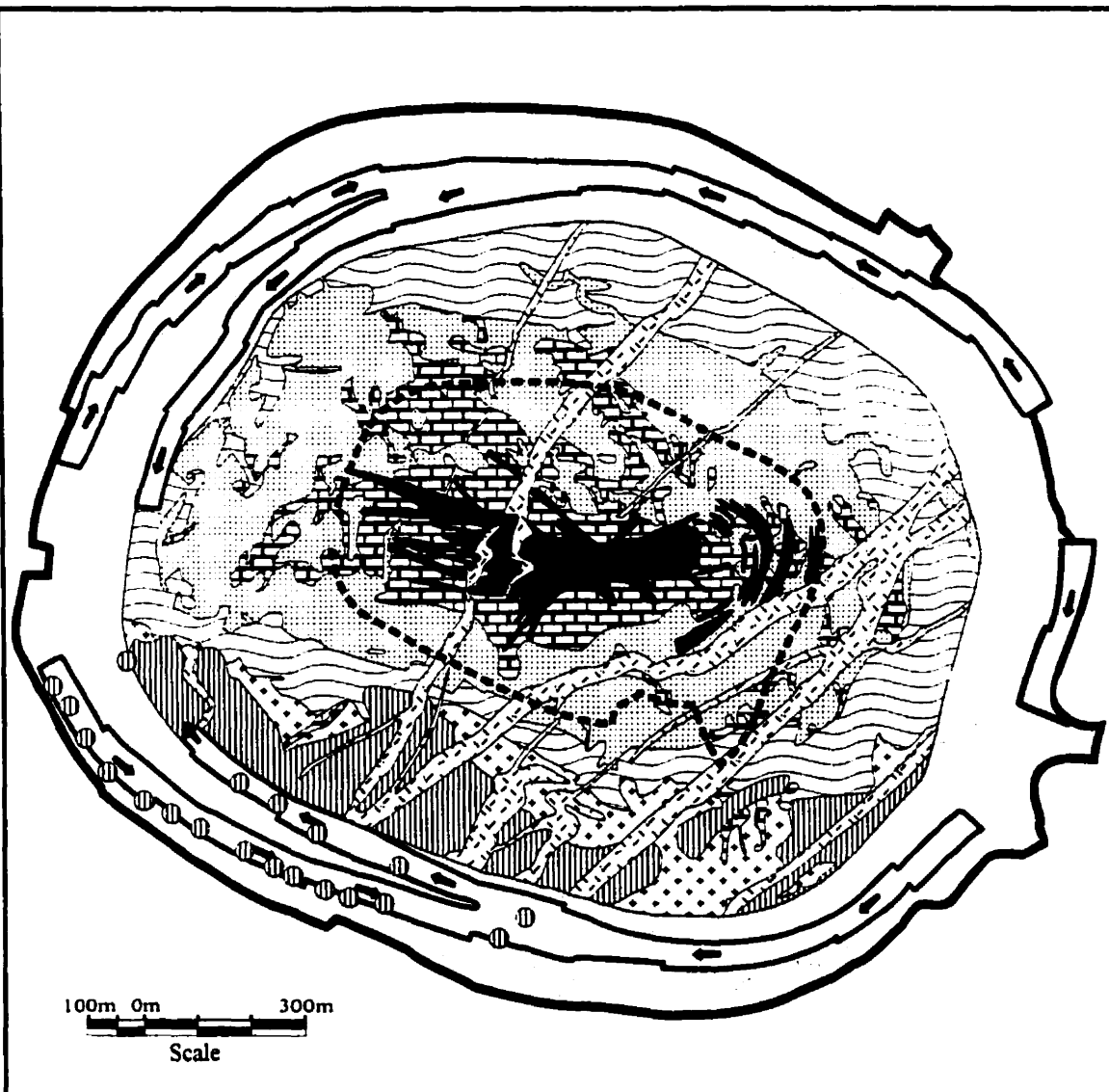
Large bodies of pegmatitic pyroxenite occur in both the northern and southern halves of the massive pyroxenite and are host to vermiculite mineralization (Hanekom *et al.*, 1965). The northern pegmatoid shows a zonation from core to rim of serpentine-phlogopite \pm apatite to phlogopite-clinopyroxene \pm apatite rocks, while southern pegmatoids are generally unzoned, consisting only of phlogopite-clinopyroxene \pm apatite. The pyroxenes are diopsidic and commonly attain lengths of 20cm.




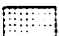
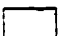






Phoscorite

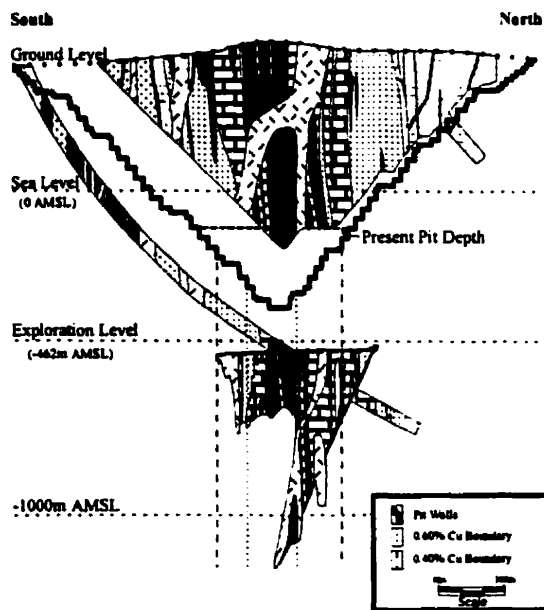
In the center of the pyroxenite is an oblong shaped core of phoscorite and carbonatite (Fig 3-2). Phoscorite forms a thick, up to 400m wide, rim which completely envelopes carbonatite, separating it from adjacent pyroxenite. Contact relationships were originally considered to be gradational between phoscorite and both carbonatite and pyroxenite (Lombaard *et al.*, 1964), however, exposures in the Phalaborwa pit suggest the outer contact with pyroxenite is abrupt (Eriksson, 1989). Lenses of carbonatite occur throughout the phoscorite and increase in frequency towards the inner contact with the carbonatite.


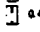

Phoscorite has an average modal composition of 35% magnetite, 25% apatite, 22% carbonate and 18% serpentine, olivine and phlogopite (Hanekom *et al.*, 1965), although bands of monomineralic magnetite or olivine are common (Lombaard *et al.*, 1964; Eriksson, 1982). Banding is roughly concentric to the shape of the phoscorite rim

Figure 3-2 Geology of the Palabora Mining Company's open pit.



-  Diabase
-  Transgressive Carbonatite
-  Banded Carbonatite
-  Phoscorite
-  Micaceous Pyroxenite
-  Feldspathic Pyroxenite
-  Fenite
-  Fenite Samples
-  Pit Area
-  Present Mining Level
-  Ramp



-  Pit Walls
-  0.60% Cu Boundary
-  0.40% Cu Boundary

(Eriksson, 1982). Magnetite is present either as early, euhedral grains or as secondary replacements of baddelyite (Van Rensburg, 1965; Aldous, 1980), while olivine occurs as either fresh or altered (serpentinized) crystals with no apparent segregation between the two (Eriksson, 1982). Olivine can contain inclusions of copper sulphides (bornite, chalcopyrite) or be included within larger sulphide grains (Aldous, 1980). Prismatic crystals and anhedral masses of apatite are both common, and calcite occurs either as disseminated grains or in veins (Eriksson, 1982). Copper sulphides comprise either early chalcopyrite, associated with olivine, or late bornite and chalcocite (Van Rensburg, 1965). Phlogopite, in the phoscorite, is found associated with olivine or as discrete crystals and shows reverse pleochroism (Eriksson, 1982).

Initially, the phoscorite was interpreted to have formed as a result of metasomatic alteration of a dunitic body, which may have been intruded prior to pyroxenite emplacement (Lombaard *et al.*, 1964). However, Eriksson (1982) considers the phoscorite to be cogenetic with the carbonatite.

Carbonatite

The central portion of the core of the complex is composed of a roughly ovoid body of carbonatite covering an area of approximately 0.4 km² (Fig. 3-2). Carbonatite magmatism occurred in two phases (Hanekom *et al.*, 1965; PMC, 1976). Intrusion of banded carbonatite, named for its concentrically zoned layers of magnetite, occurred first, followed by emplacement of transgressive carbonatite. Intrusive relationships of the two carbonatites are clear. The banded carbonatite was emplaced in the concentric pattern of the phoscorite while later transgressive carbonatite intrusion took advantage of fractures trending WNW-ESE and ENE-WSW. Dykes of transgressive carbonatite have been observed in all other members of the Phalaborwa complex (Eriksson, 1989) as well as in the host Archean complex (this study).

A number of characteristics can be used to distinguish the two carbonatite members. Perhaps the most obvious mineralogical difference between the two carbonatites is in their sulphide mineralogy (Van Rensburg, 1965; Hanekom *et al.*, 1965). The predominant sulphide of banded carbonatite is bornite while in the later carbonatite

chalcopyrite is dominant and sulphides become much more abundant. Calcite compositions also differ. Calcite in banded carbonatite is much less magnesian than that of the transgressive carbonatite, with a composition of 7.5% MgCO_3 versus 14% MgCO_3 (Lombaard *et al.*, 1964). In banded carbonatite, calcite contains exsolution lamellae of dolomite while dolomite in the transgressive carbonatite occurs as discrete grains (Van Rensburg, 1965; Eriksson, 1982). The apatite content is typically higher in transgressive carbonatite than in the banded variety and the olivine content, although low in both types, appears to be lower in the transgressive carbonatite. In banded carbonatite, olivine is rarely altered to serpentine but can be partially replaced by phlogopite, monazite or clinohumite (Eriksson, 1982). Transgressive carbonatite, although having a lower olivine content than banded carbonatite, does contain large masses of clinohumite and chondrodite crystals.

Magnetite is volumetrically and compositionally similar in banded and transgressive carbonatites but its textures differ. In banded carbonatite, magnetite occurs as discrete crystals ranging from millimetres to centimetres in diameter and shows a preferential alignment parallel to the margins of the body. Layers of magnetite, which can range from millimetres to metres in thickness, occur as discontinuous lenses ranging up to metres in length. Transgressive carbonatite contains magnetite as isolated crystals or masses, ranging in diameter from millimetres to tens of centimetres (Eriksson, 1982) which do not show a preferential alignment.

Satellite Bodies

Surrounding the main complex are numerous satellite bodies of syenite, pyroxenite and granite (Hanekom *et al.*, 1965; Eriksson, 1989). They tend to form topographic highs, but also occur as low rocky outcrops (Hanekom *et al.*, 1965), and vary from 10's of metres to 100's of metres in diameter.

Syenite is by far the most common lithology, making up the vast majority of intrusions near the periphery of the complex, and is concentrated in the southern and northern sectors. Microcline, and lesser proportions of orthoclase, are the dominant

phases in syenite and show parallel alignment. Mafic minerals comprise sodic amphiboles and pyroxenes of the arfvedsonite and aegerine-augite varieties, respectively.

Pyroxenite intrusions outside of the main complex are found in only a few localities and consist of feldspathic and massive varieties (Hanekom *et al.*, 1965). The most interesting, from an economic perspective, is the feldspathic Guide pyroxenite which is also mineralized in copper. The Guide pyroxenite is composed of pyroxene and feldspar, with the former mineral occurring either as individual crystals or poikilitically enclosed in laths of feldspar (Hanekom *et al.*, 1965). Accessory minerals include biotite, titanite and apatite, which can occur alone or as inclusions in pyroxene (Hanekom *et al.*, 1965). Sulphides consist predominantly of bornite with subordinate chalcopyrite and occur as interstitial, possibly intercumulate, crystals to pyroxene (Hanekom *et al.*, 1965). Aldous (1980) reported textural evidence of sulphides having replaced feldspar, which makes their intercumulus origin uncertain.

A granite intrusion is represented by the Kgopoeloe pipe, to the north of the complex, and consists of pink granite and granitic breccia associated with quartz syenite (Eriksson, 1989).

Carbonatite-hosted Copper Mineralization

Although copper sulphides are commonly present in carbonatite rocks (Aldous, 1980), only the Phalaborwa carbonatites host economic concentrations of copper. Copper mineralization occurs in both banded and transgressive carbonatites of the Phalaborwa complex, although it is much more abundant in the latter. Ore minerals consist predominantly of chalcopyrite and bornite, with much smaller concentrations of pyrrhotite, pentlandite, tetrahedrite, sphalerite, galena and pyrite. Owing to its economic significance, the deposit has received attention from numerous researchers (Lombaard *et al.*, 1964; PMC, 1976; Aldous, 1980), although there is no clear consensus on the processes of ore formation.

Mineralization at Phalaborwa is present as two types. Earlier banded carbonatites contain bornite as their dominant ore mineral, while transgressive carbonatites host predominantly chalcopyrite mineralization. Valleriite ($3(\text{Mg,Al})(\text{OH}_2) \bullet 2\text{FeCuS}_2$) is

present in both ore types as a late stage alteration product of the primary sulphides (PMC, 1976)

Petrographically, bornite in banded carbonatite usually occurs as small, disseminated blebs (Fig 3-3a) or, less commonly, as blebs aligned with magnetite, apatite and olivine. Banding of sulphides appears to be spatially unrelated to later fracturing events, and is considered to be of primary origin (PMC, 1976).

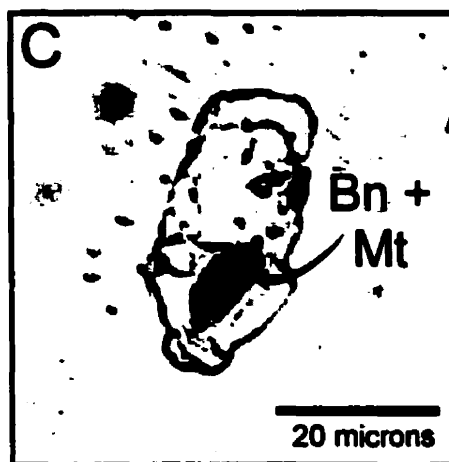
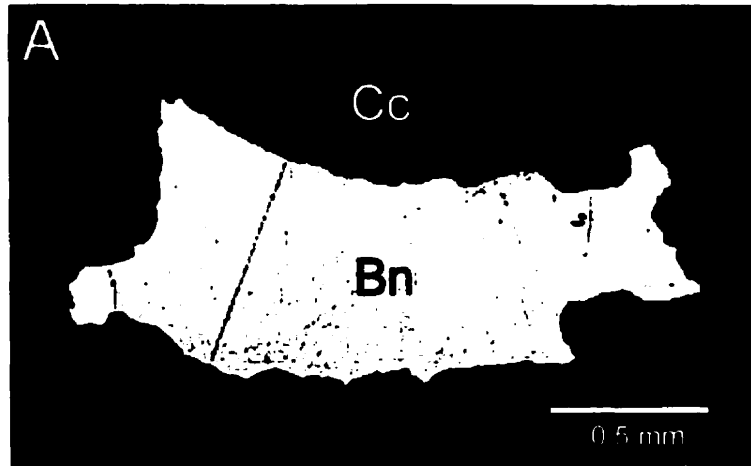
Chalcopyrite mineralization in the central transgressive carbonatite occurs most typically as thin discontinuous veinlets, either alone or in parallel sets up to 10m wide, with individual veinlets rarely exceeding 1cm (Fig 3-3b). Sulphide grains show no obvious orientation, but are usually associated with fine fractures. Dolomitization of calcite surrounding sulphide veinlets is common and forms noticeable dark grey alteration haloes. Veins and veinlets of transgressive carbonatite which invade banded carbonatite are also similarly mineralized.

A hydrothermal origin for much of the copper mineralization is generally accepted by most authors (Lombaard et al, 1964; Hanekom *et al.*, 1965; Heinrich and Moore, 1970; PMC, 1976) with fracturing of carbonatite opening pathways for mineralizing fluids which precipitated copper sulphides. Aldous (1980), however, concluded from his detailed studies of the deposit that copper mineralization in both carbonatite members was a result of primary precipitation from the carbonatite melts and deposition from circulating orthomagmatic fluids during carbonatite crystallization.

Petrographic evidence of sulphide minerals and textures supports a primary origin for copper mineralization in the guide pyroxenite, phoscorite and banded carbonatite. In each, bornite occurs as isolated blebs which are randomly distributed in the host, show no association with fracturing and contain no evidence of hydrothermal alteration. In cases where early copper mineralization does show preferred orientation, it is interpreted to be part of a magmatic layer, e.g., in magnetite layers of banded carbonatite.

Evidence of early primary magmatic mineralization has also been found in melt inclusions from pyroxenite and phoscorite (Aldous, 1980, 1986). The occurrence of copper-bearing sulphides in melt inclusions indicates that they must have been present in the melt during its emplacement (Fig. 3-3c).

Figure 3-3 Photomicrographs showing a) early bornite mineralization in banded carbonatite; b) Late chalcopyrite veinlet with associated dolomite alteration (grey) in transgressive carbonatite; and c) copper sulphide in melt inclusions from phoscorite



In contrast to bornite mineralization in banded carbonatite, late chalcopyrite ore hosted by transgressive carbonatite provides evidence of a hydrothermal origin. The occurrence of veinlets associated with fracturing and the presence of alteration haloes in the wall rock suggest that fluids took part in the transport and deposition of chalcopyrite mineralization.

Fenitization

A weak zone of fenitization, which is best developed along the western periphery of the Phalaborwa complex, occurs in both granite and granitic gneiss of the Archean complex. Little work has been done on fenitization at Phalaborwa, although Frick (1975) studied the fenites in order to rule out this process in the formation of syenites.

Three stages of fenitization were recognized in the granitic rocks and were referred to as slightly fenitized and partially fenitized granite, and fenite (Frick, 1975). The precursor was interpreted as granitic migmatite containing anhedral orthoclase and plagioclase separated by quartz, with accessory proportions of biotite and chlorite.

Slightly fenitized granite can be recognized by the growth of orthoclase along orthoclase-quartz and plagioclase-quartz boundaries (Frick, 1975). With increasing fenitization, quartz becomes less abundant and orthoclase content increases. Orthoclase crystals are anhedral and commonly separated by relict quartz. Small crystals of alkali amphibole also begin to appear at this stage at the expense of biotite and chlorite, and are commonly associated with calcite, which replaced quartz (Frick, 1975). In fenites which contain pyroxene, alkali amphibole commonly replaces this phase. With increasing intensity of alteration, the proportion of quartz decreases and the proportions of orthoclase and amphibole increase (Frick, 1975).

Dykes

The youngest intrusions in the Phalaborwa area are numerous NE – SW trending diabase dykes which cut across the complex. These dykes were originally thought by

Hanekom *et al.* (1965) to be Karoo dolerites (132 Ma), however, paleomagnetic data suggest they may be much older (1900 Ma) (Briden, 1976).

Diabase dykes range from centimetres to almost 50 metres in width and range in length from metres to just over 10 kilometres. The rocks are composed of labradoritic plagioclase and pyroxene of pigeonite composition and are typically fine-grained, although some porphyritic assemblages have been observed (Hanekom *et al.*, 1965).

References

- Aldous, R.T., 1980, Ore genesis in copper-bearing carbonatites; a geochemical, fluid inclusion and mineralogical study: Unpublished Ph.D. thesis, Imperial College, London, 365p..
- Aldous, R.T., 1986, Copper-rich fluid inclusions in pyroxenes from the Guide Copper Mine, a Satellite Intrusion of the Palabora Igneous Complex, South Africa: *Economic Geology*, v. 81, p. 143-155.
- Briden, J.C., 1976, Application of paleomagnetism to Proterozoic tectonics: *Philosoph. Trans. Royal Soc. Lond.*, v. 280, p.405-416.
- Eriksson, S.C., 1982, Aspects of the petrochemistry of the Phalaborwa Complex, northeastern Transvaal, South Africa: Unpublished Ph.D. thesis, University of the Witwatersrand, Johannesburg.
- Eriksson, S.C., 1989, Phalaborwa, a saga of magmatism, metasomatism and miscibility: in K. Bell (ed.), *Carbonatites: genesis and evolution*: London, Unwin Hyman, p. 221-254.
- Eriksson, S.C., Fourie, P.J., and De Jager, D.H., 1985, A cumulate origin for the minerals in clinopyroxenites of the Phalaborwa complex: *Transactions of the Geological Society of South Africa*, v. 88, p. 207-14.
- Frick, C., 1975, The Phalaborwa syenite intrusions: *Trans.Geol. Soc. S. Afr.*, v. 78, p. 201-213.
- Hall, A.L., 1912, The Palabora plutonic complex of the low country and its relationship to the pegmatites of the Leydsdorp mica-fields: *Transactions of the Geological Society of South Africa*, v. 15, p. 4-17.
- Hanekom, H.J., van Staden, C.M., Smit, P.J., and Pike, D.R., 1965, The geology of the Palabora Igneous Complex: *South Africa Geological Survey Handbook*, memoir 54.
- Heinrich, E.Wm., and Moore, D.G., 1970, Metasomatic potash feldspar rocks associated with igneous alkalic complexes: *Canadian Mineralogist*, v. 10, p. 571-584.
- Holmes, L.M., and Cahen, L., 1956, *Geochronologie Africaine*: Mem. Cl. Sci. Nat. Med, Acad. R. Sci. Colon. (Brussels), Fasc. 1, 169pp.
- Lombaard, A.F., Ward-Able, N.M., and Bruce, R.W., 1964, The exploration and main geological features of the copper deposit in carbonatite at Loolekop, Palabora Complex: In Haughton, S.H., ed., *The geology of some ore deposits in Southern Africa*, The geological society of South Africa, Johannesburg, p. 315-337.

- Moore, A.C., 1984, Orbicular rhythmic layering in the Palabora carbonatite, South Africa: *Geological Magazine*, v. 121, p. 53-60.
- Morgan, G.E., and Briden, J.C., 1984, Aspects of Precambrian paleomagnetism, with new data from the Limpopo mobile belt and Kaapvaal craton in southern Africa: *Physics of the Earth and Planetary Interiors*, v. 24, p. 1442-1468.
- Palabora Mining Company, 1976, The geology and the economic deposits of copper, iron and vermiculite in the Palabora Igneous Complex: a brief review: *Economic Geology*, v. 71, p. 177-192.
- Reischmann, T., 1995, Precise U/Pb age determination with baddeleyite (ZrO₂), a case study from the Phalaborwa Igneous Complex, South Africa: *S.Afr.J.Geol.*, v. 98, p. 1-4.
- Van Rensburg, W.C., 1965, Copper mineralization in the carbonate members and phoscorite, Phalaborwa, South Africa: Unpublished Ph.D. thesis, University of Wisconsin, Madison.
- Walraven, F., Armstrong, R.A., and Kruger, F.J., 1990, A chronostratigraphic framework for the north-central Kaapvaal craton, the Bushveld Complex and the Vredefort structure: *Tectonophysics*, v. 171, p. 23-48.
- Walraven, F., Frick, C.F., and Lubala, R.T., 1992, Pb-isotope geochronology of the Schiel complex, Northern Transvaal, South Africa: *South African Journal of Earth Sciences*, v. 15, p. 103-110.

**Chapter 4: Carbonate-Carbonate Liquid Immiscibility and the Formation of
Ferrocarbonatite: Evidence from Melt Inclusions in the
Amba Dongar Carbonatite Complex, India**

**David A. S. Palmer and A. E. Williams-Jones
Department of Earth and Planetary Sciences
McGill University**

Abstract

The Amba Dongar complex, India consists of a small ring structure composed of calciocarbonatite and ankerite-dominated ferrocarbonatite. Three types of solid inclusion were observed in apatite hosted by calciocarbonatite and consist of a ferroan dolomite variety (mottled inclusions), a calcite \pm barite \pm ferroan dolomite variety (multiphase inclusions) and monomineralic calcite inclusions. Petrographic evidence indicates that these inclusion types were trapped contemporaneously.

Mottled inclusions start melting at temperatures of 610°C and appear to be completely molten at temperatures >800°C. The onset of melting, of multiphase inclusions, is at slightly higher temperatures (680°C) and final melting occurs at temperatures above 1100°C. Monomineralic calcite inclusions displayed only partial melting (\approx 20%) at temperatures of 1200°C.

Consistent chemical compositions and the high temperature phase relationships, of mottled and multiphase inclusions indicates that they are trapped samples of early carbonatite melts. By contrast, the melting behaviour of monomineralic inclusions suggests that they were trapped calcite crystals. The coexistence of mottled (ferroan dolomite) and multiphase (calcitic) inclusions indicate that two chemically distinct carbonatitic liquids were present during the growth of apatite. A model involving separation of immiscible ankeritic and calcitic liquids from a parent carbonate melt is therefore proposed. It is thought that the presence of significant amounts of dissolved iron in the primary carbonate liquid affected melt structure to an extent sufficient to initiate the separation of an iron-rich liquid and a calcium-rich liquid from the parental carbonate melt. The lower density Ca-rich carbonate liquid ascended more rapidly than the conjugate iron-rich carbonate liquid, and resulted in the emplacement of early calciocarbonatite and later ferrocarbonatite at Amba Dongar.

Introduction

Field-based studies and experimental investigations of phase relationships have considerably advanced our understanding of the genesis of carbonatite magmas, even

though debate continues over whether they originate by direct melting of carbonated mantle or exsolution from a silicate magma (Le Bas, 1977; Wyllie, 1966; Gittins, 1989; Barker, 1989; Kjarsgaard and Hamilton, 1989; Lee and Wyllie, 1997, 1998). However, the subsequent evolution of these magmas has received far less attention, and consequently little is known of the processes which control this evolution. Field relationships of carbonatites indicate that carbonatitic liquids evolve in the sequence calciocarbonatite \rightarrow magnesiocarbonatite \rightarrow ferrocarbonatite, and this evolution is typically ascribed to fractionation of a carbonatite melt (Le Bas, 1989; Kjarsgaard and Hamilton, 1988; Gittins, 1989). However, although it has been shown experimentally that calciocarbonatite can be fractionated from magnesiocarbonatite (Harmer and Gittins, 1997), and that magnesiocarbonatite can be fractionated from calciocarbonatite (Lee and Wyllie, 1998), there are no data to support the notion that ferrocarbonatite can fractionate from earlier carbonatite magmas.

An alternative explanation for the existence of different carbonatite types is that they are related through liquid immiscibility. Although silicate-carbonate liquid immiscibility has been proposed to explain the formation of carbonatite magmas (Freestone and Hamilton, 1980; Kjarsgaard and Hamilton, 1989; Lee and Wyllie, 1997, 1998), carbonate-carbonate liquid immiscibility has only been considered for melts of natrocarbonatite affinity (Brooker and Hamilton, 1990; Mitchell, 1997; Nielsen *et al.*, 1997). However, it has long been accepted that liquid immiscibility occurs in iron-rich silicate systems, and results in the separation of silica-rich and iron-rich liquids (Philpotts, 1976; Roedder, 1979; Vicenzi *et al.*, 1995). Is it possible that high concentrations of iron have a similar effect on carbonatite magmas, i.e., that they cause the magma to separate into Fe-poor and Fe-rich calciocarbonatite and ferrocarbonatite magmas, respectively?

The presence of solid inclusions, which represent samples of trapped melt, potentially hold the key to understanding the evolution of carbonatite magmas. The apatite hosted by calciocarbonatite of the Amba Dongar complex, India, contains coexisting multiphase calcitic inclusions and ferroan dolomitic inclusions that we interpret to represent melt inclusions. In this paper, we characterize these solid inclusions, document their phase changes during heating and use these data to support a hypothesis

that ferrocarbonatite magmas originate by exsolving from iron-rich calciocarbonatite magmas.

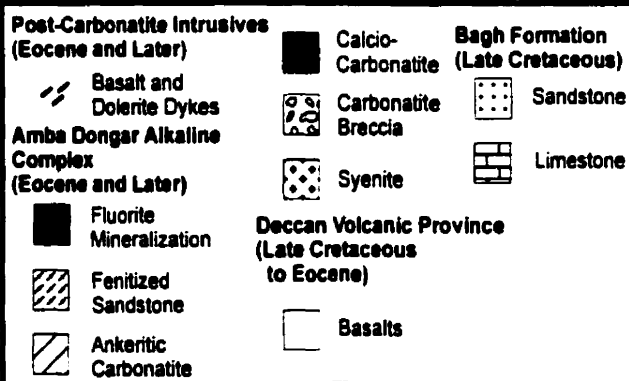
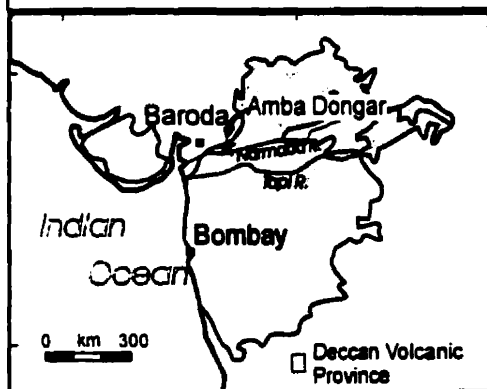
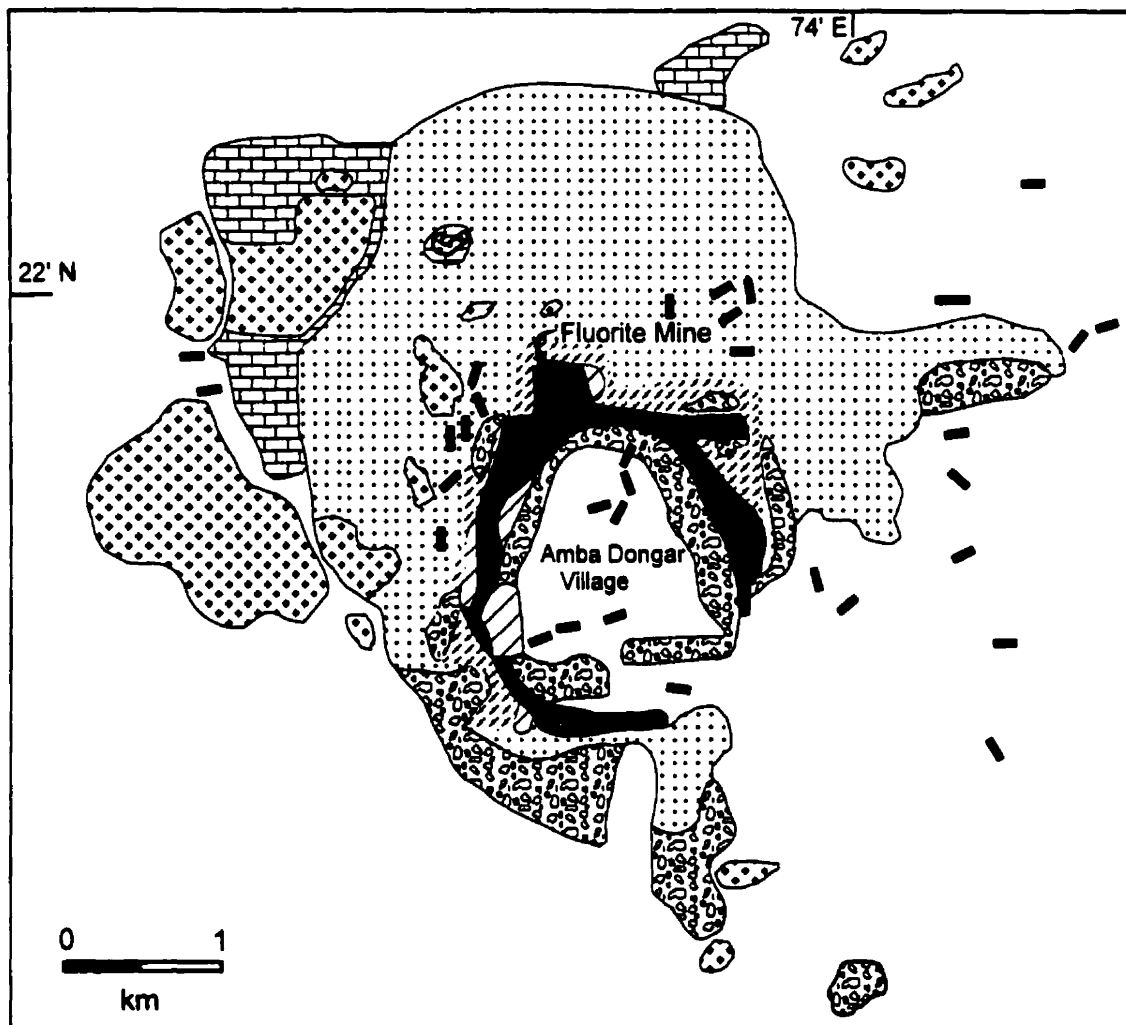
Geology of Amba Dongar

The Amba Dongar complex is located approximately 400km northeast of Bombay, India and is host to large quantities of fluorite (11.6 Mt of 30% CaF_2), that are currently being mined. It is also locally enriched in LREE (up to 10%) (S.G.Viladkar, pers. comm.). The complex is in the form of a ring and comprises carbonatite and silicate lithologies which were intruded into Deccan basalts and quartzitic sandstones of the Late Cretaceous Bagh formation (Fig.4-1). Intrusion of carbonatite and related silicate magmas occurred during the late Eocene and coincided with late stage Deccan volcanism, which is thought to have been related to a mantle plume (Simonetti *et al.*, 1995).

The first step in the emplacement of the complex was faulting activated by a highly fluidized liquid which formed a ring of carbonatite breccia. This initial faulting provided a pathway for the bulk of the magma which crystallized as an outer ring of calciocarbonatite, forming the bulk of the ring. Numerous plugs of later, fine-grained ferrocarbonatite are concentrated along the west and northwest edges of the ring structure. Bodies of syenite are randomly distributed in the surrounding country rocks. The complex is unusual in that it contains numerous small bodies of ankerite-rich ferrocarbonatite (Viladkar and Wimmenauer, 1992; Gittins and Harmer, 1997).

The calciocarbonatite at Amba Dongar shows a large variation in grain size, texture and color. Early calciocarbonatite tends to be coarser-grained, occurring as xenoliths in later, fine-grained calciocarbonatite. Both calciocarbonatite phases are generally equigranular and consist mainly of interlocking calcite crystals. A porphyritic texture is well developed, locally, with larger calcite phenocrysts set in a matrix of finer grained calcite. The proportions of other minerals in calciocarbonatite vary greatly, comprising from 1% to over 30% of the rock by volume and consist, in decreasing order of importance, of martite (hematite after magnetite), apatite, fluorite, barite, galena, pyrochlore, zircon, phlogopite and aegirine.

Figure 4-1 The geology of the Amba Dongar complex and surrounding area
(modified from Deans *et al.*, 1972).



Ferrocarbonatite is a dark red, highly oxidized, fine-grained rock dominated by ankerite and containing abundant accessory minerals in the form of hematite (after magnetite, in some cases over 50 vol. %), fluorite, barite, apatite, bastnaesite, pyrochlore, monazite, thorite, pyrite, galena and chalcopyrite (Viladkar and Wimmenauer, 1992). Two varieties of ferrocarbonatite are recognized on the basis of field relationships and accessory minerals (Viladkar and Wimmenauer, 1992). The first variety of ferrocarbonatite occurs as dykes and is characterized by a greater abundance of martite (hematite after magnetite) while the second forms small plutons and contains greater proportions of accessory fluorite, sulphates and REE minerals.

Methodology

In order to identify solids within inclusions, two preparation methods were used. The most successful involved polishing a number of apatite-bearing samples until solid inclusions intersected the surface. Two groups were prepared, one of previously homogenized and subsequently quenched inclusions and one unheated set. This enabled the characterization of bulk composition and the individual solids, respectively. The second method allowed for the analysis of opened melt inclusions on fracture surfaces prepared following the procedure of Metzger *et al.* (1977). Wave Length Dispersive Spectrometry (WDS) and Energy Dispersive Spectrometry (EDS) analyses were carried out using a JEOL 8900 superprobe equipped with a Tracor Northern energy dispersive system. WDS analyses were performed at 15 kV, with a beam diameter of 5 μ , to accommodate the small size of some inclusions, while beam rastering was employed for energy dispersive analyses, allowing rough surfaces and very small areas to be analysed.

Microthermometric experiments were conducted on solid inclusions using a Leica 1350 heating stage which is capable of attaining temperatures of approximately 1350°C. However, due to visibility problems at very high temperatures, most experiments were terminated at temperatures below 1250°C. The thermocouple was calibrated using the melting point temperatures of pure NaCl (800.4°C), NaSO₄ (884°C) and Au (1024°C) and the transition from α quartz to β quartz (573°C). The three

populations of solid inclusions, i.e, monomineralic, mottled and multiphase, discriminated on the basis of physical characteristics, were also discernable microthermometrically. Solid inclusions were considered to be homogenized when only liquid and vapour remained, as heating of inclusions to temperatures in excess of 1250°C had no effect on liquid-vapour ratios.

Solid Inclusions

Numerous solid inclusions are present in calciocarbonatite-hosted apatite and coexist with abundant fluid inclusions (Palmer and Williams-Jones, 1998, Chap. 5). Inclusion-bearing apatite comprises a single generation of primary magmatic crystals (Roelofsen, 1997). The crystals are small (<1mm long), euhedral, and occur either in isolation or in large clusters. They are randomly dispersed among the interlocking network of calcite crystals, except where concentrated locally in layers produced by flow. Although apatite crystals also occur in ferrocarbonatite, their inclusions were not of a sufficient size for study.

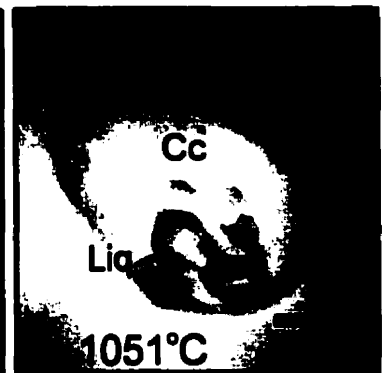
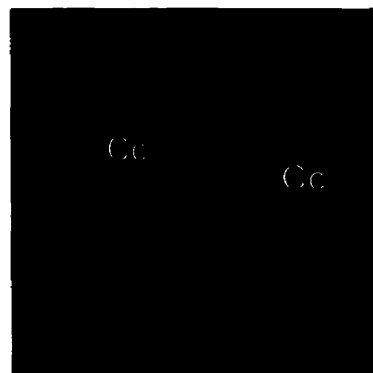
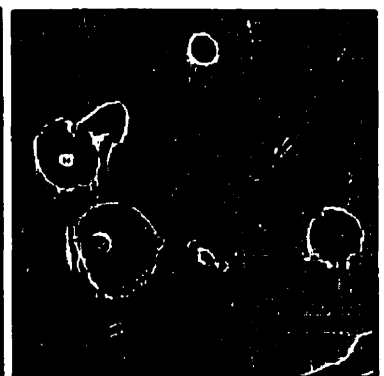
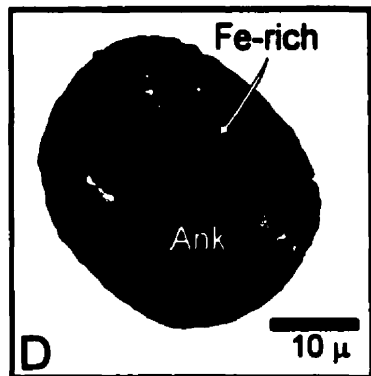
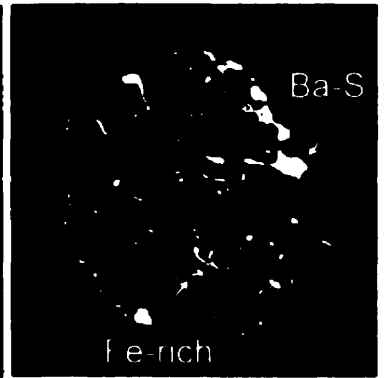
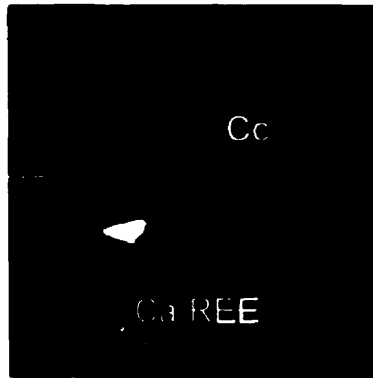
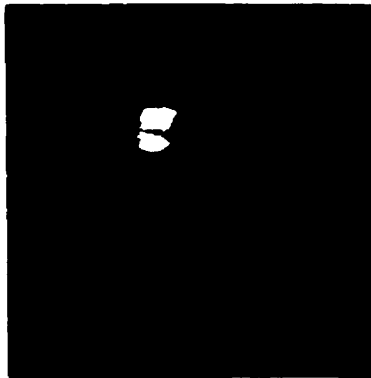
Three types of solid inclusion can be discerned, based on physical characteristics, namely mottled inclusions, containing one dominant phase, multi-phase inclusions, containing at least three separate solids, and monomineralic inclusions, composed of one, clear anisotropic phase (Fig. 4-2). The diameter of inclusions varies greatly for all types, ranging from 10 to 60 μ . The relative proportions of the three types is approximately 30%, 50% and 20%, respectively, for the mottled, multiphase and clear inclusions. Inclusions are randomly distributed in the apatite crystals and there is no evidence that they are spatially zoned in respect to type.

Mottled inclusions

Petrography

The mottled inclusions are typically round to ovoid in shape and are composed of a mottled, off-white, birefringent solid which contains small inclusions of dark material,

Figure 4-2 SEM photomicrographs of solid inclusions hosted by apatite in calciocarbonatite: A) A multiphase inclusion containing a large calcite crystal with smaller Si-, Zr-bearing and Ca²⁺-, REE-bearing phases (bright); B) An inclusion similar to A, although without the Si-Zr phase; C) A previously homogenised multiphase inclusion showing small areas of baritic and ferroan dolomitic material within a calcitic host; D) A mottled inclusion composed entirely of ferroan dolomite. Lighter areas are more iron-rich; E) A mottled inclusion composed entirely of ankerite; F) Previously homogenised solid inclusions intermediate between mottled and multiphase types. The mottled areas are ankeritic in composition, while the solid areas consist of calcite. Note the meniscus-like contact between the two phases; G) Enlargement of the inclusion from figure 4-2F; H) Two calcite inclusions; I) Plane light photomicrograph showing partial melting of a calcite crystal inclusion (1051°C).



that may represent opaque solids, and darker yellow domains which are of higher birefringence than the surrounding phase. In all mottled inclusions, the mottled phase is dominant (>75%).

Chemistry

Mottled inclusions are invariably dominated by a Fe-Mg-Ca phase which always produces low totals of between 50 and 60 wt.%, consistent with the phase being a carbonate mineral (Table 4-1). The high concentrations of Fe and Mg (up to 18.6 and 15.1%, respectively), and their inverse relationship, indicate a solid solution series between dolomite and ferroan dolomite, with a tendency towards ferroan dolomite (Fig 4-3). Some inclusions contain zones within the ferroan dolomite that were richer in Fe and these correspond to the yellow zones identified petrographically.

Multiphase Inclusions

Petrography

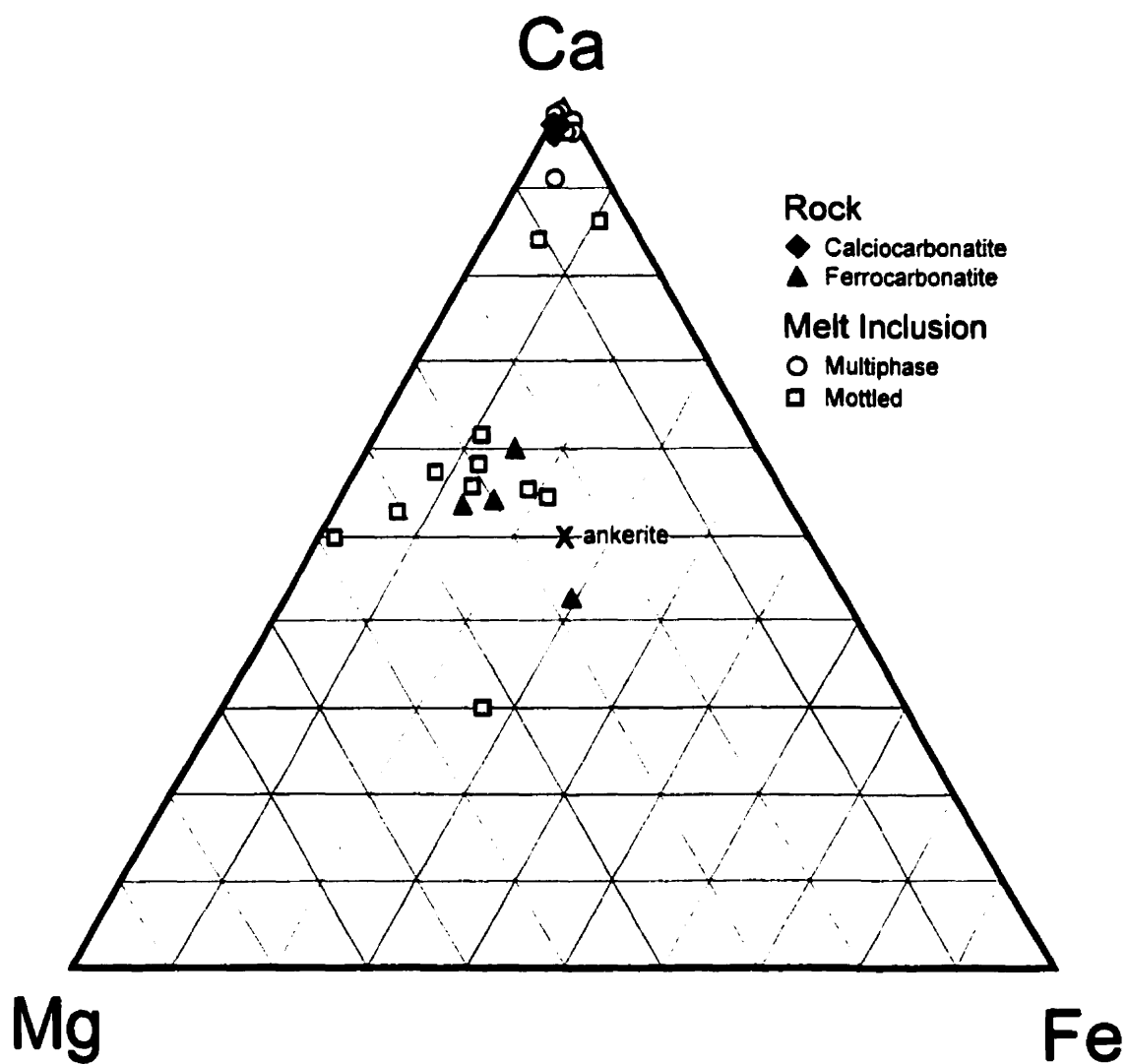
Multiphase inclusions are much clearer than the mottled inclusions, and typically are irregular to ovoid in shape with no one phase occupying more than 50% of the volume of the inclusion. Solid phases include: two off-white to colorless minerals, one strongly birefringent and the other of moderate birefringence; a light green, weakly birefringent solid; and an aggregate of orange and opaque crystals. In the majority of inclusions a vapour ± aqueous liquid phase is present, which is invariably deformed by the surrounding solids, and occupies up to 30% of the volume of an inclusion. Many multiphase inclusions commonly contain a large central crystal and two smaller crystals, of relative high density, which are commonly attached to the surface of the main solid.

Table 4-1 Compositions of mottled inclusions

	Ankeritic Inclusions										
	A-1	A-2	A-3	A-4	A-5	A-6	A-7	A-8	A-9	A-10	A-11
Wt. %											
CaO	31.48	33.06	17.41	37.20	33.33	32.53	33.04	31.18	30.06	49.76	48.44
MgO	18.63	15.48	15.38	12.79	12.23	11.80	10.64	10.44	9.76	4.40	1.29
FeO	1.61	6.06	21.77	12.08	6.88	8.87	7.68	13.57	15.12	4.20	7.56
MnO	0.29	0.53	1.53	0.81	2.24	0.61	4.03	0.69	0.63	0.21	0.16
BaO	0.02	0.07	0.01	0.28	0.00	0.05	0.01	0.05	0.00	0.09	0.02
SrO	0.79	0.98	0.38	0.55	0.84	0.54	0.61	0.24	0.12	0.57	0.00
Na ₂ O	0.04	0.10	0.08	0.14	0.08	0.13	0.07	0.02	0.07	0.08	0.00
K ₂ O	0.01	0.02	0.02	0.03	0.02	0.03	0.02	0.01	0.01	0.03	0.02
P ₂ O ₅	0.08	0.06	0.10	1.06	0.10	0.56	0.14	0.10	0.15	1.57	0.20
SiO ₂	0.13	0.13	0.02	0.04	0.14	0.02	0.08	0.00	0.03	0.04	0.49
*CO ₂	46.92	43.52	43.32	35.02	44.14	44.87	43.68	43.71	44.05	39.04	41.83
Cat. %											
Ca	14.25	15.78	8.51	19.95	16.01	28.40	29.15	27.64	26.73	44.88	43.96
Mg	13.91	12.19	12.40	11.31	9.69	14.33	13.07	12.88	12.09	5.53	1.63
Fe	0.52	2.08	7.64	4.65	2.37	6.04	5.29	9.39	10.50	2.95	5.35
Mn	0.10	0.18	0.55	0.32	0.78	0.42	2.81	0.48	0.44	0.15	0.11
Ba	0.00	0.01	0.00	0.04	0.00	0.01	0.00	0.01	0.00	0.02	0.01
Sr	0.16	0.21	0.09	0.13	0.18	0.26	0.29	0.12	0.06	0.28	0.00
Na	0.03	0.09	0.07	0.13	0.06	0.20	0.11	0.03	0.12	0.12	0.00
K	0.01	0.01	0.01	0.02	0.01	0.03	0.02	0.01	0.01	0.03	0.02
P	0.05	0.03	0.06	0.73	0.06	0.39	0.10	0.07	0.11	1.12	0.14
Si	0.09	0.09	0.01	0.03	0.10	0.02	0.06	0.00	0.02	0.04	0.41
C	70.89	69.33	70.67	62.67	70.73	49.91	49.10	49.37	49.93	44.87	48.37

* CO₂ by difference

Figure 4-3 Compositions of multiphase and mottled inclusions and calciocarbonatites and ferrocarbonatites in the ternary system Ca-Mg-Fe (cat.%). Multiphase inclusions are compositionally similar to calciocarbonatites and mottled inclusions to ferrocarbonatites. The two outlying mottled inclusions (anomalously high Ca) represent the segregated calcite-ferroan dolomite inclusions seen in Figure 4-2f and g. Note the inverse correlation between Fe and Mg for mottled inclusions indicating solid solution.



Chemistry

Analyses of unheated multiphase solid inclusions indicate the presence of a Ba-, S-bearing mineral, probably barite, which corresponds to the strongly birefringent phase, and a Ca-rich mineral, most likely calcite, which dominates the inclusion (Fig. 4-3). Bulk compositions of homogenised inclusions are similar, with between 48 and 53 wt.% CaO, 5-7 wt.% BaO and approximately 1.3 wt.% SrO (Table 4-2), however, small zones of Fe-, Mg-rich material are present, locally, and probably represent ferroan dolomite (Fig. 4-2x, Table 4-3). EDS analysis also indicates the presence of significant Sr, La and Ce. The two small attached crystals mentioned above are composed of Zr (with detectable amounts of Si) and LREE, and may be zircon and a REE carbonate, such as bastnaesite, respectively (Table 4-4). The density differences seen in secondary electron images (SEI) between the calcite and these phases also supports their being bastnaesite and zircon (Fig. 4-2a,b).

Mixed Inclusions

A group of inclusions, containing both ferroan dolomite and calcite, was identified through backscattered electron imaging (Fig. 4-2f,g). This type, which was observed only in preheated samples, showed a strong segregation of the two phases with material of ferroan dolomitic composition forming a meniscus-shaped contact with the calcite. Unfortunately, inclusions containing a large percentage of ferroan dolomite, darken upon heating and phase transitions at temperatures above $\approx 800^{\circ}\text{C}$ could not be determined.

Table 4-2 Compositions of homogenised multiphase inclusions

	Multiphase Inclusions				
	MP-1	MP-2	MP-3	MP-4	MP-5
Wt.%					
CaO	53.07	48.25	52.69	52.98	48.96
MgO	0.52	0.39	0.44	0.28	0.21
FeO	0.09	0.24	0.16	0.39	0.48
MnO	0.06	0.02	0.11	0.03	0.16
BaO	7.21	5.65	3.23	2.71	3.88
SrO	1.32	1.37	1.21	1.46	0.89
Na ₂ O	0.09	0.11	0.08	0.12	0.14
K ₂ O	0.03	0.04	0.02	0.05	0.04
P ₂ O ₅	0.48	0.52	0.32	0.41	0.38
SiO ₂	0.01	0.00	0	0	0
*CO ₂	37.11	43.41	41.74	41.57	44.86
Cat.%					
Ca	50.73	44.94	48.46	48.67	44.86
Mg	0.70	0.51	0.56	0.36	0.27
Fe	0.07	0.17	0.11	0.28	0.34
Mn	0.05	0.01	0.08	0.02	0.12
Ba	2.01	1.54	0.87	0.73	1.04
Sr	0.68	0.69	0.60	0.73	0.44
Na	0.16	0.18	0.13	0.20	0.23
K	0.03	0.05	0.02	0.05	0.04
P	0.37	0.38	0.23	0.30	0.28
Si	0.01	0.00	0.00	0.00	0.00
C	45.20	51.53	48.92	48.66	52.38

* CO₂ by difference

**Table 4-3 EDS analyses of phases in homogenised
multiphase inclusions**

Sample phase	ME-1 barite	ME-2 ankerite	ME-3 Cc + Brt
Wt. %			
CaO	6.29	18.64	83.97
MgO	1.39	9.21	0.00
FeO	0.00	55.34	0.00
MnO	0.00	1.78	1.01
BaO	59.59	4.32	9.68
Na ₂ O	1.52	0.94	0.96
K ₂ O	0.00	0.00	0.06
La ₂ O ₃	0.00	2.93	0.00
Ce ₂ O ₃	0.00	2.94	0.00
SO ₃	30.71	1.90	3.13
Cat. %			
Ca	12.61	23.26	92.45
Mg	3.87	18.96	0.00
Fe	0.00	49.56	0.00
Mn	0.00	1.62	0.81
Ba	34.87	1.57	3.11
Na	5.53	2.04	1.84
K	0.00	0.00	0.07
La	0.00	0.90	0.00
Ce	0.00	0.90	0.00
S	43.12	1.19	1.73

Cc calcite, Brt barite

Table 4-4 EDS analyses of crystals in opened multiphase inclusions

	XI-1	XI-2	XI-3	XI-4	XI-5	XI-6	XI-7
	Cc	Sr-Cc	Bs+Str+Cc	Cc+Ba	Cc+Str	Cc+Str	Cc+Str
Wt. %							
CaO	96.71	92.78	38.35	40.67	73.35	66.36	83.89
MgO	0.19	0.31	0.00	0.03	0.00	1.23	0.65
FeO	1.00	0.56	0.00	0.73	1.78	1.44	0.71
BaO	0.34	1.57	2.67	38.94	1.62	2.24	1.33
SrO	1.53	4.02	34.29	2.40	19.30	24.94	11.50
Na ₂ O	0.23	0.44	0.00	0.94	0.00	1.82	1.47
K ₂ O	0.00	0.00	0.51	0.00	0.00	0.00	0.00
La ₂ O ₃	0.00	0.33	10.41	4.93	3.73	1.97	0.45
Ce ₂ O ₃	n.a.	n.a.	13.77	2.54	n.a.	n.a.	n.a.
SO ₃	0.00	0.00	0.00	8.82	0.23	0.00	0.00
Cat. %							
Ca	97.58	95.47	57.60	63.17	84.22	76.00	88.52
Mg	0.27	0.44	0.00	0.06	0.00	1.96	0.96
Fe	0.79	0.45	0.00	0.89	1.59	1.29	0.58
Ba	0.10	0.47	1.17	17.65	0.54	0.75	0.41
Sr	0.84	2.24	27.87	2.02	11.99	15.46	6.57
Na	0.43	0.81	0.00	2.64	0.00	3.77	2.80
K	0.00	0.00	0.91	0.00	0.00	0.00	0.00
La	0.00	0.12	5.38	2.63	1.47	0.78	0.16
Ce	n.a.	n.a.	7.07	1.35	n.a.	n.a.	n.a.
S	0.00	0.00	0.00	9.59	0.18	0.00	0.00

Cc - calcite; Sr-Cc - strontian calcite?; Str - strontianite; Brt - barite; Bs - bastnaesite

Monomineralic Inclusions

Petrography

Monomineralic inclusions consist of a strongly anisotropic phase. They are typically larger than either mottled or multiphase inclusions and are either well rounded or ovoid in shape.

Chemistry

Monomineralic inclusions are, without exception, homogeneous in composition. EDS analyses only yield peaks for Ca (Table 4-5) and, based on petrographic and compositional data, the mineral is interpreted to be calcite.

High Temperature Phase Relations

Monomineralic Inclusions

Monomineralic (i.e., calcite) inclusions began melting in the temperature range 750-850°C and at 1100°C had undergone approximately 10-20% melting. Temperature increases to 1200°C caused no further melting.

Mottled Inclusions

Mottled solid inclusions showed the lowest initial melting temperatures of the three types of inclusions. The first phase to melt is the small yellow phase, which did so over a relatively wide temperature interval, from 430 to 590°C. Between 610 and 660°C ferroan dolomite began to melt, however, the bulk of the ferroan dolomite melted at temperatures between

Table 4-5 Compositions of Calcite Inclusions

	Calcite						
	C-1	C-2	C-3	C-4	C-5	C-6	C-7
Wt. %							
CaO	52.83	56.55	53.64	54.13	54.48	54.76	56.32
MgO	0.91	0.71	0.08	0.30	0.11	0.18	0.51
FeO	0.08	0.63	0.41	0.14	0.27	0.50	0.96
MnO	0.10	0.26	0.27	0.09	0.16	0.15	0.04
BaO	0.22	0.13	0.00	0.12	0.03	0.00	0.02
SrO	0.49	0.18	0.00	0.66	0.00	0.03	0.00
Na ₂ O	0.02	0.05	0.02	0.05	0.09	0.03	0.00
K ₂ O	0.01	0.02	0.43	0.02	0.26	0.01	0.01
P ₂ O ₅	0.08	0.24	0.00	0.18	0.02	0.11	0.33
SiO ₂	0.02	0.02	0.00	0.01	0.01	0.03	0.10
*CO ₂	45.25	41.25	45.15	44.30	44.57	44.22	41.71
Cat. %							
Ca	47.03	50.84	47.74	48.40	48.53	48.87	50.58
Mg	1.12	0.88	0.10	0.37	0.14	0.22	0.64
Fe	0.05	0.44	0.28	0.09	0.19	0.35	0.67
Mn	0.07	0.18	0.19	0.06	0.11	0.11	0.03
Ba	0.06	0.03	0.00	0.03	0.01	0.00	0.01
Sr	0.23	0.09	0.00	0.32	0.00	0.01	0.00
Na	0.04	0.07	0.03	0.08	0.14	0.05	0.00
K	0.01	0.02	0.45	0.03	0.28	0.01	0.01
P	0.06	0.17	0.00	0.12	0.01	0.07	0.24
Si	0.02	0.01	0.00	0.01	0.01	0.02	0.08
C	51.32	47.26	51.20	50.48	50.58	50.29	47.74

* CO₂ by difference

660 and 790°C (Fig 4-4). Darkening of the inclusions at temperatures in excess of 700°C made the temperature of final homogenization difficult to determine, although 800°C can be taken as a minimum.

Multiphase Inclusions

Multiphase solids typically have higher initial melting temperatures than the mottled ferroan dolomite inclusions. Calcite is the first mineral to melt, and generally does so at temperatures between 680 and 740°C (Fig 4-5, 4-6). However, in two inclusions calcite began melting at approximately 460 and 640°C, respectively. The unidentified green mineral was the next to start melting, at temperatures between 880 and 995°C, followed by barite at temperatures above 1000°C, and orange material above 1050°C. Final homogenization of all inclusions, to liquid and vapour, occurred at temperatures above 1100°C.

Discussion

The occurrence of three distinct types of solid inclusion which show an intimate association, spatially, poses an interesting problem. This spatial association suggests that the three inclusion types also share a close temporal association, and owing to the primary nature of the apatite (Roelofsen, 1997), the small size of the crystals (<200µ long) and the random orientation of inclusions, the trapping of these three types of inclusion can be considered to have been synchronous. Secondary features, such as localization of inclusions along fractures or a linear distribution, as was described by Ting *et al.* (1994) for solid inclusions from the Sukulu carbonatite, Uganda, are absent at Amba Dongar.

Melt versus Trapped Solid

The most important question to be addressed is the origin of the inclusions, i.e., are they trapped melt or solids? The clear, calcite-only inclusions are unlikely to

Figure 4-4 Melting behaviour of mottled inclusions: A) No change at 261°C; B) initial melting of inclusion and formation of vapour bubble prior to darkening of inclusion (649°C).

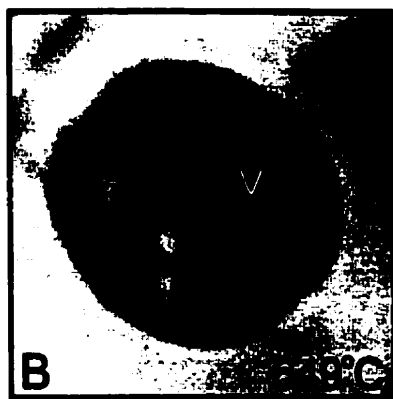


Figure 4-5 Melting behaviour of a multiphase inclusion: A) at 285°C showing S1, S2, S3 and S4 solids; B) initial melting of S1 at 735°C; C) continued melting (948°C); D) Initial melting of the central solid (S2) at 974°C; E) S1 now liquid, S2 continues melting; F) Extensive melting of S3 and formation of vapour bubble (V) at 1020°C; G) Initial melting of S4 at 1049°C; H) S4 almost melted, the inclusion is composed almost entirely of liquid and vapour (1107°C); I) The quench product at 25°C.

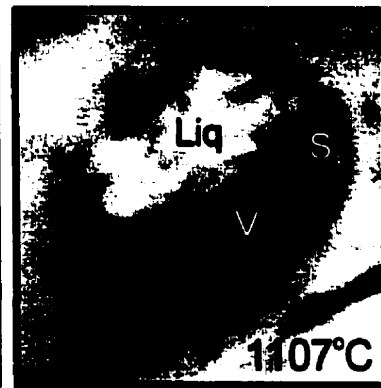
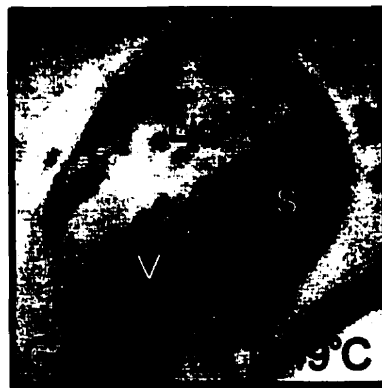
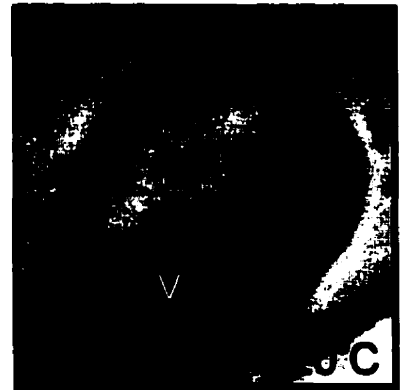
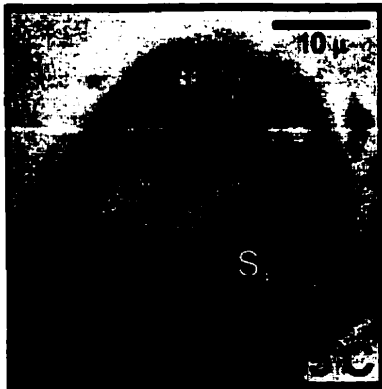
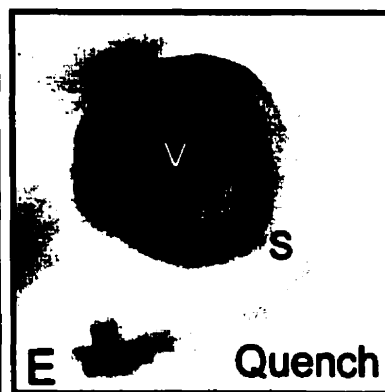
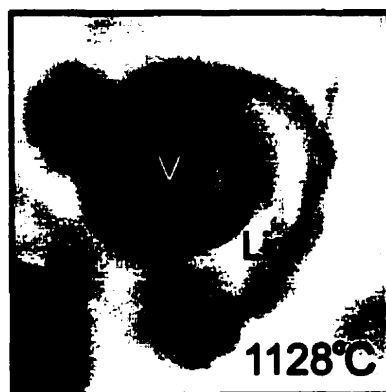
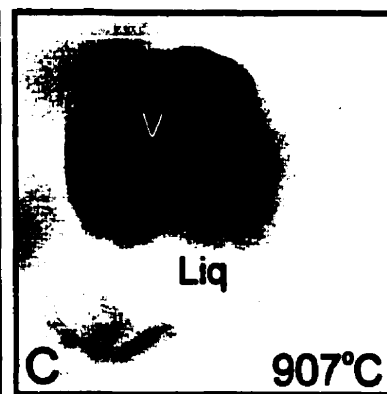
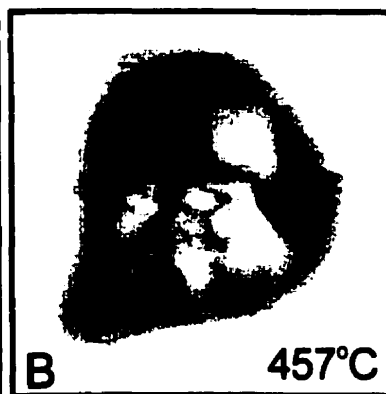
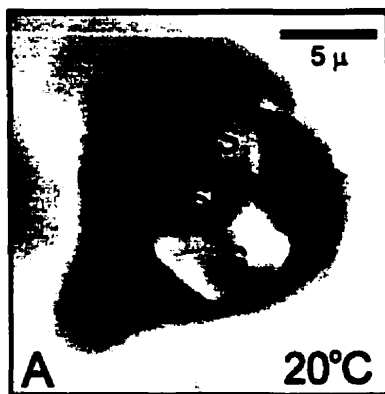


Figure 4-6 Melting behaviour of a multiphase inclusion: A) at 20°C showing S1, S2 and S3 solids; B) Initial melting? in the center of the inclusion at 457°C; C) One solid remains in the liquid (L) + vapour (V) at 907°C; D) L-V homogenization at 1128°C; E) Quench product at 20°C.



represent trapped liquids based on their melting behaviour. With a maximum of 20% melting at temperatures of 1200°C, these inclusions almost certainly do not represent a eutectic melt although they could possibly represent a sub-liquidus melt. However, the absence of other phases in these inclusions makes it more likely that they are trapped calcite crystals.

Based on chemistry and phase relationships, there is a high degree of probability that mottled and multiphase inclusions represent trapped carbonatitic liquids. The compositions of these two types of inclusions are very similar to those of ferro- and calciocarbonatites, respectively (Table 4-6, Fig. 4-3). Multiphase inclusions, on average, have similar concentrations of Ca, Fe, Mg and P to representative samples of calciocarbonatite from the Amba Dongar complex, however, barium and strontium contents are higher, and silicon lower, in the inclusions than the bulk rock. On the other hand, calciocarbonatite is locally enriched in Sr and has been partly silicified (Palmer and Williams-Jones, 1996).

Mottled inclusions have remarkably consistent compositions which, as noted above, are very similar to those of ferrocarbonatite. Concentrations of Ca, Fe, Mg, P and Sr in mottled inclusions all fall within the corresponding ranges for the ferrocarbonatites (Table 4-6, Fig. 4-3). Ba contents, however, are much lower in the inclusions, but this can be attributed to the difficulty of analysing heterogeneous quench products, because barite has been observed in some mottled inclusions. As is the case for multiphase inclusions, the SiO₂ contents of mottled inclusions are much lower than those of ferrocarbonatite, and suggest that the latter may be anomalously enriched in silica due to subsolidus silicification (see above).

Although the compositions of multiphase and mottled inclusions differ in some respects from those of calcio- and ferrocarbonatite, respectively, the consistency in the compositions of the two sets of inclusions is strong support for their representing trapped liquids. If the solid inclusions represented trapped solids the compositional variance would be much higher than that analysed.

The temperatures of phase changes measured during microthermometric analyses of multiphase and mottled inclusions agree well with those obtained in experimental

Table 4-6 Average compositions of Melt Inclusions (MI_{AVG}) and representative analyses of calciocarbonatites and ferrocarbonatites

	Calciocarbonatites						Ferrocarbonatites				
	+ MI _{AVG}	AD008	AD053	AD016b	AD026a	*1	+ MI _{AVG}	AD-012b2	AD-013d	AD-002c	*2
wt. %											
SiO ₂	0.00	9.01	3.76	2.43	6.13	2.49	0.10	8.15	11.69	16.03	1.8
TiO ₂	n.a.	0.04	0.07	0.01	0.12	n.d.	n.a.	0.14	0.36	0.05	0.04
Al ₂ O ₃	n.a.	0.45	0.06	0.08	0.11	n.d.	n.a.	0.04	0.33	0.25	0.07
Fe ₂ O ₃	0.27	1.62	1.19	0.37	2.36	1.05	9.58	9.15	16.61	7.05	10.65
MnO	1.07	0.27	0.24	0.22	0.54	0.63	0.08	3.21	3.76	3.17	1.42
MgO	0.37	0.18	0.08	0.16	1.87	0.48	11.17	9.82	8.88	10.35	10.3
CaO	51.19	50.49	53.77	53.96	45.21	50.87	34.32	24.62	18.96	23.04	34.8
Na ₂ O	0.11	n.d.	n.d.	n.d.	0.02	0.09	0.07	0.33	0.41	0.29	n.d.
K ₂ O	0.04	0.22	n.d.	0.07	0.38	n.d.	0.02	0.01	0.02	0.02	n.d.
P ₂ O ₅	0.42	0.64	2.19	0.22	0.63	1.08	0.38	1.66	0.94	0.38	0.24
LOI	n.a.	37.2	38.1	40.6	38		n.a.	25.47	26.59	30.42	13.38
CO ₂	41.74	n.a.	n.a.	n.a.	n.a.	40.8	42.73	n.a.	n.a.	n.a.	39.79
ppm											
Ba	40634	2337	3741	7732	8247	10020	485	79500	52400	44400	3680
Sr	9371	1864	2700	9058	1801	2960	3832	4715	4684	6382	3480
Zr	n.a.	113	94	13	62	70	n.a.	39	113	73	90
Y	n.a.	60	117	51	111	180	n.a.	193	363	200	440
Nb	n.a.	32	97	38	418	95	n.a.	200	395	48	140
Total	100.20	100.78	100.53	100.53	97.08		98.86	90.57	93.86	95.51	99.89
cat. %											
Si	0.00	7.68	3.21	2.08	5.18	4.14	0.08	7.22	10.40	13.87	1.50
Ti	n.a.	0.03	0.04	0.01	0.08	n.d.	n.a.	0.09	0.24	0.03	0.03
Al	n.a.	0.45	0.06	0.08	0.11	n.d.	n.a.	0.04	0.35	0.25	0.07
Fe	0.19	1.15	0.85	0.26	1.66	1.41	6.64	6.78	12.36	5.10	7.44
Mn	0.77	0.19	0.17	0.16	0.38	0.85	0.05	2.41	2.83	2.32	1.00
Mg	0.47	0.23	0.10	0.20	2.35	1.15	13.79	12.98	11.79	13.35	12.84
Ca	47.08	46.12	49.20	48.93	40.80	87.22	30.46	23.37	18.08	21.35	31.17
Na	0.18	n.d.	n.d.	n.d.	0.03	0.28	0.12	0.57	0.71	0.49	n.d.
K	0.04	0.24	n.d.	0.08	0.39	n.d.	0.02	0.01	0.02	0.02	n.d.
P	0.31	0.46	1.58	0.16	0.45	1.46	0.28	1.25	0.71	0.28	0.17
C	48.90	43.24	44.46	47.25	48.15	2.43	48.33	41.89	40.13	40.85	45.41
Ba	1.53	0.09	0.14	0.29	0.30	0.70	0.02	3.08	2.04	1.68	0.13
Sr	0.55	0.11	0.16	0.53	0.10	0.32	0.22	0.29	0.29	0.38	0.20
Zr	n.a.	0.01	0.01	0.00	0.00	0.01	n.a.	0.00	0.01	0.00	0.00
Y	n.a.	0.00	0.01	0.00	0.01	0.02	n.a.	0.01	0.02	0.01	0.02
Nb	n.a.	0.00	0.01	0.00	0.02	0.01	n.a.	0.01	0.02	0.00	0.01

*1-2 data taken from Viladkar and Wimmensauer (1992)

+ MI_{AVG} multiphase melt inclusions ++ MI_{AVG} mottled melt inclusions

n.d. not detected

n.a. not analyzed

investigations of synthetic carbonatite systems and in other melt inclusion studies. The eutectic temperature in the synthetic system which most closely models the composition of mottled inclusions, $\text{CaO-MgO-CO}_2\text{-H}_2\text{O}$, is generally accepted to be approximately 650°C at 2 kbar, while that of the system appropriate for modeling multiphase inclusions, $\text{CaO-CO}_2\text{-H}_2\text{O}$, is also approximately 650°C , at the same pressure (Wyllie and Tuttle, 1960; Fanelli *et al.*, 1986; Wyllie, 1989). Although phase changes were observed in mottled inclusions at temperatures as low as 450°C , ferroan dolomite, which is the main phase in these inclusions, began melting at temperatures between 610 and 660°C and homogenized at temperatures above 800°C . Melting of multiphase inclusions commenced at temperatures between 640 and 740°C , and complete homogenization occurred at temperatures slightly above 1100°C . The agreement between temperatures of initial melting of ferroan dolomite in mottled inclusions and calcite in multiphase inclusions to the eutectic temperatures in the systems $\text{CaO-MgO-CO}_2\text{-H}_2\text{O}$ and $\text{CaO-CO}_2\text{-H}_2\text{O}$, respectively, is further support for the hypothesis that these solid inclusions represent trapped melts.

On the basis of the evidence presented above, we therefore conclude that multiphase and mottled inclusions represent samples of the carbonatite liquids responsible for the crystallization of calciocarbonatites and ferrocarbonatites, respectively. We further conclude from the close spatial, and thus temporal, association of multiphase and mottled inclusions, that two carbonate melts, one of calcitic composition and the other of ankeritic composition, coexisted at Amba Dongar.

Carbonatite Evolution

Fractionation is still the most widely accepted process to explain the evolution from calciocarbonatite \Rightarrow magnesiocarbonatite \Rightarrow ferrocarbonatite. Harmer and Gittins (1997) have argued that a primary magnesian carbonatite melt could produce the full range of carbonatites observed in nature. The reaction of an ascending Mg-rich carbonatite melt with wherlitic wall rocks would drive the melt to more calcic compositions, producing calciocarbonatite at an early stage. Once the conduit had been armoured by calciocarbonatite, emplacement of more magnesian melts would follow.

However, investigations in the system $\text{CaO}-(\text{MgO} + \text{FeO})-(\text{Na}_2\text{O} + \text{K}_2\text{O})-(\text{SiO}_2 + \text{Al}_2\text{O}_3 + \text{TiO}_2)-\text{CO}_2$ by Lee and Wyllie (1998) show that calciocarbonatites can only originate from carbonate melts separated immiscibly from silicate melts, not from primary, mantle-derived carbonate melts, and that magnesiocarbonatite cannot be produced by immiscibility. According to this study, dolomitic carbonatite can only form from a primary carbonate melt or, contrary to Gittins and Harmer (1997), through fractionation of a calciocarbonatite melt (Lee and Wyllie, 1998). Significantly, neither study nor any other, to our knowledge, has demonstrated how fractionation leads to late-stage generation of ferrocarbonatite.

If fractionation were responsible for the production of ferrocarbonatite liquids at Amba Dongar, then melt trapped, at any given time, as inclusions in apatite should have a fixed composition, reflecting a particular stage in the evolution of the system. This is not the case as two chemically distinct types of melt inclusions, i.e., multiphase and mottled inclusions, were apparently trapped synchronously. The only way to obtain a range of compositions by fractionation, i.e., calcitic to ferroan dolomite, would be to have entrapment occur over a long interval of crystallization, and this would result in an outward zonation in inclusions of Ca- to Fe-rich compositions. However, this is not supported by the distribution of calcitic and ferroan dolomite melt inclusions, which is random, and the absence of zoning in apatite suggestive of re-equilibration with a changing melt composition (Roelofsen, 1997). As well, the process of fractionation would necessitate a cumulate origin for calciocarbonatite rocks at Amba Dongar, a concept which is difficult to reconcile with the production of the outer ring of fine-grained carbonatite breccia. Fluid inclusion evidence for apatite formation at approximately 12 kbar also argues against a cumulate origin for the calciocarbonatite (Palmer and Williams-Jones, 1998, Chap. 5). If calcite was a liquidus phase at 12 Kb, then the calcite cumulates would have to ascend approximately 35 km before their final emplacement just below the present erosional surface, a highly improbable occurrence. The presence of porphyritic varieties of calciocarbonatite, large calcite crystals in a finer grained calcite matrix (Viladkar, 1981), also suggests that a wholly cumulate origin for these rocks is unlikely, as it would require a bimodal distribution in calcite growth rates.

An alternative process that can, in principle, explain the diversity of carbonatite compositions is that of carbonate-carbonate liquid immiscibility. Experimental studies in the system $\text{SiO}_2\text{-Al}_2\text{O}_3\text{-CaO-Na}_2\text{O-CO}_2$ by Brooker and Hamilton (1990) have documented the occurrence of three coexisting liquids, one silicate, one Ca-carbonate and one Ca-Na carbonate. Carbonate-carbonate liquid immiscibility was also reported by Mitchell (1997) in natural lavas erupted from the Oldoinyo Lengai volcano, Tanzania. The liquids consisted of a carbothermal brine, which crystallized gregoryite, sodian sylvite, potassium neighborite and a Ba-rich carbonate, and a Na-rich carbonate liquid. Nielsen *et al.* (1997) have identified carbonate-silicate, Ca-carbonate and Ca-Na-carbonate solid inclusions in melilitite of the Gardiner complex, Greenland which are thought to represent trapping of immiscible melilititic and calciocarbonatite melts, and a third high temperature, immiscible Na-rich carbonate liquid.

Although the preceding evidence indicates that liquid immiscibility occurs in natrocarbonatite systems, the lack of data for the CaO-MgO-FeO-CO_2 system at liquidus temperatures seriously hampers evaluation of the role that carbonate-carbonate liquid immiscibility may play in the formation of ferrocarbonatite. However, it is worth noting that Fe-enriched silicate magmas commonly separate into Fe-rich and Fe-poor liquids (Philpotts, 1976; Roedder, 1979; Vicenzi *et al.*, 1995). Further indications of the possible role of Fe in causing carbonate-carbonate immiscibility are provided by subsolidus relationships in the system $\text{CaCO}_3\text{-MgCO}_3\text{-FeCO}_3$. Goldsmith *et al.* (1962) observed a large field of immiscibility between ferroan calcite and calcian siderite at temperatures ranging from 600 to 800°C, which is consistent with the absence, in nature, of a $\text{CaFe}(\text{CO}_3)_2$ mineral (Davidson *et al.*, 1994; Chai and Navrotsky, 1996). Although this is only a solid state relationship, it is promising that Ca and Fe are mutually incompatible in carbonate solids, and it is possible that this behaviour extends to carbonate liquids.

In Fe-enriched silicate systems, liquid immiscibility has been attributed to the crystal field effects associated with the d_6 electronic configuration of Fe^{2+} (Hudon, 1998). The Fe^{2+} ion has its d orbitals oriented at an angle to the x-y-z axes, which results in less shielding of the nucleus of the ion and, consequently, permits the ion to exert greater coulombic forces (Hudon, 1998). The inability of the Fe^{2+} ion to shield itself results in exaggeration of the interactive forces within the melt, i.e., repulsion, and acts to promote

silicate liquid immiscibility (Hess, 1995, 1996; Hudon, 1998). It is therefore reasonable to predict that the behaviour of the Fe^{2+} ion will play a similar role in promoting liquid immiscibility in Fe-rich carbonate melts.

Despite the fact that carbonate-carbonate liquid immiscibility has only been demonstrated for natrocarbonatite systems, there are compelling arguments that such immiscibility, and not fractionation, was responsible for the formation of ferrocarbonatite at Amba Dongar. Along with the temporal arguments which support the coexistence of two carbonate liquids at Amba Dongar, further physical evidence supporting carbonate-carbonate liquid immiscibility can be gleaned from microscopic examination of the multiphase inclusions. The presence of two coexisting liquids during heating of multiphase melt inclusions (Fig. 4-7) indicates that immiscible liquids were present at the time of trapping, and were compositionally similar to calcite and ferroan dolomite/ankerite, respectively. The dominance of Ca in one liquid, evident in X-ray analyses of this material, suggests that it is calcic, while the strong correlation between Fe and Mg, and the lack of elements other than Ca, indicates that the other is ankeritic (Figs. 4-8, 4-9). The meniscus shaped margin of ferroan dolomite, in contact with calcite, within mixed inclusions also indicates that Fe-rich liquids were present during apatite growth (Fig. 4-2f, g), and therefore coexisted with liquids which were trapped as multiphase inclusions, i.e., calcic carbonatite magma.

Model

It is proposed that the intrusion of ferrocarbonatites at Amba Dongar was initiated by formation of carbonate magmas directly from the mantle. Isotopic evidence suggests that carbonatite liquids intruded at Amba Dongar were either related to mantle plume activity, which was responsible for the extrusion of flood basalts, or from direct partial melting of an enriched mantle source (Simonetti and Bell, 1995). Experimental studies indicate that carbonate liquids produced in such a manner are dolomitic in composition (Wallace and Green, 1988; Dalton and Wood, 1993; Sweeney, 1994), and the significant volumes of ferrocarbonatite present at Amba Dongar suggest that these liquids were also

Figure 4-7 The formation of two liquids in a multiphase inclusion at high temperature: A) At 955°C an outer layer of vapour obscures melting phenomena; B) The retreating vapour mantle reveals the presence of a second phase within liquid (1032°C); C) the second liquid is evident at the meniscus between liquid 1 and vapour (V) at 1051°C.

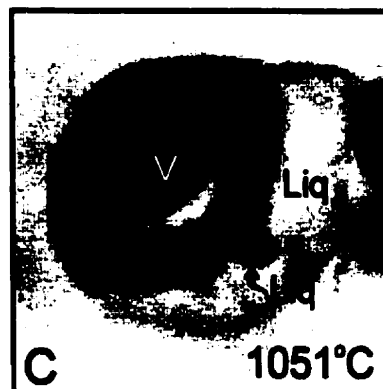
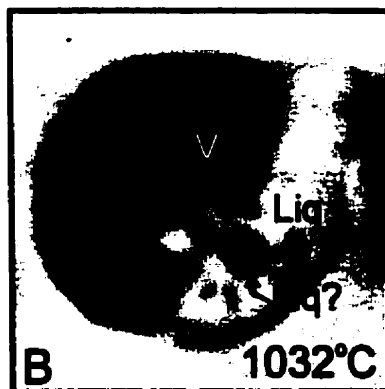
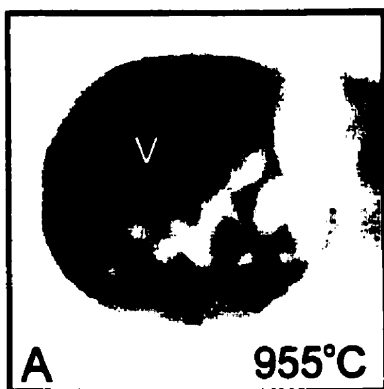


Figure 4-8 A) Backscattered electron image of a homogenised multiphase melt inclusion showing small patches of Fe-rich material; B) X-ray map for Ca; C) X-ray map for Mg; D) X-ray map for Fe.

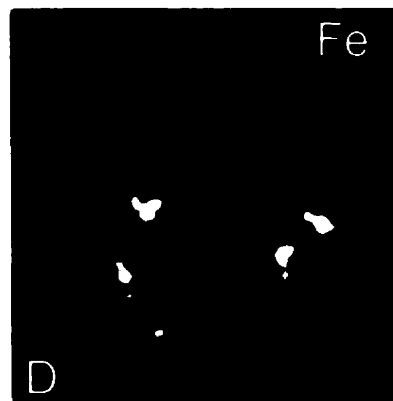
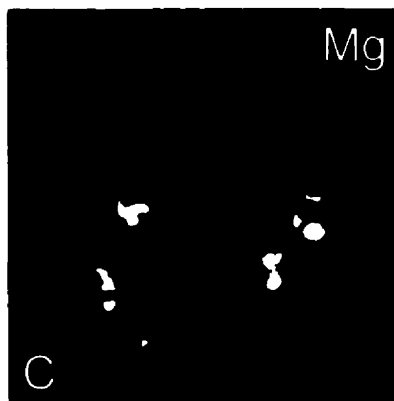
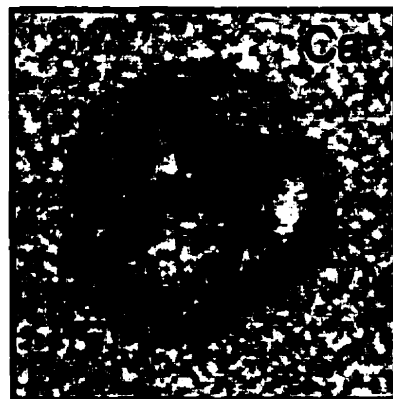
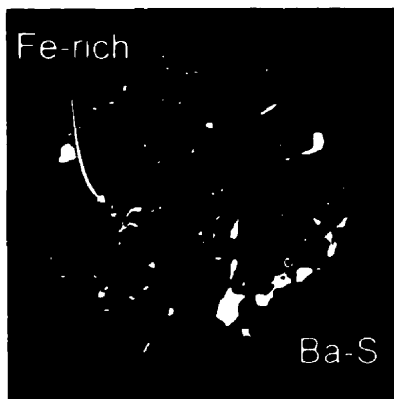
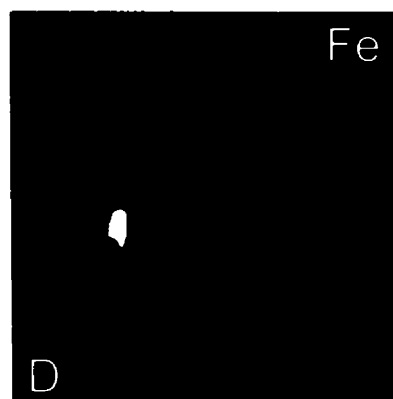
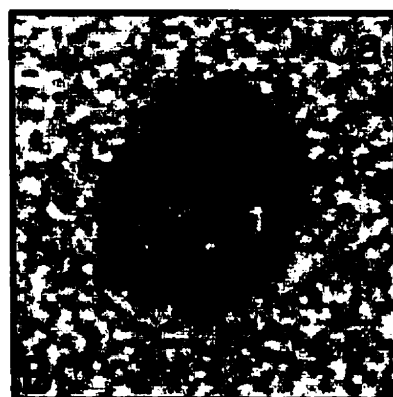
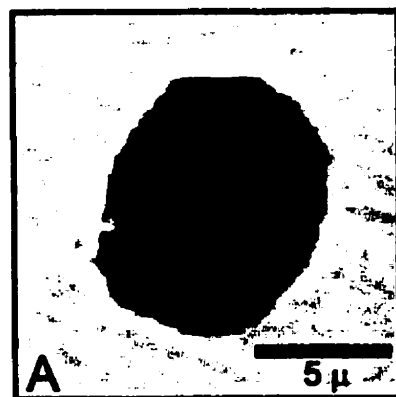


Figure 4-9 A) Backscattered electron image of a homogenised multiphase melt inclusion; B) X-ray map for Ca; C) X-ray map for Mg; D) Xray map for Fe.



enriched in iron. The rising magma experienced a loss of volatiles at a pressure of approximately 12 kbar (Palmer and Williams-Jones, 1998, Chap. 5) causing rapid cooling of the melt until the liquidus temperature of apatite was reached (1100°C). The rapidly changing conditions, i.e., decreasing pressure and temperature and loss of volatiles, induced separation of two carbonate liquids of ankeritic and calcitic compositions, respectively, which were trapped in the crystallizing apatite as mottled and multiphase inclusions.

The separation of Ca- and Fe-rich carbonate liquids allowed, not only the sharp contacts observed in the field, but also the timing relationships. The ankeritic liquid, being denser than the calcitic liquid (based on mineral densities), sank and ponded towards the bottom of the upwelling magma, allowing the intrusion of calciocarbonatite to occur first. Continued ascent of magma eventually led to intrusion of ferrocarnatite as plugs or dykes, along zones of weakness related to the earlier emplacement of the calciocarbonatite.

Conclusions

Three types of solid inclusion were found to coexist in apatite, and comprise a mottled variety, composed almost entirely of ferroan dolomite, a multiphase variety, which contains calcite and subordinate ankerite and barite, and a monomineralic variety consisting of calcite. The compositions and melting relationships of the two former types are consistent with their representing trapped samples of carbonatitic melts, while the monomineralic inclusions behave as trapped solids, i.e., they are only melted partially at temperatures exceeding 1200°C. The temperatures of initial melting of mottled inclusions ranged between 610 and 660°C, while those of multiphase inclusions were between 680 and 740°C. This is consistent with experimentally determined eutectic temperatures for the systems CaO-MgO-CO₂-H₂O and CaO-CO₂-H₂O, which are approximately 650°C (Wyllie and Tuttle, 1960; Fanelli *et al.*, 1986; Wyllie, 1989). Although homogenization temperatures of mottled inclusions were not observed, multiphase inclusions were completely molten at temperatures above 1100°C. The random distribution of mottled and multiphase inclusions in single apatite crystals and the

lack of evidence indicating prolonged growth of the host, i.e., zoned crystals, indicate that inclusions were temporally associated, and suggests that ferrocarbonatite and calciocarbonatite are related through liquid immiscibility. This conclusion is supported by the formation of two immiscible liquids in multiphase inclusions, observed during heating, and the presence of mixed ferroan dolomite-calcite inclusions which are interpreted to represent heterogeneous entrapment of the two liquids.

Although carbonate-carbonate immiscibility has been documented in natrocarbonatite systems (Brooker and Hamilton, 1990; Mitchell, 1997; Nielsen *et al.*, 1997), this study provides the first evidence that it can also occur in the CaO-MgO-FeO-CO₂ system. We propose that the ferrocarbonatites at Amba Dongar were the products of carbonate-carbonate immiscibility in a Fe-rich magma, and suggest that this mechanism may explain the genesis of ferrocarbonatites elsewhere.

References

- Aldous, R.T., 1980, Ore genesis in copper-bearing carbonatites; a geochemical, fluid inclusion and mineralogical study: Unpublished Ph.D. thesis, Imperial College, London, 365p..
- Barker, D.S., 1989, Field relations of carbonatites: *in* K. Bell (ed.), Carbonatites: genesis and evolution: London, Unwin Hyman, p. 38-69.
- Brooker, R.A. and Hamilton, D.L., 1990, Three-liquid immiscibility and the origin of carbonatites: *nature*, v. 346, p. 459-462.
- Chai, L., and Navrotsky, A., 1996, Synthesis, characterization and energetics of solid solution along the dolomite-ankerite join, and implications for the stability of ordered $\text{CaFe}(\text{CO}_3)_2$: *American Mineralogist*, v. 81, p. 1141-1147.
- Dalton, J.A., and Wood, B.J., 1993, The compositions of primary carbonate melts and their evolution through wallrock reaction in the mantle: *Earth and Planetary Science Letters*, v. 119, p. 511-525.
- Davidson, P.M., Symmes, G.H., Cohem, B.A., Reeder, R.J., and Lindsley, D.H., 1994, Synthesis of the new compound $\text{CaFe}(\text{CO}_3)_2$ and experimental constraints on the $(\text{Ca,Fe})\text{CO}_3$ join: *Geochimica et Cosmochimica Acta*, v. 58, p. 5105-5109.
- Fanelli, M.F., Cava, N., and Wyllie, P.J., 1986, Calcite and dolomite without portlandite at a new eutectic in $\text{CaO-MgO-CO}_2\text{-H}_2\text{O}$, with applications to carbonatites: In *Morphology and phase equilibria of minerals: Proceedings 13th General Meeting International Mineralogical Association, Bulgarian Academy of Sciences, Sofia*, p. 313-322.
- Freestone, I.C., and Hamilton, D.L., 1980, The role of liquid immiscibility in the genesis of carbonatites – an experimental study: *Contrib. Mineral. Petrol.*, v. 73, p. 105-117.
- Gittins, J., 1989, The origin and evolution of carbonatite magmas: *in* Bell, K., (ed.), Carbonatites: genesis and evolution: London, Unwin Hyman, p. 149-176.
- Gittins, J., and Harmer, R.E., 1997, What is ferrocarbonatite? A revised classification: *Journal of African Earth Sciences*, v. 25, p. 159-168.
- Goldsmith, J.R., Graf, D.L., Witters, J., and Northrop, D.A., 1962, Studies in the system $\text{CaCO}_3\text{-MgCO}_3\text{-FeCO}_3$: 1. Phase relations; 2. a method for major-element spectrochemical analysis; 3. compositions of some ferroan dolomites: *Journal of Geology*, v. 70, p. 659-688.

- Harmer, R.E., and Gittins, J., 1997, The origin of dolomitic carbonatites: field and experimental constraints: *Journal of African Earth Sciences*, v. 25, p. 5-28.
- Hess, P.C., 1995, Thermodynamic mixing properties and the structure of silicate melts, *Rev. Mineral.*, v. 32, p. 145-190.
- Hess, P.C., 1996, Upper and lower critical points: thermodynamic constraints on the solution properties of silicate melts: *Geochim. Cosmochim. Acta*, v. 60 (13), p. 2365-2377.
- Hudon, P., 1998, The study of melts in the ternary CaO-MgO-SiO₂ at high pressures and the nature of immiscibility in binary systems: Unpublished Ph.D. thesis, McGill University, Montreal.
- Kjarsgaard, B.E., and Hamilton, D.L., 1989, The genesis of carbonatites by immiscibility: in K. Bell (ed.), *Carbonatites: genesis and evolution*: London, Unwin Hyman, p. 388-404.
- Kjarsgaard, B.E., and Hamilton, D.L., 1988, Liquid immiscibility and the origin of alkali-poor carbonatites: *Mineralogical Magazine*, v. 52, p. 43-55.
- Le Bas, M.J., 1977, *Carbonatite-Nephelinite Volcanism*: John Wiley and Sons, Toronto.
- Lee, W.-J., and Wyllie, P.J., 1998, Petrogenesis of carbonatite magmas from mantle to crust, constrained by the system CaO-(MgO + FeO*)-(Na₂O + K₂O)-(SiO₂ + Al₂O₃ + TiO₂)-CO₂: *Journal of Petrology*, v. 39, p. 495-517.
- Lee, W.-J., and Wyllie, P.J., 1997, Liquid immiscibility between nephelinite and carbonatite from 1.0 Gpa to 2.5 Gpa compared with mantle melt compositions: *Contrib. Mineral. Petrol.*, v. 127, p. 1-16.
- Lide, D.R., ed., 1995, *Handbook of chemistry and physics*, 76th edition, 1995-1996: CRC Press Inc., New York.
- Metzger, F. W., Kelly, W. C., Nesbitt, B. E., and Essene, E. J., 1977, Scanning Electron microscopy of daughter minerals in fluid inclusions: *Economic Geology*, v. 72, p. 141-152.
- Mitchell, R.H., 1997, Carbonate-carbonate immiscibility, neighborite and potassium iron sulphide from Oldoinyo Lengai natrocarbonatite: GAC/MAC Annual Meeting May 19-21: Abstract Volume, p. A104.

- Nesbitt, B.E., and Kelly, W.C., 1977, Magmatic and Hydrothermal inclusions in carbonatite of the Magnet Cove Complex, Arkansas: *Contrib. Mineral. Petrol.*, v. 63, p. 271-294.
- Nielson, T. F. D., Solovova, I. P., and Veksler, I. V., 1997, Parental melts of melilitolite and origin of alkaline carbonatite: evidence from crystallized melt inclusions, Gardiner complex: *Contrib. Mineral. Petrol.*, v. 126, p. 331-344.
- Palmer, D.A.S., and Williams-Jones, A.E., 1996, Genesis of the carbonatite-hosted fluorite deposit at Amba Dongar, India: Evidence from fluid inclusions, stable isotopes and whole rock-mineral geochemistry: *Economic Geology*, v. 91, p. 934-950.
- Palmer, D.A.S., and Williams-Jones, A.E., 1998, Fluid evolution of the Amba Dongar carbonatite complex, India: Unpublished Ph.D. thesis, McGill University, Montreal, Chapter 5.
- Philpotts, A.R., 1976, Silicate liquid immiscibility: Its probable extent and petrogenetic significance: *American Journal of Science*, v. 276, p. 1147-1177.
- Rankin, A.H. and Le Bas, M.J., 1974, Liquid Immiscibility between silicate and carbonate melts in naturally occurring ijolite magma: *Nature*, v 250, p. 206-209.
- Reischmann, T., 1995, Precise U/Pb age determination with baddeleyite (ZrO_2), a case study from the Phalaborwa Igneous Complex, South Africa: *S.Afr.J.Geol.*, v. 98, p. 1-4.
- Roedder, E., 1979, Silicate liquid immiscibility in magmas: In *The Evolution of the Igneous Rocks: Fiftieth Anniversary Perspectives*, p. 15-57.
- Simonetti, A., and Bell, K., and Viladkar, S.G., 1995, Isotopic data from the Amba Dongar Carbonatite Complex, west-central India: Evidence for an enriched mantle source: *Chemical Geology*, v. 122, p. 185-198.
- Sweeney, R.J., 1994, Carbonatite melt compositions in the earth's mantle: *Earth and Planetary Science Letters*, v. 128, p. 259-270.
- Ting, W., Rankin, A. H. and Woolley, A. R., 1994, Petrogenetic significance of solid carbonate inclusions in apatite of the Sukulu carbonatite, Uganda: *Lithos*, v. 31, p. 177-187.
- Vicenzi, E.P., Green, T.H., and Sie, S.H., 1995, Immiscible silicate liquids at high pressure: The influence of melt structure on elemental partitioning: *Nuclear Instruments and Methods in Physics Research B*, v. 104, p. 470-475.

- Viladkar, S.G., 1981, The carbonatites of Amba Dongar. Gujarat, India: Bulletin of the Geological Society of Finland, v. 53, p. 17-28.
- Viladkar, S.G. and Wimmenauer, W., 1992, Geochemical and Petrological Studies on the Amba Dongar Carbonatites (Gujarat, India): Chem Erde, v. 52, p. 277-291.
- Wallace, M.E., and Green, D.H., 1988, An experimental determination of primary carbonatite magma composition: Nature, v. 335, p. 343-346.
- Woolley, A.R. and Kempe, D.R.C., 1989, Carbonatites: nomenclature, average chemical compositions, and element distribution: *in* K. Bell (ed.), Carbonatites: genesis and evolution: London, Unwin Hyman, p.1-37.
- Wyllie, P.J., 1989, Origin of carbonatites: evidence from phase equilibrium studies: *in* K. Bell (ed.), Carbonatites: genesis and evolution: London, Unwin Hyman, p.149-176.
- Wyllie, P.J., 1966, Experimental studies of carbonatite problems: the origin and differentiation of carbonatite magmas: *in* Tuttle, O.F., and Gittins, J., eds., Carbonatites: London, Wiley & Sons, p. 311-352.
- Wyllie, P.J. and Tuttle, O.F., 1960, The system $\text{CaO-CO}_2\text{-H}_2\text{O}$ and the origin of carbonatites: Journal of Petrology, v. 1, p. 1-46.

Bridge to Chapter 5

In the previous chapter, solid inclusions observed in apatite of calciocarbonatite were characterized with respect to composition and phase changes at high temperature. It was concluded that these inclusions represent samples of trapped carbonatite magmas produced by carbonate-carbonate liquid immiscibility. The compositions of the liquids were similar to calciocarbonatite and ferrocarbonatite, and existed at temperatures greater than 800°C.

Primary fluid inclusions are spatially associated with melt inclusions and this provided an opportunity to characterize the aqueous fluids which were in equilibrium with the carbonatite melts. In Chapter 5 the composition, pressure-temperature conditions and evolution of these orthomagmatic fluids are discussed based on microthermometric experiments and decrepitate analyses. Fluid inclusions were also observed in quartz hosted by fenites surrounding the complex. These fluid inclusions were similarly characterized, and used to determine the relationship between orthomagmatic fluids and fenitization.

**Chapter 5: Fluid Evolution of the Amba Dongar
Carbonatite Complex, India**

**D. A. S. Palmer and A. E. Williams-Jones
Department of Earth and Planetary Sciences
McGill University**

Abstract

A variety of primary fluid inclusions have been identified in apatite hosted by calciocarbonatite of the Amba Dongar complex, India and in quartz of the surrounding fenitized sandstones. Calcite from calciocarbonatite also hosts fluid inclusions, however, their origins are uncertain. Fluid inclusions in apatite comprise liquid- and vapour-rich liquid-vapour inclusions (LV and VL, respectively), liquid-vapour inclusions containing up to two solids (LVS) and liquid-vapour inclusions containing more than two solids (LVMS). Based on scanning electron microscopic analyses of solids and decrepitate residues from LVS and LVMS inclusions, minerals consist of complicated mixtures of carbonates (calcite, ankerite, nahcolite, gregoryite/kalicinite, burbankite), sulphates (arcanite) and three complex Si-bearing phases which also contain Ca-Mg, Al-Na-Ca-Sr and Al-K-Ca-Sr. Calcite- and quartz-hosted inclusions are dominantly LV inclusions, although VL varieties are present.

Microthermometric experiments of fluid inclusions in apatite indicate average homogenization temperatures of 254, 335 and 521°C for LV, LVS and LVMS inclusions, respectively. Quartz-hosted inclusions homogenize at temperatures ranging from 262°C to 122°C, with decreasing temperatures corresponding to decreasing intensity of fenitization, while calcite-hosted inclusions homogenize at an average temperature of 155°C. The low temperature phase behaviour of all inclusions indicates that the aqueous fluids are NaCl-, KCl-bearing brines with salinities between 15 and 1.5 wt.%. In addition, LVS, LVMS, VL(ap) and VL(qtz) inclusions contain CO₂ and CH₄.

The compositions of decrepitate residues indicate that LVS and LVMS inclusions were dominated by S and HCO₃⁻, respectively, and had low Na/(Na+K) ratios (<0.5). LV(ap) and LV (qtz) inclusions contain Cl⁻ as the dominant anion in solution and are strongly depleted in K relative to LVS and LVMS inclusions, with Na/(Na+K) values >0.6 and >0.9 for LV (ap) and LV(qtz) inclusions, respectively.

Microthermometric data and compositions of residues from decrepitated fluid inclusions suggest an evolutionary trend of LVS⇒LVMS⇒LV (ap) ⇒LV (qtz). Estimated temperatures and pressures of trapping of aqueous fluids, based on isochoric projections of fluid inclusions, and melt inclusion studies by Palmer and Williams-Jones

(1998; Chap. 4), are between 875 and 1000°C and >8Kb for LVS inclusions; <875°C and <8Kb for LVMS inclusions; <650°C and <4 Kb for LV (ap) inclusions; and <260°C and <500 bars for fenitizing fluids, i.e., LV(qtz). The chemical evolution of the fluids, represented by the different fluid inclusion types, involved an increasing activity of Cl⁻ anion, increasing Na/(Na+K) and decreased activity of S and HCO₃⁻.

Introduction

Over the past thirty years it has become widely recognized that large volumes of aqueous fluids are released during the emplacement of carbonatites, and that they are responsible for the fenitization that is associated with these intrusives (Currie and Ferguson, 1971; Kresten and Morogan, 1986; Wyllie, 1989; Gittins *et al.*, 1990; Bailey and Hampton, 1990; Morogan 1994). However, relatively little research has focussed on the nature of these aqueous fluids or the evolution of their compositions during carbonatite crystallization.

Fluid inclusions provide the most direct method of studying orthomagmatic fluids exsolved from carbonatite magmas but, as of yet, there has been comparatively little published on this aspect of carbonatite genesis. The little information that is available, however, shows a fluid evolution that is repeated among many carbonatites (Rankin, 1975; Nesbitt and Kelly, 1977; Andersen, 1986; Ting *et al.*, 1994; Morogan and Lindblom, 1995; Samson *et al.*, 1995a). Typically, there is a single, low salinity, carbonic fluid which evolves into a low CO₂/H₂O, moderate to high salinity fluid and a moderate to high CO₂/H₂O, low salinity fluid (Andersen, 1986; Morogan and Lindblom, 1995; Poutianien, 1995). The composition of these inclusion fluids is varied and is reflected by the numerous carbonate, sulphate, halide and oxide daughter/trapped minerals which they contain (Rankin, 1975; Nesbitt and Kelly, 1977; Ting *et al.*, 1994; Samson *et al.*, 1995b).

This paper uses data obtained from primary fluid inclusions in apatite, hosted by calciocarbonatite, and in quartz and feldspar, hosted by fenitized sandstone, to reconstruct the PTX conditions of evolving aqueous fluids exsolved during emplacement of carbonatites at Amba Dongar, India.

Geology

The Amba Dongar complex is located approximately 400km northeast of Bombay, India in the western part of the Deccan volcanic province (Fig. 5-1). The intrusion of carbonatite magma, during the late Eocene, coincided with the extrusion of flood basalts, with which the carbonatites are spatially associated. The complex is situated adjacent the Narmada rift, which was opened along a site of earlier faulting as India moved over a mantle plume (Karkare and Srivistava, 1990; Simonetti *et al.*, 1995).

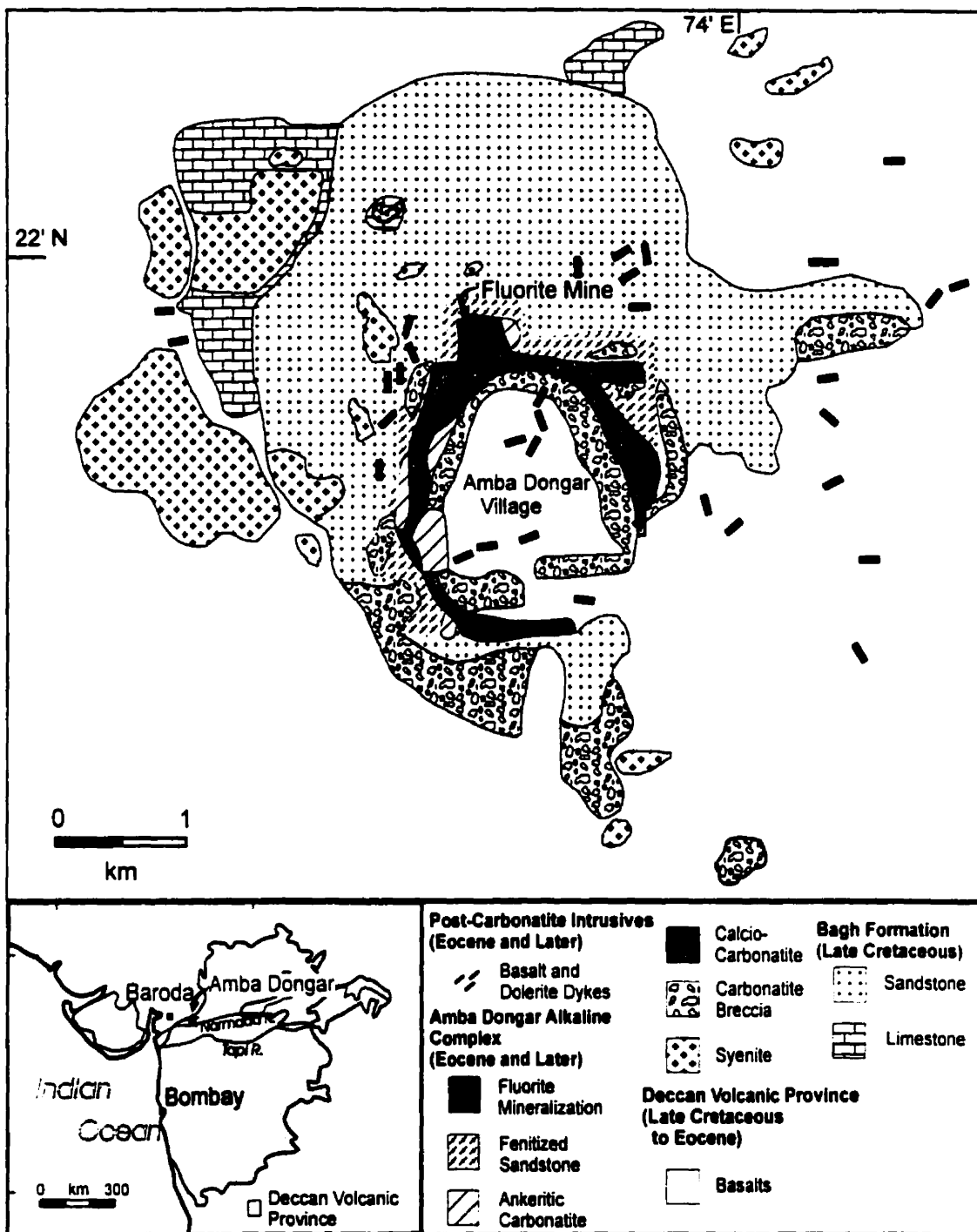
The complex consists of an outer ring of carbonatite breccia and an inner ring of calciocarbonatite, which form the main topographic feature of the ring. Numerous plugs of fine-grained ankeritic carbonatite are concentrated along the west and northwest edges of the ring structure, while bodies of syenite are randomly distributed in the surrounding country rocks. The complex hosts large quantities of fluorite (11.6Mt of 30% CaF_2) which are currently being exploited, and locally contains ore grades of LREE (up to 10% (Viladkar, pers. comm.)).

Deans *et al.* (1972) and Viladkar (1981) have developed a chronological sequence for intrusion of the ring. Initial faulting at Amba Dongar was triggered by a highly fluidized liquid which formed the ring of carbonatite breccia and provided a pathway for later melts which crystallized calciocarbonatite. Following emplacement of the main ring, iron-rich melts were intruded to form the smaller bodies of ankeritic carbonatite. Deposition of the large fluorite deposit was the last event, and resulted from interaction of late stage orthomagmatic fluids with meteoric water (Palmer and Williams-Jones, 1996).

Carbonatites

Calciocarbonatite, which forms the dominant lithology of the ring, is composed of equigranular grains of calcite with accessory apatite, hematite, pyrochlore and

**Figure 5-1 The geology of the Amba Dongar complex and surrounding area
(modified from Deans et al., 1972)**



fluorite. The grain size is highly variable and, porphyritic varieties, consisting of large calcite phenocrysts set in a matrix of finer grained calcite, occur locally. Flow banding is evident as an alignment or segregation of accessory minerals.

Ankeritic varieties of carbonatite are easily distinguished from calciocarbonatite, by their red colour, and fine-grain size. Pseudomorphs of hematite after magnetite are common in the ankeritic carbonatite, and can comprise up to 50% of the rock, by volume. Accessory minerals include fluorite, barite, bastnaesite, pyrochlore and monazite. Small dykes of ankeritic carbonatite are commonly found within the calciocarbonatite.

Fenites

An aureole of potassic metasomatism is well developed in sandstones surrounding the carbonatites. Sodic and sodic-potassic fenitization of sandstones is also reported but is only found in drill core and is not exposed on surface (Viladkar, 1986). Roelofsen (1997) has determined that the precursor to many sodic fenites is ijolite and not sandstone, as was originally thought (Viladkar, 1986).

The precursor of potassic fenites in all cases is quartzitic sandstone of the Late Cretaceous Bagh formation. The quartz-rich nature (>96% SiO₂) of the host rock facilitates the identification of potassic fenites, which consist of variable proportions of quartz and secondary potassium feldspar. Potassic metasomatism varies in intensity with distance from the margin of the intrusion, with fenites proximal to carbonatites containing over 80% potassium feldspar and those at distances of approximately 150m away containing less than 5%. The feldspar minerals are microcline and orthoclase, with the former predominating (Roelofsen, 1997). Muscovite is present in the fenites, although in small quantities (<5%), and only in the higher grade fenites proximal to carbonatite.

Fluid Inclusions

Primary fluid inclusions were identified in apatite and calcite, in calciocarbonatite, and in quartz and feldspar within potassically fenitized Bagh sandstone (Fig. 5-2).

Fluid Inclusions in Apatite

Fluid inclusions in apatite may be subdivided into four groups: liquid-rich, liquid-vapour inclusions (LV); vapour-rich, liquid-vapour inclusions (VL); liquid-vapour inclusions containing up to two solids (LVS); and liquid-vapour inclusions containing more than two solid phases, or multiphase inclusions (LVMS). Over 50% of inclusions in apatite are LV type inclusions, approximately 30% are LVS inclusions and less than 20% are LVMS inclusions.

Apatite in calciocarbonatite hosts only primary inclusions, which are typically restricted to the cores of crystals (Fig. 5-3). Fluid inclusion shapes range from spherical to cylindrical (parallel to the C axis), and their dimensions can range from microns to tens of microns in diameter, or length. Inclusion shape or size cannot be used to discriminate among different groups of inclusions, except for VL inclusions which are invariably spherical. The vapour in LV and VL inclusions occupies from 10 to over 90% of the volume of an inclusion. Some inclusions contain a second liquid, CO₂ (see below). LVS inclusions typically contain less than 40 vol.% vapour and less than 20 vol.% solids, while LVMS inclusions contain less than 40 vol.% vapour, but typically over 50 vol.% of solids. The latter inclusions are thought to represent solid-bearing inclusions described by Roedder (1973).

Petrographic examination of LVMS inclusions indicates that up to five solid phases can be present in a single inclusion. Solids in LVS inclusions are typically colorless, with one being strongly birefringent and the other weakly birefringent. LVMS inclusions can contain a colored mineral, pale to dark green in plane polarized light, an opaque phase and birefringent and nonbirefringent, colorless minerals.

Figure 5-2 Fluid inclusions in apatite (calciocarbonatite) and quartz (fenite) at Amba Dongar. A) CO₂-rich vapour-liquid (VL) inclusion in apatite; B) Coexisting LV and VL inclusions in apatite; C) CO₂-bearing LVS inclusion in apatite with only one solid phase; D) LVS inclusion in apatite with only one solid phase; E) LVS inclusion in apatite with two solid phases; F) LVS inclusion in apatite with two solid phases; G) LVMS inclusion in apatite with three solid phases; H) LVMS inclusion in apatite with at least five solid phases; I) LV inclusion in quartz in fenitised sandstone; J) CO₂-bearing LV inclusion in quartz in fenitised sandstone; K) SEM image of an opened LVMS inclusion containing two carbonate minerals and potassium sulphate (arcanite – K₂SO₄); L) SEM image of solids from LVMS inclusions on the surface of apatite crystal. The solids include carbonates and K-, Na- and Al-bearing silicates.

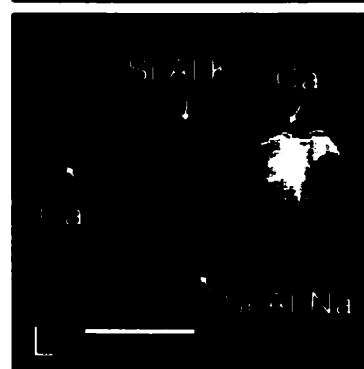
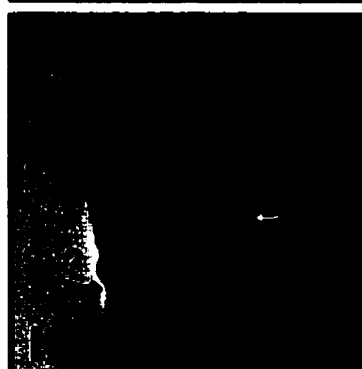
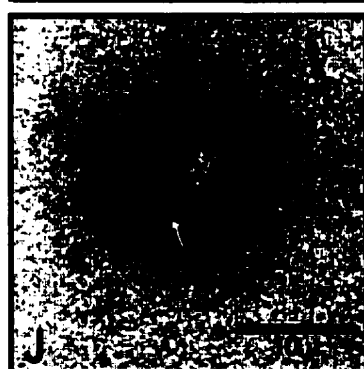
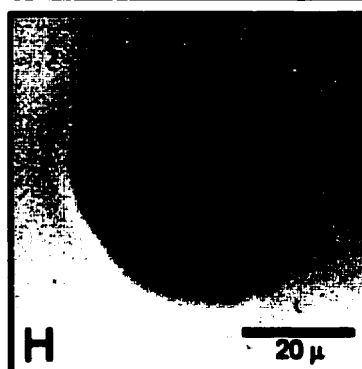
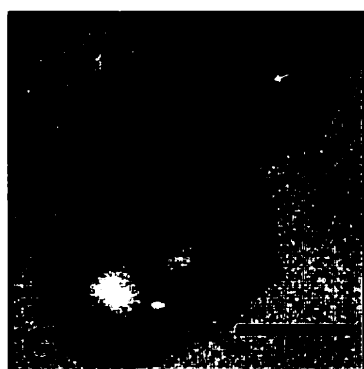
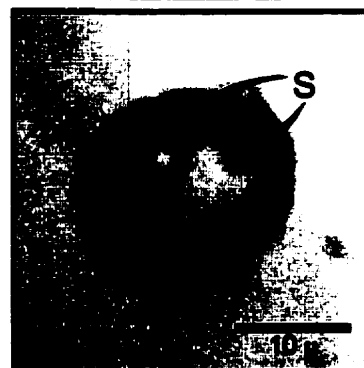
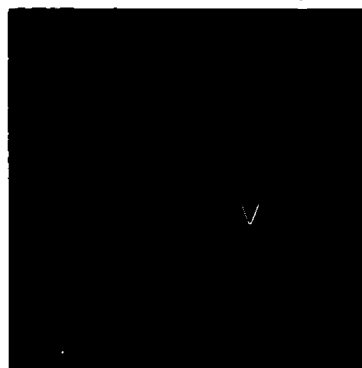
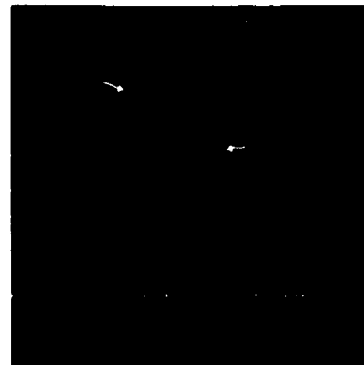
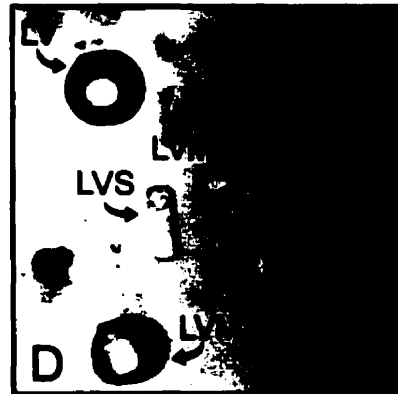


Figure 5-3 Photomicrographs of fluid inclusion-bearing apatite crystals in calciocarbonatite. Microphotographs A, B and C show groupings of fluid inclusions in the center of crystals. Microphotograph D is a magnification of the apatite crystal in C, showing that inclusions comprise a random distribution of LV-, VL-, LVS- and LVMS-types.



Solids

Solids in LVMS inclusions were identified by SEM analysis of opened fluid inclusions following the methods of Metzger *et al.* (1977) (Fig. 5-2K,L). The most commonly observed solids produce spectra for Ca, Ca-Mg-Fe, Ca-Sr, Ca-Sr-La and Ca-Na-K (Table 5-1). The lack of silicon and the petrographic characteristics of the various crystals, suggest that they are carbonate or bicarbonate minerals, probably calcite, Mg-Fe calcite, burbankite ($\text{Ca}_3(\text{Sr,Ba,La,Ce})_3(\text{CO}_3)_5$) and possibly nahcolite ($\text{NaH}(\text{CO}_3)$) or gregoryite ($(\text{Na,K,Ca})_2\text{CO}_3$), respectively. One opened inclusion contained four distinct phases, namely arcanite? (K_2SO_4), ankerite, calcite, and a much smaller fourth solid which contains silica (Fig 5-2K). A number of crystals were found on the surface of apatite which also contain silica (Fig5-2L). Three distinctly different crystal types were recognized, based on composition. These contain Ca-Sr-Si-Mg, Si-Sr-Al-K-Ca and Si-Sr-Al-Na-Ca, and may represent mixtures of carbonates and silicates or minerals of the cancrinite series. In Si-bearing solids, strontium contents may be exaggerated due to the interference between Si and Sr spectral lines (Poirier, pers. comm.).

Fluid Inclusions in Calcite

Two populations of fluid inclusions were observed in calcite of calciocarbonatite, namely liquid- (>60%) and vapour-rich varieties of liquid-vapour inclusions (LVcc, VLcc). The distinction between primary and secondary inclusions is difficult, however, a division was made between inclusions occurring along planes (secondary) and those which are randomly distributed within the host mineral (possibly primary). Both LV and VL inclusions are small, <10 μ in diameter, and irregularly shaped. Although all inclusions contain both liquid and vapour, the volume ratios of these phases span a range from 0.1 to just under 1. SEM analyses of opened fluid inclusions in calcite revealed that a small proportion contain a Sr-rich mineral, probably strontianite, however, no solid-bearing fluid inclusions were recognized using a petrographic microscope.

Table 5-1 SEM analyses of inclusion solids

ID#	S-1	S-2	S-3	S-4	S-5	S-6	S-7	S-8	S-9
	Cc	Sl-Sr	Cc+Str	Cc	Cc+Si-Al-K	Cc+Si-Al-Na	Arc + Cc	Fe-Mg Cc	Cc + Fe
cat. % (renormalized)									
Si	0.68	36.70	n.d.	4.08	29.81	24.71	0.90	0.14	0.24
Al	0.03	0.21	n.d.	0.48	4.03	4.39	0.42	0.09	0.19
Ca	97.07	49.14	77.98	91.27	51.44	55.85	60.82	82.32	94.27
Mg	0.27	1.27	2.69	1.51	n.d.	n.d.	n.d.	7.32	0.56
Fe	0.78	0.83	n.d.	0.15	0.74	n.d.	0.23	4.87	1.32
Na	0.21	1.22	0.60	0.04	0.24	6.04	1.03	1.25	0.79
K	n.d.	n.d.	n.d.	0.01	4.93	0.27	19.23	1.02	0.87
S	n.d.	n.d.	n.d.	0.14	n.d.	0.78	15.87	1.82	1.20
Ba	0.12	0.61	1.20	0.23	n.d.	n.d.	0.71	0.28	n.d.
La	n.d.	0.03	0.00	0.01	0.01	n.d.	n.d.	n.d.	n.d.
Sr	0.83	10.00	17.53	2.08	8.81	7.98	0.80	0.89	0.55

Cc - calcite; Str - strontianite; Arc - arcanite

n.d. - not detected

Fluid Inclusions in Quartz and Feldspar

Primary fluid inclusions hosted by quartz in fenitized sandstone are irregular in shape and range from a few microns to tens of microns in diameter (Fig 5-2I,L). They are predominantly LV inclusions (>90%), although some vapour-rich inclusions are present. The latter increase in frequency with increasing intensity of fenitization. In liquid-rich varieties, vapour bubbles make up less than 20% of the inclusion volume.

The fluid inclusions analysed in fenites were hosted by quartz overgrowths on pre-existing quartz grains and are deemed primary (Fig. 5-4). Support for their primary origin comes from petrographic observations which reveal the absence of quartz overgrowths in unaltered sandstone, and their increasing frequency with increasing intensity of fenitization. Although large losses of SiO₂ from sandstone during fenitization imply that quartz underwent extensive dissolution it is also plausible that, due to local disequilibrium, this dissolution was accompanied by some precipitation of quartz which produced the polygonal quartz overgrowths that trapped the fenitizing fluid.

Owing to the nature of the host mineral, fluid inclusions in feldspar are uncommon, and where present, are small (<5 μ) and irregularly shaped. The turbid nature of the feldspar makes identification of primary or secondary origins nearly impossible, however, microthermometric data were obtained on a small number of feldspar-hosted inclusions.

Microthermometry

Fluid inclusion microthermometry was carried out on fluid inclusions within apatite, calcite, quartz and feldspar using a Fluid Inc. modified, U.S.G.S gas flow, heating/freezing stage (Reynolds, 1992). Accuracies of $\pm 0.2^{\circ}\text{C}$ and $\pm 1.0^{\circ}\text{C}$ were achieved for subzero and higher temperatures, respectively, by calibration using synthetic CO₂ and H₂O inclusions. Results are presented in Table 5-2 and Figure 5-5.

Figure 5-4 Photomicrograph of secondary quartz overgrown on quartz grain in fenitised sandstone. The overgrowth imparts a hexagonal form not seen in quartz grains of unaltered sandstone.



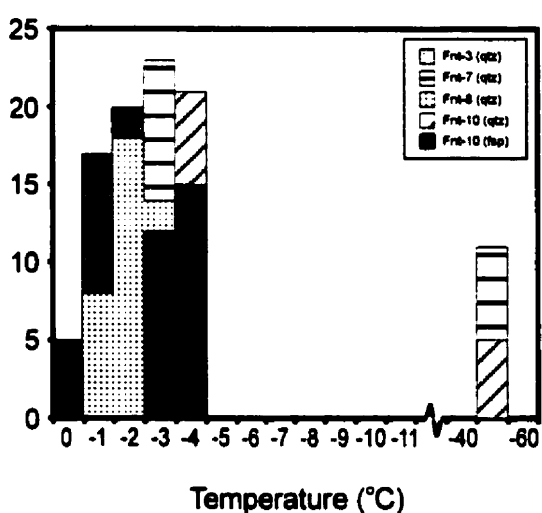
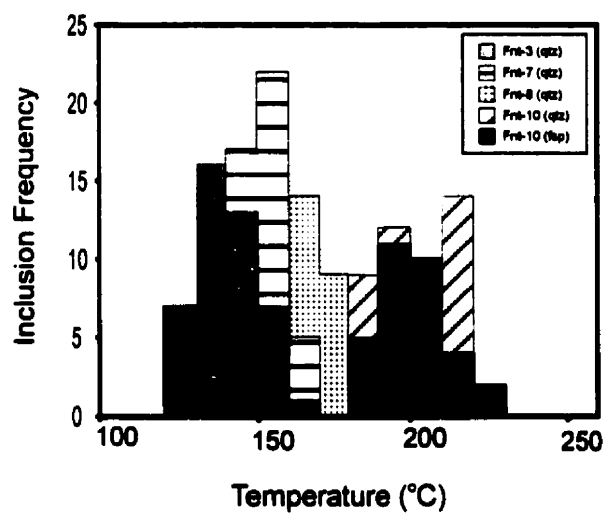
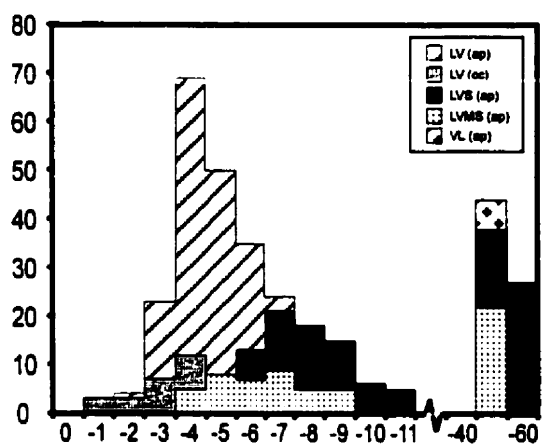
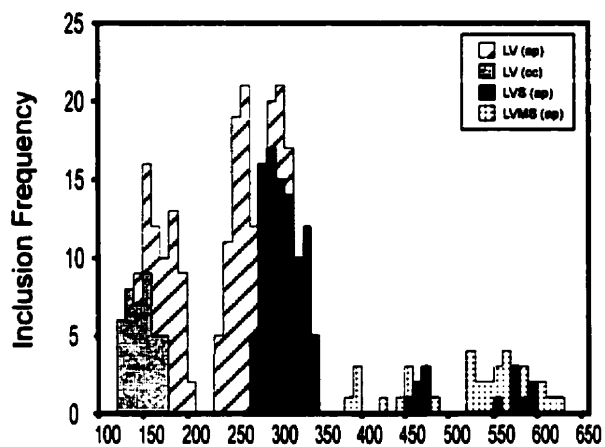
Table 5-2 Fluid inclusion data

Type	#inclusions	Th + (mean) °C	Te °C	Tmice °C	Salinity wt. % NaCl-KCl eq.
*LV (ap)	224	142 - 341 (254)	>-27	-2.1 to -8.2	3.4 - 11.4
*LVS	107	271 - 584 (335)	>-27	-2.6 to -11.8	4.1 - 15.2
*LVMS	38	324-628 (521)	>-27	-4.3 to -9.4	6.5 - 12.7
*LV (cc)	40	120 - 191 (155)	>-27	-1.2 to -8.3	2.0 - 12.1
**LV (qtz)	208	122 - 262 (180)	>-23	-0.7 to -5.2	1.5 - 8.5

* Salinity calculated using Na/Na+K ratio of 0.75 (Hall *et al.*, 1988)

** Salinity calculated using Na/Na+K ratio of 0.90 (Hall *et al.*, 1988)

Figure 5-5 Histograms showing A) homogenization temperatures for fluid inclusions in apatite and calcite; and B) final ice melting temperatures; C) homogenization temperatures for fluid inclusions in quartz; and D) final ice melting temperatures.

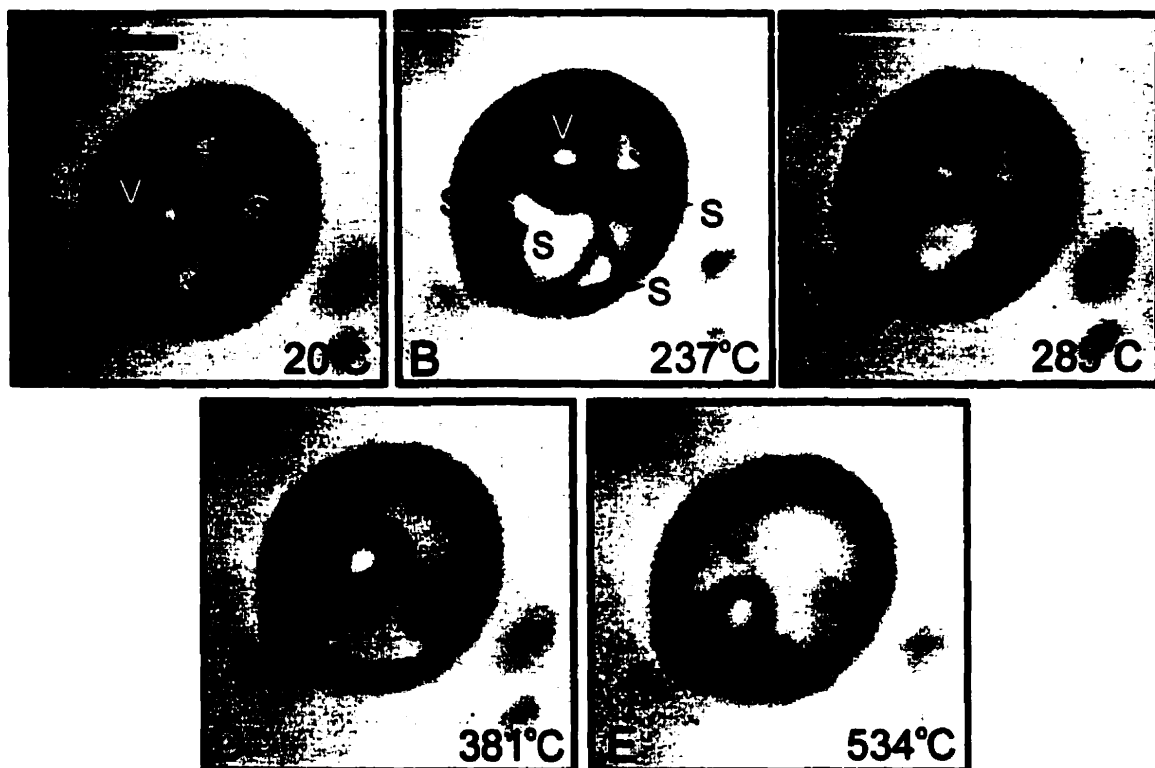


Results from Apatite

Homogenization temperatures of LV fluid inclusions hosted by apatite in calciocarbonatite range between 148 and 342°C, with three distinct populations ranging between 148 and 208°C, 230 and 300°C and 280 and 342°C. Homogenization temperatures of vapour-rich inclusions could not be determined due to the shape of the inclusion (ovoid) or decrepitation prior to homogenization. Homogenization of vapour to liquid in the majority of LVS inclusions occurs at temperatures similar to those for LV inclusions, i.e., between 270 and 340°C. Small numbers of LV inclusions homogenise at significantly higher temperatures, mainly between 450 and 470°C and 550 and 590°C. Final homogenization of fluid inclusions is typically by daughter mineral dissolution. In the case of inclusions containing only one solid, this temperature is between 430 and 498°C. The final homogenization of LVS inclusions containing two solids is similar, i.e., between 406 and 481°C. By contrast, the other solid dissolves at much lower temperatures, namely between 150 and 214°C. The liquid and vapour phases in inclusions containing more than two solids (LVMS) homogenize at much higher temperatures than LVS inclusions, i.e., between 384 and 628°C. Daughter minerals dissolve over a wide interval of temperature. However, four distinct groups of dissolution temperatures can be discerned at, 120 to 178°C, 218 to 265°C, 340 to 364°C and 417 to 488°C. These sub-groupings presumably represent different minerals (Fig. 5-6).

Temperatures of initial melting of ice (T_e) in LV inclusions were all greater than -27°C, well above the observed melting points of fluids containing CO_2 or CaCl_2 and are interpreted to reflect dominance by NaCl (+ KCl). Sub-groups of LV inclusions discerned from homogenization temperatures are not evident from their melting behaviour. Final ice melting temperatures of liquid-vapour inclusions range between -8.2 and -2.1°C, corresponding to salinities of 12.5 to 3.8 Wt.% NaCl eq. (Hall *et al.*, 1988). Most LV inclusions show an inverse correlation between ice melting and homogenization temperatures. VL inclusions commonly melt at temperatures between -56.8 and -57.6°C, consistent with the presence of significant concentrations of CO_2 and minor

Figure 5-6 Photomicrographs of LVMS inclusion in apatite showing phase changes during heating. A) At 20°C the vapour bubble is deformed by solid phases, and no liquid is observable. B) at 237°C the liquid phase is visible and five separate solids can be identified. C) Dissolution of solids progress (285°C) and at 381°C (D) only three solids remain, including an opaque. E) At 534°C the opaque mineral is still present, the one remaining transparent solid has almost dissolved and the vapour bubble has begun to shrink in size. Decrepitation of the inclusion occurred before fluid homogenization or dissolution of the opaque (548°C).



concentrations of another gas, probably CH₄ and/or N₂ (Burrus, 1981). With further heating of inclusions containing a second liquid, the CO₂ fraction homogenizes to vapour between 29.3 and 30.2°C. CO₂ triple point and homogenization temperatures indicate that up to 0.3 XCH₄ is present in the inclusion fluids (Burrus, 1981).

Unlike LV inclusions, T_e values of solid-bearing inclusions show a bimodal distribution. The first sign of melting occurs at temperatures less than -56.6°C, while the second is at temperatures greater than -27°C. The lower eutectic ranges between -56.7 and -62.3°C, for LVS inclusions, while that of LVMS inclusions has a much narrower range, between -57.6 and -58.0°C. The occurrence of melting well below -56.6°C, the eutectic temperature for the system CO₂-H₂O, indicates the presence of significant quantities of dissolved CH₄ and N₂ in the inclusion fluids. The majority of solid-bearing inclusions have initial temperatures of ice melting in the range of -27 to -24°C, i.e., close to the metastable eutectic for the NaCl-KCl-H₂O system (Roedder, 1984). These inclusions have a slightly wider range of temperatures of final ice melting than LV inclusions. LVS inclusions show the greatest range of T_{mice} values, between -11.8 and -2.6°C, corresponding to salinities of 16.4 to 4.6 Wt.% NaCl eq. (Hall *et al.*, 1988), while LVMS inclusions have a more restricted range between -9.4 and -4.3°C (13.9 to 7.2 Wt.% NaCl eq.). Temperatures at which CO₂ liquid homogenizes to vapour range between 24 and 30°C.

Results for calcite

The temperature of homogenization of LV fluid inclusions hosted by calcite from carbonatite ranged between 120 and 192°C. Sub-groupings occur within the data and are centered at 190, 180, 160 and 150°C, and typically represent distinct samples. Homogenization temperatures could not be measured for inclusions in which vapour occupies greater than 20 vol%.

Temperatures of initial ice melting were all greater than -27°C, corresponding to the NaCl + KCl system and well above the melting points of fluids containing CO₂ and CaCl₂. Temperatures of final ice melting of liquid-vapour inclusions range between -9.2

and -1.2°C , corresponding to salinities of 13.6 to 2.3 Wt.% NaCl eq. (Hall *et al.*, 1988). The sub-groups discerned from homogenization temperatures are absent in the low temperature data. Temperatures of melting for vapour-rich inclusions occur between -56.8 and -57.6°C indicating the presence of significant amounts of CO_2 . The triple point temperature suggests a small amount of another gas, most probably CH_4 . With further heating, CO_2 liquid homogenized to vapour between 29 and 30.2°C .

Results for Quartz and Feldspar

The majority of fluid inclusions analysed in fenites were hosted by quartz, with only one sample yielding inclusion measurements for feldspar. Homogenization temperatures for liquid-vapour inclusions ranged between 120 and 262°C , with the higher temperatures corresponding to more strongly fenitized samples. The mean and median of the homogenization temperatures of liquid-vapour inclusions in feldspar are similar to those in quartz from the same sample. As with fluid inclusions in apatite and calcite, vapour-rich inclusions yielded no homogenization temperature data.

Temperatures of initial ice melting in liquid-vapour inclusions in quartz were all greater than -23°C , indicating that the fluid is an aqueous NaCl ($\pm\text{KCl}$) solution with little or no dissolved CO_2 . Final ice melting occurs at higher temperatures and over a smaller range than those in carbonatite, i.e., between -0.7 and -4.9°C , corresponding to salinities of 1.5 to 7.9 Wt.% NaCl eq. (Hall *et al.*, 1988). However, the inverse correlation between liquid-vapour homogenization and final ice melt temperatures observed for LV inclusions in apatite is still evident in quartz-hosted LV inclusions. Vapour-rich inclusions in quartz have a triple point of -56.4 to -56.8°C , indicating the presence of CO_2 . Further heating caused homogenization of CO_2 liquid to vapour between 29.8 and 31°C .

Decrepitates

In order to more fully characterize the composition of the fluids, analyses of fluid inclusion decrepitate residues were performed on polished sections of apatite and calcite,

and quartz, from carbonatite and fenite, respectively. Cleaned, fluid inclusion-bearing chips were heated to 450°C, carbon-coated and the decrepitate residues analysed using a Jeol superprobe, equipped with a Tracor Northern Energy Dispersive Spectrometry (EDS) system. In order to minimize errors resulting from evaporation and NaCl-KCl creep (Haynes *et al.*, 1988), the time interval between decrepitation and analysis was kept to a maximum of two hours.

Results

Decrepitate residues were found on all sample surfaces and consisted of irregular, roughly spherical mounds in quartz and apatite, and linear ridges which generally developed along cracks or cleavage planes in calcite. The residues were most densely concentrated on calcite, followed by quartz, then apatite.

Apatite

The analysis of decrepitate residues by EDS on apatite, or calcite, creates some difficulties in evaluating true composition, as the substrate causes background contamination of elements such as Ca, an element that is potentially in significant concentrations in the residue. Samson *et al.* (1995b) have developed a computational method for removing the substrate contribution of elements, but this is only useful for minerals which contain an element not found in the decrepitate, such as phosphorous in apatite. Analyses of residues on calcite and quartz, therefore, cannot be corrected as Ca and Si are possible fluid constituents.

Corrected analyses of apatite residues (AD061) indicate that precipitates contain significant concentrations of Na, K, Ba, Fe, S and Cl, and minor, but consistent, concentrations of La and Ce (Table 5-3). The contents of Al and Si are either minor or cannot be interpreted reliably. The correlation between the x value and C_{Ca} in Samson *et al.* (1995b) suggests that in most samples Ca is a minor component. Highly anomalous values of Ca, Si, Sr, Al, Ti and Mg were obtained for some residues but these may have

Table 5-3 EDS analyses of decrepitate residues from apatite-hosted fluid inclusions (calcioarbonatite)

Type*	Ca	Na	K	Fe	Ba	Cl	S	Si	Al	Mg	Sr	La	Ce	P	$\frac{Na}{Na+K}$	$\frac{S}{Cl}$	Charge
Cat.% (renormalized)																	
LV	0.00	35.29	1.94	0.46	0.11	54.95	7.18	0.00	0.00	0.00	0.00	0.04	0.03	0.00	0.95	0.13	-21.0
LV	0.00	37.25	1.62	0.00	0.53	55.67	4.94	0.00	0.00	0.00	0.00	0.00	0.00	0.00	0.96	0.09	-19.0
LV	0.00	37.60	0.69	0.00	0.00	52.19	6.72	1.24	0.00	0.00	0.00	0.07	0.05	0.00	0.98	0.13	-17.3
LV	0.00	27.59	7.39	4.85	0.00	30.12	28.61	0.00	0.00	0.00	0.00	0.00	0.14	0.00	0.79	0.95	-7.0
LV	0.00	22.03	17.53	0.13	0.01	34.48	20.68	0.00	0.00	0.00	0.00	0.21	0.16	0.00	0.56	0.60	-5.2
LV	0.00	34.55	8.74	2.10	0.00	43.29	8.71	1.95	0.02	0.00	0.00	0.00	0.01	0.00	0.80	0.20	-3.3
LV	0.00	45.02	2.43	0.65	0.00	44.44	7.19	0.00	0.27	0.00	0.00	0.00	0.01	0.00	0.95	0.16	-0.3
LV	0.00	37.30	2.07	0.24	0.92	49.28	9.39	0.57	0.00	0.00	0.00	0.09	0.13	0.00	0.95	0.19	-14.0
LV	0.00	36.05	3.62	0.66	0.00	53.57	5.82	0.17	0.00	0.00	0.00	0.03	0.08	0.00	0.91	0.11	-16.5
LV	0.00	39.99	1.28	0.92	0.00	48.77	8.56	0.05	0.12	0.00	0.00	0.17	0.13	0.00	0.97	0.18	-11.3
LV	0.00	32.38	6.62	5.21	0.09	38.08	17.45	0.00	0.00	0.00	0.00	0.11	0.06	0.00	0.83	0.46	-5.2
LV	0.00	25.02	15.16	0.80	1.04	41.78	14.24	1.62	0.26	0.00	0.00	0.07	0.01	0.00	0.62	0.34	-7.8
LV	0.00	30.22	9.58	0.98	0.33	46.98	9.75	1.97	0.02	0.00	0.00	0.00	0.17	0.00	0.76	0.21	-11.4
LV	0.00	44.27	4.95	0.91	0.00	40.60	8.69	0.24	0.00	0.00	0.00	0.20	0.14	0.00	0.90	0.21	4.7
LV	0.00	37.14	0.72	0.00	0.00	53.60	7.10	1.31	0.00	0.00	0.00	0.08	0.05	0.00	0.98	0.13	-19.3
LV	0.00	28.49	7.63	3.09	0.00	31.10	29.54	0.00	0.00	0.00	0.00	0.00	0.15	0.00	0.79	0.95	-8.2
LV	0.00	22.80	16.97	0.14	0.02	37.30	22.37	0.00	0.00	0.00	0.00	0.23	0.17	0.00	0.57	0.60	-8.6
LVS	0.00	17.65	35.08	4.64	0.00	3.46	34.84	0.00	0.00	0.00	0.00	0.00	0.15	0.00	0.33	10.06	34.2
LVS	0.00	18.46	36.70	4.85	0.00	4.20	35.11	0.50	0.00	0.00	0.00	0.01	0.16	0.00	0.33	8.37	35.8
LVS	0.00	17.04	36.41	0.44	0.00	4.87	38.34	0.00	0.00	0.00	0.00	0.02	0.02	0.38	0.32	7.88	29.6
LVS	0.00	16.85	37.76	0.87	0.00	5.32	38.53	0.24	0.00	0.00	0.00	0.01	0.02	0.39	0.31	7.24	30.5
LVS	0.00	13.96	32.05	0.44	0.00	6.89	43.75	0.00	0.00	0.00	0.00	0.02	0.02	0.38	0.30	6.35	17.5
LVS	0.00	13.07	36.24	1.14	0.00	6.99	41.82	0.18	0.00	0.00	0.00	0.11	0.02	0.43	0.27	5.99	22.0
LVS	0.00	15.96	32.58	1.61	1.06	8.85	36.00	3.24	0.62	0.00	0.00	0.08	0.00	0.00	0.33	4.07	23.0
LVS	0.00	18.58	30.40	1.51	0.99	8.89	35.61	3.03	0.58	0.00	0.00	0.05	0.00	0.00	0.38	4.01	23.5
LVMS	43.86	0.00	5.12	0.00	0.43	0.49	3.34	0.00	46.35	0.00	0.00	0.00	0.00	0.41	0.00	6.83	25.1
LVMS	27.65	0.30	0.72	0.35	0.07	1.11	13.95	36.72	0.51	1.70	16.77	0.03	0.01	0.00	0.29	12.56	7.0
LVMS	27.96	6.14	19.59	0.00	0.29	3.15	7.57	4.17	31.15	0.00	0.00	0.00	0.00	0.00	0.24	2.41	32.9
LVMS	30.69	6.82	3.95	17.04	0.16	3.38	13.34	6.19	18.31	0.00	0.00	0.01	0.11	0.00	0.63	3.94	24.7
LVMS	40.26	8.58	1.51	21.46	0.20	4.27	0.50	0.00	23.06	0.00	0.00	0.01	0.14	0.00	0.85	0.12	36.5
LVMS	21.03	11.83	15.50	0.25	0.05	5.79	8.93	27.34	9.25	0.00	0.00	0.02	0.01	0.00	0.43	1.54	27.7
LVMS	12.43	22.99	22.60	0.32	0.21	9.66	12.49	1.96	17.03	0.00	0.00	0.15	0.14	0.00	0.50	1.29	36.2
LVMS	11.28	27.04	20.48	0.38	0.00	11.36	19.88	0.00	0.00	0.00	0.00	0.18	0.17	2.40	0.57	1.75	32.0

* division of fluid inclusion types based on daughter mineral content

been produced by daughter minerals or trapped solids. Elevated Ca contents may indicate calcium carbonate or sulphate, while high Si concentrations in decrepitates may reflect the silicate solids discussed earlier.

Calcite

Residues of fluid inclusions hosted by calcite are similar to those from apatite, and consist predominantly of Na, K, Ba, Fe, S and Cl (Table 5-4). Because of contamination by the substrate, Ca concentrations cannot be estimated. Strontium values are consistently high, suggesting that they have not been significantly affected by substrate contamination. La and Ce are both present in most analyses, but their low concentrations, and the inability to correct for the calcite substrate, make their values unreliable. However, like Sr, they show no correlation with Ca content and suggest the presence of LREE in the residues.

Quartz

Numerous analyses of decrepitate residues were obtained on quartz from fenites of varying grade (Table 5-5). Residues contain consistently high proportions of Cl, moderate Na and lesser proportions of S, Fe and Ba. Minor concentrations of Ca and K occur in most decrepitates, and Al and Ti can be detected in roughly half of the samples. La is also present but Ce is noticeably absent. Fenite grade has little effect on the composition of precipitates, with the exception of K, which tends to be lower in samples of lower grade.

Table 5-4 EDS analyses of decreptate residues from calcite-hosted fluid inclusions (calciocarbonatite)

Type	Ca	Na	K	Fe	Ba	Cl	S	Si	Al	Mg	Sr	La	Ce	P	<u>Na</u> Na+K	<u>S</u> Cl	Charge
Cat.% (renormalized)																	
LV	89.11	1.29	3.40	0.69	0.00	0.61	0.00	0.58	0.61	1.72	0.43	0.00	0.00	0.27	0.28	0.00	4.4
LV	44.34	9.13	19.49	0.00	0.28	20.78	3.09	0.00	0.61	0.00	0.96	0.02	0.00	0.80	0.32	0.15	6.4
LV	84.89	2.52	5.33	0.00	0.00	2.94	2.14	0.00	0.00	0.00	2.10	0.05	0.03	0.00	0.32	0.73	3.8
LV	51.82	6.55	13.85	0.12	0.00	22.62	2.13	0.47	0.31	0.00	0.66	0.05	0.01	0.00	0.32	0.09	-3.2
LV	53.16	8.73	16.01	0.00	0.40	14.30	3.87	0.93	0.55	0.00	0.52	0.03	0.02	0.45	0.35	0.27	8.7
LV	81.73	3.93	6.64	0.00	0.82	5.06	0.18	1.10	0.00	0.00	0.51	0.04	0.00	0.00	0.37	0.03	5.8
LV	61.38	7.44	10.85	0.00	0.00	14.69	2.11	0.31	0.87	0.00	1.07	0.05	0.06	0.00	0.41	0.14	2.5
LV	31.36	14.38	19.67	0.00	0.00	25.65	7.69	0.00	0.09	0.20	0.33	0.01	0.00	0.00	0.42	0.30	4.6
LV	55.98	9.85	12.93	0.00	0.00	15.56	3.47	1.35	0.00	0.00	0.88	0.00	0.00	0.00	0.43	0.22	5.5
LV	37.21	15.79	17.32	0.67	0.08	19.63	8.25	0.25	0.48	0.00	0.23	0.00	0.00	0.09	0.48	0.42	9.7
LV	84.40	2.44	2.34	0.33	0.83	5.12	1.17	0.53	1.51	0.00	0.55	0.03	0.02	0.00	0.51	0.23	-0.3
LV	93.35	1.41	1.33	0.49	0.17	1.48	0.00	0.37	0.00	0.00	0.00	0.00	0.00	0.06	0.52	0.00	1.6
LV	73.38	8.91	7.97	0.25	0.98	5.33	2.02	0.00	0.09	0.00	1.07	0.00	0.00	0.00	0.53	0.38	11.2
LV	68.15	6.81	5.85	0.00	0.28	10.52	0.65	0.60	0.00	5.99	0.45	0.00	0.00	0.00	0.54	0.06	2.0
LV	90.89	3.06	2.49	0.41	0.00	0.71	0.81	0.00	0.06	0.00	0.86	0.01	0.01	0.00	0.55	1.14	4.6
LV	71.03	8.52	6.32	1.85	0.00	4.10	4.69	0.54	0.81	0.00	0.51	0.01	0.00	0.89	0.57	1.14	9.4
LV	75.85	6.63	4.62	0.09	0.00	10.48	0.77	0.00	0.60	0.00	0.79	0.00	0.04	0.09	0.59	0.07	0.4
LV	81.69	6.35	4.25	1.16	0.13	5.33	0.00	0.00	0.13	0.16	0.48	0.00	0.00	0.00	0.60	0.00	5.9
LV	85.52	4.50	2.84	0.32	0.10	1.63	1.53	0.00	0.92	0.00	1.32	0.07	0.07	0.07	0.61	0.84	5.2
LV	85.82	6.09	3.33	0.33	0.00	1.51	1.41	0.00	0.11	0.00	0.91	0.01	0.00	0.00	0.65	0.93	7.4
LV	73.26	11.34	5.70	0.37	0.00	6.12	2.03	0.25	0.19	0.00	0.45	0.04	0.02	0.00	0.67	0.33	10.1
LV	87.85	6.27	3.04	0.71	0.00	0.91	0.14	1.02	0.00	0.00	0.00	0.00	0.05	0.00	0.67	0.15	8.7
LV	91.33	1.92	0.91	0.88	0.00	0.99	0.00	1.21	0.00	0.00	2.09	0.00	0.00	0.67	0.68	0.00	2.3
LV	67.42	12.98	5.33	0.00	1.41	9.36	1.01	0.42	0.00	0.00	1.50	0.03	0.00	0.54	0.71	0.11	9.2
LV	78.52	10.37	3.82	0.00	0.00	3.02	3.20	0.13	0.18	0.00	0.76	0.00	0.00	0.00	0.73	1.06	9.6
LV	83.03	7.52	2.73	0.00	0.53	1.59	2.70	0.24	0.71	0.00	0.94	0.00	0.00	0.00	0.73	1.70	7.6
LV	90.58	5.03	1.61	0.30	0.87	0.48	0.00	0.85	0.00	0.00	0.26	0.04	0.00	0.00	0.76	0.00	6.8
LV	82.34	9.40	2.99	0.00	0.00	1.50	1.63	0.00	0.04	0.00	1.17	0.00	0.00	0.17	0.76	1.09	10.1
LV	81.90	8.24	2.61	0.81	0.00	1.70	1.81	0.00	0.50	0.00	0.18	0.05	0.03	0.82	0.76	1.06	8.7
LV	88.35	6.06	1.68	0.00	0.70	0.34	1.23	0.00	0.12	1.48	0.00	0.04	0.00	0.00	0.78	3.65	7.1
LV	78.99	10.22	1.49	0.58	1.04	3.70	0.68	0.00	0.52	0.00	1.39	0.06	0.00	0.00	0.87	0.18	8.5

Table 5-5 EDS analyses of decrepitate residues from quartz-hosted fluid inclusions (fentes)

Sample	Type	Ca	Na	K	Fe	Ba	Cl	S	Si	Al	Mg	Sr	La	Ce	P	<u>Na</u> Na+K	<u>S</u> Cl	Charge
Cat. % (renormalized)																		
Fnt-10	LV	0.77	6.54	0.18	0.00	0.00	12.93	2.24	76.84	0.08	0.00	0.00	0.00	0.00	0.00	0.97	0.17	-6.9
Fnt-10	LV	0.84	7.90	0.52	0.73	0.01	13.43	2.53	74.03	0.00	0.00	0.00	0.00	0.00	0.00	0.94	0.19	-5.5
Fnt-10	LV	0.85	12.53	1.30	0.38	0.00	19.49	1.09	62.47	1.88	0.00	0.00	0.00	0.01	0.00	0.91	0.06	-5.6
Fnt-10	LV	0.14	9.69	0.40	0.57	0.00	12.83	0.92	75.28	0.17	0.00	0.00	0.00	0.00	0.00	0.96	0.07	-2.8
Fnt-10	LV	0.00	8.45	0.00	0.17	0.88	11.41	1.60	77.31	0.00	0.00	0.00	0.03	0.00	0.00	1.00	0.14	-3.2
Fnt-10	LV	0.15	2.05	0.01	0.10	0.02	2.60	0.09	94.10	0.00	0.00	0.00	0.02	0.01	0.00	1.00	0.03	-0.5
Fnt-10	LV	0.33	7.93	0.15	0.30	0.00	7.94	0.38	82.01	0.31	0.00	0.00	0.02	0.01	0.00	0.98	0.05	0.3
Fnt-8	LV	0.42	7.27	0.00	0.24	0.00	13.67	0.78	77.56	0.00	0.00	0.00	0.03	0.03	0.00	1.00	0.06	-6.5
Fnt-8	LV	0.19	6.80	0.01	0.00	0.00	11.06	1.42	77.57	2.65	0.00	0.00	0.00	0.00	0.00	1.00	0.13	-4.9
Fnt-8	LV	0.66	16.23	0.15	0.59	0.00	20.10	7.01	54.71	0.08	0.00	0.00	0.02	0.00	0.00	0.99	0.35	-6.6
Fnt-8	LV	0.28	18.12	0.29	0.02	0.24	21.88	3.72	55.43	0.00	0.00	0.00	0.01	0.01	0.00	0.98	0.17	-5.1
Fnt-8	LV	0.83	12.05	2.03	0.00	0.15	18.12	0.75	65.59	0.00	0.00	0.00	0.06	0.04	0.00	0.86	0.04	-3.9
Fnt-8	LV	0.10	7.66	0.00	1.14	0.00	7.96	0.27	82.82	0.00	0.00	0.00	0.00	0.03	0.00	1.00	0.03	0.2
Fnt-3	LV	1.87	1.96	0.00	0.02	0.10	2.65	1.27	91.10	0.00	0.36	0.00	0.01	0.30	0.00	1.00	0.48	-0.3
Fnt-3	LV	1.91	0.73	0.42	0.41	0.00	1.37	0.30	93.78	0.00	0.58	0.00	0.00	0.01	0.00	0.63	0.22	0.8
Fnt-3	LV	1.13	2.24	0.00	0.22	0.00	3.31	0.00	93.10	0.00	0.00	0.00	0.00	0.00	0.00	1.00	0.00	-0.4
Fnt-3	LV	1.68	1.82	0.11	0.00	0.00	2.42	0.00	92.89	0.00	0.00	0.00	0.00	0.01	0.00	0.94	0.00	0.4

Discussion

Fluid Types

In order to unravel the fluid history of the Amba Dongar carbonatites, it is first necessary to determine the parageneses of the various inclusion types observed. The extreme diversity and lack of any spatial distribution of primary inclusions within a single apatite crystal poses an interesting problem. Six types of inclusion comprising two types of solid inclusions (Palmer and Williams Jones, 1998, Chap. 4) and four types of aqueous fluid inclusions can exist over areas of only tens of square microns within apatite. The aqueous inclusions can be divided into four groups based on physical characteristics, LV, VL, LVS and LVMS. Temperature and compositional information for these fluid inclusions support the divisions and provide much more accurate criteria for the discrimination of fluids than is possible petrographically. Only LV and VL fluid inclusions are hosted by calcite and by quartz overgrowths in fenites. However, the origin of calcite-hosted fluid inclusions is uncertain, and these inclusions are therefore not considered in the following discussion.

In apatite, all fluid inclusions appear to be primary and to have been trapped pene-contemporaneously, however, the wide range of compositions of aqueous fluids for different inclusion types indicate that they could not have been trapped simultaneously. As well, pressures of entrapment, based on isochoric projections of CO₂-bearing inclusions and independent temperature estimates of fluids, for different inclusion types are too widely separated for the respective inclusions to represent coexisting fluids. The only alternative, therefore, is that trapping occurred over a period of time during and following apatite growth by primary and secondary processes. At high temperatures the process of annealing fractures in a fluid medium may be efficient enough to erase the evidence of secondary processes, producing the observed primary relationships (Roedder, 1984).

Fluid compositions

In addition to physical differences, the fluid inclusions also show a number of chemical differences. Perhaps the most revealing chemical dissimilarity among inclusions is their content of incondensable gases. LV inclusions in apatite contain no measurable quantities of CO₂, whereas VL, LVS and LVMS inclusions contain appreciable concentrations of CO₂. The CO₂-bearing inclusions can be further distinguished on the basis of gas phase composition. In VL and LVMS inclusions, the gas phase is essentially pure CO₂, while in LVS inclusions it contains a mixture of CO₂ with up to 0.3 X_{CH₄} (Burrus, 1981). VL inclusions in quartz contain pure CO₂, while LV inclusions are CO₂-free.

The absence of chloride-bearing phases in either LVS (birefringent minerals) or LVMS inclusions (EDS identification) allows for the interpretation of salinities estimated from microthermometric data. Temperature-salinity relationships for LV (ap), LVS and LVMS inclusions permit clear discrimination among the three groups, although some LVS inclusions plot within the LVMS group and may be misclassified (Fig. 5-7). Salinities of solid-bearing inclusions show slightly higher values than those of solid-free inclusions. Temperatures of homogenization for LV (qtz) inclusions of fenites overlap values for LV (ap) inclusions, however salinities are lower.

Further differences among the three groups are also evident in the compositions of decrepitate residues and the nature of the solid minerals. The presence of solid phases in fluid inclusions raises the question of whether they constitute trapped or daughter minerals. The consistent volume proportions of the various solids in LVS and LVMS inclusions suggest the latter, however, the abundance of minerals in LVMS inclusions makes the discrimination between trapped solids or daughter minerals difficult. In LVMS inclusions, these minerals consist of Ca-carbonates, K-sulphate, K-Na-Al silicates and an Fe-rich opaque mineral. Unfortunately, the solids in LVS inclusions could not be identified, however, decrepitate analyses suggest some possibilities. Three groups of decrepitates could be distinguished based on their charge imbalance (either positive or negative), the presence of Ca, and their S/Cl and Na/Na+K ratios (Fig. 5-8).

Figure 5-7 Salinity versus temperature diagrams for A) apatite-hosted (calciocarbonatite) and B) quartz-hosted (fenite) fluid inclusions.

Salinity (Wt.% NaCl-KCl)

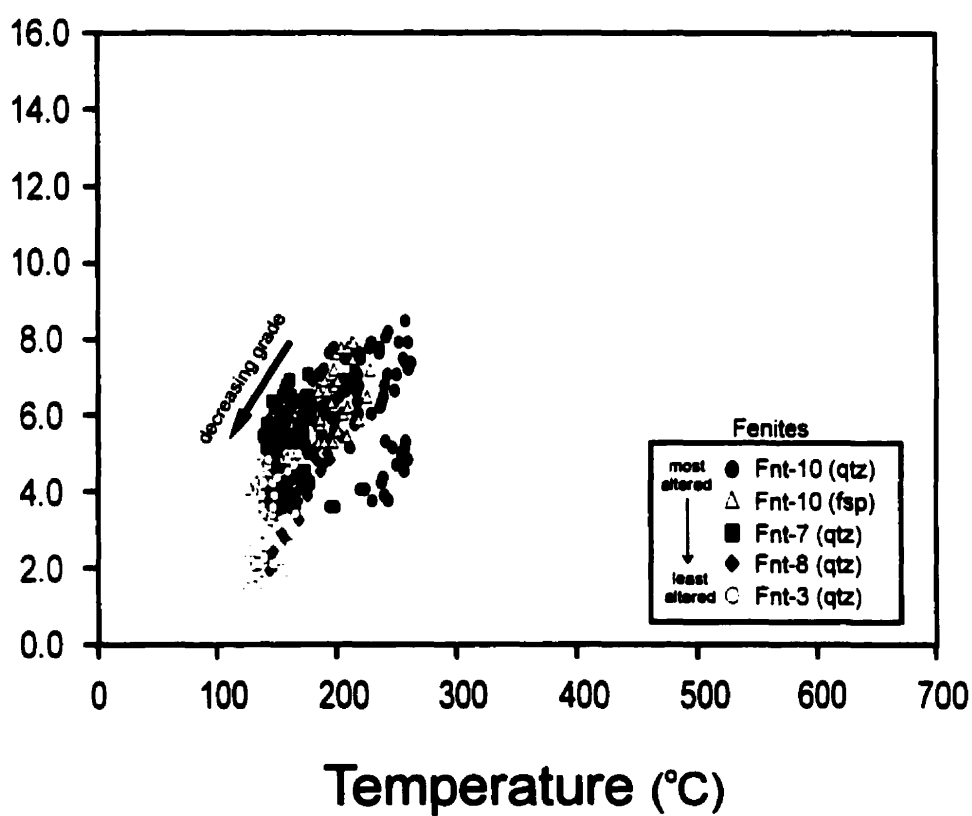
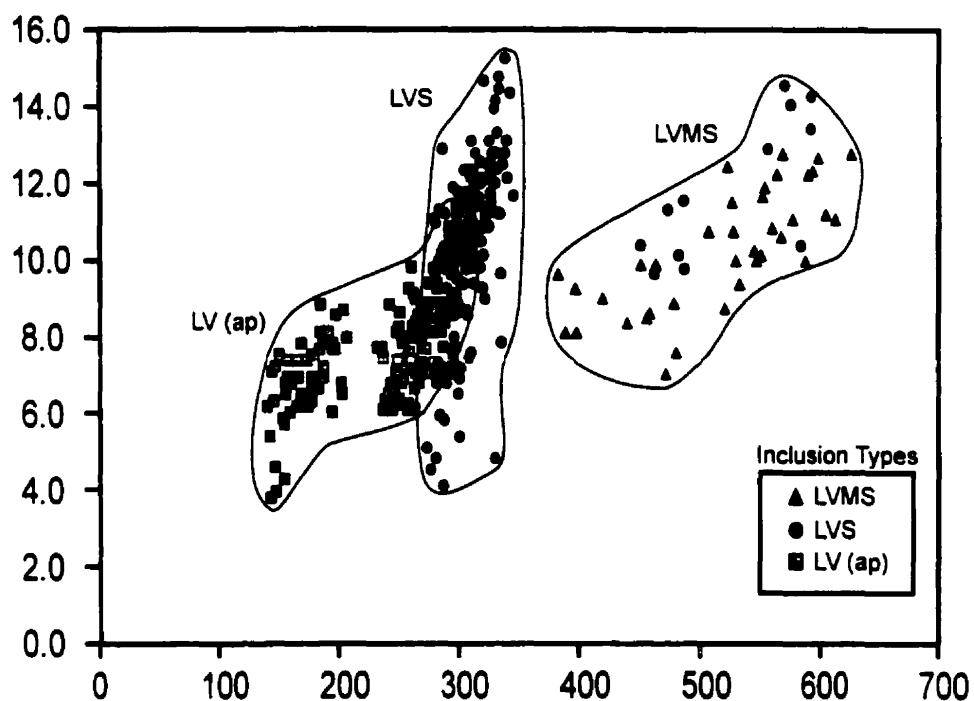
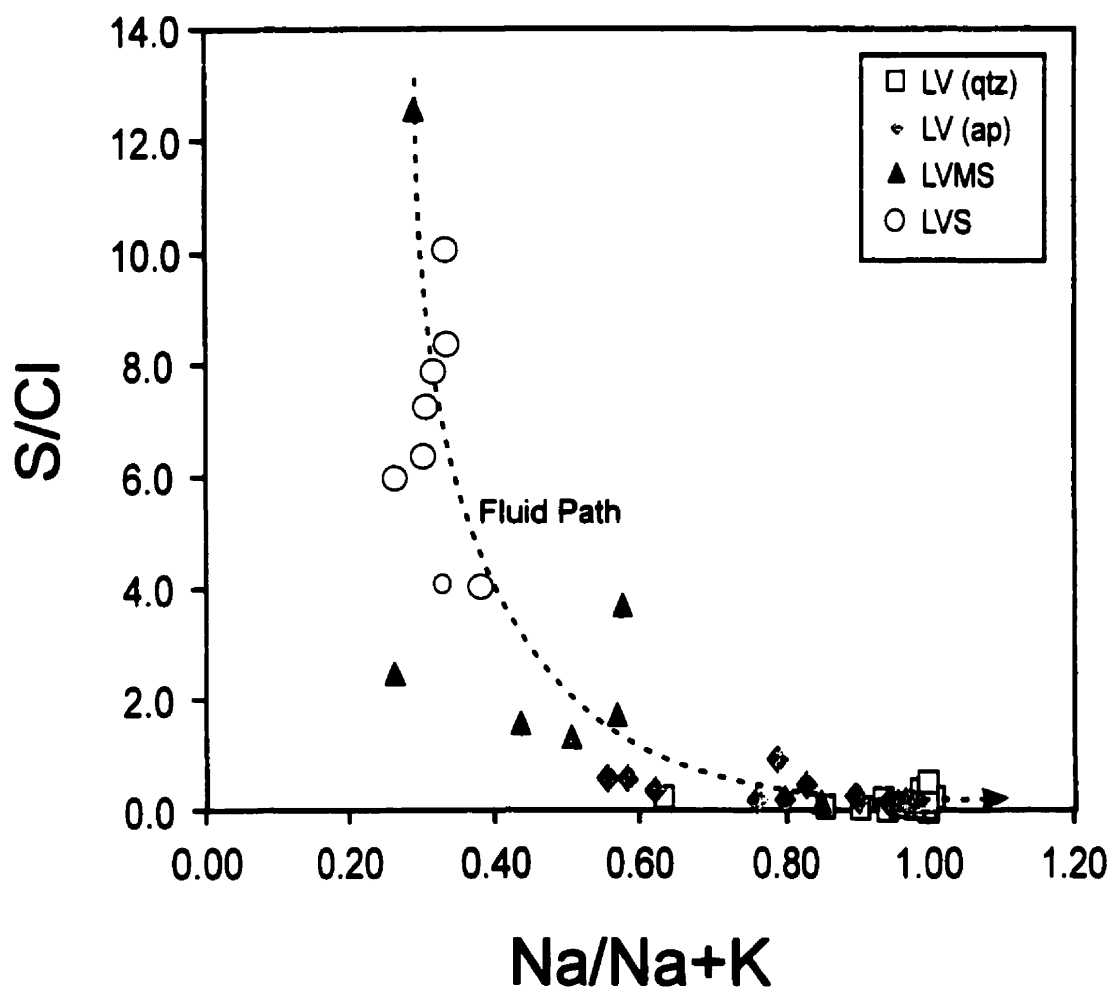


Figure 5-8 Na/Na+K versus S/Cl diagram showing compositions of decrepitate residues from LVS, LVMS, LV (ap) and LV (qtz) inclusions. Inclusions describe a trend of decreasing sulphur and increasing chlorine, with the increasing dominance of sodium over potassium, corresponding to the sequence LVS \Rightarrow LVMS \Rightarrow LV (ap) \Rightarrow LV (qtz) (path indicated by dotted line).



Residues which have high concentrations of Ca are typically low in Cl and S, indicating a dependence of Ca on some other anion, i.e., carbonate species. Na and K are both present in these residues, together with relatively high Al and in one case high Si. These decrepitate residues represent LVMS inclusions. This is inferred from previous daughter mineral identifications in which multiple (more than two) associated solids, some containing Na, K, Al and Si, were observed. One of the two Ca-deficient sets consistently shows an excess negative charge while the other shows positive charge imbalance. Na/K and S/Cl ratios also reflect the differences between the two groups (Fig. 5-8), with decrepitate residues dominated by K and S having positive charge surplus, and those that are Na-rich and dominated by the Cl⁻ ion having a negative charge imbalance. As LV inclusions are solid-free, and minerals identified in LVS inclusions cannot be halides (both birefringent), it is suggested that LV (ap) inclusions are represented by the chloride-dominated decrepitate residues, while LVS inclusions produced the S-, K-rich decrepitate residues. One of the solids in LVS inclusions is therefore interpreted to be arcanite, while the positive charge imbalance suggests that the other solid is composed of carbonate, and in the absence of Ca, may be nahcolite or kalinite (KHCO₃).

Analyses of residues from LV and VL inclusions in quartz suggest that the fluids were NaCl brines which carried significant sulfur and small proportions of Fe. Potassium is present in much smaller proportions than in other fluid inclusions, which have Na/(Na+K) ratios consistently above 0.9 (Fig. 5-8).

Analyses of decrepitate residues can be used in conjunction with microthermometric data to provide quantitative estimates of fluid compositions. Element concentrations were calculated using salinities determined from microthermometry, the ratio of Cl concentration in analyses to Cl concentration in fluid inclusions and the relationship between Cl and the various cations in decrepitate analyses (Appendix I). The proportions of CO₂ and CH₄ were calculated using FLINCOR (Brown, 1989) and estimated by the method of Burrus (1981), respectively. The concentration of HCO₃⁻ was calculated on the assumption that it is the dominant species and accounts for all anion deficiency in the decrepitate analyses.

Molal concentrations of selected elements in inclusion fluids in apatite are:

LV (ap): Na 1.44 K 0.27 Fe 0.05 Ba 0.008 Cl 1.9 S 0.53

LVS: Na 6.13 K 10.65 Fe 0.45 Cl 1.9 S 14.48 HCO₃⁻ 7.86 CO₂ >1.06 CH₄ <0.45

LVMS: Na 4.91 K 5.25 Ca 12.62 Ba 0.08 Al 8.46 Cl 2.30 S 4.69 HCO₃⁻ 11.87 CO₂ 3.25.

Although Ca, HCO₃⁻ and Al have high concentrations in LVMS inclusions, the large volume percentage of daughter minerals containing these components indicates that the values are not unreasonable. The absence of halide minerals in inclusions suggests that salinity estimates are also reasonable. The ratios of ions would, however, remain the same at any [Cl⁻], as their values are set by decrepitate analyses and an increase or decrease in [Cl⁻] would only raise or lower the absolute concentrations of other ions accordingly.

The lack of solids in quartz-hosted inclusions simplifies the calculation of absolute fluid compositions based on fluid inclusion microthermometry and decrepitate residues. The average molal concentrations of selected elements in quartz-hosted fluid inclusions are

LV (qtz) Cl 1.3 Na 0.89 S 0.143 K 0.07 Ca 0.05 Fe 0.04 Ba 0.02

LV (qtz): Cl 0.9 Na 0.66 S 0.14 K 0.02 Ca 0.24 Fe 0.02 Ba 0.004

LV (qtz): Cl 0.6 Na 0.42 Ca 0.41 K 0.33 S 0.10 Fe 0.04 Ba .01

for high, medium and low grade fenites, respectively.

Fluid Evolution

The distinct compositional and temperature trends point to the presence of at least three physically separate fluids during the formation of the Amba Dongar carbonatites. The occurrence of CO₂-bearing and CO₂-free inclusions at first glance suggests the

possibility of CO₂ immiscibility, a phenomenon which has been shown to be more common in geologic fluids than originally thought (Johnson, 1991; Duan *et al.*, 1995). The solvus position at temperatures comparable to those of entrapment (see below), however, indicates that the concentrations of CO₂ in LVS and LVMS inclusions, <0.02 XCO₂ and <0.06X CO₂, respectively, are much too low to represent the exsolution of CO₂-rich fluids from CO₂-bearing brines (Shmulovich and Plyasunova, 1993; Duan *et al.*, 1995). As well, the expected differences in salinity between the aqueous and CO₂ endmembers are not evident; LV, LVS, LVMS and even VL inclusions have overlapping salinity ranges. The fluids are therefore not considered to have been in equilibrium with each other and represent an evolutionary history of one or more fluids.

The chemical characteristics of the inclusion fluids provide the strongest evidence for the presence of an evolving orthomagmatic fluid during carbonatite emplacement at Amba Dongar. It can be assumed that hydrothermal fluids responsible for fenitization were exsolved during carbonatite emplacement and therefore represent an evolved form of one or more parental hydrothermal solutions. Given this assumption a number of chemical indicators can be used to describe the evolution of the fluids.

Figure 5-9a-c are ternary diagrams representing the composition of the four fluids, Lv (ap), Lv (qtz), LVS and LVMS in the Na-K-Cl, Na-K-S and Cl-S-HCO₃⁻ systems. In all cases, the fluids show a consistent evolutionary trend, from least evolved to most evolved, of LVS⇒LVMS⇒LV (ap) ⇒LV (qtz). In figure 5-9a this sequence corresponds to a trend of increasing Na/K with increasing Cl, while in figure 5-9b the sequence is marked by a trend of decreasing S with increasing Na/K. The same sequence of fluids is repeated when Cl and S are compared to HCO₃⁻. Figure 5-9c shows that LVS fluids evolve to LVMS fluids by decreasing S and increasing HCO₃⁻ at relatively constant Cl, and then decreasing HCO₃⁻ and increasing Cl.

Locations of fluid inclusion populations on a T-Salinity diagram also provides evidence of evolving hydrothermal fluids. In Figure 5-10 it can be seen that the slope of the trend for LVMS and LV(ap) inclusions continues through to the LV (qtz) inclusions of higher homogenization temperatures. A sharp decrease in salinity of LV (qtz) inclusions, however, occurs over the lower temperature range and corresponds to lower grades of fenitization. This may be a result of dilution and cooling of fluids through

Figure 5-9 Ternary diagrams showing compositional trends of apatite- and quartz-hosted fluid inclusions in calciocarbonatite and fenite, respectively. The systems A) Na-K-Cl⁻ and B) Na-K-S, and C) Cl⁻, S and HCO₃⁻.

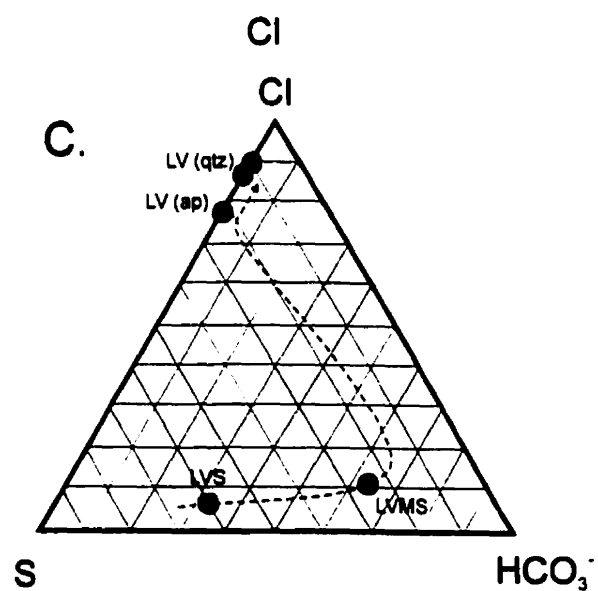
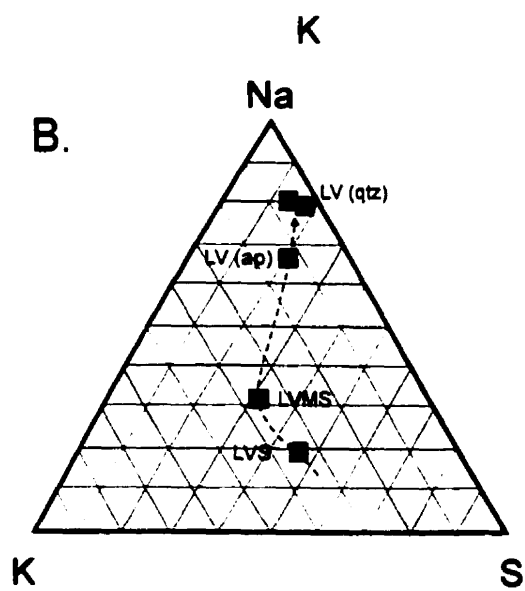
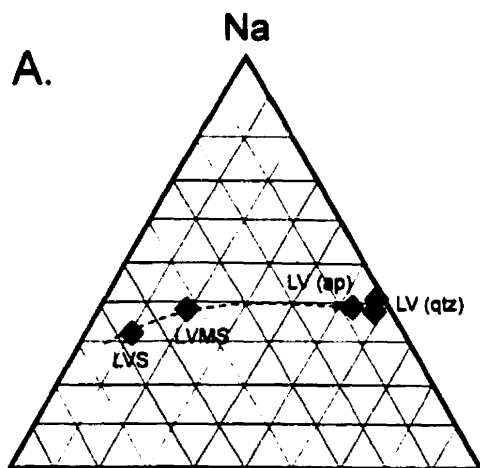
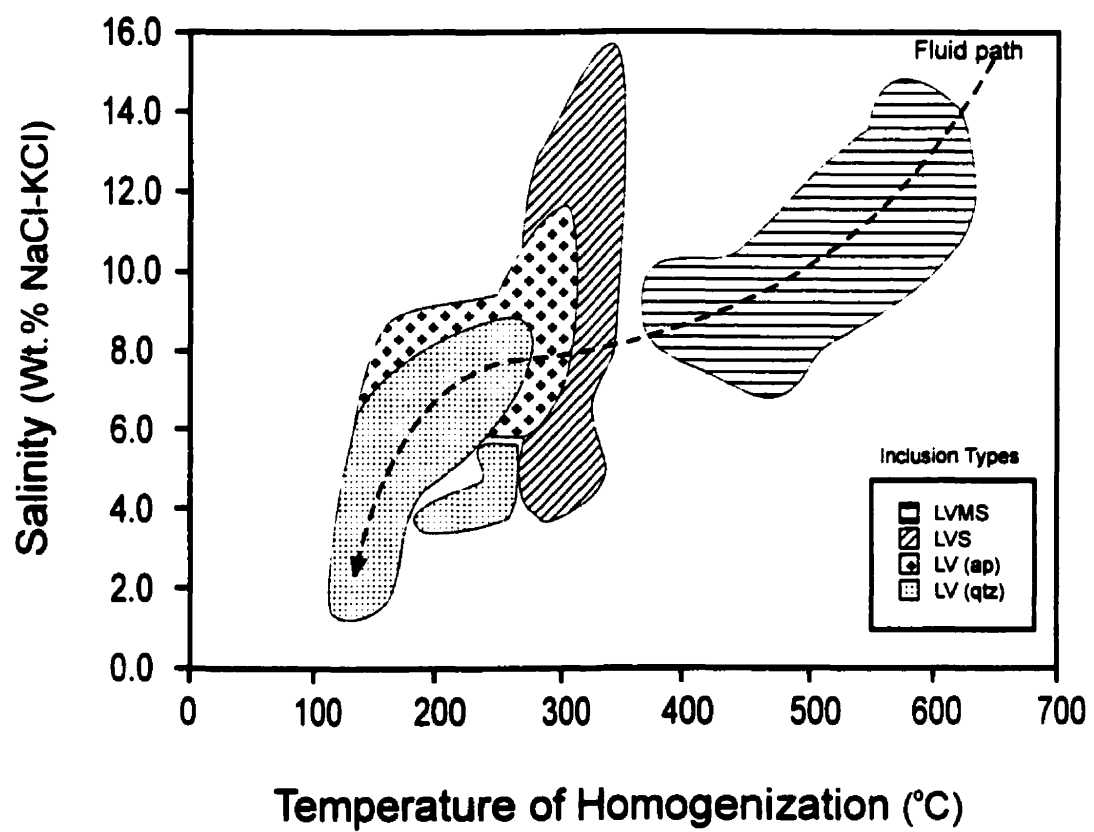


Figure 5-10 Temperature versus salinity diagram for apatite- and quartz-hosted fluid inclusions showing an inferred fluid path for LVMS and LV (ap) fluid inclusions (dotted line). LVS inclusions are not part of the proposed path as isochoric corrections place them at higher pressures than either LVMS or LV (ap) inclusions.



interaction with surrounding meteoric waters which would have effectively halted fenitization. This is confirmed by decrepitate analyses of low grade fenite-hosted inclusions (Fnt-3, Table 5-5) which indicate higher Ca concentrations and low formation temperatures ($<200^{\circ}\text{C}$), conditions similar to those determined for meteoric fluids by Palmer (1994) which were, in part, responsible for fluorite mineralization. The LVS inclusions, although represented on the graph are not involved in this particular fluid path. Isochoric projection of LVS inclusions indicate that they were formed at significantly higher pressures than LVMS or LV (ap) inclusions (see below).

Pressure and Temperature

Estimation of pressure and temperature conditions of evolving fluids is difficult. Earlier analyses of the stratigraphic location of the Amba Dongar carbonatites and CO_2 content of fluid inclusions by Palmer and Williams-Jones (1996) has shown that emplacement of the carbonatite was at shallow depth corresponding to pressures between 75 and 100 bars. Average homogenization temperatures (T_h) were determined to be 335, 521 and 254°C , for LVS, LVMS and LV(ap) inclusions, respectively. If it can be assumed that fluid trapping occurred during or after final emplacement of carbonatite, then the trapping temperatures are roughly equivalent to the homogenization temperatures. However, because of the low pressure the T_h values of LVS inclusions are much lower than expected, given that they represent the initial fluid and would have been trapped at near magmatic temperatures. It therefore follows that they were trapped at relatively high pressures, i.e., before emplacement of the carbonatites. Although homogenization temperatures of LVMS inclusions are within the range of the currently accepted eutectic temperatures for synthetic carbonatites in the system $\text{CaO-CO}_2\text{-H}_2\text{O}$ (Wyllie, 1989), it is likely that they were somewhat higher, i.e., that LVMS inclusions were also trapped at much higher pressures than those of final carbonatite emplacement. The same argument was used by Andersen (1986), Poutiainen (1995) and Samson *et al.* (1995a) to explain low homogenization temperatures of primary fluid inclusions in apatite for other complexes.

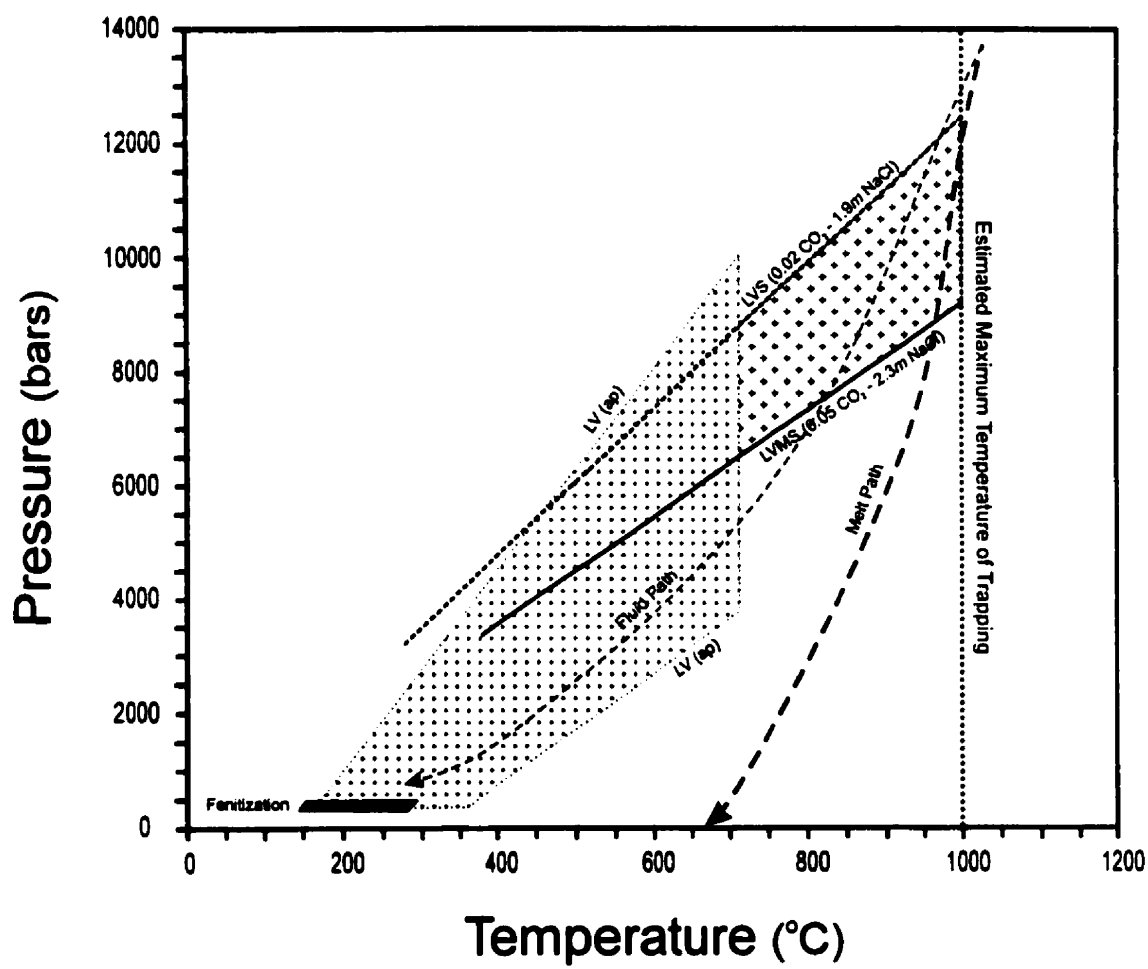
In order to reliably estimate pressure from fluid inclusions, temperature data must be evaluated independently. Studies by Palmer and Williams-Jones (1998, Chap. 4) of melt inclusions in apatite hosting the fluid inclusions indicate eutectic temperatures of approximately 700°C for calciocarbonatite and liquidus temperatures in the range 1050-1150°C. It is therefore reasonable to conclude that the exsolution of orthomagmatic fluid would have taken place between these two temperatures, i.e., after significant crystallization but before complete solidification of the magma. Assuming that this temperature was below 1000°C, the corresponding pressures would have been less than 12.5 Kb (Fig. 5-11). This pressure is equivalent to a depth of approximately 35 km, indicating that entrapment occurred near the base of the crust.

Figure 5-11 describes a probable P-T path followed by the fluids after exsolution, and the predicted sequence of trapping of fluid types along this path. Based on this reconstruction, the earliest aqueous fluids were of the LVS type, and were trapped at temperatures between 900 and 1000°C and at pressures between 11 and 12.5 Kb. The rapidly ascending LVS fluid eventually intersected isochors for LVMS inclusions at an estimated maximum temperature of 875°C and a pressure of 8 kbars. With decreasing pressure and temperature the evolving fluid traversed the conditions under which LV (ap) inclusions were trapped, estimated by the melt inclusion eutectic temperatures, to be <4 kbars and <650°C, and eventually intersected the pressure-temperature conditions of fenite formation, at <500 bars and <262°C, respectively.

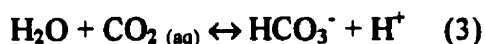
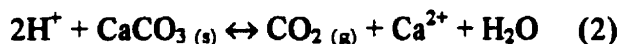
Fluid Model

From the physico-chemical conditions discussed above, it is proposed that exsolution of an aqueous fluid at Amba Dongar occurred at temperatures between 900 and 1000°C and pressures approaching 12.5 Kb, equivalent to a depth of approximately 35 kms, and was recorded by trapping of LVS inclusions. This early formed fluid was S- and K-rich and contained significant Na, Fe, HCO_3^- , CO_2 and CH_4 . Although Cl^- was not the dominant anion in solution, it was present in sufficient quantities for the fluid to be considered a moderate salinity brine. The subsequent evolution of this fluid was towards higher HCO_3^- and CO_2 concentrations and lower S, K, Na, Cl and Fe

Figure 5-11 Isochoric projection of LVS, LVMS, LV (ap) and LV (qtz) fluid inclusions. The heavy dotted line represents the assumed P-T path of the melt based on melt inclusion studies from Amba Dongar by Palmer and Williams-Jones (1998). The lighter dotted line represents the possible path of the fluid based on fluid inclusion homogenization and assumed melt temperatures. Isochores for the NaCl-H₂O-CO₂ and CO₂-free systems were calculated using FLINCOR (Brown, 1989). The maximum temperature of trapping was estimated from melt inclusion studies of Palmer and Williams-Jones (1998).



concentrations as recorded by LVMS inclusions, which were probably trapped at temperatures and pressures below 875°C and 8 Kb, respectively. The most distinguishing features of the fluid at this stage were that it contained high concentrations of Ca and was CH₄-free, the latter indicating a change in fluid composition towards a higher oxidation state. The following reactions can be used to explain the changes which are inferred to have taken place in the fluid:



With saturation of CO₂ in fluids represented by LVS inclusions, the loss of CO₂ (g) effectively reduced CH₄ concentrations through Reaction 1. VL (ap) inclusions are inferred to represent entrapment of the escaping volatiles. The escaping CO₂ would also have had the effect of driving Reaction 2 to the right, producing additional Ca²⁺, and with decreasing temperature the CO₂ would have reacted with H₂O to produce HCO₃⁻ via Reaction 3. The acidity required to drive these reactions could have been produced by the oxidation of the S-bearing LVS fluid through Reaction 4, or through the disassociation of species due to decreasing temperature. The increasing Na/K ratio from LVS to LVMS inclusions may indicate progressive reaction of the fluid with wall rocks as the magma ascended, i.e., fenitization at depth. This potassic metasomatism would have acted to drive fluid compositions toward higher Na/K ratios, which is supported by the most evolved fluids, i.e., those trapped as LV (ap) inclusions, which have Na/K ratios greater than unity.

The marked reduction in Ca, HCO₃⁻, CO₂, and most other ions from LVMS to LV(ap) fluids was probably caused by continued reaction of wall rocks as well as the crystallization and removal of the Ca-, Na- and K-bearing minerals, observed in LVMS

inclusions, as the evolving aqueous fluid cooled. These two processes could have effectively increased Na/K ratios and reduced the overall content of dissolved species to produce fluids which were trapped as LV (ap) type inclusions. The upper limits of temperature and pressure under which LV(ap) inclusions were trapped are constrained to have been below the lower estimate of conditions for LVMS inclusions (<650°C and <4 Kb), while the lower limits would have intersected the field of fenitization (<500 bars, <260°C). At shallow depths the reaction of the more evolved fluid, represented by LV(ap) inclusions, with quartzitic sandstone caused extensive growth of potassium feldspar at the expense of quartz which severely depleted the fluid in its remaining K and Al, creating high Na/K ratios in the fluid. These fluids were trapped as LV (qtz) inclusions and became progressively less concentrated with distance from the intrusion. The outer limit of fenitization was marked by interaction of the carbonatite-derived fluids with Ca-bearing meteoric waters, which diluted them further and re-introduced Ca. The temperature barrier, formed by the meteoric water cell, stopped fenitization from progressing further.

Conclusions

Fluid inclusions trapped by apatite and calcite in calciocarbonatite and quartz of potassic fenites of Amba Dongar record the complex evolution of an orthomagmatic fluid exsolved from carbonatite magma. Three types of fluid inclusion were observed in apatite and consist of LVS inclusions, which contain liquid, vapour and up to two solids (arcanite, nahcolite?), LVMS inclusions containing liquid, vapour and more than two, and up to five, solids (calcite, ankerite, arcanite, nahcolite?, Fe-oxide) and LV inclusions which contain only liquid and vapour. In calcite and quartz, inclusions are limited to LV-types.

LVS inclusions represent the first fluid exsolved by carbonatites, and were trapped at temperatures between approximately 900 and 1000°C and pressures between 11 and 12.5 Kb, corresponding to depths of 30-35 kms. Later fluids consisted, in order of trapping, of LVMS and LV(ap) types and were trapped at pressures <8 Kb and <4 Kb (<22 and <11 kms), respectively and temperatures between 650 and 875°C and 300 and

650°C. Temperatures of fenitization, based on the homogenization of LV inclusions in quartz, decreased with increasing distance from the intrusion, starting at approximately 260°C for higher grade fenites and declining to 120°C for the lowest grade fenites. Pressure conditions of fenitization were less than 500 bars and probably closer to 100 bars (Palmer and Williams-Jones, 1996), corresponding to depths of < 1.5 km.

Based on decrepitate analyses and bulk salinities, early aqueous fluids, represented by LVS inclusions, had moderate salinity (15-4 wt.% NaCl-KCl), were K-rich, Na- and Fe-bearing, and contained high concentrations of SO_4^{2-} and lesser HCO_3^- and Cl^- . Carbon dioxide was the main dissolved gas species and was accompanied by minor methane. During ascent, the fluids evolved towards lower K, Na, Fe and S concentrations, lower salinities (12-6 wt.% NaCl-KCl), higher $f\text{O}_2$ (loss of CH_4) and higher concentrations of Ca, HCO_3^- and CO_2 . LV(ap) inclusions represent the final stage in the evolution of the fluid in equilibrium with the carbonatite magmas. This stage was marked by an increase in the concentration of Na relative to K and a greater anionic dependence on Cl^- , although the salinity range was lower (11-3 wt.% NaCl). Sulphur was present in much lower concentrations and CO_2 was absent.

The reaction of the aqueous fluids, represented by LV(ap) inclusions, with sandstones surrounding the complex removed appreciable quantities of K, S and Ca, from the fluid, and resulted in much higher Na/K ratios. The salinities of these fluids, determined from LV (qtz) inclusions, were lower (8-1 wt.% NaCl eq.), and decreased with increasing distance from the margin of the intrusion.. Approximately 150m from the contact, fenitization was effectively halted by dilution and cooling of fenitizing fluids through interaction with Ca-bearing meteoric fluids.

References

- Andersen, T., 1986, Magmatic fluids in the Fen carbonatite complex, S.E. Norway: *Contrib. Mineral. Petrol.*, v. 93, p. 491-503.
- Bailey, D.K., and Hampton, C.M., 1990, Volatiles in alkaline magmatism: *Lithos*, v. 26, p. 157-165.
- Brown, P.E., 1989, FLINCOR: A microcomputer program for the reduction and investigation of fluid inclusion data: *Amer. Mineral.*, v. 74, p. 1390-1393.
- Burruss, R.C., 1981, Analysis of phase equilibria in C-O-H-S fluid inclusions: *Mineral. Assoc. Canada, Short Course Handbook 6*, p. 39-74.
- Currie, K.L. and Ferguson, J., 1971, A study of fenitization around the alkaline complex at Callender Bay, Ontario, Canada: *Canadian Journal of Earth Sciences*, v. 8, p. 498-517.
- Deans, T., Sukheswala, R.N., Sethna, S.F. and Viladkar, S.G., 1972, Metasomatic feldspar rocks (potash fenites) associated with the fluorite deposits and carbonatites of Amba Dongar, Gujarat, India: *Trans. Inst. Min. Metall. (sect. B: earth sci.)*, v. 81, p. B1-B9.
- Duan, Z., Moller, N., and Weare, J.H., 1995, Equation of state for the NaCl-H₂O-CO₂ system: Prediction of phase equilibria and volumetric properties: *Geochim. Cosmochim. Acta*, v. 59 (14), p. 2869-2882.
- Gittins, J., Beckett, M.F., and Jago, 1990, Composition of the fluid accompanying carbonatite magma: A critical examination, *American Mineralogist*, v. 75, p. 1106-1109.
- Hall, D.L., Sterner, S.M., and Bodnar, R.J., 1988, Freezing point depression of NaCl-KCl-H₂O solutions: *Econ. Geol.*, v. 83, p. 197-202.
- Haynes, F.M., Sterner, S.M., and Bodnar, R.J., 1988, Synthetic fluid inclusions in natural quartz. IV. Chemical analyses of fluid inclusions by SEM/EDA: Evaluation of method: *Geochim. et Cosmochim. Acta*, v. 52, p. 969-977.
- Johnson, E.L., 1991, Experimentally determined limits for H₂O-CO₂-NaCl immiscibility in granulites: *Geology*, v. 19, p. 925-928.
- Karkare, S.G. and Srivistava, R.K., 1990, Regional dyke swarms related to the Deccan Trap Alkaline province, India: *in* A.J. Parker, P.C. Rickwood and D.H. Tucker (eds.), *Mafic Dykes and Emplacement Mechanisms, Proceedings of the Second International Dyke Conference, Adelaide, South Australia, September, 1990*, p. 335-347.

- Kresten, P., and Morogan, V., 1986, Fenitization at the Fen complex, southern Norway: *Lithos*, v. 19, p. 27-42.
- Metzger, F. W., Kelly, W. C., Nesbitt, B. E., and Essene, E. J., 1977, Scanning Electron microscopy of daughter minerals in fluid inclusions: *Economic Geology*, v. 72, p. 141-152.
- Morogan, V., 1994, Ijolite versus carbonatite as sources of fenitization: *Terra Nova*, v. 6, p. 166-176.
- Morogan, V. and Lindblom, S. 1995, Volatiles Associated with the alkaline – carbonatite magmatism at Alnö, Sweden: a study of fluid and solid inclusions in minerals from the Långersholmen ring complex: *Contrib. Mineral. Petrol.* V 122, p. 262-274.
- Nesbitt, B.E., and Kelly, W.C., 1977, Magmatic and Hydrothermal inclusions in carbonatite of the Magnet Cove Complex, Arkansas: *Contrib. Mineral. Petrol.*, v. 63, p. 271-294.
- Palmer, D A S . 1994, Geology and geochemistry of the Amba Dongar carbonatite-hosted fluorite deposit, India: Unpublished M.Sc. thesis, McGill University, Montreal, 110p..
- Palmer, D A S . and Williams-Jones, A.E., 1996, Genesis of the carbonatite-hosted fluorite deposit at Amba Dongar, India: Evidence from fluid inclusions, stable isotopes and whole rock-mineral geochemistry: *Economic Geology*, v. 91, p. 934-950
- Palmer, D.A.S., and Williams-Jones, A.E., 1998, Carbonate-carbonate liquid immiscibility and the formation of ferrocarbonatite: evidence from melt inclusions in the Amba Dongar carbonatite complex, India: Unpublished Ph.D. thesis, McGill University, Montreal, Chapter 4.
- Poutiainen, M., 1995, Fluids in the Siilinjärvi carbonatite complex, eastern Finland: Fluid inclusion evidence for the formation conditions of zircon and apatite: *Bull. Geol. Soc. Finland*, v. 67, part 1, p. 3-18.
- Rankin, A.H., 1975, Fluid inclusion studies in apatite from carbonatites of the Wasaki area of western Kenya: *Lithos*, v. 8, p. 123-136.
- Reynolds, T.J., 1992, Fluid Inc. adapted U.S.G.S. gas-flow heating/freezing system: *Instruction Manual*.
- Roedder, E., 1973, Fluid inclusions from the fluorite deposits associated with carbonatite at Amba Dongar, India, and Okorusu, South West Africa: Metasomatic feldspar rocks (potash fenites) associated with the fluorite deposits and carbonatites of Amba

- Dongar, Gujarat, India: Discussion and contributions: Trans. Inst. Min. Metall. (sect. B: earth sci.), v. 82, p. B35-B39.
- Roedder, E., 1984, Fluid Inclusions: Reviews in Mineralogy Vol. 12, P.H. Ribbe (ed.), Mineral. Soc. Am., 644p.
- Roelofsen, J.N., 1997, The primary and secondary mafic silicates of two alkaline anorogenic complexes: Strange Lake (Quebec-Labrador) and Amba Dongar (Gujarat, India): Unpublished Ph.D. thesis, McGill University, Montreal, 489p..
- Samson, I.M., Weining, L., and Williams-Jones, A.E., 1995, The nature of orthomagmatic hydrothermal fluids in the Oka carbonatite, Quebec: evidence from fluid inclusions: Geochim. Cosmochim. Acta, v. 59, p. 1963-1977.
- Samson, I.M., Williams-Jones, A.E., and Weining, L., 1995b, The chemistry of hydrothermal fluids in carbonatites: Evidence from leachate and SEM-decrepitate analysis of fluid inclusions from Oka, Quebec, Canada: Geochim. Cosmochim. Acta, v. 59, p. 1979-1989.
- Shmulovich, K.I., and Plyasunova, N.V., 1993, Phase equilibria in ternary system formed by H₂O and CO₂ with CaCl₂ or NaCl at high T and P: Geochem. Intl., v. 30 (12), p. 53-71.
- Simonetti, A., and Bell, K., and Viladkar, S.G., 1995, Isotopic data from the Amba Dongar Carbonatite Complex, west-central India: Evidence for an enriched mantle source: Chemical Geology, v. 122, p. 185-198.
- Ting, W., Burke, E.A.J., Rankin, A.H., and Woolley A.R., 1994, Characterization and petrogenetic significance of CO₂, H₂O and CH₄ fluid inclusions in apatite from the Sukulu carbonatite, Uganda: Eur. J. Mineral., v. 6, p. 787-803.
- Viladkar, S.G., 1981, The carbonatites of Amba Dongar. Gujarat, India: Bulletin of the Geological Society of Finland, v. 53, p. 17-28.
- Viladkar, S.G., 1986, Fenitization at the Amba Dongar Carbonatite alkalic complex, India: in M. Gabriel (ed), Symposium New Mineral Raw Materials: Proceedings, p. 170-189.
- Wyllie, P.J., 1989, Origin of carbonatites: evidence from phase equilibrium studies: in K. Bell (ed.), Carbonatites: genesis and evolution: London, Unwin Hyman, p.149-176.

Bridge to Chapter 6

In the previous chapter, the PTX conditions of aqueous fluids exsolved from carbonatite were determined by microthermometric experiments and decrepitate analyses of primary fluid inclusions. In Chapter 6, the compositions of fluids responsible for fenitization are inferred from mass balance calculations based on analyses of bulk rock composition and compared to those of the fluid types discussed in Chapter 5. This method of determining fluid composition is particularly useful for trace elements and REE, which are typically in low concentrations, and are not reliably obtained from fluid inclusion analyses. The quantification of the mass changes which accompanied fenitization allowed for the calculation of the water-rock ratio, based on the amount of quartz removed and silica solubility at the conditions of fenitization. This, in turn, permitted the concentrations of the trace elements and the REE in the fluid to be determined by supplying the multiplier needed to extract these data from the mass changes experienced by the fenites.

**Chapter 6: Fenitization Associated with the Amba Dongar
Carbonatite Complex, India**

**D. A. S. Palmer and A. E. Williams-Jones
Department of Earth and Planetary Sciences
McGill University**

Abstract

The Amba Dongar complex, India, consists of a carbonatite ring structure which was intruded into Deccan basalts and Late Cretaceous, quartz-rich (>96 wt. % SiO₂) sandstones of the Bagh formation. The aqueous fluids exsolved during crystallization of the carbonatite were responsible for intense fenitization of the surrounding sandstone, manifested as the replacement of quartz by potassium feldspar.

The quartz-rich nature of the sandstone precursor facilitates the characterization of fenites, and permits accurate estimation of the mass exchanges that occurred between sandstone and fenitizing fluids. Mass balance calculations based on Gresens' (1967) volume factor method and the isocon method of Grant (1986) indicate that fenitization was accompanied by significant losses of Si and additions of K, Al, Ca, Ba, Fe, La, Ce, F, Rb, Sr, Y and HREE. Given the precursor composition, mass additions must necessarily have come from fluids, and this suggests that carbonatite-derived hydrothermal fluids contain significant K, Al, Ca, Ba, Fe, F, Rb, Sr, Y and REE, particularly the LREE.

Water-rock ratios calculated from the solubility of silica under the conditions of fenitization and mass balance estimates of SiO₂ loss indicate that a minimum of 72.2 litres of solution/100g of rock was required to produce high grade fenites (W/R = 722). Calculations based on the feldspar hydrolysis reaction and the volume of water required for fenitization indicate that a minimum of 1.2×10^{-8} m of dissolved Al was present in the initial fenitizing solutions. By contrast, calculations based on the mass of Al added during alteration and the water/rock ratio, indicate that the minimum concentration of Al in the fenitizing fluid was 1.6×10^{-3} m. This latter value is considered a more reasonable estimate of the true concentration of Al in the fluid. Concentrations of trace elements and REE calculated using mass changes in conjunction with the water-rock ratio yield values comparable to those reported for geothermal waters in alkaline igneous settings.

Introduction

The almost ubiquitous presence of metasomatic alteration haloes surrounding carbonatites provides an indirect method of studying carbonatite-derived fluids through

their interaction with country rocks. Large volumes of literature have been published on this fenitization (McKie, 1966; Currie and Ferguson, 1971; Kresten and Morogan, 1986; Viladkar, 1986; Wyllie, 1989; Roelofsen, 1997). However, only a few studies have quantified mass changes (Palmer and Williams-Jones, 1998b, Chap.8; Morogan 1994), the others being restricted to qualitative descriptions of the mineralogical and gross chemical changes of fenites.

Comparisons of the major and trace element compositions of fenite and its unaltered equivalent can be used to quantify the exchanges of mass between rock and fluid by performing simple mass balance calculations (Gresens, 1967; Grant, 1986). This method makes it possible to determine the true gains and losses of elements during fenitization possible by taking into account mass or volume changes which accompanied the alteration.

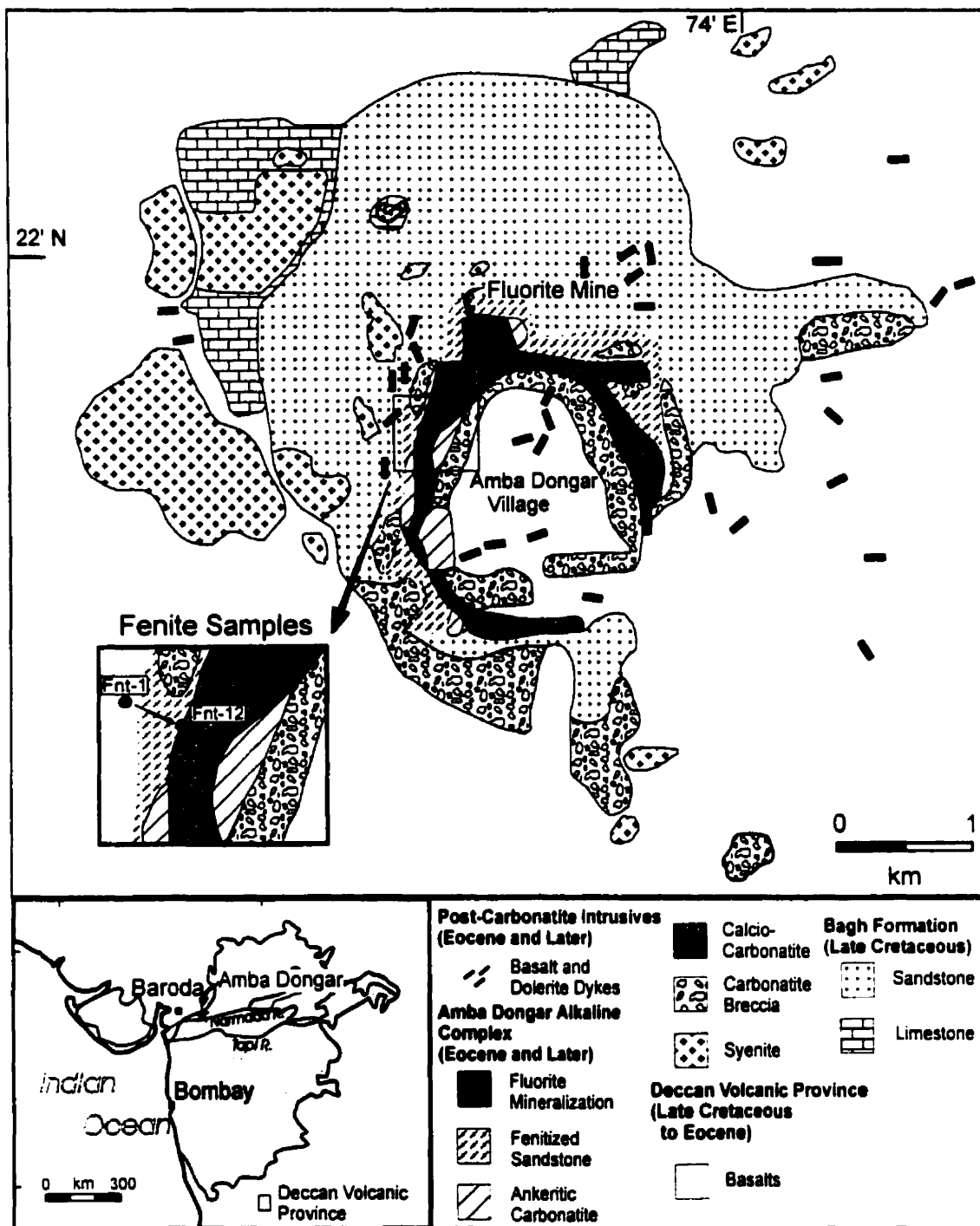
This paper uses fenites of the Amba Dongar complex, India to reconstruct the compositions of aqueous fluids which were responsible for potassic fenitization of the surrounding country rocks. These intrusions are in an ideal setting in which to study fluids generated by carbonatite magmatism owing to the fact that they are hosted by sandstone containing >96 wt.% SiO₂. This simple mineralogy of the precursor enables the mineralogical and chemical changes that accompanied fenitization to be quantified with unprecedented accuracy.

Geology

The Amba Dongar alkaline complex was intruded into the western part of the Deccan province, India during the Late Eocene (Fig. 6-1) and is temporally and spatially associated with Deccan volcanism (Karkare and Srivistava, 1989; Simonetti *et al.*, 1995). The complex is hosted by Deccan flood basalts as well as quartzitic sandstones and limestones of the Late Cretaceous Bagh formation.

The complex is dominated by a carbonatite ring structure surrounded by numerous syenitic intrusions. Emplacement of carbonatite was initiated as an injection of fluidized calciocarbonatitic liquid which formed a carbonatite breccia, and was followed by intrusion of the main outer ring of calciocarbonatite. In the western half of the ring,

**Figure 6-1 The geology of the Amba Dongar complex and surrounding area
(modified from Deans et al., 1972).**



numerous small plugs and dykes of ankeritic ferrocarbonatites were, in turn, emplaced along the outer margins of the calciocarbonatite. During the waning stages of carbonatite magmatism, fluids were exsolved from the crystallizing carbonatites and were responsible for the formation of a well developed fenite aureole in the sandstones surrounding the complex as well as deposition of economic quantities of fluorite within carbonatite (11.6 Mt., 30% CaF_2) (Deans *et al.*, 1973; Palmer and Williams-Jones, 1996).

Carbonatites

Calciocarbonatite at Amba Dongar is composed of medium- to coarse-grained calcite occurring as an interlocking arrangement of equigranular crystals. Porphyritic varieties of calciocarbonatite, consisting of coarse euhedral calcite crystals set in a finer grained calcitic matrix, occur locally. Accessory minerals are common, and consist of ubiquitous apatite and local disseminations of pyrochlore and fluorite.

The plugs and dykes of ferrocarbonatite, which were intruded during the last stages of carbonatite magmatism, are fine-grained, red-coloured and are predominantly composed of ankerite. Locally, pseudomorphs of hematite after magnetite can make up to 50% of the rock. Accessory minerals include, in decreasing order of importance, barite, fluorite, monazite, bastnaesite and pyrochlore.

Bagh Formation

Unaltered Late Cretaceous Bagh sandstones and limestones surround the complex to the east, west and north. In the vicinity of the complex, sandstone consists almost entirely of quartz (>96 wt.% SiO_2) with grains ranging in size from that of silt to those of small pebbles. Quartz grains are subround to round with irregular grain boundaries and are generally well sorted.

Limestone occurs to the northwest of the ring and is separated from carbonatites by sandstone. It is composed of thinly to moderately bedded marl, which displays gentle folding.

Fenites

Potassic, sodic and sodic-potassic fenites have been reported from Amba Dongar (Deans *et al.*, 1972; Viladkar, 1986; Roelofsen, 1997). In earlier studies only the potassic fenites, which are exposed on surface, were described. However, sodic and sodic-potassic fenites were later located during diamond drilling in the northern portion of the ring. The precursor in all cases was originally thought to have been quartzitic sandstones of the Bagh Formation (Viladkar, 1986), however, fenitized examples of volcanic and plutonic ijolitic rocks are now known (Roelofsen, 1997)

Potassic Fenites

Potassic fenitization occurs along the western, northern and eastern margins of the ring complex in the surrounding sandstones and decreases in intensity with increasing distance from the carbonatite. The highest grade fenites are composed almost entirely of microcline and orthoclase (up to 90%), the former mineral being predominant (Roelofsen, 1997). Microcline occurs as subhedral, tabular crystals which preserve the grain-size of the original rock, while orthoclase crystals are more poorly formed and enclose significant quantities of disseminated sericite. The grain size, however, is similar. Minor proportions of coarse muscovite occur along both quartz-quartz and quartz-feldspar boundaries and rare albite grains can be found interspersed among K-feldspar crystals. Much of the quartz in fenite appears more ragged than that in the unaltered sandstone and almost invariably contains fine, pervasive fractures. In some cases, however, relict quartz grains have been mantled by a shell of euhedral quartz, imparting a hexagonal form to the grains.

Sodic Fenites

Sodic and sodic-potassic fenites have been observed only in deeper sections of the complex and are classified into three groups based on mineralogy (Viladkar, 1986;

Roelofsen, 1997). The most sodic variety is referred to as ultrasodic fenite, and consists of an assemblage of anhedral to subhedral albite with minor relict quartz and rare, fine-grained aegirine-augite (Viladkar, 1986). Sodic fenite, which has only been found in one location, is composed of albite (greater than 50%), subordinate aegirine-augite and relict quartz grains (Viladkar, 1986). The third group is represented by sodic-potassic fenites, and has been subdivided into two sub-types comprising an orthoclase-aegirine-apatite-calcite variety and a microperthite-aegirine-augite-orthoclase-albite variety. It has been proposed, based on feldspar mineralogy (Viladkar, 1986), that the assemblage containing orthoclase is lower temperature and therefore related to carbonatite-derived hydrothermal fluids while the microperthite-orthoclase-albite assemblage represents higher temperatures and was formed by aqueous fluids exsolved from an unexposed ijolite. The precursor to sodic and sodic-potassic fenites was originally thought to be the quartzitic Bagh sandstones (Viladkar, 1986), however, Roelofsen (1997) has shown that most samples of these fenites were originally ijolite.

Alteration Chemistry

The major, trace and rare earth element compositions of samples of altered and unaltered sandstone were analysed in order to evaluate mass changes that accompanied fenitization (Table 6-1). Major elements were analysed by X-ray Fluorescence (XRF) while trace element and rare earth element (REE) concentrations were determined by XRF and Instrumental Neutron Activation Analysis (INAA).

Figures 6-2 and 6-3 show the concentrations of selected major and minor elements, respectively, plotted versus the concentration of SiO_2 , an indicator of alteration intensity. As might be expected, SiO_2 content decreases towards the complex, i.e., with increasing intensity of alteration. This is also readily apparent in normative mineral calculations (CIPW, Newpet) of progressively fenitized rock which show a large decrease in quartz towards the complex (Fig. 6-4).

Major element plots (Fig. 6-2) show, not surprisingly, continuous increases in Al_2O_3 and K_2O with decreasing SiO_2 , while the content of Na_2O rises only slightly, and remains effectively constant in the more intensely fenitized sandstone. The

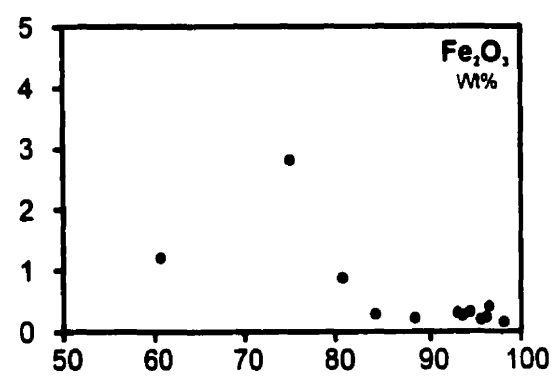
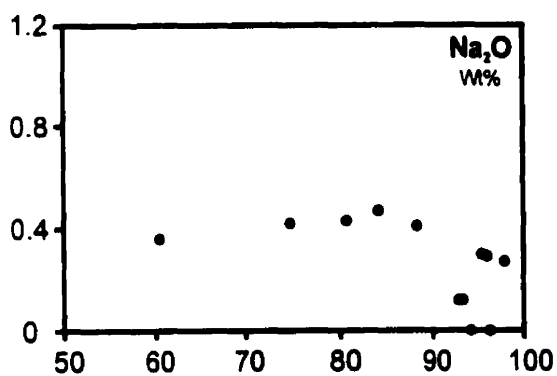
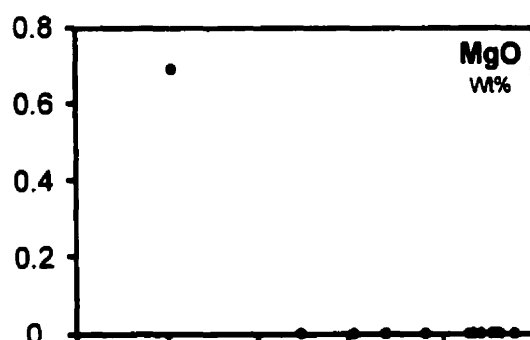
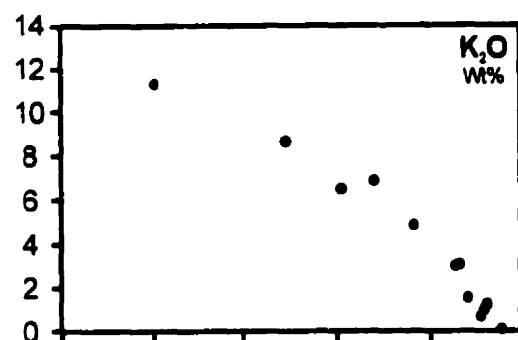
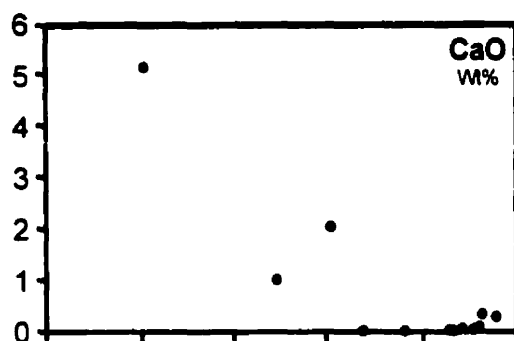
Table 6-1 Chemical compositions of unaltered (Fnt-1) and progressively altered sandstone (Fnt-2 - 12)

Sample	Fnt-1	Fnt-2	Fnt-3	Fnt-4	Fnt-5	Fnt-6	Fnt-7	Fnt-8	Fnt-9	Fnt-10	Fnt-11	Fnt-12
Type	ssl	ssl	ssl	fenite	fenite	fenite	fenite	fenite	fenite	fenite	fenite	fenite
Wt. %												
SiO ₂	97.92	96.36	96.05	95.41	94.20	93.29	92.79	88.06	83.82	80.44	74.73	60.36
TiO ₂	0.32	0.041	0.16	0.06	0.071	0.028	0.030	0.13	0.08	0.12	0.64	0.102
Al ₂ O ₃	0.18	2.08	1.35	2.58	1.26	1.70	1.69	5.51	8.14	7.58	10.28	13.25
Fe ₂ O ₃	0.14	0.40	0.23	0.2	0.32	0.25	0.31	0.22	0.28	0.88	2.81	1.21
MnO	n.d.	0.018	0.01	n.d.	0.009	0.005	0.007	n.d.	n.d.	0.01	0.02	0.064
MgO	n.d.	n.d.	n.d.	n.d.	n.d.	n.d.	n.d.	n.d.	n.d.	n.d.	n.d.	0.69
CaO	0.27	0.32	0.07	0.03	0.04	n.d.	0.01	n.d.	n.d.	2.03	1	5.14
Na ₂ O	0.27	n.d.	0.29	0.3	n.d.	0.12	0.12	0.41	0.47	0.43	0.42	0.36
K ₂ O	0.06	1.18	0.93	0.66	1.48	3.01	2.94	4.79	6.82	6.46	8.61	11.25
P ₂ O ₅	0.01	0.017	0.03	0.01	0.014	0.014	0.019	0.02	0.01	0.05	0.02	2.410
LOI	0.32	0.27	0.22	0.66	0.53	0.07	0.11	0.18	0.24	1.82	1.55	2.90
ppm												
F	130	150	230	180	190	170	200	160	200	210	380	3000
Cr ₂ O ₃	49	72	30	n.d.	53	47	56	n.d.	n.d.	n.d.	57	10
V	43	4	76	18	6	6	6	25	26	76	323	109
Rb	2	29.9	23	15	40.3	77.6	76.5	112	162	129	160	229
Sr	9	24.9	27	23	32.9	60.8	57.4	74	67	142	79	1076
Nb	32	7.0	49	2	8.7	7.8	7.9	62	15	39	55	130
Pb	1.3	2.7	5.4	6.1	6.8	10.1	14.7	22	11	38	34	425
U	n.d.	4.2	n.d.	n.d.	4.1	4.8	4.8	n.d.	n.d.	n.d.	n.d.	n.d.
Th	5	0.7	4	7	2.7	1.2	1.3	6	10	13	7	63
Y	3	8.4	6	3	10.7	11.5	11.5	5	n.d.	7	9	76
Zr	90	50.3	206	67	82.9	75.5	71.0	86	62	99	1878	59
Co	140	2	150	120	1	n.d.	n.d.	94	100	66	n.d.	n.d.
Sc	0.8	0.2	1.3	0.6	0.5	0.3	0.3	0.9	0.6	0.6	n.d.	9.3
Ta	4	n.d.	4	3	n.d.	n.d.	n.d.	3	3	2	n.d.	n.d.
La	7	9	36	11	13.9	8.9	9	21	21	46	86.3	168
Ce	12	18	18	26	29	11	15	31	39	53	98	1300
Nd	10	7	15	11	10	11	13	15	16	27	38	95
Sm	0.4	0.8	1.1	1.1	2.2	0.6	0.7	1.7	1.9	2.3	5.9	24
Eu	0.2	0.2	0.4	0.3	0.4	0.2	0.2	0.6	0.7	1	2.1	8.3
Yb	0.7	0.2	1.19	0.7	0.3	0.6	0.7	0.9	0.7	0.9	1.2	3.5
Lu	0.1	0.1	0.16	n.d.	0.06	0.09	0.13	0.12	0.1	0.13	0.18	0.58
Total	99.54	100.74	99.49	99.99	99.97	100.57	100.10	99.43	99.99	100.04	100.59	99.32

n.d. not detected

ssl sandstone

Figure 6-2 Major element compositions of progressively fenitised Bagh sandstone (indicated by decreasing concentration of SiO_2).



SiO₂ (Wt.%)
← Progressive Fenitization

SiO₂ (Wt.%)
← Progressive Fenitization

Figure 6-3 Minor element compositions of progressively fenitised Bagh sandstone (indicated by decreasing concentration of SiO_2).

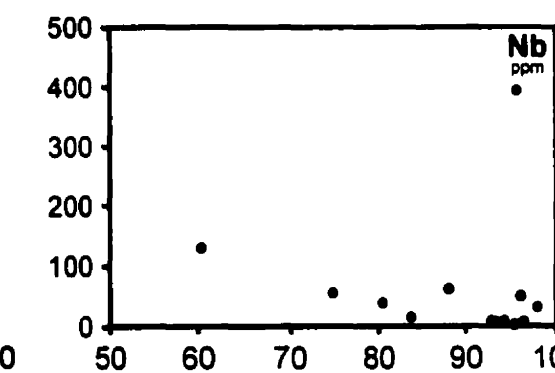
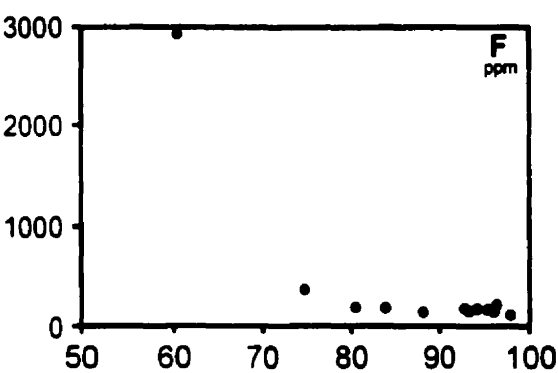
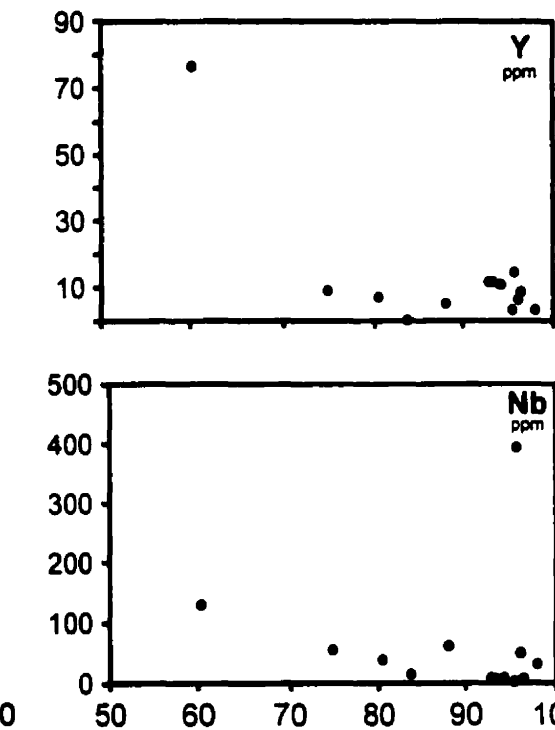
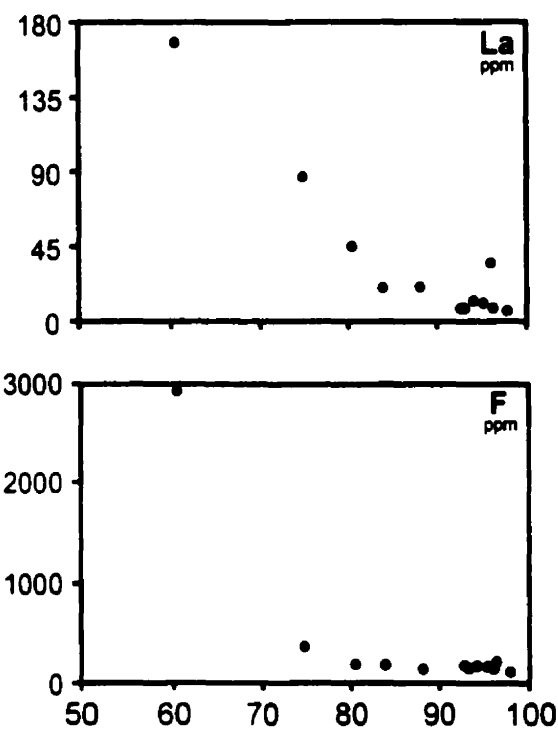
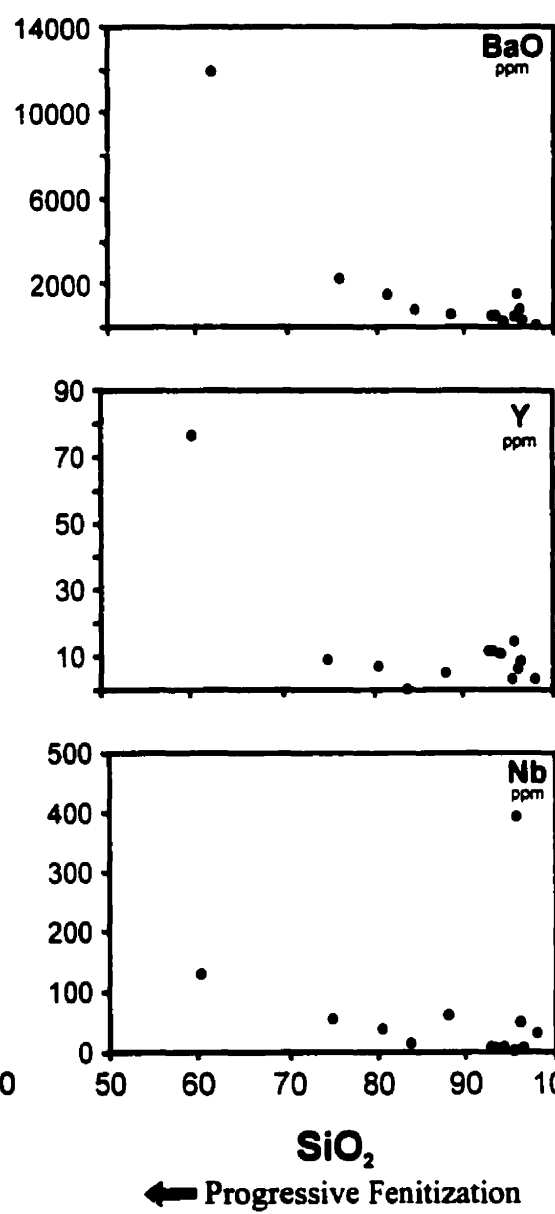
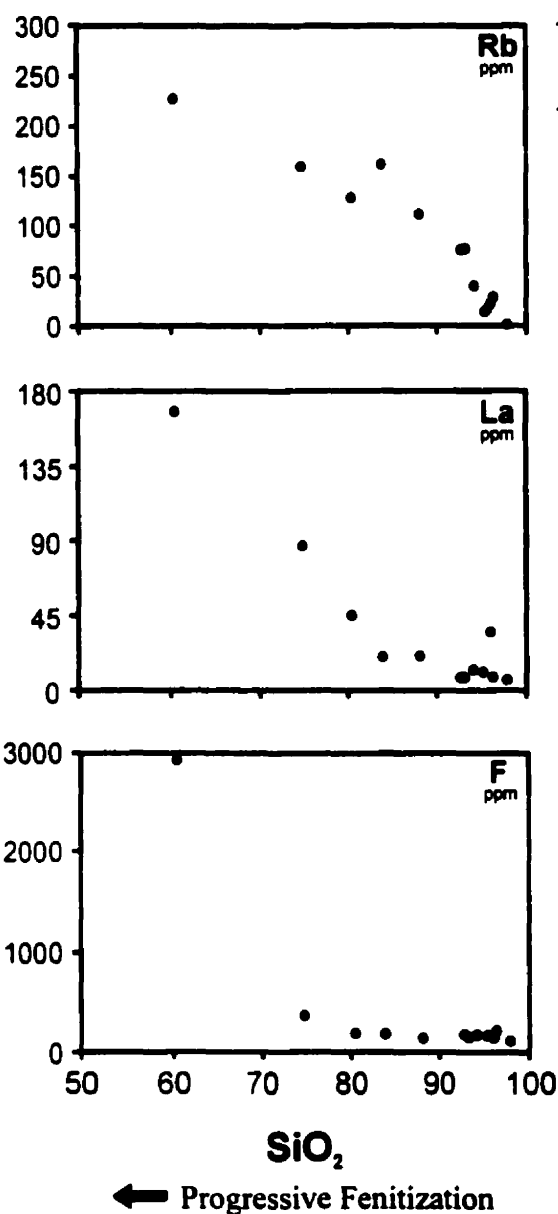
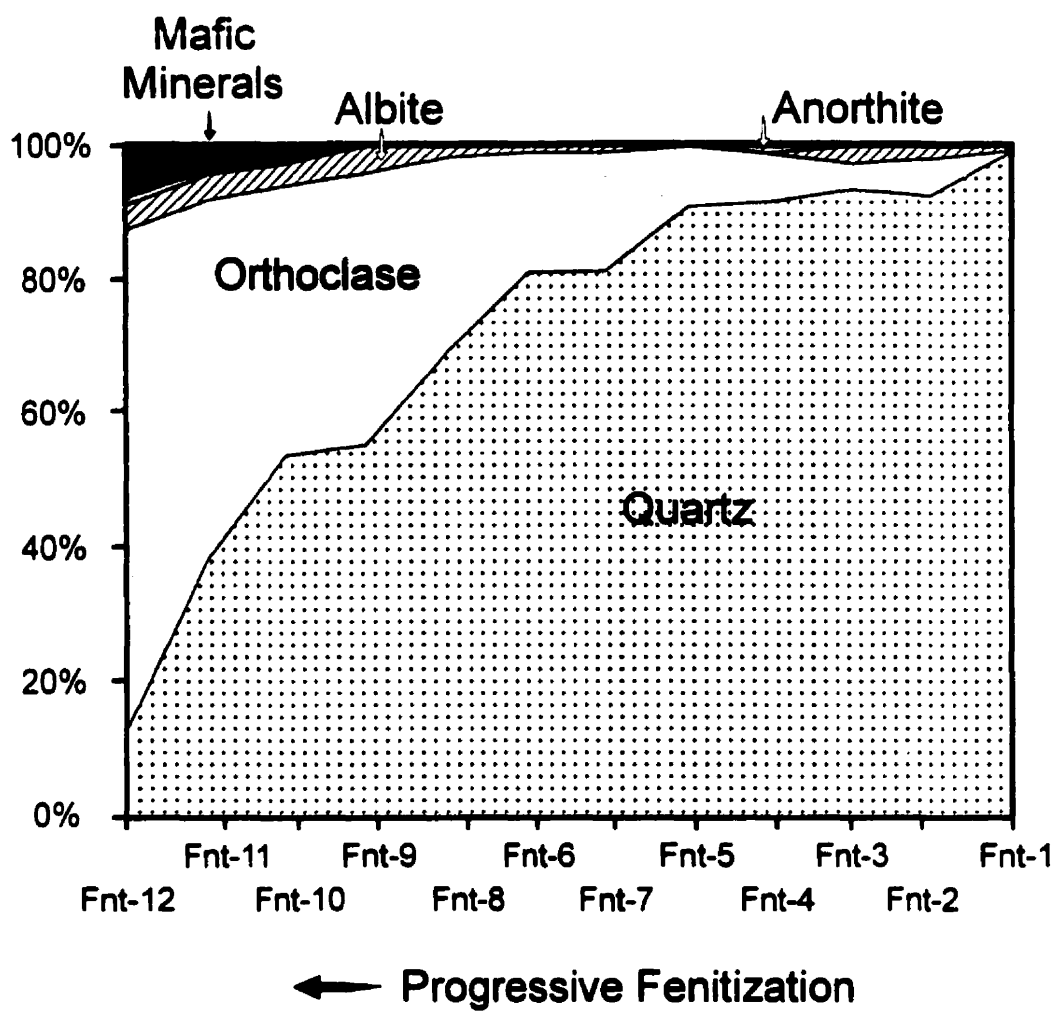


Figure 6-4 Normative mineralogy of progressively fenitised Bagh sandstone.



concentrations of CaO and Fe_2O_3 also rise sharply, but only where alteration is the most intense. The MgO and fluorine contents are essentially constant (The MgO concentration is below detection) except in the most altered fenite, which is strongly enriched in these components (Figs. 6-2 and 6-3). Rubidium concentration, like that of K_2O , increases steadily with increasing degree of alteration while Ba behaves similarly to Ca, with only slight increases in peripheral fenites and sharp increases in samples proximal to the carbonatite intrusion (Fig. 6-3). Nb displays a trend of increasing concentration with increasing intensity of alteration, but is not enriched to the same degree in the high grade fenite as other elements.

The concentration of La (representing the LREE) shows a relatively steady increase with increasing degree of fenitization (Fig. 6-3). By contrast, Y, which is a surrogate to the HREE has a low, and essentially unchanged concentration in all samples except for the highest grade fenite in which it is highly enriched.

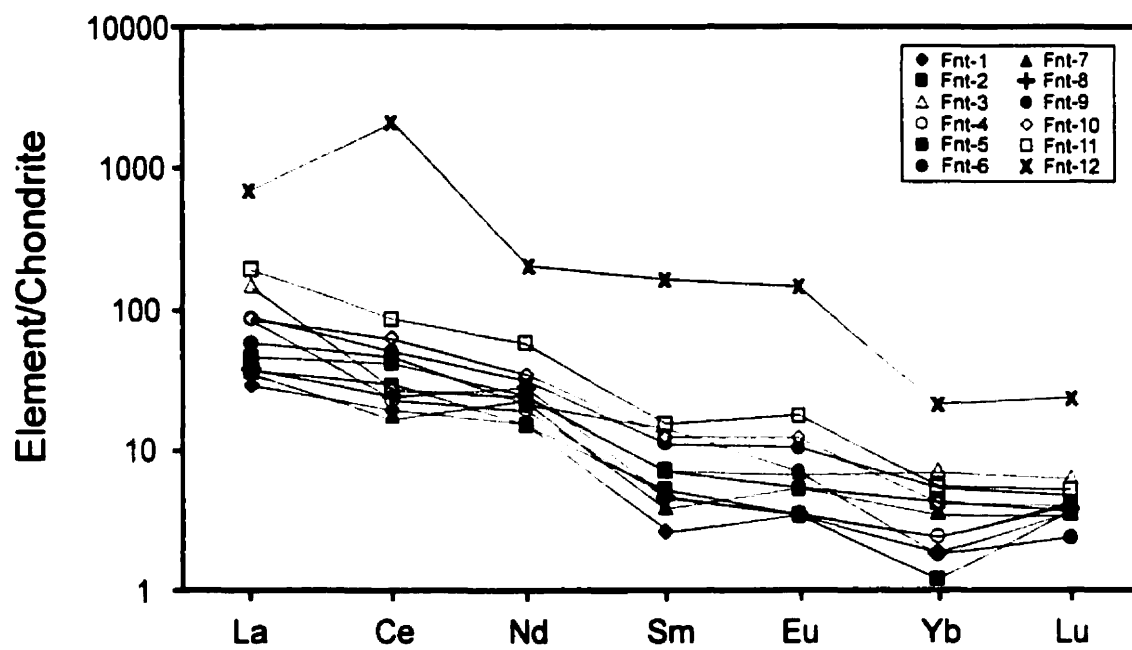
Chondrite normalized REE profiles of fenites are LREE enriched and lack a Eu anomaly (Fig. 6-5). The most elevated LREE values occur in the highest grade fenites and REE content consistently increases with increasing intensity of fenitization. However, HREE distributions are more irregular with some higher grade fenites having lower HREE contents than lower grade fenites.

Mass Balance

The isocon method of Grant (1986) and Gresens' (1967) volume factor method were chosen to illustrate and calculate mass exchanges which occurred between unaltered Bagh sandstone and fenitizing fluids. For this purpose it is necessary to identify an immobile element or assume a volume factor.

Selecting an immobile element is inherently difficult in clastic sedimentary rocks because of the heterogeneous distribution of detrital grains, particularly zircon and rutile. This produces large variations in the precursor concentrations of a number of potentially immobile elements, and coupled with the extreme reactivity of carbonatite fluids, poses an almost insurmountable problem in identifying volume changes between altered and unaltered sedimentary rocks. However, the simple nature of the precursor, almost pure

Figure 6-5 Chondrite-normalized rare earth element (REE) profiles for unaltered and altered Bagh sandstone, where Fnt-1 is unaltered sandstone and Fnt-12 is the most strongly fenitized sample.



quartz, and the uncomplicated nature of the alteration, replacement of quartz by potassium feldspar, allows volume changes to be roughly estimated thereby fixing isocons. Petrographic studies of unaltered and altered sandstone show that there were no changes, other than mineralogical, which would have compromised volume relationships (e.g., porosity). Based on the densities of quartz and microcline, the volume difference between the quartz-rich host rock and a fenite which has undergone complete replacement by potassium feldspar is, at most, 4%.

Rough correlations between common immobile elements, such as Ti and Cr, and Y and Th, also support the assumption of minor volume changes. However, in Bagh sandstone, the distribution of these elements is very heterogeneous because of their concentrations in heavy minerals and this is reflected in volume factors based on best fits of isocons to immobile elements (no volume change in low grade fenite and up to 38% volume loss in higher grade fenites). Therefore, volume changes are better estimated petrographically. As well, the assumption of near volume for volume replacement errs on the side of caution and produces values which can be considered minima.

Isocon diagrams for seven progressively fenitised Bagh sandstones are presented in Figure 6-6. These samples represent a section oriented perpendicular to the sandstone/carbonatite contact and extending approximately 150m from the contact to allow the full spectrum of fenite grades to be characterized. The solid line on each graph represents an isocon of slope M^A/M^O , and is defined by the largest number of potentially immobile elements. This line relates to Gresens' (1967) volume factor through the equations:

$$M^A/M^O = f_v (\rho^A/\rho^O) \quad (1)$$

and

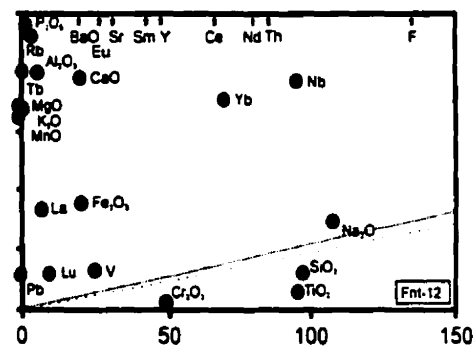
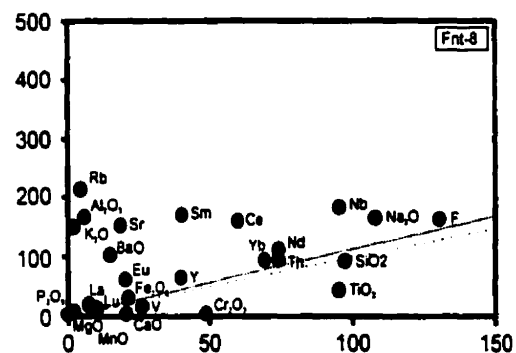
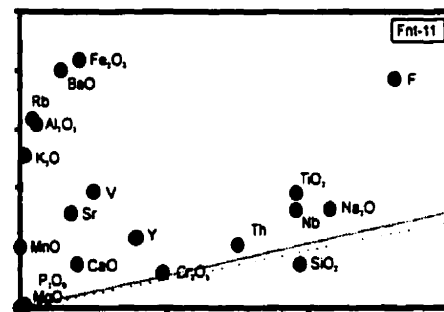
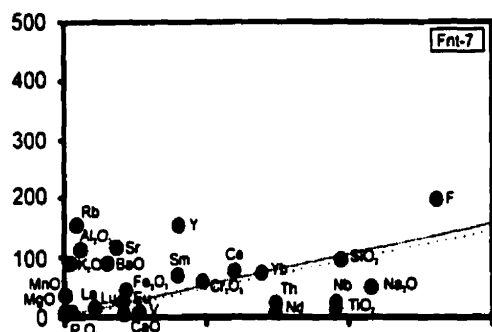
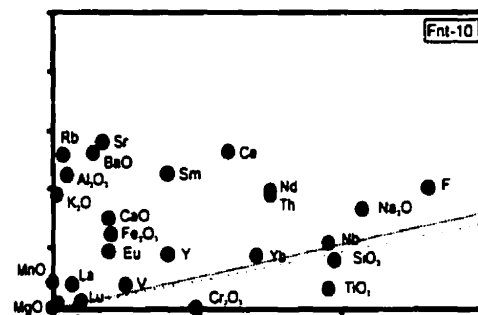
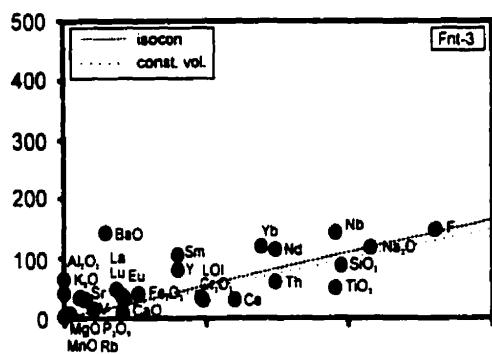
$$(\Delta C_i/C_i^O) = (M^A/M^O)(C_i^A/C_i^O) - 1 \quad (2)$$

and, finally

$$(\Delta C_i/C_i) = f_v (\rho^A/\rho^O)(C_i^A/C_i^O) - 1 \quad (3)$$

Figure 6-6 Isocon digrams for six progressively fenitized Bagh sandstones (Fnt-3, 7, 8, 10, 11, 12) versus unaltered sandstone (Fnt-1) (c.f. Grant, 1986). Elements which plot above the dotted line (isocon) were added and those which plot below were removed during fenitization. The line of constant volume (lighter dotted line) is plotted for reference.

Altered



Unaltered (Fnt-1)

where M is mass, C_i is the concentration of element i , ρ is specific gravity, f_v is the volume factor and A and O are the altered and original rocks, respectively. Elements above the line have undergone mass gains during fenitization, while those below have been depleted. The isocons in samples Fnt-3 and 8, Fnt-10 and 11 and Fnt-12 correspond to mass factors of 0.99, 0.98 and 0.97, respectively, and therefore mass losses of 1, 2 and 3%. Results of mass change calculations are given in Table 6-2.

Mass losses

During fenitization, SiO_2 underwent the greatest mass loss, and the largest absolute mass change with 0.9 to 36 g of SiO_2 removed per 100 g_{rock} . Although the precursor consisted almost entirely of quartz, other elements were present in small proportions and their mass changes can also be determined. CaO underwent losses of between 2000 and 2700 ppm, corresponding to changes of -74 and -100% of the initial concentration of 2700 ppm, but only in the lower grade fenites. Ta and Co experienced minor losses that were independent of the intensity of fenitization. The same is true for Zr and Sc, except in the high grade fenites where there was a large gain in Zr (1842 ppm, Fnt-11) and a small gain in Sc (8 ppm, Fnt-12). Sc and Ta gains are within the range of acceptable error, however the Zr gain is unexpectedly large and is probably an artifact of an anomalously high primary concentration of detrital zircon.

Mass Gains

The replacement of quartz by feldspar during fenitization at Amba Dongar requires that there was addition of K_2O and Al_2O_3 to the unaltered sandstones. These elements show gains between 0.9 and 12 g/100 g_{rock} compared to a concentration of 0.06 g/100g in the unaltered rock, and 1 and 14 g/100 g_{rock} , compared to a concentration of 0.18g/100g in the precursor, respectively, with the larger additions corresponding to higher degrees of fenitization. BaO and F show gains ranging from 745 to 12 172 ppm and 21 to 2 957 ppm, respectively, compared to concentrations in the precursor of 82 and 130 ppm, while CaO shows significant increases, 0.76-1.8g/100g in the mid to high grade

Table 6-2 Mass transfers (MT) for fertilized sandstone

Sample	Fnt-1 unaltered	Fnt-3 altered	MT	% change	Fnt-7 altered	MT	% change	Fnt-8 altered	MT	% change	Fnt-10 altered	MT	% change	Fnt-11 altered	MT	% change	Fnt-12 altered	MT	% change
g/kg precursor																			
SiO ₂	97.92	96.05	-2.77	-3	92.79	-6.00	-6	88.06	-10.69	-11	80.44	-19.00	-19	74.73	-25.30	-26	60.36	-39.27	-40
TiO ₂	0.32	0.16	-0.16	-50	0.03	-0.29	-91	0.13	-0.19	-6	0.12	-0.20	-63	0.64	0.30	94	0.10	-0.22	-69
Al ₂ O ₃	0.18	1.35	1.16	643	3.69	3.48	1931	5.51	5.28	2932	7.58	7.26	4032	10.28	9.81	5450	13.25	12.70	7053
Fe ₂ O ₃	0.14	0.23	0.09	63	0.31	0.17	119	0.22	0.08	36	0.88	0.72	517	2.81	2.59	1850	1.21	1.04	740
MnO	nd	0.01	0.01	---	0.01	0.01	---	0.00	0.00	---	0.01	0.01	---	0.02	0.02	---	0.06	0.06	---
MgO	nd	nd	---	---	nd	---	---	nd	---	---	nd	---	---	nd	---	---	0.69	0.67	---
CaO	0.27	0.07	-0.20	-74	0.01	-0.26	-96	0.00	-0.27	-100	2.03	1.72	638	1.00	0.70	260	5.14	4.72	1750
Na ₂ O	0.27	0.29	0.02	6	0.12	-0.15	-56	0.41	0.14	50	0.43	0.15	56	0.42	0.14	51	0.36	0.08	30
K ₂ O	0.06	0.93	0.86	1435	2.94	2.85	4754	4.79	4.68	7808	6.46	6.28	10464	8.61	8.31	13844	11.25	10.87	18120
P ₂ O ₅	0.01	0.03	0.02	197	0.02	0.01	88	0.02	0.01	98	0.05	0.04	391	0.02	0.01	94	2.41	2.33	23319
g/1000 kg precursor																			
BaO	82	820	730	891	494	407	497	571	484	590	1473	1363	1663	2244	2099	2559	11908	11489	14011
Cr ₂ O ₃	49	30	-19	-39	56	6	13	0	-49	-100	0	-49	-100	57	6	13	10	-39	-80
V	43	76	32	75	6	-37	-86	25	-18	-42	76	32	73	323	271	630	109	63	146
F	130	150	19	14	200	68	52	160	28	22	210	76	58	380	239	184	3000	2785	2142
LOI	0.32	0.22	-0.10	-32	0.11	-0.21	-66	0.18	-0.14	-44	1.82	1.47	458	1.55	1.19	371	2.90	2.50	781
Rb	2	23	21	1039	77	74	3689	112	109	5447	129	125	6228	160	153	7674	229	220	11002
Sr	9	27	18	197	57	48	532	74	64	714	142	130	1448	79	68	753	1076	1037	11519
Nb	32	49	17	52	8	-24	-76	62	29	92	39	6	20	55	21	67	130	95	296
Pb	nd	nd	---	---	15	15	---	nd	---	---	nd	---	---	nd	---	---	425	413	---
U	nd	nd	---	---	5	5	---	nd	---	---	nd	---	---	nd	---	---	0	0	---
Th	5	4	-1	-21	1	-4	-74	6	1	19	13	8	155	7	2	36	63	57	1130
Y	3	6	3	98	12	8	280	5	2	65	7	4	129	9	6	192	76	71	2368
Zr	90	206	114	127	71	-20	-22	86	-5	-5	99	7	8	1878	1735	1928	59	-32	-36
Co	140	150	9	6	nd	---	---	94	-47	-33	66	-75	-54	nd	---	---	nd	---	---
Sc	1	1	0	61	nd	---	---	1	0	11	1	0	-26	nd	---	---	9	8	1030
La	7	36	29	409	9	2	27	21	14	197	46	38	545	86	77	1098	168	156	2232
Ce	12	18	6	49	15	3	24	31	19	156	53	40	333	98	83	694	1300	1251	10427
Nd	10	15	5	49	0	-10	-100	15	5	49	27	16	165	38	27	269	95	82	823
Sm	0.4	1.1	0.7	172.4	0.7	0.3	73.4	1.7	1.3	321.0	2.3	1.9	464.2	5.9	5.3	1333.3	24.0	22.9	5730.3
Eu	0.2	0.4	0.2	98.1	0.2	0.0	-0.4	0.6	0.4	197.2	1.0	0.8	390.6	2.1	1.8	920.3	8.3	7.9	3932.6
Yb	0.7	1.2	0.5	68.4	0.7	0.0	-0.9	0.9	0.2	27.4	0.9	0.2	26.1	1.2	0.5	66.6	3.5	2.7	385.9
Lu	0.1	0.2	0.1	58.5	0.1	0.0	28.8	0.1	0.0	18.9	0.1	0.0	27.6	0.2	0.1	74.9	0.6	0.5	463.6

nd Not detected

fenites, compared to the original concentration of 0.27 g/100g. Rb and Sr show large mass gains in all samples, 21-233 ppm and 18-1 100 ppm, respectively, when compared to initial concentrations in the precursor of 2 and 9 ppm. Although Th was lost in the two least altered samples, Fnt-3 and Fnt-7, it was gained (1-60 ppm) in all other fenites. All REE experienced mass gains, in all samples, with the largest gains being recorded by La, Ce and Nd, with values of 165, 1 325 and 87 ppm, respectively, in the highest grade fenite. These gains are well above the initial concentrations of La, Ce and Nd in unaltered sandstone of 7, 12 and 10 ppm, respectively.

Discussion

As mentioned above, the quartz-rich nature of Bagh sandstone permits accurate estimations of the mass exchanges which occurred between rock and fenitizing fluids. An important feature of fenites is that they yield valuable information on the trace element contents of fenitizing fluids, data which are difficult to obtain with any accuracy from fluid inclusion studies.

Mass Changes During Fenitization

Mass balance calculations for fenitized sandstone confirm that there were major additions of K_2O , Al_2O_3 , Fe_2O_3 , Ba, and significant additions of La, Ce, F, Rb, Sr, Y, and HREE, and that the sizes of these additions to sandstone increased with increasing intensity of fenitization. The addition of Ca occurred only in higher grade fenites (Fnt-10, 11, 12) and Na, although consistently added, was not present in significant concentrations, and showed no evidence of increasing concentration, with increasing intensity of fenitization. SiO_2 is the only component which underwent consistent, and progressive, losses with increasing degree of alteration, and in fact experienced the greatest mass transfer of all components (-39 g/100g_{rock}, Fnt-12). Magnesium was only detected in the highest grade fenite (Fnt-12), and only a limited concentration (0.69 wt. %).

The quartz-rich composition of the fresh sandstone (almost 98 wt.% SiO₂) used in the calculations requires that all elements added during fenitization were almost entirely introduced by the fenitizing fluids. Although Ca was a significant component of the fenitizing fluids, it was quickly removed during the initial stages of alteration, probably due to fluorite precipitation (Richardson and Holland, 1979). Sodium, a major element in the fenitizing fluids (Palmer and Williams-Jones, 1998a, Chap. 5), was not added in significant amounts to rocks. This is consistent with the absence of albite and can be explained by the relatively low temperature of the fenitization, <300°C (Palmer and Williams-Jones, 1998a, Chap. 5). At 300°C, a K/Na ratio of <0.1 is required to stabilize albite based on calculations using SUPCRT92 (Johnson *et al.*, 1991). By contrast, the K/Na ratio of the fenitizing fluid is estimated, from analyses of fluid inclusions by Palmer and Williams-Jones (1998b, Chap. 5), to have been ≈0.2. The stable alkali feldspar for this fluid composition at 300°C is microcline with a composition > Or₉₅ (Rubie and Gunter, 1983)

Water-Rock Ratios

The removal of large amounts of quartz from sandstones during fenitization indicates that the fluid was extremely undersaturated with respect to silica. Maximum water-rock ratios can therefore be determined for the alteration if the solubility of quartz is known at the conditions of fenitization. Quartz solubility is dependent almost entirely on temperature, except at high pH (>8) or high ionic strengths (>3 molal NaCl; Rimstidt, 1997). Fluid inclusion studies of fenites by Palmer and Williams-Jones (1998b, Chap. 5) have determined the temperatures under which a number of fenites formed as a function of distance from the carbonatite. Approximately 25m from the margin of the intrusion, the temperature of the fenitizing fluid was approximately 260°C, and, could not have been greater than 320°C because the confining pressure was ≈100 bars and there is no evidence of boiling (Roedder, 1984). Thermodynamic calculations (Johnson *et al.*, 1991), based on a temperature of 300°C, indicate that fenitizing fluids could contain up to 0.009m, or 540ppm, SiO_{2(aq)}. Therefore, the removal of 39 g/100g_{rock}, or 390 000ppm, of SiO₂ from sandstone during the formation of high grade fenite, determined from mass

balance calculations, would require a water- rock ratio of 722. However, it must be remembered that inherent in this calculation of water/rock ratios are assumptions that the initial fluids were silica-free and that the removal of quartz by dissolution occurred at 100% efficiency. The first assumption, although probably not entirely valid, is reasonable given the source of the fluid, i.e., a carbonatite magma largely devoid of silica. The second assumption is also considered reasonable as the unaltered rocks consisted almost entirely of quartz, and the kinetics of quartz dissolution at high temperature (>200°C) are rapid, i.e., equilibrium is quickly attained (Mountain, 1992; Rimstidt, 1997).

Calculated Fluid Composition

On the basis of the mass balance calculations presented earlier, the principal elements added to the sandstone during fenitization were K and Al. The concentration of K in the fluid was estimated from fluid inclusion data to be 0.27 (Palmer and Williams-Jones, 1998a, Chap. 5) and that of Al can be calculated from the solubility of K-feldspar. The latter, however, requires independent estimates of m_{Si} and pH. As discussed above, m_{SiO_2} was 0.009m and pH can be estimated from the fact that high grade fenites contain muscovite, i.e., conditions were close to the feldspar-muscovite boundary.

At 300°C the K-feldspar-muscovite boundary occurs at a pH of approximately 5.4, based on the reaction:



(Log K calculated using SUPCRT92; Johnson *et al.*, 1991). However, this is a minimum value because it assumes quartz saturation. If the activity of silica were one or two orders of magnitude lower, pH would increase to 8.4 and 11.4, respectively.

The concentration of Al in equilibrium with potassium feldspar was calculated from the reaction:



using a hydrolysis constant for potassium feldspar at 300°C determined using SUPCRT92 (Johnson *et al.*, 1991) and thermodynamic data for aluminum hydroxide complexes from Shock *et al.* (1997). The complex $\text{Al}(\text{OH})_3^0$ was used to represent dissolved Al, as it is the dominant form of aluminum at the pH range of the fenitizing fluid (Castet, 1991). Activity coefficients of dissolved species were determined using the computer program EQ3 (Wolery, 1992). The concentration of dissolved Al in equilibrium with potassium feldspar at 300°C was calculated to be approximately $1.2 \times 10^{-8}\text{m}$. This is a minimum value because, as noted earlier, the molality of SiO_2 used in the calculation was that of quartz saturation, whereas the actual concentration may have been orders of magnitude lower. Another method of determining the minimum concentration of Al in fenitizing solutions is to divide the number of moles of Al_2O_3 added to high grade fenites by the volume of water calculated from the water-rock ratio (722). Based on this calculation, the fenitizing fluids must have had approximately 5 orders of magnitude more dissolved Al ($1.6 \times 10^{-3}\text{m}$) than the value calculated above. We believe that this latter value provides a much more realistic estimate of the concentration of Al in the fenitizing fluids on the grounds that the water/rock ratio is reasonable, i.e., similar to or less than that calculated for hydrothermal alteration elsewhere (Wood and Williams-Jones, 1994; Reed, 1997). The former value implies an extremely unrealistic water/rock ratio of 10^7 . We therefore conclude that the concentration of Al was probably of the order of 10^{-3}m , which is similar to values measured for acid-sulphate geothermal waters (Giggenbach, 1997).

As mentioned earlier, mass balance calculations provide an opportunity to estimate concentrations of trace elements in fenitizing fluids, something that is usually not possible from analyses of fluid inclusions. Table 6-3 presents the minimum molal concentrations of selected trace elements and REE in the fenitizing solutions, based on a water-rock ratio of 722, or 72.2 litres per 100g of rock and the mass gains reported in Table 6-2. The most abundant minor elements in solution are P, F, Ba and Sr, having minimum concentrations of 2.13×10^{-4} , 1.9×10^{-4} , 9.7×10^{-5} and $1.53 \times 10^{-5}\text{m}$, respectively, followed closely by Rb, Nb and Y, at minimum concentrations of 3.3×10^{-6} , 1.3×10^{-6} and

Table 6-3 Concentration of trace elements in fenitizing solutions
based on 77.2 litres of water per 100g of rock.

Element	Mass Gain		Concentration
	g/100g _{rock}	moles	molality
P ₂ O ₅	2.33	0.016	2.13E-04
BaO	1.15	7.49E-03	9.71E-05
F	0.28	0.015	1.90E-04
Rb	0.022	2.57E-04	3.34E-06
Sr	0.10	1.18E-03	1.53E-05
Nb	9.46E-03	1.02E-04	1.32E-06
Th	5.65E-03	2.44E-05	3.15E-07
Y	7.10E-03	7.99E-05	1.04E-06
Sc	8.24E-04	1.83E-05	2.37E-07
La	0.016	1.12E-04	1.46E-06
Ce	0.125	8.93E-04	1.16E-05
Nd	8.23E-03	5.71E-05	7.39E-07
Sm	2.29E-03	1.52E-05	1.97E-07
Eu	7.87E-04	5.18E-06	6.70E-08
Yb	2.70E-04	1.56E-06	2.02E-08
Lu	4.64E-05	2.65E-07	3.43E-09

1.0×10^{-6} m, respectively. Th and Sc have the lowest minimum concentrations, 3.2×10^{-7} and 2.4×10^{-7} m, respectively.

The LREE elements La and Ce display minimum concentrations of 1.2×10^{-5} and 1.5×10^{-6} m, respectively, while the remaining REE, Nd, Sm, Eu, Yb and Lu, are at very low concentrations, 7.4×10^{-7} , 2×10^{-7} , 6.7×10^{-8} , 2.0×10^{-8} and 3.4×10^{-9} m, respectively. These values are very similar (less than one log unit difference) to those determined by VanMiddlesworth (1997) for REE in thermal waters of the Bitterroot lobe of the Idaho Batholith and to Salton Sea and East Pacific Rise thermal waters (Michard *et al.*, 1983, 1984; Michard, 1989). La values determined for fenitizing fluids are also comparable to those in aqueous fluid associated with the Copper Flat porphyry system determined by Norman *et al.* (1989).

Conclusions

The Amba Dongar complex contains a well developed aureole of potassic fenites in sandstones surrounding the carbonatite ring. Fenitization was characterized by additions, to the rock, of K, Al, Ca, Ba, Fe, F, Rb, Sr, Y and REE, particularly the LREE and losses of Si, while Na concentrations remained unchanged. The quartz-rich nature of sandstone allowed for accurate estimation of the mass changes of these elements which occurred during fenitization.

Thermodynamic calculations of Al concentration in fenitizing fluids, based on the hydrolysis of K-feldspar reaction, indicate that a minimum of approximately 1.2×10^{-8} m Al was present in fenitizing solutions. By contrast, the concentration calculated from the mass of Al added to the rock during fenitization and a water/rock ratio estimated from quartz solubility and SiO_2 mass loss is 1.6×10^{-3} m. This value is similar to that measured in geothermal waters and is considered to provide the better estimate of the actual concentration of Al in the fenitizing fluid. Minimum trace element concentrations, including those of the REE, calculated from mass changes and the water/rock ratio are also comparable to those measured in modern geothermal systems.

References

- Castet, S., 1991, Solubilité de la boehmite et spéciation de l'aluminium dissous dans les solutions aqueuses à haute température (90-350°C) détermination expérimentale et modélisation: unpublished Ph.D. Thesis, Paul Sabatier University, Toulouse, France, 116p.
- Currie, K.L. and Ferguson, J., 1971, A study of fenitization around the alkaline complex at Callender Bay, Ontario, Canada: *Canadian Journal of Earth Sciences*, v. 8, p. 498-517.
- Deans, T., Sukheswala, R.N., Sethna, S.F. and Viladkar, S.G., 1972, Metasomatic feldspar rocks (potash fenites) associated with the fluorite deposits and carbonatites of Amba Dongar, Gujarat, India: *Trans. Inst. Min. Metall. (sect. B: earth sci.)*, v. 81, p. B1-B9.
- Deans, T., Sukheswala, R.N., Sethna, S.F. and Viladkar, S.G., 1973, Metasomatic feldspar rocks (potash fenites) associated with the fluorite deposits and carbonatites of Amba Dongar, Gujarat, India: Discussion and contributions: *Trans. Inst. Min. Metall. (sect. B: earth sci.)*, v. 82, p. B33-B40.
- Giggenbach, W.F., 1997, The origin and evolution of fluids in magmatic-hydrothermal systems: In: Barnes, H.L., ed., *Geochemistry of Hydrothermal Ore Deposits*, John Wiley & Sons Inc., Toronto, p. 737-798.
- Grant, J.A., 1986, The isocon diagram-A simple solution to Gresens' equation for metasomatic alteration: *Economic Geology*, v. 81, p. 1976-1982.
- Gresens, R.L., 1967, Composition-volume relationships of metasomatism: *Chem. Geol.* v. 2, p. 47-65.
- Johnson, J.W., Oelkers, E.H., and Helgeson, H.C., 1991, Supcrt92: a software package for calculating the standard molal thermodynamic properties of minerals, gases, aqueous species, and reactions from 1 to 5000 bars and 0° to 1000°C: *Computer Geoscience*, v. 18, p. 899-947.
- Karkare, S.G. and Srivistava, R.K., 1990, Regional dyke swarms related to the Deccan Trap Alkaline province, India: in A.J. Parker, P.C. Rickwood and D.H. Tucker (eds.), *Mafic Dykes and Emplacement Mechanisms, Proceedings of the Second International Dyke Conference*, Adelaide, South Australia, September, 1990, p. 335-347.
- Kresten, P., and Morogan, V., 1986, Fenitization at the Fen complex, southern Norway: *Lithos*, v. 19, p. 27-42.

- McKie, D., 1966, Fenitization: in Tuttle, O.F., and Gittins, J., eds., Carbonatites: London, Wiley & Sons, p. 261-294.
- Michard, A., 1989, Rare earth element systematics in hydrothermal fluids: *Geochim. Cosmochim. Acta*, v. 53, p. 745-750.
- Michard, A., Albarede, G., Michard, J.F., Minster, J.L., Charlou, J.L., and Tan, N., 1983, Rare-earth element and uranium in high temperature solutions from the East Pacific Rise hydrothermal vent field (13°N): *Nature*, v. 303, p. 795-797.
- Michard, A., Albarede, G., Michard, J.F., Minster, J.L., Charlou, J.L., and Tan, N., 1983, Chemistry of solutions from the 13°N East Pacific Rise hydrothermal site: *Earth Planet. Sci. Lett.*, v. 67, p. 297-307.
- Morogan, V., 1994, Ijolite versus carbonatite as sources of fenitization: *Terra Nova*, v. 6, p. 166-176.
- Mountain, B.W., 1992, Fluid-rock interaction paths: Natural and experimental examples: Unpublished Ph.D. thesis, McGill University, Montreal.
- Norman, D.I., Kyle, P.R., and Baron, C., 1989, Analysis of trace elements, including rare earth elements, in fluid inclusion liquids: *Econ. Geol.*, v. 84 (1), p. 162-166.
- Palmer, D.A.S., and Williams-Jones, A.E., 1996, Genesis of the carbonatite-hosted fluorite deposit at Amba Dongar, India: Evidence from fluid inclusions, stable isotopes and whole rock-mineral geochemistry: *Economic Geology*, v. 91, p. 934-950.
- Palmer, D.A.S., and Williams-Jones, A.E., 1998a, Fluid evolution of the Amba Dongar carbonatite complex, India: Unpublished Ph.D. thesis, McGill University, Montreal, Chapter 5.
- Palmer, D.A.S., and Williams-Jones, A.E., 1998b, Fenitization associated with the Phalaborwa complex, South Africa: Unpublished Ph.D. thesis, McGill University, Montreal, Chapter 8.
- Reed, M.H., 1997, Hydrothermal alteration and its relationship to ore fluid composition: In: Barnes, H.L., ed., *Geochemistry of Hydrothermal Ore Deposits*, John Wiley & Sons Inc., Toronto, p. 303-366.
- Richardson, C. and Holland, D., 1979a, The solubility of fluorite in hydrothermal solutions, an experimental study: *Geochimica et Cosmochimica Acta*, v. 43, p. 1313-1325.

- Rimstidt, J.D., 1997, Gangue mineral transport and deposition: In: Barnes, H.L., ed., *Geochemistry of Hydrothermal Ore Deposits*, John Wiley & Sons Inc., Toronto, p. 487-516.
- Roedder, E., 1984, Fluid Inclusions: Reviews in Mineralogy Vol. 12, P.H. Ribbe (ed.), Mineral. Soc. Am., 644p.
- Roelofsen, J.N., 1997, The primary and secondary mafic silicates of two alkaline anorogenic complexes: Strange Lake (Quebec-Labrador) and Amba Dongar (Gujarat, India): Unpublished Ph.D. thesis, McGill University, Montreal, 489p..
- Rubie, D.C., and Gunter, W.D., 1983, The role of speciation in alkaline igneous fluids during fenite metasomatism: *Contrib. Mineral. Petrol.*, v. 82, p. 165-175.
- Shock, E.L., Sassani, D.C., Willis, M., and Sverjensky, D.A., 1997, Inorganic species in geologic fluids: Correlations among standard molal thermodynamic properties of aqueous ions and hydroxide complexes: *Geochim. Cosmochim. Acta*, v. 61 (5), p.907-950.
- Simonetti, A., and Bell, K., and Viladkar, S.G., 1995, Isotopic data from the Amba Dongar Carbonatite Complex, west-central India: Evidence for an enriched mantle source: *Chemical Geology*, v. 122, p. 185-198.
- VanMiddlesworth, P.E., 1997, Determination of REE, Th and U concentrations in thermal waters of the Lochsa, Salmon and Stanley regions of the Bitterroot lobe of the Idaho Batholith: Unpublished M.Sc. Thesis, University of Idaho, Moscow, 190p..
- Viladkar, S.G., 1986, Fenitization at the Amba Dongar Carbonatite alkalic complex, India: *in* M. Gabriel (ed), *Symposium New Mineral Raw Materials: Proceedings*, p. 170-189.
- Wolery, T.J., 1992, *Eq3/6*, a software package for the geochemical modeling of aqueous systems: Lawrence Livermore National Laboratory, University of California, Livermore.
- Wood, S.A., and Williams-Jones, A.W., 1994, The aqueous geochemistry of the rare-earth elements and yttrium 4. Monazite solubility and REE mobility in exhalative massive sulfide-depositing environments: *Chem. Geol.*, v. 115, p. 47-60.
- Wyllie, P.J., 1989, Origin of carbonatites: evidence from phase equilibrium studies: *in* K. Bell (ed.), *Carbonatites: genesis and evolution*: London, Unwin Hyman, p.149-176.

Bridge to Chapter 7

The preceding three chapters used solid inclusions, fluid inclusions and fenitization to characterize the melts and aqueous fluids that were present during the emplacement of the Amba Dongar complex, India. It was concluded that carbonate-carbonate liquid immiscibility was responsible for the formation of calciocarbonatite and ferrocarbonatite. The evolution of the aqueous fluids was documented, with respect to temperature, pressure and composition, from exsolution of the fluids at depths of 35 km until final emplacement of the carbonatite near surface.

The following chapters use similar methods to investigate the melt and fluid evolution of another carbonatite-bearing complex, the Phalaborwa complex, South Africa. This complex differs from Amba Dongar in that it is dominated by pyroxenite and contains a copper deposit within the carbonatites. Also, whereas the evidence for aqueous fluids at Amba Dongar is plentiful, carbonatite melts at Phalaborwa appear to have contained much less dissolved water. The information obtained is used to determine the controls on copper mineralization in carbonatite.

**Chapter 7: Solid Inclusions from the Phalaborwa complex, South Africa:
Evidence of silicate-carbonate immiscibility**

**D. A. S. Palmer and A. E. Williams-Jones
Department of Earth and Planetary Sciences,
McGill University**

Abstract

The Phalaborwa complex, South Africa, is composed of both silicate and carbonate lithologies which were intruded into Archean granites and granitic gneisses. The complex is host to a large (≈ 400 Mt) copper deposit, with an average grade of 0.69% Cu. Copper mineralization can be divided into early bornite (phoscorite, banded carbonatite) and late chalcopyrite (transgressive carbonatite) stages.

Numerous solid inclusions are present in apatite hosted by phoscorite and transgressive carbonatite. Consistent compositions and high temperature phase relationships indicate that solid-vapour and solid-liquid-vapour inclusions represent trapped samples of melt.

Solid-vapour inclusions in phoscorite are composed of two solids which show compositional and petrographic similarities to calcite and magnetite, and a third high magnesian silicate. The proportions of calcite and the magnesian silicate in the inclusions are similar, while magnetite comprises less than 10% of the volume of an inclusion. A small proportion ($<5\%$) of vapour can usually be observed. Analyses of some solid-vapour inclusions also reveal spectral peaks for Cu and S and indicate that a Cu-Fe sulphide is also present. Apatite in transgressive carbonatite hosts two populations of solid inclusion comprising solid and solid-liquid-vapour. The solids comprise calcite and a magnesian silicate, with calcite making up well over 50% of the inclusion. Fluid present in solid-liquid-vapour inclusions, typically comprises less than 10% of the inclusion volume and is a saline Mg-, Fe- and S-bearing NaCl-KCl brine (≈ 22 wt.% NaCl eq.). Na/Na+K ratios are consistently between 0.4 and 0.6.

Heating of solid-vapour inclusions in phoscorite produces initial melting at temperatures of around 450°C. In the temperature range 740 to 800°C, two immiscible liquids are present with silicate and carbonate compositions. At temperatures above 800°C the inclusion homogenizes to a single liquid plus vapour, and on cooling separates again into two liquids. Solid inclusions in transgressive carbonatites have initial melting temperatures in the range 550 to 670°C and homogenize above 750°C. Temperatures of initial and final melting of solid-liquid inclusions overlap those of solid-vapour inclusions.

Consistent compositions and high temperature phase relationships indicate that solid-vapour and solid-liquid-vapour inclusions represent trapped samples of melt. These melt inclusions provide evidence that silicate-carbonate liquid immiscibility occurred in the liquids which were responsible for the formation of carbonate-bearing lithologies. Although liquid immiscibility was important in removing Si from the carbonate-rich melt, silicate and carbonate rocks are not related by liquid immiscibility. Fractionation is still considered to have been dominant in the formation of the Phalaborwa complex. The presence of Cu-bearing sulphides in solid-vapour inclusions hosted by phoscorite indicates that Phalaborwa magmas were enriched in Cu before emplacement. Solid-liquid-vapour inclusions provide the first evidence of a separate magmatic aqueous fluid phase at Phalaborwa and support a hydrothermal origin for copper mineralization in transgressive carbonatite.

Introduction

Numerous theories have been proposed for the formation of carbonatite magmas over the last 40 years with the two most widely favoured being silicate-carbonate liquid immiscibility (Freestone and Hamilton, 1980; Kjarsgaard and Hamilton, 1988; Lee and Wyllie, 1996, 1997, 1998) and direct melting of the mantle (Wallace and Green, 1988; Gittins, 1988; Sweeny, 1994; Harmer and Gittins, 1997). The subsequent evolution of the carbonatite magma is typically ascribed to fractionation of the parental liquid, although there have been some suggestions that carbonate-carbonate immiscibility may also play a role (Brooker and Hamilton, 1990; Mitchell, 1997; Nielsen *et al.*, 1997; Palmer and Williams-Jones, 1998a, Chap. 4).

Silicate-carbonate liquid immiscibility has been shown to occur in numerous synthetic systems (Freestone and Hamilton, 1980; Kjarsgaard and Hamilton, 1988; Lee and Wyllie, 1996, 1997) and examples have also been reported for natural systems (Rankin and Le Bas, 1974; Amundsen, 1987; Nielsen *et al.*, 1997). In natural and experimental systems, silicate and carbonate liquids co-exist at similar temperatures, ranging between 900 and <1300°C (Rankin and Le Bas, 1974; Freestone and Hamilton, 1980; Hamilton and Kjarsgaard, 1993; Lee and Wyllie, 1997; Nielsen *et al.*, 1997). The

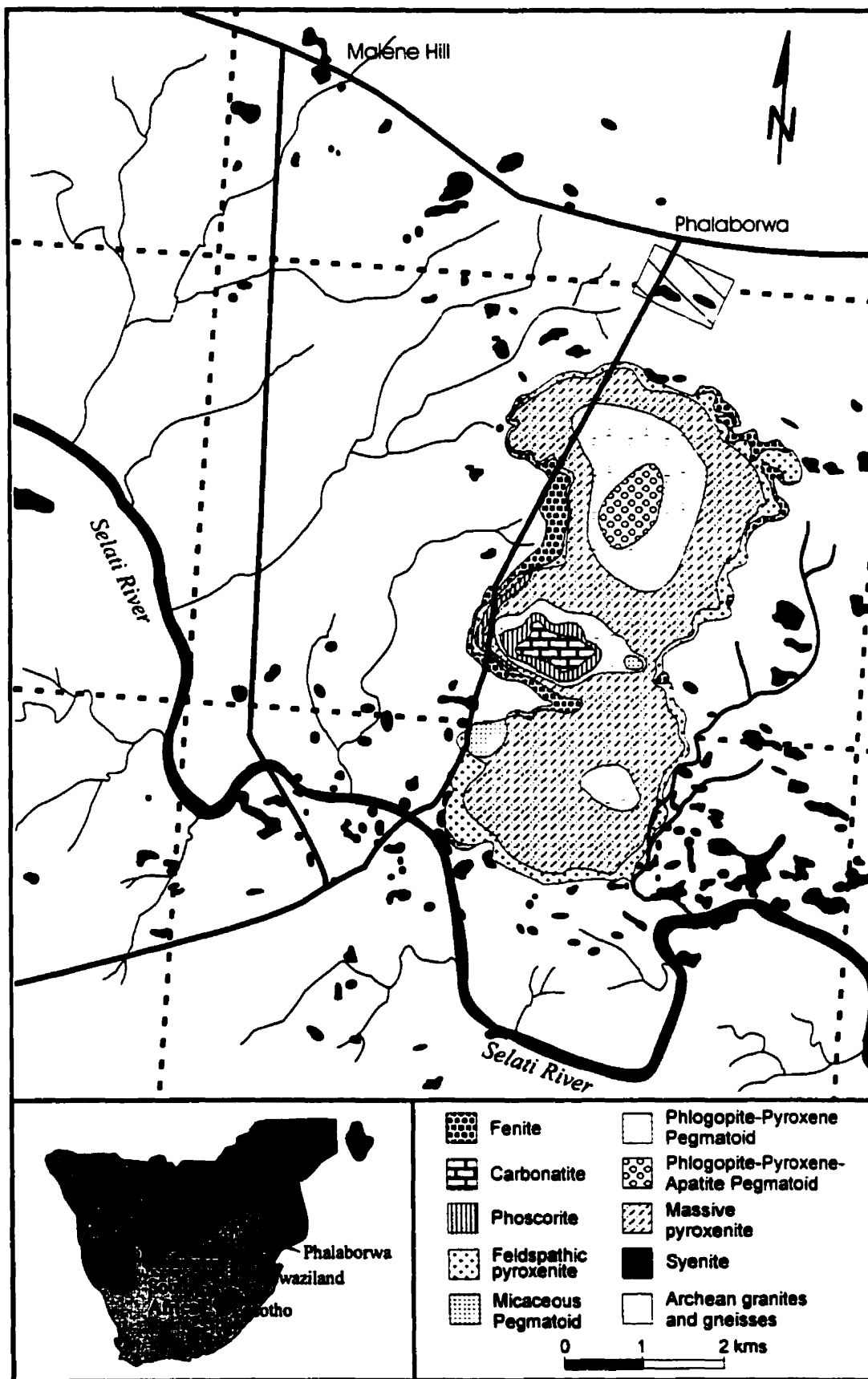
composition of silicate and carbonate liquids produced experimentally are diverse, and include nephelinite, melilitite and phonolite and natrocarbonatite and calciocarbonatite, respectively (Freestone and Hamilton, 1980; Kjarsgaard and Hamilton, 1988; Lee and Wyllie, 1997). Reports of naturally occurring immiscible melts are restricted to melilitite, basalt and peridotite and calciocarbonatite, magnesiocarbonatite and natrocarbonatite, respectively (Amundsen, 1987; Nielsen *et al.*, 1997)

New data from solid inclusions identified in apatite from phoscorite and transgressive carbonatite of the Phalaborwa complex, South Africa, indicate that they are samples of trapped melts which existed during emplacement of the respective lithologies. The behaviour of these melt inclusions suggests that, although silicate-carbonate immiscibility played an important role in the formation of the host phoscorite and carbonatite, it cannot explain the presence of the large volumes of silicate rocks at Phalaborwa. Rather, liquid immiscibility served only to remove silica from early carbonate-rich liquids.

Geology

The Phalaborwa complex is located in the northeastern part of South Africa's Transvaal province and is composed of both silicate and carbonatite lithologies (Fig. 7-1). The complex, which has been dated at between 2047 and 2061 Ma (Eriksson, 1989; Reischmann, 1995), was intruded into Archean granites and granitic gneisses (Hannekom, 1965) and began with the formation of a large kidney shaped lobe of pyroxenite which was later cored by phoscoritic and carbonatitic magmas. Numerous small bodies of syenite were emplaced within the surrounding Archean granites and gneisses both during and after intrusion of the complex. Late NE-SW trending diabase dykes cut both the complex and the country rocks, and are thought to be Precambrian in age (≈ 1900 Ma) (Briden, 1976). An aureole of fenitization is weakly developed in granites and gneisses around the carbonatites, suggesting that hydrothermal fluids were present during emplacement of the complex (Frick, 1975; Eriksson, 1982; Palmer and Williams-Jones, 1998b, Chap. 8).

Figure 7-1 The geology of the Phalaborwa complex, South Africa (modified from Hanekom et al., 1965 and Frick, 1975).



Economic quantities of copper mineralization make Phalaborwa unique among carbonatite intrusions. Initial reserves were calculated at over 400 Mt, grading, on average, 0.69% Cu (Palabora Mining Company, 1976) as bornite and chalcopyrite. Gold, platinum and zircon are recovered as by-products from the copper ore. Economic deposits of vermiculite and phosphate also occur in the complex, and are hosted by pyroxenite.

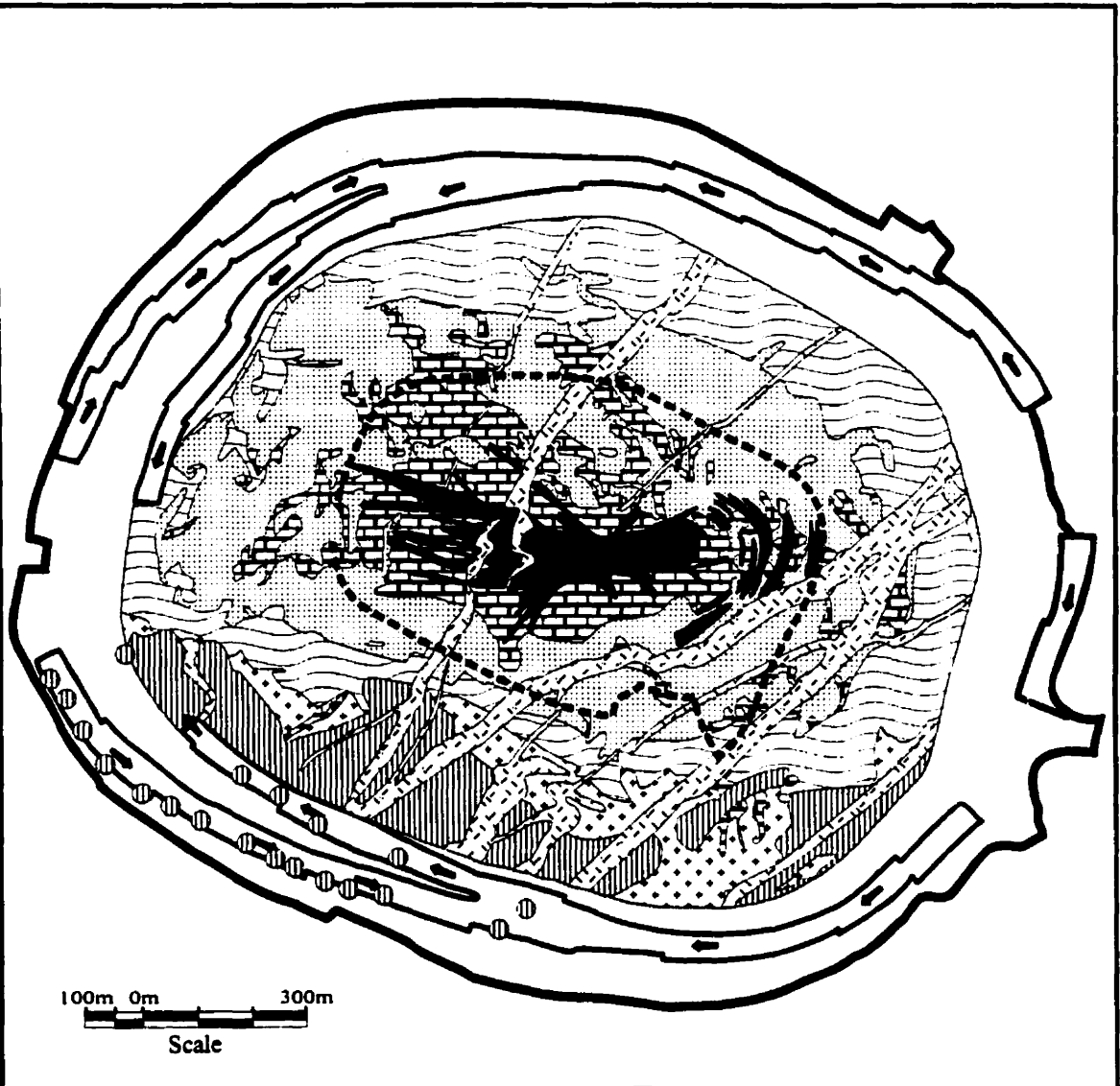
Pyroxenite










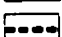
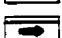
Pyroxenite is the dominant lithology of the complex and can be subdivided into four main types based on mineralogical and textural characteristics. These four pyroxenite types may be distinguished by the following descriptors: massive; micaceous; pegmatitic; and feldspathic. Contacts between one pyroxenite type and another are sharp. Recent studies by Eriksson (1989) suggest that all four pyroxenite subtypes were formed by primary crystallization from the parental magmas, and not, as was first thought for phlogopite-rich pyroxenites, by secondary hydrothermal processes (Eriksson, 1982). All pyroxenites consist dominantly of diopsidic pyroxene and contain variable proportions of phlogopite and calcic plagioclase. Apatite is an ubiquitous accessory mineral. Massive pyroxenites are mineralogically homogeneous and contain minor proportions of apatite and phlogopite interstitial to diopside, while micaceous pyroxenites differ only through an increase in phlogopite content. Pegmatitic pyroxenites comprise serpentine-bearing and non serpentine-bearing varieties of phlogopitic pyroxenite, located in the northern and southern sections of the complex, respectively. Feldspathic pyroxenite is characterized by large (up to several centimetres in diameter) anhedral microcline crystals. The spatial restriction of this pyroxenite to the margins of the main pyroxenite body is interpreted to indicate a cumulate origin (Eriksson, 1989).

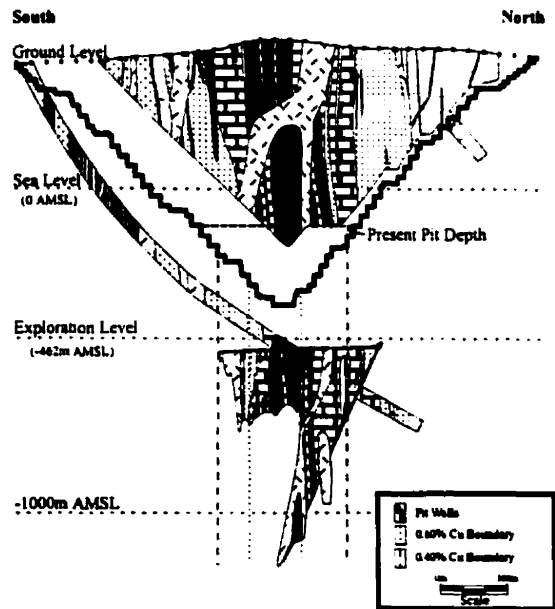
Phoscorite

Separating pyroxenite and carbonatite is a unit referred to locally as phoscorite (Fig 7-2), composed of a thick (up to 400m) ring of apatite-rich, magnetite-

Figure 7-2 The geology of Palabora Mining Company's open pit.



-  Diabase
-  Transgressive Carbonatite
-  Banded Carbonatite
-  Phoscorite
-  Micaceous Pyroxenite
-  Feldspathic Pyroxenite
-  Fenite
-  Fenite Samples
-  Pit Area
-  Present Mining Level
-  Ramp



carbonate-magnesian silicate-bearing rock originally thought to represent gradational zoning between pyroxenite and carbonatite. More recent studies, however, (Palabora Mining Company, 1976), have identified sharp contacts between pyroxenite and phoscorite and a primary origin for phoscorite involving cogenesis with carbonatite, is now proposed (Eriksson, 1989).

The average modal composition of phoscorite, calculated by Hannekom (1965) from mill data, is 35% magnetite, 25% apatite, 22% carbonate and 18% olivine-serpentine and phlogopite. Accessory baddelyite, commonly replaced by magnetite (Van Rensburg, 1965), and copper sulphides are also present.

Carbonatite

Carbonatites are the youngest members of the main complex and consist of an early banded variety, named for its distinctive concentric bands of magnetite which parallel the outer ring of phoscorite, and a later transgressive variety, which was intruded along WNW and ENE trending fractures (Fig. 7-2). Both carbonatite types are composed of fine- to coarse-grained calcite with accessory copper sulphides, apatite and olivine. Magnetite can reach abundances locally of well over 50%.

The two carbonatite types are readily distinguished by their sulphide mineralogy, with banded carbonatite containing dominantly bornite, and transgressive carbonatite, which hosts the bulk of the copper mineralization, containing dominantly chalcopyrite. The composition of calcite, which is more magnesian in transgressive carbonatite, has also been proposed as a means of discriminating between carbonatite types (Eriksson, 1989). Although magnetite concentrations are similar in the two carbonatite types, there are differences in the textures of magnetite. Magnetite in banded carbonatite is often found in massive lenses with individual crystals aligned parallel to the outer margin of the carbonatite. In transgressive carbonatite, magnetite crystals lack a preferred orientation, although they do occur locally in massive pods.

Apatite

Apatite, which hosts the solid inclusions investigated in this study, is found in all lithologies of the complex. It occurs as abundant, variably sized (mms to cms), euhedral to subhedral crystals in both carbonatite and phoscorite and may be interstitial to or occur as included solids in the major rock-forming minerals (Aldous, 1980). Aldous (1980) divided apatite into three types based on its occurrence in pyroxenite, phoscorite and carbonatite and concluded that, although it is probably primary magmatic mineral, a hydrothermal origin cannot be ruled out. Our discovery of possible melt inclusions in apatite of transgressive carbonatite and phoscorite, confirm its primary origin in both these lithologies.

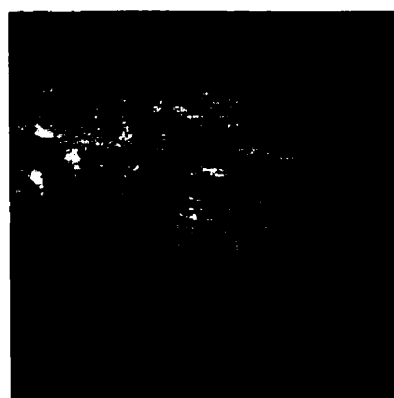
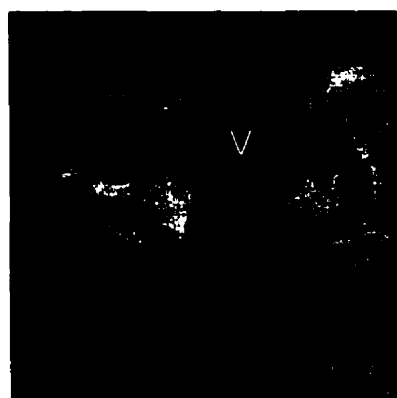
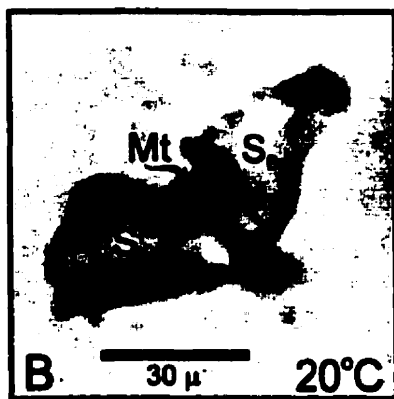
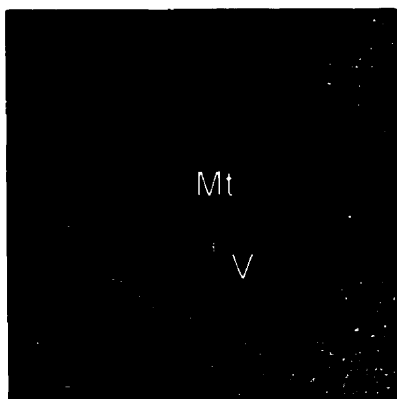
Solid inclusions

Numerous multiphase solid inclusions were identified in apatite hosted by phoscorite and transgressive carbonatite at Phalaborwa. Only solid-vapour inclusions were recognized in phoscorite, while solid-vapour and solid-liquid-vapour types were found in transgressive carbonatite (Fig. 7-3).

Solid-Vapour Inclusions in Phoscorite

Randomly dispersed throughout apatite crystals in phoscorite are numerous, small ($<60\mu$), ovoid to cigar-shaped, solid-vapour inclusions containing three separate solid phases and one fluid phase (Fig. 7-3a). The two dominant solids divide the inclusion in almost equal parts, and consist of a light green, strongly anisotropic mineral and a colorless mineral with no obvious birefringence. At the boundary between these two solids there is almost invariably a small, hexagonal opaque which occupies no more than 20% by area of the section of the inclusion viewed in the microscope. Between the inner wall and the outer surface of the inclusion, generally at the contact between the two

Figure 7-3 Solid inclusions in apatite from phoscorite and transgressive carbonatite. Photomicrographs of: A) and B) solid inclusions from phoscorite containing magnesian silicate (S), calcite (S_{Br}), magnetite (Mt) and a vapour phase (V); C) a solid inclusion from transgressive carbonatite containing calcite (S_{Br}) and subordinate magnesian silicate (S) and a large vapour (V) phase; and D) a solid inclusion from transgressive carbonatite containing calcite (S_{Br}), magnesian silicate (dark upper solid), an undetermined third solid and a mixture of liquid and vapour H_2O (H_2O_{V+L}).



dominant solids, is a small, dark, irregularly shaped phase which, upon heating, proves to be vapour.

Solid-Vapour Inclusions in Transgressive Carbonatite

Solid inclusions hosted within apatite crystals of transgressive carbonatite are small ($<20\mu$), irregularly shaped bodies which contain only three phases, two solids and a vapour phase. The two solids comprise a colorless, highly birefringent phase, which generally occupies over 50 vol.% of the inclusion, and a weakly colored green solid of indeterminate birefringence which rarely occupies over 10% of the inclusion volume. The fluid phase, which is usually irregularly shaped due to the crystallization of the solid phases, can occupy as much as 40% of the inclusion's section.

Solid-Liquid-Vapour -Bearing Inclusions in Transgressive Carbonatite

A number of liquid and vapour-bearing solid inclusions were identified within apatite of transgressive carbonatite. These inclusions contain up to four solids and consist of a large, colorless birefringent mineral, occupying over 50% of the inclusion volume and three smaller, irregularly shaped, non birefringent solids. The fluid phase consists of both vapour and liquid which are invariably in contact with at least two of the smaller solids. Visually, the volume of aqueous fluid never exceeds 10% of the total volume of an inclusion.

Composition of Solid Inclusions

In order to identify the solid phases in the inclusions, electron microprobe energy dispersive spectrometric (EDS) analyses were performed on samples of apatite from phoscorite and transgressive carbonatite which had been polished to the level of the inclusion (Table 7-1, 2, 3, 4).

Table 7-1 Semi-quantitative analyses of calcite and dolomite in opened melt inclusions (phoscorite)

cation%	C-1	C-2	C-3	C-4	C-5	D-1	D-2	D-3	D-4
wt.%	calcite					dolomite			
SiO ₂	0.15	0.66	0.75	1.76	—	—	—	1.79	1.27
MgO	0.63	2.72	2.18	0.64	0.49	14.49	21.61	7.21	5.39
MnO	—	—	—	—	—	—	—	1.08	1.02
FeO	0.73	—	1.74	0.40	0.53	9.57	4.29	—	0.60
CaO	93.87	92.81	82.29	85.67	93.84	55.55	52.75	61.62	65.10
Na ₂ O	—	0.36	—	0.43	—	—	—	—	—
K ₂ O	0.45	0.84	0.40	—	—	—	—	—	0.56
BaO	—	1.45	1.03	—	0.16	—	—	0.77	0.99
SO ₃	0.77	—	0.41	2.49	0.60	0.61	0.83	1.43	14.68
CuO	0.86	0.76	—	1.18	—	0.41	—	1.40	0.83
La ₂ O ₃	—	—	3.16	—	0.61	—	1.39	0.40	2.33
Ce ₂ O ₃	—	—	3.00	—	0.19	—	3.19	—	0.66
P ₂ O ₅	1.37	—	4.05	7.31	2.05	18.60	15.47	19.10	4.83
cat.%									
Si	0.00	0.01	0.01	0.02	—	—	—	0.05	0.03
Mg	0.01	0.04	0.04	0.01	0.05	0.58	0.80	0.33	0.21
Mn	—	—	—	—	—	—	—	0.03	0.02
Fe	0.01	—	0.02	0.00	0.00	0.21	0.09	—	0.01
Ca	0.98	0.93	0.93	0.96	0.95	1.21	1.11	1.58	1.70
Na	—	—	—	—	—	—	—	—	—
K	0.01	0.01	0.01	—	—	—	—	—	0.02
Ba	—	0.01	0.00	—	—	—	—	0.00	0.01
S	0.01	—	0.01	0.03	0.03	0.01	0.01	0.02	0.18

— not detected

Table 7-2 Semi-quantitative analyses of magnesian silicate in opened melt inclusions (phoscorite)

cation%	O-1	O-2	O-3	O-4	O-5	O-6	O-7	O-8	O-9
wt.%					olivine				
SiO ₂	38.25	13.39	19.56	21.98	25.47	38.31	31.57	37.30	23.33
MgO	57.96	53.98	50.31	42.75	34.06	58.68	42.35	53.00	56.38
MnO	0.64	8.05	11.86	6.10	6.73	—	—	—	7.49
FeO	3.11	—	5.77	1.32	3.06	3.01	6.92	2.71	—
Na ₂ O	—	—	—	2.85	—	—	—	0.17	1.60
K ₂ O	0.04	—	—	—	—	—	2.78	—	—
BaO	—	5.79	—	3.39	—	—	4.14	—	—
SO ₃	—	5.31	5.88	0.68	6.12	—	3.64	0.32	2.28
CuO	—	10.45	—	12.46	21.11	—	8.60	3.07	8.09
La ₂ O ₃	—	3.02	4.24	6.27	3.06	—	—	3.43	—
cat.%									
Si	0.90	0.36	0.53	0.60	0.75	0.90	0.84	0.91	0.57
Mg	2.03	2.16	2.03	1.73	1.50	2.05	1.69	1.94	2.05
Mn	0.01	0.18	0.27	0.14	0.17	—	—	—	0.15
Fe	0.06	—	0.13	0.03	0.08	0.06	0.15	0.06	—
Na	—	—	—	0.15	—	—	—	0.01	0.08
K	0.00	—	—	—	—	—	0.09	—	—
Ba	—	0.06	—	0.04	—	—	0.04	—	—
S	—	0.07	0.07	0.01	0.08	—	0.01	0.00	0.03
Cu	—	0.21	—	0.26	0.47	—	0.17	0.06	0.15
La	—	0.03	0.04	0.06	0.03	—	—	0.03	—
Mg#	0.95	1.00	0.94	0.98	0.97	0.97	0.92	0.97	1.00

— not detected

**Table 7-3 Semi-quantitative analyses of Fe-oxides and chalcopyrite in
opened melt inclusions (phoscorite)**

cation%	F-1	F-2	F-3	F-4	CP-1	CP-2
wt. %	Fe-Ox				CPY	
SiO ₂	1.61	0.05	---	---	0.08	0.05
MgO	11.46	10.20	0.87	3.98	1.11	0.69
FeO	64.96	79.72	57.48	55.99	18.84	18.46
CaO	9.11	4.55	38.71	35.82	9.82	17.50
Na ₂ O	---	0.28	1.13	1.22	6.02	3.42
K ₂ O	---	---	---	---	---	0.32
BaO	---	---	---	---	0.81	---
SO ₃	0.36	---	0.53	0.05	25.63	22.90
CuO	0.04	1.80	---	0.14	19.18	13.91
La ₂ O ₃	1.74	0.11	---	0.75	1.79	---
Ce ₂ O ₃	2.17	---	---	0.53	0.75	---
P ₂ O ₅	7.44	2.48	1.02	1.25	15.54	22.07
Si	0.03	0.00	---	---	---	---
Mg	0.28	0.25	0.02	0.10	0.10	0.08
Fe	0.90	1.11	0.80	0.78	1.00	1.16
Ca	0.67	0.04	0.02	0.61	---	0.17
Na	---	0.01	0.04	0.04	0.74	0.50
K	---	---	---	---	---	0.03
Ba	---	---	---	---	0.02	---
S	0.00	---	0.01	0.00	1.22	1.29
Cu	---	---	---	---	0.92	0.79

--- not detected

Table 7-4 Semi-quantitative analyses of melt leakage on apatite surface (Phoscorite)

cation%	m-1	m-2	m-3	m-4	m-5	m-6	m-7	m-8
wt. %								
SiO ₂	4.61	3.13	—	49.46	0.74	0.41	9.08	42.94
Al ₂ O ₃	4.85	3.84	1.48	14.27	—	—	7.59	—
MgO	5.38	3.60	0.49	1.77	4.04	1.89	0.81	35.49
FeO	3.58	3.16	0.53	2.67	1.51	0.54	0.64	—
CaO	38.48	39.22	93.84	9.56	73.64	68.78	44.77	18.43
Na ₂ O	0.39	0.82	—	12.10	—	0.31	4.46	—
K ₂ O	0.06	—	—	0.58	0.27	0.65	0.42	—
BaO	0.16	—	0.16	0.80	—	—	—	—
SO ₃	11.71	2.37	0.60	0.18	0.48	0.68	0.58	0.02
CuO	0.93	0.37	—	0.71	0.03	—	0.17	—
La ₂ O ₃	—	—	0.61	0.66	—	2.25	—	—
Ce ₂ O ₃	—	0.80	0.19	—	0.66	—	—	—
P ₂ O ₅	29.06	42.59	2.05	7.23	17.61	23.13	31.49	3.12
cat. %								
Si	0.08	0.05	—	0.82	0.01	0.01	0.15	0.71
Al	0.10	0.08	0.03	0.28	—	—	—	—
Mg	0.13	0.09	0.01	0.04	0.10	0.05	0.02	0.88
Fe	0.05	0.04	0.01	0.04	0.02	0.01	0.01	—
Ca	0.33	0.18	1.64	0.07	1.09	0.94	0.41	0.28
Na	0.01	0.03	—	0.39	—	0.01	0.14	—
K	0.00	—	—	0.01	0.01	0.01	0.01	—
Ba	0.00	—	—	0.01	—	—	—	—
S	0.15	0.03	0.01	0.00	0.01	0.01	0.01	0.00
Cu	—	—	—	—	—	—	0.00	—
La	—	—	—	—	—	—	0.15	—

— not detected

Solid-Vapour Inclusions from Phoscorite

Phase compositions are remarkably similar among solid inclusions in phoscorite-hosted apatite. The highly birefringent solid, which dominates the inclusion, consists of a Ca-rich, Mg-bearing mineral with a Mg/Ca cation ratio between 0.12 and 0.72. This mineral is probably calcite, Mg-calcite or dolomite (Table 7-1). The colorless birefringent phase is a magnesian silicate, with average Mg and Si cationic proportions of 1.9 to 0.7, respectively (Fig 7-4a, Table 7-2). Unfortunately, the small opaque mineral was never observed on the polished inclusion surface, however, strong peaks for Fe were obtained (cation proportions >1) in a number of analyses, and it is inferred to be an iron oxide (Table 7-3). Aldous (1980), identified small chalcopyrite crystals associated with magnetite in olivine-hosted solid inclusions from phoscorite. The presence of Cu, Fe and S in analyses of opened solid inclusions in apatite (Table 7-3), indicates that opaque minerals in inclusions may also include chalcopyrite. In a number of cases, solid inclusions leaked during heating and analyses of the leak products confirmed the presence of Cu, Fe and S (Fig. 7-4b, Table 7-4).

The analysis of material which leaked from inclusions during heating provided further quantification of bulk compositions (Table 7-4). Although proportions are variable, analyses indicate that solid inclusions are composed mainly of Ca, Mg and Si. Calcium generally dominates the composition of melt leaks followed by Si, then Mg with average cation proportions of 0.34, 0.21 and 0.13, respectively.

Solid-Vapour Inclusions from Transgressive Carbonatite

Energy dispersive spectra for polished inclusions and the precipitates of melt leaks indicate that the bulk composition of solid-vapour inclusions is dominated by Ca (cation proportions of 0.88 to 0.98), has elevated S (0.16 to 0.33) and minor concentrations of Si, Mg (0.02 and 0.03, respectively) (Table 7-5). As for inclusions from phoscorite, the two solid phases present in solid-vapour inclusions from transgressive carbonatite are calcite and a magnesian silicate. Although chemical

Figure 7-4 SEM photomicrographs of: A) Mg-Si solid in opened melt inclusion in apatite of phoscorite. Spot O-1 corresponds to an analysis in Table 7-2; and B) melt leakage on apatite surface (phoscorite). Spots m-1,2,3 and 4 correspond to analyses in Table 7-4;

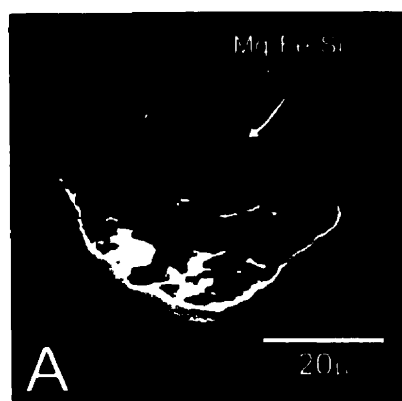


Table 7-5 Semi quantitative analyses of melt inclusion leakage residues (ML) and solids (S) on apatite of transgressive carbonatite

	ML-1	ML-2	ML-3	ML-4	ML-5	ML-6	S-1	S-2	S-3	S-4	S-5
cat. %	melts						solids				
Si	---	---	---	---	0.02	0.01	0.04	1.26	0.47	---	1.15
Al	0.01	0.01	0.01	0.00	0.00	---	---	---	---	---	---
Mg	---	---	---	---	0.03	0.07	0.15	2.37	2.41	0.02	1.24
Mn	---	---	---	---	---	---	---	---	---	---	---
Fe	---	0.01	0.01	0.00	---	---	0.00	0.15	0.10	1.63	0.09
Ca	0.98	0.95	0.93	0.97	0.88	0.89	0.80	0.09	1.00	1.46	0.69
Na	---	---	0.01	0.02	0.02	---	---	---	---	0.33	---
K	0.01	0.01	0.01	0.01	0.01	0.01	0.01	---	0.02	0.04	0.02
Ba	0.00	0.02	0.01	---	---	0.03	0.00	0.07	---	---	---
S	0.23	0.22	0.33	0.33	0.16	0.16	0.00	0.14	0.01	0.00	0.00
Cu	---	0.01	0.03	---	---	---	---	---	---	0.49	0.01
La	---	---	---	---	---	---	0.00	---	---	0.03	0.12
Ce	---	---	---	---	0.03	---	---	0.06	---	0.01	0.69
Mineral ID							calcite	olivine	Cc+Ol	Cc+Cpy	olivine

Cc - calcite; Ol - olivine; Cpy - chalcopyrite

components are almost identical to those of solid inclusions from phoscorite, the concentrations of Si and Mg are much lower, corresponding to very small proportions of magnesian silicate within these inclusions.

The two dominant phases in solid-liquid-vapour inclusions in transgressive carbonatite, are also calcite and a magnesian silicate. However, the presence of an aqueous fluid implies a somewhat more complex bulk composition. In order to determine the composition of the associated aqueous phase, solid-liquid-vapour inclusions were decrepitated and the residues analysed by EDS (Table 7-6). Results indicate that the aqueous fluid is a NaCl-KCl brine with minor proportions of Mg, Fe and S. Na/Na+K ratios are consistently around 0.5. Charge balance calculations indicate that the fluid contains unaccounted for anionic species, probably HCO_3^- or CO_3^{2-} .

Microthermometric Results

High temperature phase changes in solid inclusions were investigated using a Leica 1350 heating stage calibrated using the melting points of pure NaCl (800.4°C), NaSO₄ (884°C) and Au (1024°C) and the transition from α quartz to β quartz (573°C). Temperatures of phase changes in aqueous fluid-bearing inclusions were measured on a U.S.G.S gas-flow fluid inclusion stage using liquid and gaseous nitrogen as a cooling medium. Calibration was accomplished using synthetic H₂O and CO₂ fluid inclusions, achieving an accuracy of $\pm 0.2^\circ\text{C}$.

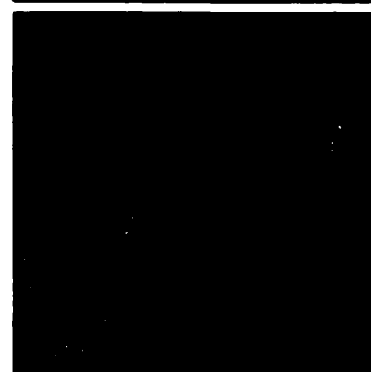
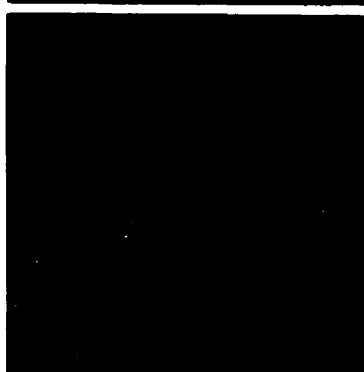
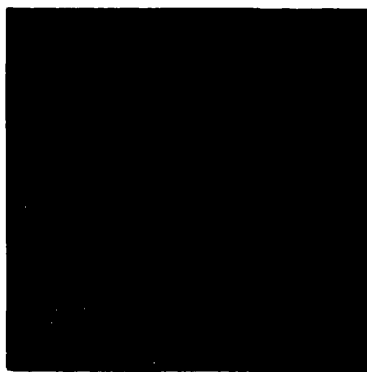
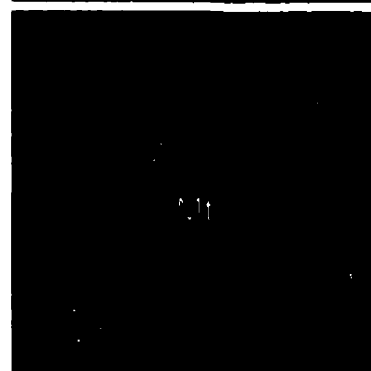
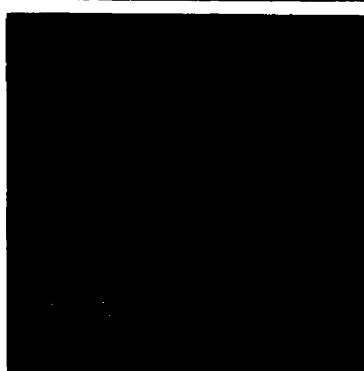
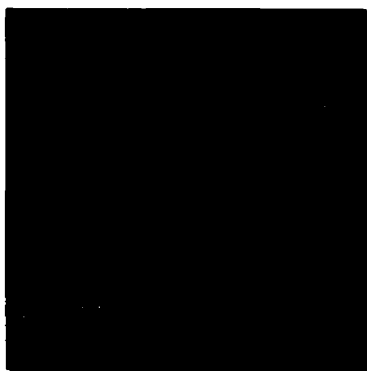
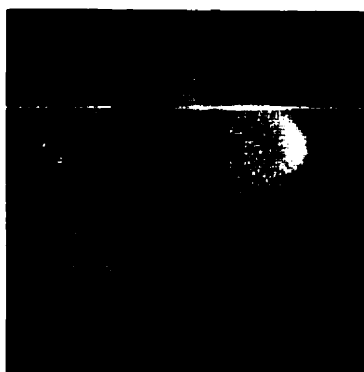
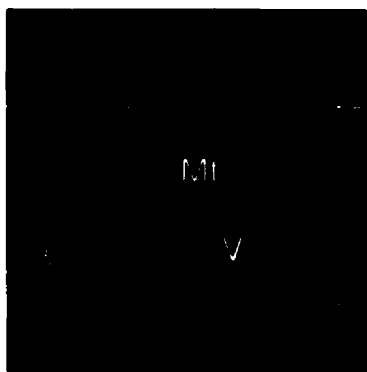
Solid-Vapour Inclusions in Phoscorite

The first changes in solid-vapour inclusions in phoscorite consistently occurred at temperatures between 429 and 480°C (Fig. 7-5c), and consisted of a reduction in the size of the vapour bubble and its disappearance. Melting of solids commenced at temperatures between 635 and 690°C and appeared to occur simultaneously in both carbonate and silicate solids (Fig. 7-5d). At the same time as melting begins, a vapour bubble appeared in the liquid fraction. With continued heating, greater quantities of liquid are produced and the presence of two immiscible liquids becomes apparent, one

**Table 7-6 Semi quantitative analyses of melt inclusion decrepitates on apatite of
transgressive carbonatite**

	D-1	D-2	D-3	D-4	D-5	D-6	D-7
cat. %							
Cl	26.76	40.00	45.91	45.31	46.79	49.04	44.46
S	0.66	2.03	0.35	---	0.39	0.55	0.59
Na	17.99	21.57	24.55	19.13	31.91	27.72	22.67
K	17.77	25.29	28.52	32.57	19.11	22.09	31.57
Ca	33.49	4.23	---	---	---	---	0.36
Mg	2.86	4.40	0.30	1.15	0.69	---	0.16
Fe	0.21	---	0.30	---	0.65	0.06	0.14
Ce	---	---	---	---	0.42	---	0.04
Si	0.27	2.49	0.08	0.49	0.04	0.34	---
Al	---	---	---	1.35	---	0.20	---
Na/Na+K	0.50	0.5	0.5	0.4	0.6	0.6	0.4
Na/Cl	0.67	0.54	0.53	0.42	0.68	0.57	0.51
charge	26.95	10.15	7.28	6.96	4.70	0.51	9.81

Figure 7-5 Melting behaviour of melt inclusions in phoscorite-hosted apatite. A) solid inclusion at 20°C in plane polarized light. B) same inclusion in cross polarized light showing the inclusion divided approximately in half by birefringent (Ca-carbonate) and non-birefringent (Mg-Si solid) phases. The central opaque is assumed to be magnetite while the dark area in the lower right hand edge behaves like a vapour phase. C) At 476°C the vapour phase is almost gone. D) Initial melting in transparent solids begins at approximately 689°C. E) Production of vapour with continued melting at 706°C. F) The presence of two liquids becomes apparent (764°C). G) Increased melting is accompanied by an increase in the size of the vapour bubble (767°C). H) Only two liquids and vapour remain (793°C) and I) quenched liquids with vapour.



green in color and the other colorless, with the vapour bubble tending to stay within the colorless liquid (Fig 7-5f, 7-6c). Between temperatures of 740 and 800°C no solid material remains. Magnetite, which is the last phase to disappear, melts at temperatures of up to 800°C (Fig 7-5h). Homogenization of the two liquids to one occurred at temperatures in excess of 800°C (Fig. 7-6f) but even with heating to 1250°C, the vapour bubble did not dissolve. Cooling of the homogenous liquid caused it to separate back into two liquids at temperatures between 800 and 650°C confirming the occurrence of liquid immiscibility (Fig. 7-6g). The two phases were interpreted to be liquid as their outer boundaries would change shape in response to movement of the vapour bubble.

Solid-Vapour Inclusions in Transgressive Carbonatite

On heating, the vapour phase within solid-vapour inclusions hosted by apatite in transgressive carbonatite began to increase in size at temperatures between 420 and 460°C, at times occupying greater than half the visible area of the inclusion. Melting of the large carbonate solid commenced at temperatures between approximately 550 and 670°C and continued to between 700 and 774°C, at which temperatures the small colorless solid (magnesian silicate) started to melt. Melting terminated between 750 and 850°C with only liquid and vapour remaining. There was no evidence for two separate liquids either during heating or cooling of the inclusions.

Solid-liquid-vapour Inclusions in Transgressive Carbonatite

During heating of aqueous liquid-vapour -bearing solid inclusions in apatite hosted by transgressive carbonatite (Fig 7-7), two of the solids began to dissolve at temperatures between 200 and 266°C and 300 and 388°C, respectively, and by 450°C both solids had dissolved completely. The decomposition of the solids was interpreted to represent dissolution not melting because of the low temperatures and the presence of aqueous fluid. Homogenization of vapour to aqueous liquid occurred at temperatures between 430 and 542°C. Changes in the shape of the dominant solid, calcite, occurred between 604 and 668°C and were interpreted to represent initial melting of the former

Figure 7-6 Melting behaviour of melt inclusions in phoscorite-hosted apatite showing immiscible separation on cooling. A) Inclusion at 20°C in plane polarized light showing two solids and a dark area of vapour. The upper solid is Ca-carbonate while the lower solid is an Mg-Si mineral. B) Initial melting of carbonate phase at 716°C. C) Final melting of the carbonate phase and continued melting of the Si-bearing solid at 760°C. D) Two coexisting liquids (773°C). E) The carbonate liquid dissolving in the silicate liquid (821°C). F) The two liquids homogenized to a single liquid at 897°C. G) On cooling the homogeneous liquid separates back into two liquids (668°C). H) and I) Showing the birefringent nature of quench solid S2.

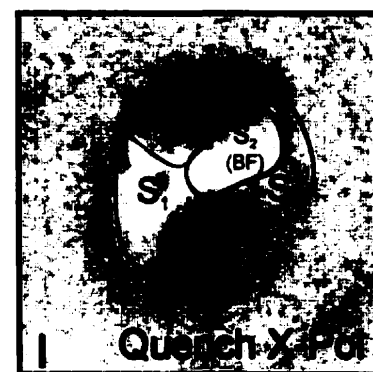
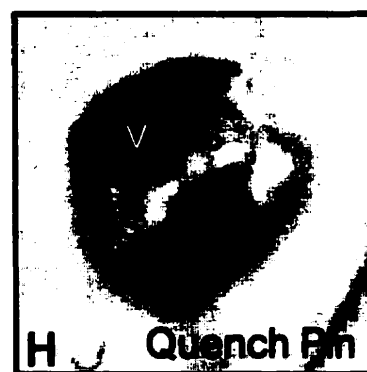
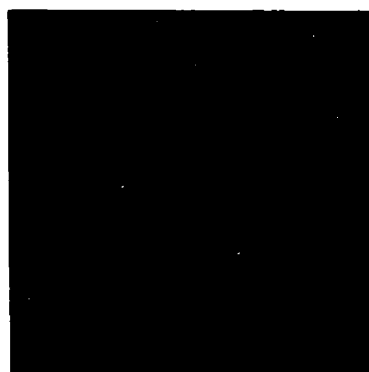
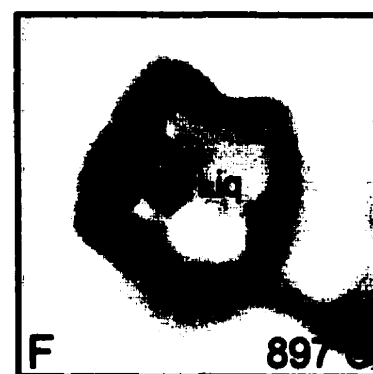
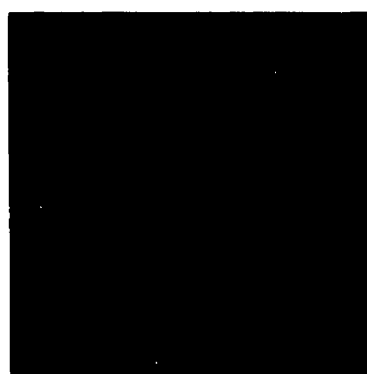
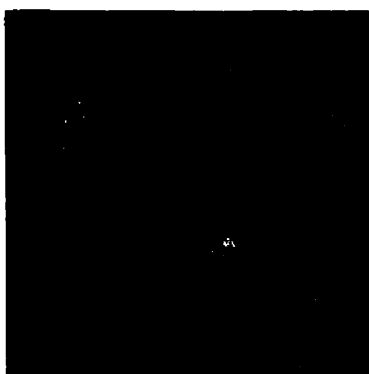
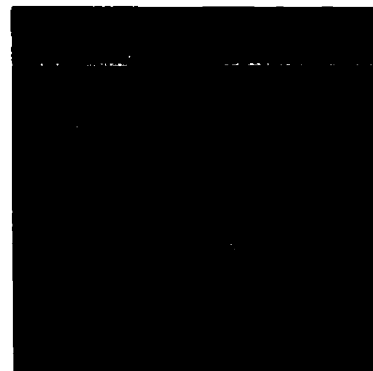
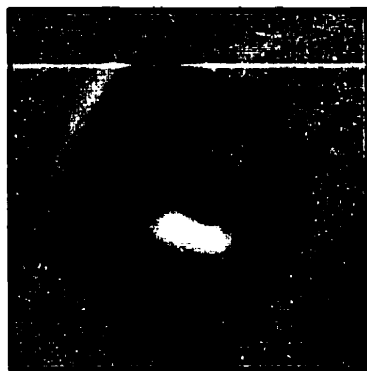
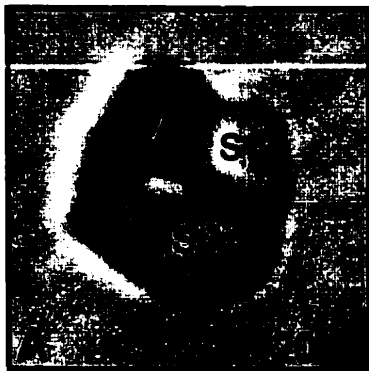
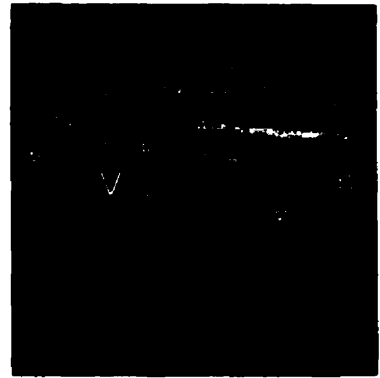
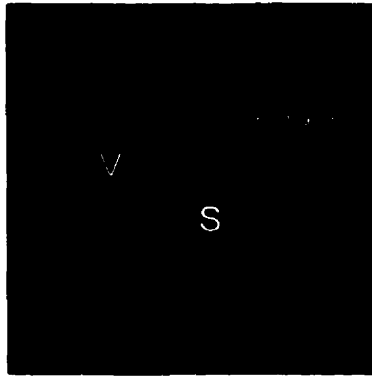
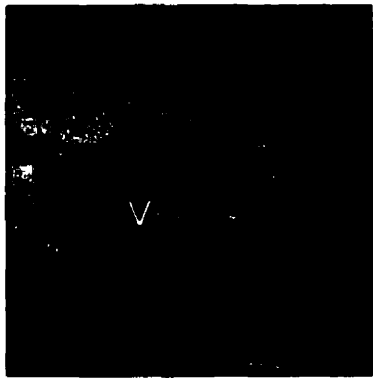
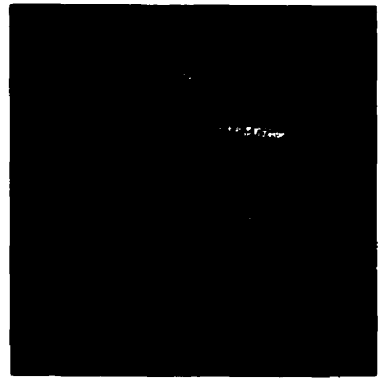
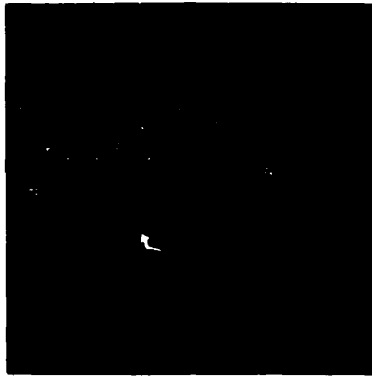


Figure 7-7 Dissolution and melting behaviour of aqueous liquid-vapour-bearing melt inclusions in transgressive carbonatite.



melt fraction of the inclusion. All inclusions homogenized to a single liquid plus vapour at temperatures below 850°C. As with the solid-vapour inclusions, there was no evidence of a second liquid. The behaviour of the aqueous fluid during melting was not observed clearly, as inclusions with fluid volumes of greater than 2-3%, typically decrepitated at temperatures between 450 and 550°C. Those inclusions which did not decrepitate had lesser proportions of aqueous fluid, and the interactions between aqueous fluid and melt were not easily resolved due to the small size of the inclusions.

Low temperature microthermometry was performed on aqueous fluid-bearing inclusions in order to determine the composition of the aqueous phase. Temperatures of initial and final melting of ice, in all inclusions, fell within a restricted range of temperatures between -21.3 and -24.1°C consistent with the system NaCl-KCl-H₂O and corresponding to salinities of approximately 22 wt.% NaCl-KCl (Hall *et al.*, 1988). Decrepitate analyses confirm that the fluids are chloride brines, and indicate that the Na/(Na+K) ratios are between 0.4 and 0.6 and that there are minor, but consistent, concentrations of Mg, Fe and S (Table 7-6).

Discussion

Solid inclusions in apatite of both phoscorite and transgressive carbonatite displayed consistent, and reproducible, melting behaviour and chemical compositions, and are therefore interpreted to represent trapped samples of melt. The evidence provided by melt inclusions trapped in phoscorite indicates that immiscible silicate and carbonate liquids were involved in the formation of the Phalaborwa complex. The compositional data suggest that one of the liquids had a bulk composition similar to a magnesian calcite and the other a bulk composition dominated by Mg, subordinate Si and significant Fe, Mn and S, hereafter referred to as the high magnesian silicate liquid. Magnetite was also present and microthermometric data presented above suggest that it was in fact the first mineral to crystallize from phoscoritic melts.

Olivine-hosted melt inclusions in phoscorite studied by Aldous (1980) are compositionally different from those in apatite, with the main silicate phase consisting of phlogopite. Although temperatures of initial melting were documented by Aldous

(1980), homogenization of inclusions was not observed due to darkening of the host mineral at high temperatures. He concluded that olivine was the first mineral to crystallize from the magma based on petrographic relationships (Aldous, 1980). However, the presence of a high magnesian silicate liquid in apatite-hosted melt inclusions would suggest otherwise, i.e., that apatite crystallized prior to olivine, trapping the parental liquid from which olivine crystallized.

Melt inclusions in transgressive carbonatite comprise two types which differ only in the proportions of aqueous fluid. Compositionally, solid phases in the two groups of inclusions are similar with Ca-carbonate predominating. Evidence of small proportions of a Si-Mg phase are provided by analyses of opened inclusions, although separate liquids were not observed upon heating of these inclusions. This is predictable, however, as inferred bulk compositions are not suggestive of systems which are favourable for liquid immiscibility, i.e., low SiO₂, high CaCO₃ (Lee and Wyllie, 1997, 1998). Initial melting and homogenization temperature ranges also overlap for both aqueous fluid-bearing and solid+vapour inclusions and the two types of inclusions are thought to represent samples of the same melt. The variable content of aqueous fluid is interpreted to reflect heterogeneous mechanical trapping of a physically separate aqueous phase.

Crystallization History

The formation of phoscorite at Phalaborwa occurred through a process of silicate-carbonate immiscibility which produced a magnesian calciocarbonatitic liquid and a high magnesian silicate liquid, which crystallized calcite and olivine, respectively. Magnetite and apatite are thought to represent liquidus phases of the parental melt and therefore began crystallizing before separation occurred. The process of liquid immiscibility, rather than being responsible for the formation of carbonatite, is considered to have essentially refined the composition of the existing silica-bearing, carbonate-rich melt which then crystallized banded carbonatite. The separation of the high magnesian silicate liquid, which produced olivine, may also have been responsible for reducing the concentration of Mg in the carbonate liquid to levels where a magnesian calcite, rather than dolomite, crystallized. This may indicate, in this case at least, that calciocarbonatite

can form from an originally Mg-rich melt, if the magma exsolves a silicate liquid into which Mg is preferentially partitioned.

One of the implications of the above discussion is that liquid immiscibility was not responsible for the formation of pyroxenite and only occurred in the melt which crystallized phoscorite and carbonatite. The generation of pyroxenite by liquid immiscibility would have required that fractionation of carbonates from the conjugate carbonate liquid take place, in order to produce bulk compositions suitable for liquid immiscibility to re-occur. This is unlikely as silicates are the first phases to crystallize in the conjugate carbonate melt, driving the liquid away from the miscibility gap (Lee and Wyllie, 1998). Eriksson (1982, 1989) also concluded that, although the relationships between phoscorite and carbonatite are poorly understood, the main lithologic features of Phalaborwa were not a result of liquid immiscibility.

The late stage transgressive carbonatite is notable in that it is the only carbonate-rich melt to contain significant amounts of water, indicated by the absence of aqueous liquid-vapour-bearing melt inclusions and fluid inclusions in banded carbonatite. This, together with compositional differences from banded carbonatite, more magnesian calcite but lower proportions of magnesian silicate, indicate that transgressive carbonatite probably represents the final fractionated aliquots of carbonatite liquid which were forcefully injected into earlier banded carbonatite.

The development of the Phalaborwa complex is therefore thought to have involved intrusion of pyroxenite followed by later intrusions of a silicate-carbonate liquid. This liquid crystallized magnetite and apatite, the latter trapping samples of the melt, and then separated into two immiscible liquids, one carbonate-rich and the other silicate-rich. Magnesium was partitioned into the silicate liquid, and crystallized olivine upon cooling. The Mg-depleted carbonate melt also crystallized olivine, as predicted by experimentally determined phase diagrams (Lee and Wyllie, 1998), and then crystallized magnesian calcite. Dolomite was not stable in banded carbonatite due to the removal of significant Mg through separation of the Mg-rich silicate melt. Continued fractionation of the carbonate liquid, at depth, produced the later Mg-enriched, olivine poor, transgressive carbonatite which was injected along fractures in the crystallizing banded carbonatite and phoscorite.

Copper Mineralization

The absence of fluid inclusions or aqueous fluid-bearing melt inclusions in apatite of banded carbonatite and phoscorite and the presence of copper sulphides in melt inclusions hosted by phoscorite supports a primary magmatic origin for the early bornite copper mineralization.

The presence of a previously unidentified aqueous phase in transgressive carbonatite provides further support for the hydrothermal origin of copper mineralization in transgressive carbonatite (Hanekom, 1965; Van Rensburg, 1965; Aldous, 1980). Although copper was not identified in residues from solid-liquid-vapour melt inclusion decrepitates, the presence of S and Mg in the NaCl-KCl brine would suggest that this fluid could have been responsible for the deposition of copper sulphides as well as the dolomitization of calcite surrounding chalcopyrite mineralization.

Early copper mineralization at Phalaborwa was probably the result of primary crystallization of bornite from a carbonate melt which was enriched in Cu and S (no evidence for the presence of an immiscible sulphide liquid was found in melting experiments). This style of mineralization dominated the early phoscorite and banded carbonatite but was replaced by deposition of chalcopyrite from hydrothermal fluids in the later transgressive carbonatites. Transgressive carbonatite magmatism probably represented a late stage fractionation of the melts which crystallized banded carbonatite. These late stage products were probably water saturated, or at least enriched in H₂O compared to earlier melts, and provided the aqueous fluids which transported Cu and S.

Conclusions

Three types of solid inclusions were identified in apatite hosted by carbonate-bearing lithologies of the Phalaborwa complex and are comprised of solid-vapour inclusions in phoscorite, consisting of equal volumes of calcite and magnesian silicate with subordinate iron oxide, Fe-Cu sulphides and vapour; solid-vapour inclusions in transgressive carbonatite, composed of calcite with subordinate magnesian silicate and

vapour; and solid-liquid-vapour inclusions in transgressive carbonatite, consisting of calcite, subordinate magnesian silicate and vapour and a small volume of aqueous fluid containing two daughter minerals.

Solid-vapour inclusions in phoscorite represent the trapping of two immiscible liquids of carbonate and silicate compositions. Temperatures of initial melting were determined to be between 635 and 690°C, while the two liquids coexisted at temperatures between 740 and 800°C. Above temperatures of 800°C only one liquid (+ vapour) was present, which separated back into two liquids during cooling.

Solid-vapour and solid-liquid-vapour inclusions show no evidence of liquid immiscibility and formed only one liquid during heating experiments. Temperatures of initial melting, were between 550 and 670°C and 604 and 668°C, respectively for solid-vapour and solid-liquid-vapour inclusions, while homogenization occurred at temperatures above 750°C and below 850°C, for both types of inclusions.

The consistent phase ratios and relationships for solid inclusions indicate that they are samples of melts trapped in apatite during crystallization of phoscorite and transgressive carbonatite. Owing to the occurrence of carbonate-silicate liquid immiscibility in phoscoritic melts, it is suggested that liquid immiscibility was not responsible for the formation of pyroxenites and carbonatites at Phalaborwa but occurred in phoscorite magma only to the extent of removing unwanted silica. Following separation the carbonate liquid evolved into banded then transgressive carbonatite. The evolution of this carbonate-bearing liquid resulted in an increase in dissolved water in later melts which were exsolved as an aqueous fluid.

The presence of copper sulphides in melt inclusions in phoscorite and the blebby nature of bornite mineralization in banded carbonatite suggest that it was crystallized directly from these melts. However, the presence of an aqueous fluid in transgressive carbonatite magmas, and the localization of chalcopyrite mineralization along fractures, with accompanying dolomitization of calcite, suggest that late copper mineralization was precipitated from hydrothermal fluids.

References

- Aldous, R.T., 1980, Ore genesis in copper-bearing carbonatites; a geochemical, fluid inclusion and mineralogical study: Unpublished Ph.D. thesis, Imperial College, London, 365p..
- Amundsen, H.E.F., 1987, Evidence for liquid immiscibility in the upper mantle: *Nature*, v. 327, p. 692-695.
- Briden, J.C., 1976, Application of paleomagnetism to Proterozoic tectonics: *Philosophical Transactions of the Royal Society of London*, v. 280, p. 405-416.
- Brooker, R.A. and Hamilton, D.L., 1990, Three-liquid immiscibility and the origin of carbonatites: *nature*, v. 346, p. 459-462.
- Eriksson, S.C., 1982, Aspects of the petrochemistry of the Phalaborwa Complex, northeastern Transvaal, South Africa: Unpublished Ph.D. thesis, University of the Witwatersrand, Johannesburg.
- Eriksson, S.C., 1989, Phalaborwa, a saga of magmatism, metasomatism and miscibility: *in* K. Bell (ed.), *Carbonatites: genesis and evolution*: London, Unwin Hyman, p. 221-254.
- Freestone, I.C., and Hamilton, D.L., 1980, The role of liquid immiscibility in the genesis of carbonatites – an experimental study: *Contrib. Mineral. Petrol.*, v. 73, p. 105-117.
- Frick, C., 1975, The Phalaborwa syenite intrusions: *Trans.Geol. Soc. S. Afr.*, v. 78, p. 201-213.
- Gittins, J., 1988, The origin of carbonatites: *Nature*, v. 335, p. 295-296.
- Hall, D.L., Sterner, S.M., and Bodnar, R.J., 1988, Freezing point depression of NaCl-KCl-H₂O solutions: *Econ. Geol.*, v. 83, p. 197-202.\
- Hamilton, D.L., and Kjarsgaard, B.A., 1993, The immiscibility of silicate and carbonate liquids: *S.Afr. J. Geol.*, v. 96, p. 139-142.
- Hanekom, H.J., van Staden, C.M., Smit, P.J., and Pike, D.R., 1965, The geology of the Palabora Igneous Complex: *South Africa Geological Survey Handbook, memoir 54*.
- Harmer, R.E., and Gittins, J., 1997, The origin of dolomitic carbonatites: field and experimental constraints: *journal of African Earth Sciences*, v. 25, p. 5-28.
- Kjarsgaard, B.E., and Hamilton, D.L., 1988, Liquid immiscibility and the origin of alkali-poor carbonatites: *Mineralogical Magazine*, v. 52, p. 43-55.

- Lee, W-J., and Wyllie, P.J., 1996, Liquid immiscibility in the join $\text{NaAlSiO}_3\text{-CaCO}_3$ at 2.5 GPa and the origin of calciocarbonatite Magmas : *Journal of Petrology*, v. 38, p. 1113-1135.
- Lee, W-J., and Wyllie, P.J., 1997, Liquid immiscibility between nephelinite and carbonatite from 1.0 Gpa to 2.5 Gpa compared with mantle melt compositions: *Contrib. Mineral. Petrol.*, v. 127, p. 1-16.
- Lee, W-J., and Wyllie, P.J., 1998, Petrogenesis of carbonatite magmas from mantle to crust, constrained by the system $\text{CaO-(MgO + FeO}^*\text{)-(Na}_2\text{O + K}_2\text{O)-(SiO}_2\text{ + Al}_2\text{O}_3\text{ + TiO}_2\text{)-CO}_2$: *Journal of Petrology*, v. 39, p. 495-517.
- Mitchell, R.H., 1997, Carbonate-carbonate immiscibility, neighborite and potassium iron sulphide from Oldoinyo Lengai natrocarbonatite: GAC/MAC Annual Meeting May 19-21: Abstract Volume, p. A104.
- Nielson, T. F. D., Solovova, I. P., and Veksler, I. V., 1997, Parental melts of melilitolite and origin of alkaline carbonatite: evidence from crystallized melt inclusions, Gardiner complex: *Contrib. Mineral. Petrol.*, v. 126, p. 331-344.
- Palabora Mining Company, 1976, The geology and the economic deposits of copper, iron and vermiculite in the Palabora Igneous Complex: a brief review: *Economic Geology*, v. 71, p. 177-192.
- Palmer, D.A.S., and Williams-Jones, A.E., 1998a, Carbonate-carbonate liquid immiscibility and the formation of ferrocarbonatite: evidence from melt inclusions in the Amba Dongar carbonatite complex, India: Unpublished Ph.D. thesis, McGill University, Montreal, Chapter 4.
- Palmer, D.A.S., and Williams-Jones, A.E., 1998b, Fenitization associated with the Phalaborwa complex, South Africa: Unpublished Ph.D. thesis, McGill University, Montreal, Chapter 8.
- Rankin, A.H. and Le Bas, M.J., 1974, Liquid Immiscibility between silicate and carbonate melts in naturally occurring ijolite magma: *Nature*, v 250, p. 206-209.
- Reischmann, T., 1995, Precise U/Pb age determination with baddeleyite (ZrO_2), a case study from the Phalaborwa Igneous Complex, South Africa: *S.Afr.J.Geol.*, v. 98, p. 1-4.
- Sweeney, R.J., 1994, Carbonatite melt compositions in the earth's mantle: *Earth and Planetary Science Letters*, v. 128, p. 259-270.
- Van Rensburg, W.C., 1965, Copper mineralization in the carbonate members and phoscorite, Phalaborwa, South Africa: Unpublished Ph.D. thesis, University of

Wisconsin, Madison.

Wallace, M.E., and Green, D.H., 1988, An experimental determination of primary carbonatite magma composition: *Nature*, v. 335, p. 343-346.

Bridge to Chapter 8

In chapter 7, melt inclusions identified in apatite hosted by phoscorite and transgressive carbonatite are analysed, and the data used to show that silicate-carbonate immiscibility occurred in melts which produced phoscorite, and that fractionation was responsible for the formation of the younger carbonatites. The presence of copper sulphides in melt inclusions from phoscorite suggests that early-stage copper mineralization is primary magmatic in origin. Although no primary fluid inclusions were observed in apatite, melt inclusions in transgressive carbonatite contain an aqueous fluid which was analysed microthermometrically, and the data used to interpret its composition.

Fenites surrounding pyroxenite and carbonatite are characterized in Chapter 8 and the mass changes to these rocks, that accompanied fenitization, are used to interpret the chemistry of the fenitizing fluids. This allowed further characterization of the aqueous fluids identified in Chapter 7, as well as identification of the fluids exsolved from pyroxenite. With this information, late-stage copper mineralization is linked to aqueous fluids.

**Chapter 8: Fenitization Associated with the
Phalaborwa Complex, South Africa**

**D. A. S. Palmer and A. E. Williams-Jones
Department of Earth and Planetary Sciences
McGill University**

Abstract

The early Proterozoic Phalaborwa complex, South Africa (2060 Ma) consists of a large kidney shaped intrusion of pyroxenite which was later cored by phoscorite and subsequently intruded by banded (early) and transgressive (late) carbonatites. The carbonate rocks are host to 400 Mt of early bornite and late chalcopyrite ores grading, on average, 0.69% Cu. A zone of fenitization is developed in Archean granites and granitic gneisses surrounding the complex, indicating that hydrothermal fluids were active during its emplacement.

Two episodes of fenitization can be discerned based on chemical and mineralogical changes, and consist of regional fenitization associated with pyroxenite emplacement and contact fenitization associated with carbonatite intrusion. Whole rock compositions of fenitized granite and granitic gneiss indicate that regional and contact fenitization were accompanied by significant gains in K, Ca, Ba, Mg, Fe, Sr, Th and LREE, and losses in Si and Na. However, the replacement of diopside by richterite and chemical changes in potassium feldspar in both fenite types indicate that fluids responsible for contact fenitization were enriched in Mg, and probably contained more Na, compared to pyroxenite-derived fluids.

Dolomitization of calcite surrounding chalcopyrite veinlets in transgressive carbonatite suggests that Mg-enriched orthomagmatic fluids exsolved from carbonatite were responsible for copper mineralization. The primary magmatic nature of bornite mineralization in early banded carbonatites suggests that late chalcopyrite ore was either hydrothermally remobilised from primary sulphides or formed by partitioning of Cu, Fe and S from the melt into an aqueous fluid.

Introduction

The Phalaborwa copper deposit in South Africa is a rare example of copper concentration in a carbonatite, and the only one in which this concentration reached economic levels (Palabora Mining Company, 1976). Two theories on the genesis of the copper mineralization have received serious consideration, namely the deposition of

copper minerals wholly by hydrothermal fluids (Hanekom *et al.*, 1965; Heinrich, 1970; Palabora Mining Company, 1976) and a hybrid primary magmatic/auto metasomatic model (Aldous, 1980). The localization of chalcopyrite mineralization along fractures in late carbonatite intrusives (transgressive carbonatite) is convincing evidence for hydrothermal deposition (Hanekom, 1965; Palabora Mining Company, 1976; Aldous, 1980), however, Aldous (1980) also interpreted copper sulphide-bearing melt inclusions in early carbonate-bearing rocks (phoscorite) as evidence for primary crystallization of bornite \pm chalcopyrite in early carbonatite intrusives (banded carbonatite).

In order to evaluate the processes which were responsible for copper deposition at Phalaborwa, it is necessary to unravel both the magmatic and hydrothermal evolution of the carbonatites. Aldous (1980) was hampered by the lack of fluid inclusions in apatite within carbonatite and was obliged to work only with the abundant melt inclusions hosted by diopside and olivine of the pyroxenite and phoscorite, respectively. The results, however, provided direct evidence of primary magmatic copper sulphides in pyroxenite and phoscorite melts. Palmer and Williams-Jones (1998b, Chap. 7) observed melt inclusions in apatite of the phoscorite and identified aqueous fluid-bearing melt inclusions in transgressive carbonatite, providing the first evidence of orthomagmatic fluids associated with carbonatite. The aureole of fenitised rock surrounding the complex supplies further evidence that a hydrothermal system was active during emplacement of silicate and/or carbonate-bearing rocks.

The objective of this study is to characterise aqueous fluid(s) responsible for fenitization of country rocks, determine their source(s) and establish their relationship to copper mineralization. Bulk rock analyses of fenites and their precursors, manipulated using the methodology of Gresens (1967) and Grant (1986) were employed to quantify the mass changes which occurred between fluid and rock. Small scale mineralogical changes, which were not recognized by whole rock analyses, provided additional information on rock/fluid interactions. The calculation of mass changes in fenites proved to be an accurate method of interpreting the composition of fenitizing fluids.

Geology

The Phalaborwa complex is located in the northeastern Transvaal, South Africa and consists of early Proterozoic (2060 Ma) (Reischmann, 1995) silicate and carbonatite rocks which intruded Archean granites and granitic gneisses (Hanekom *et al.*, 1965; Eriksson, 1982). Intrusion of the complex began with a large-kidney shaped lobe of pyroxenite which was later cored by phoscoritic and carbonatitic magmas (Fig 8-1). During both syn and post-intrusion periods, numerous small bodies of syenite were emplaced within the surrounding Archean granites and gneisses. This was followed by intrusion of a large number of southwest trending diabase dykes thought to be Precambrian in age (≈ 1900 Ma) (Briden, 1976). An aureole of weakly fenitized granite and gneisses surrounds the complex, suggesting that hydrothermal fluids were present during the emplacement of the complex (Frick, 1975; Eriksson, 1982).

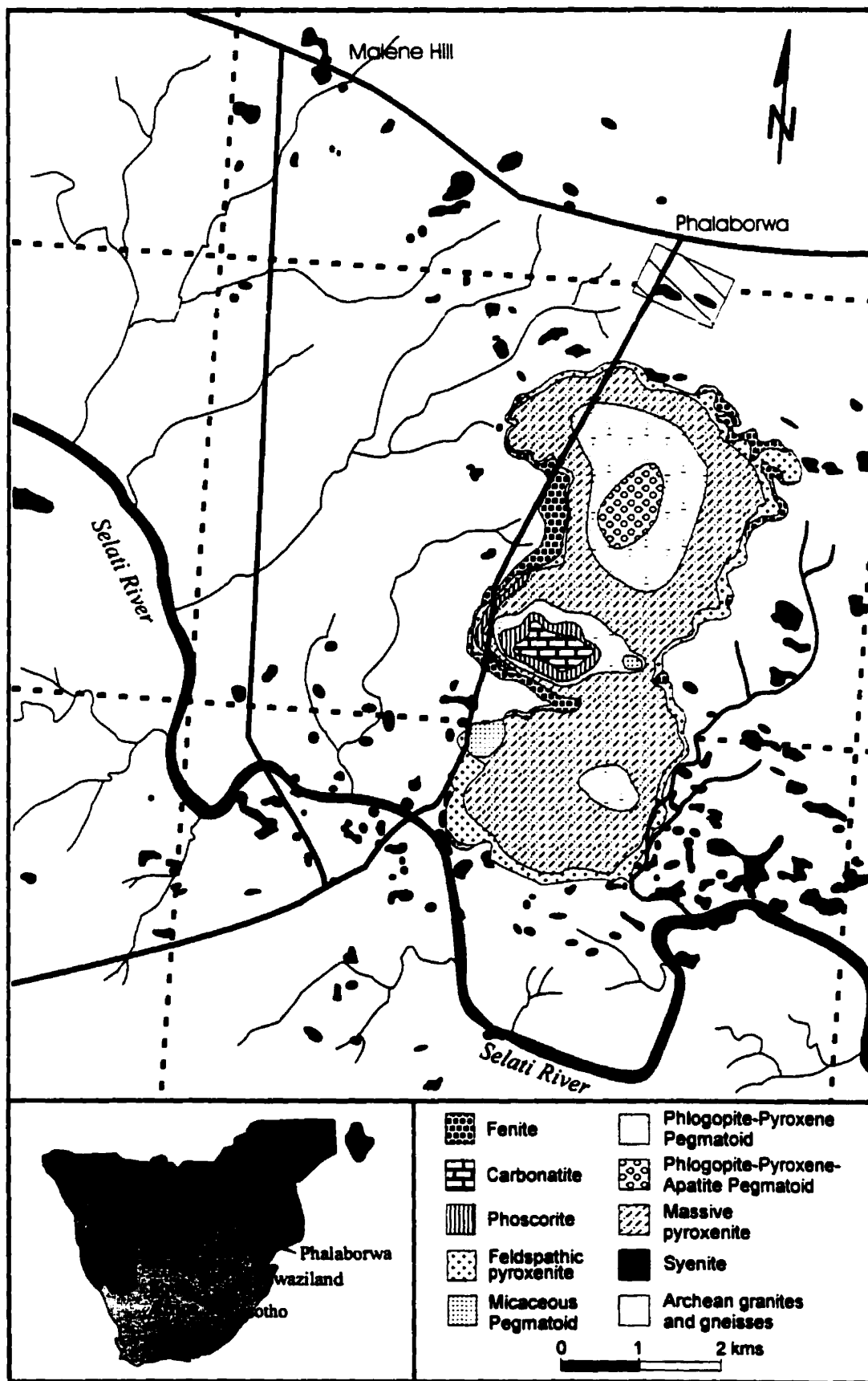
The Phalaborwa alkaline complex is unique in that it contains the only known economic copper deposit hosted by carbonatite. Mineralization consists of bornite- or chalcopyrite-rich ore with initial reserves of over 400 Mt, grading, on average, 0.69% Cu (Palabora Mining Company, 1976). By-products of Au, Pt and Zr are recovered from the copper ore, and economic deposits of vermiculite and phosphate (as apatite) are hosted by pyroxenite and phoscorite, respectively.

Pyroxenite

Pyroxenite forms the earliest, and volumetrically, the dominant, lithology of the complex and can be sub-divided into massive, micaceous, pegmatitic and feldspathic varieties. Contact relationships are typically sharp between pyroxenites and the host granites and gneisses. Recent studies of the pyroxenites by Eriksson (1989) suggest that they were formed by primary crystallization of the parental magmas, and not, as was first thought for phlogopite-rich pyroxenites, by secondary hydrothermal processes (Eriksson, 1982).

Common to all varieties of pyroxenite is the presence of diopsidic pyroxene and accessory apatite. Phlogopite contents are highly variable and range from minor

Figure 8-1 The geology of the Phalaborwa complex, South Africa (modified from Hanekom et al., 1965 and Frick, 1975).



(massive pyroxenites), to major (glimmerites). Feldspathic pyroxenites contain abundant, large (up to centimetres in size), anhedral microcline crystals and are spatially restricted to the margins of the main pyroxenite body. Eriksson (1989) considers feldspathic pyroxenite to be of cumulate origin.

Phoscorite

Forming a barrier between pyroxenite and the central carbonatites is a thick (up to 400m) ring of an apatite-rich, magnetite-carbonate-olivine rock, locally called phoscorite (Fig. 8-2). This lithology was originally thought to represent a gradational transition between pyroxenite and carbonatite, however, geologists of the Palabora Mining Company (PMC), have observed sharp contacts between pyroxenite and phoscorite and a primary origin, linking phoscorite to carbonatite, is now proposed (Eriksson, 1989).

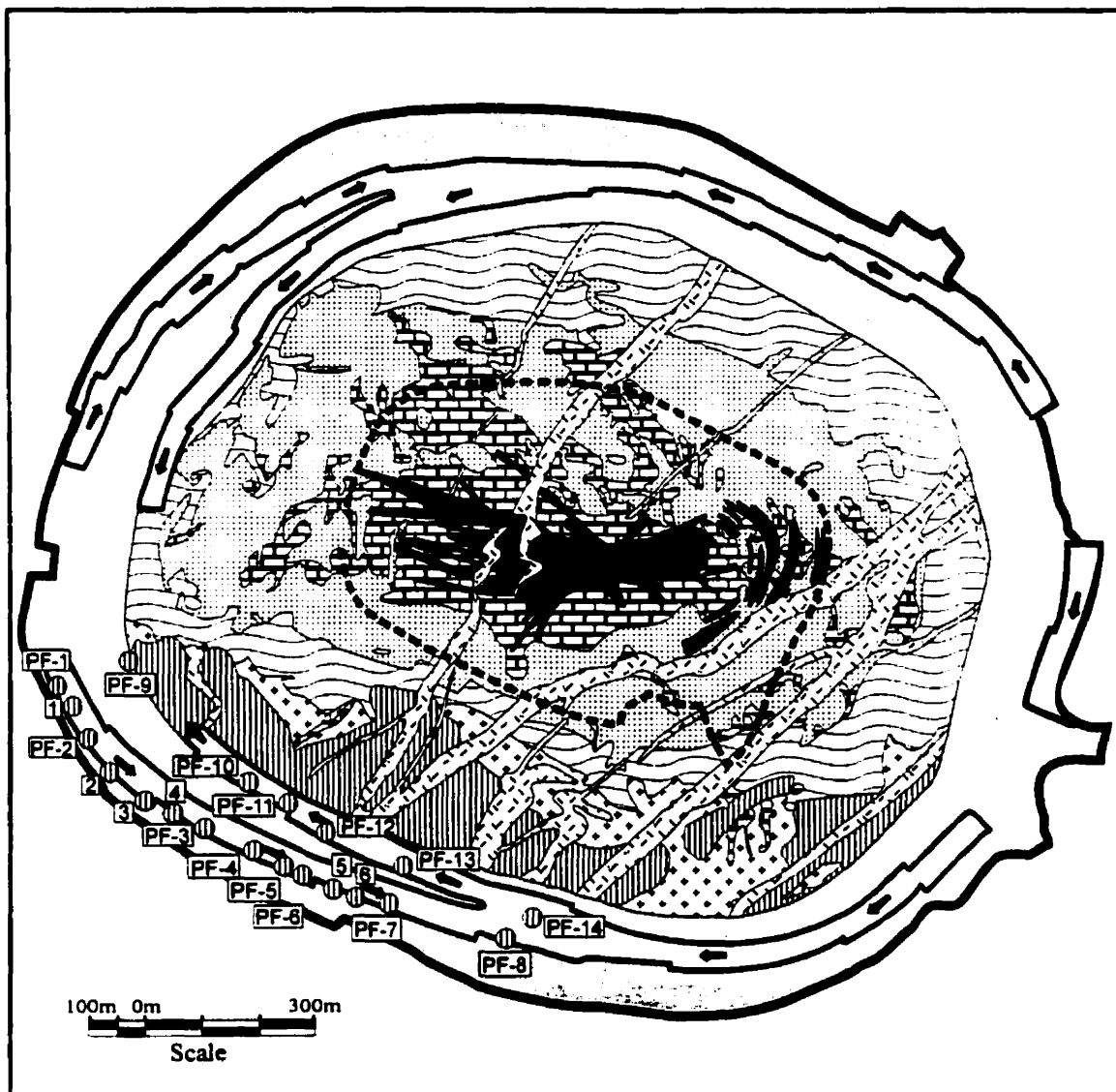
The average modal composition of phoscorite, calculated by Hanekom *et al.* (1965) from mill results, is 35% magnetite, 25% apatite, 22% carbonate and 18% olivine-serpentine and phlogopite. Baddelyite, which is commonly replaced by magnetite (Van Rensburg, 1965), and copper sulphides are the main accessory minerals.




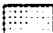
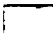






Carbonatite

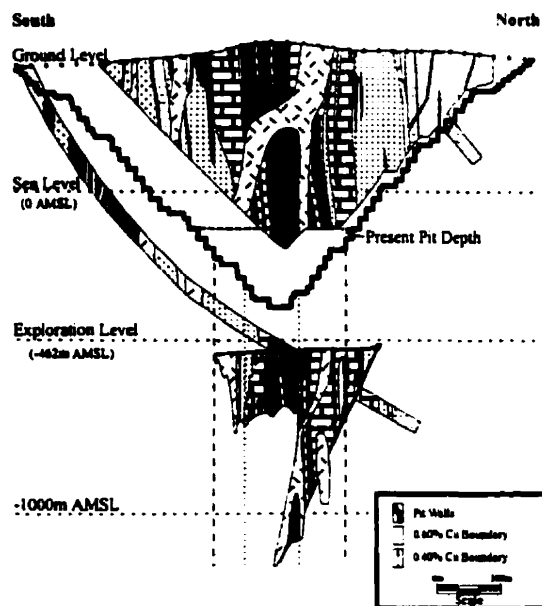
Carbonatites are the youngest members of the main complex and were intruded in two phases. The earliest intrusion was banded carbonatite, named for its distinctive concentric layers of magnetite, which are oriented parallel to the outer ring of phoscorite. Later intrusions produced transgressive carbonatite, which was preferentially intruded along WNW and ENE trending fractures (Fig. 8-2). Both banded and transgressive carbonatites are composed of fine- to coarse-grained calcite with accessory copper-iron sulphides, apatite and olivine. Magnetite, which is always present as an accessory phase, locally reaches abundances of over 50%.

The principal feature distinguishing the two carbonatite types is their sulphide mineralogy. Banded carbonatite has bornite as its dominant sulphide mineral, while transgressive carbonatite, which hosts the majority of the copper mineralization, contains

Figure 8-2 The geology of the Phalaborwa open pit.



-  Diabase
-  Transgressive Carbonatite
-  Banded Carbonatite
-  Phoscorite
-  Micaceous Pyroxenite
-  Feldspathic Pyroxenite
-  Fenite
-  Fenite Samples
-  Pit Area
-  Present Mining Level
-  Ramp



predominantly chalcopyrite. Calcite compositions can also be used to distinguish between carbonatite types, with transgressive carbonatite containing the more magnesian varieties. Although magnetite concentrations are similar in the two carbonatite types, in banded carbonatite, magnetite crystals are commonly aligned parallel to the outer margins of the carbonatite, whereas, in transgressive carbonatite, magnetite crystals are randomly oriented.

Copper mineralization

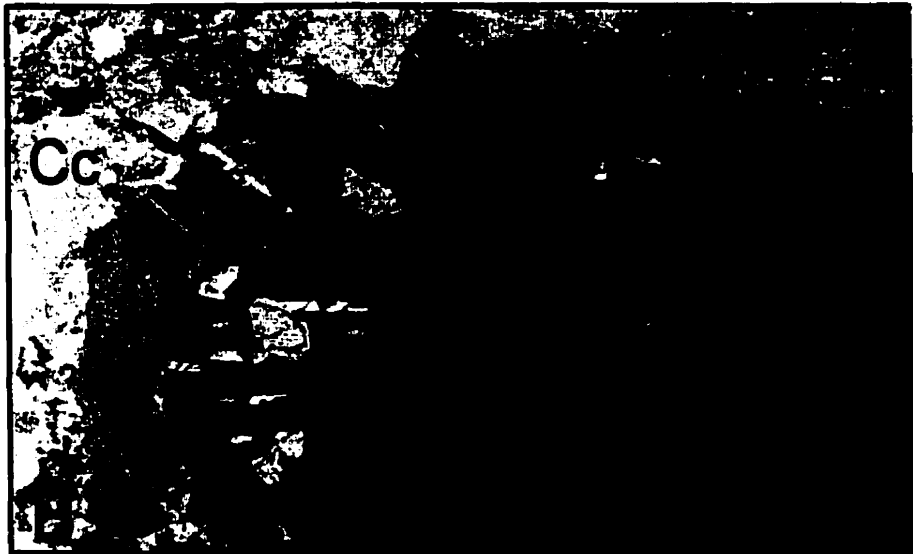
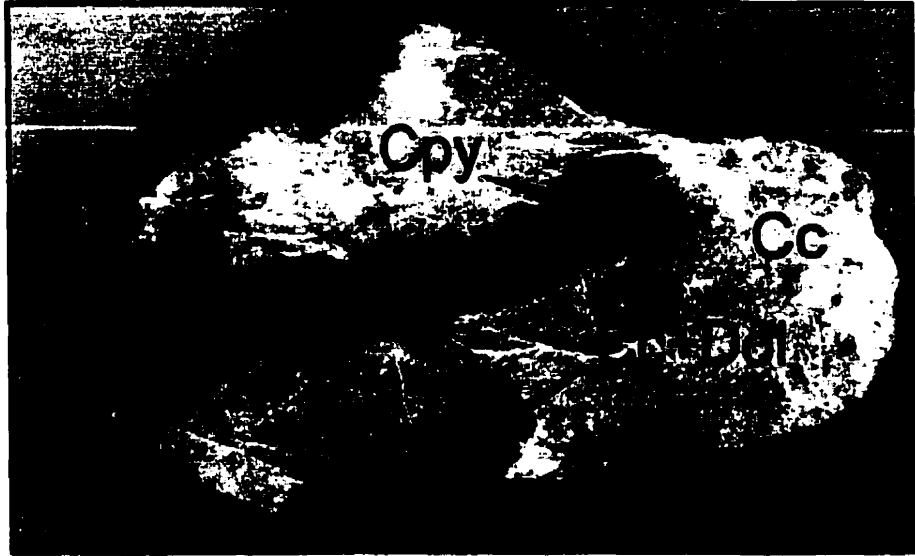
Two stages of mineralization can be distinguished; an early bornite-dominated stage, associated with banded carbonatite; and a later chalcopyrite-rich stage hosted by transgressive carbonatite. Although bornite and chalcopyrite are dominantly early and late, respectively, they are commonly found together in both stages. Accessory sulphide minerals include pyrrhotite, pentlandite, tetrahedrite, sphalerite, galena and pyrite.

Early copper mineralization occurs as small disseminated blebs of bornite, which are locally associated with magnetite, apatite and olivine. Bornite, in banded carbonatite, is not spatially associated with late fractures and is considered to be a primary magmatic mineral (PMC, 1976). Chalcopyrite in transgressive carbonatite is more typically found either as isolated, discontinuous veinlets (Fig. 8-3a) or swarms of veinlets up to 10m wide in which individual veinlets rarely exceed 1cm in width. While sulphide crystals show no preferred orientation, veinlets tend to be associated with fine fractures in the carbonatite (Aldous, 1980). The introduction of chalcopyrite, and associated magnetite, was often accompanied by the replacement of calcite by dolomite in the surrounding calciocarbonatite (Fig. 8-3a,b). Veins and dykes of transgressive carbonatite, which cut banded carbonatite, show a similar style of mineralization to the larger bodies of transgressive carbonatite.

Fenitization

The host granites and granitic gneisses are only weakly fenitized near their contacts with the alkaline complex, although evidence of fenitization has been observed

Figure 8-3 Features of transgressive carbonatite A) Chalcopyrite with an alteration halo consisting of dolomite after calcite. B) Photomicrograph showing dolomite that has replaced calcite surrounding magnetite which was introduced with chalcopyrite.



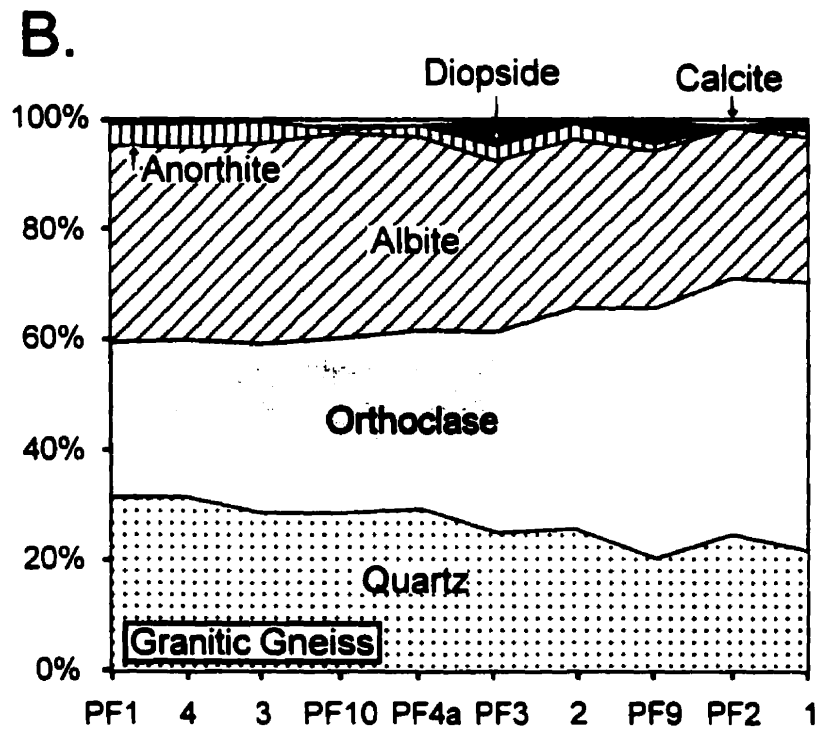
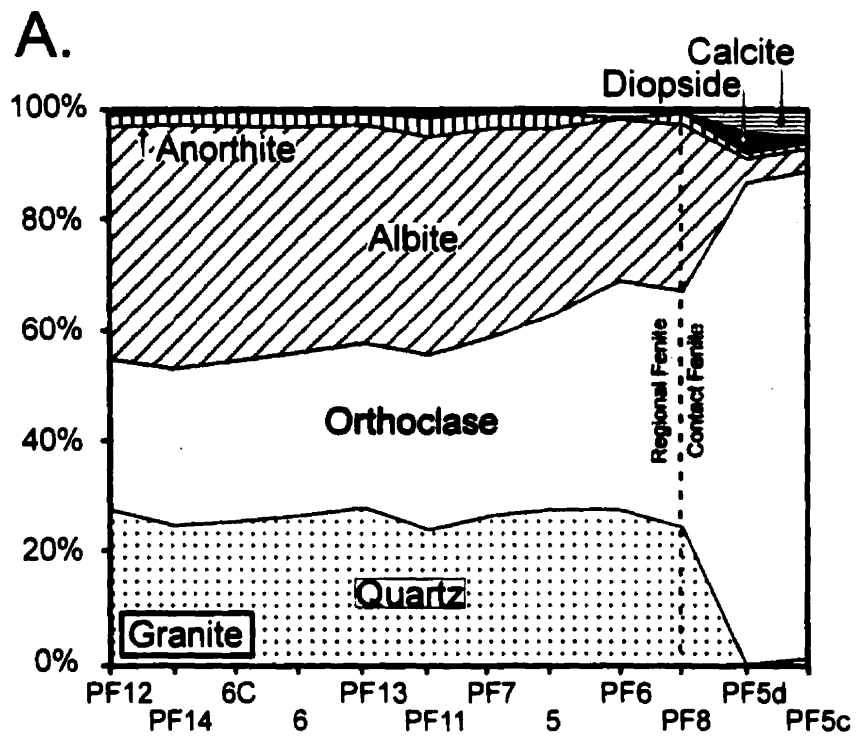
up to 5 km away from the margins (Eriksson, 1982). Unaltered gneiss is a white, medium- to coarse-grained equigranular rock composed of orthoclase, albite, quartz and biotite, while the later granite is pink in colour and lacks biotite. Two styles of fenitization can be distinguished, namely contact fenitization, which surrounds carbonatite dykes, and regional fenitization, which surrounds pyroxenite. Regional fenitization at Phalaborwa has not significantly altered the appearance of the precursor lithologies except for imparting a slight greenish hue due to the addition of green diopside (<10%), which commonly occurs as small (< 1cm) disseminated grains or thin (<1cm) veinlets. Contact fenites, which have only been observed in granite, are noticeably different from their precursor, having lost almost all of their original quartz, along with the addition of pyroxene (Fig. 8-4)

Frick (1975), in seeking to explain the origins of the syenitic bodies, provided the only detailed descriptions of fenites at Phalaborwa. He described the fenitization as the growth of orthoclase at the expense of quartz and plagioclase along quartz-orthoclase and quartz-plagioclase boundaries, and therefore considered it to be wholly potassic in nature. Petrographic examination of both granite and granitic gneiss fenites, during the course of the present study, however, has provided evidence that the fenitization was of a sodi-potassic nature.

Earlier pyroxenite veinlets and disseminations have been observed in which pyroxene has been partially or completely replaced by a blue alkali amphibole (Fig. 8-5a,b), varying in composition from richterite to winchite and edenite. Single disseminated crystals of pyroxene in contact and regional fenites are commonly only replaced partially by amphibole, typically with sharp contacts between the two minerals, while veinlets in contact fenites are preferentially replaced along their margins. The proportion of amphibole increases significantly near carbonatite dykes which cut granite, however, pyroxene in regional fenites is commonly replaced.

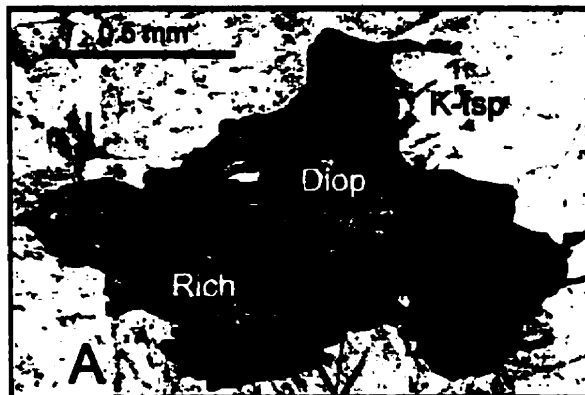
Granite or granitic gneiss surrounding pyroxene veinlets commonly contains a halo of clouded feldspar (Fig. 8-5c), suggesting alteration by aqueous fluids associated with the veinlet. The halo itself is typically half the width of the vein but is continuous along its length.

Figure 8-4 Normative mineral plots for A) fenitized granite and B) fenitized granitic gneiss. See Figure 8-2 for sample locations.



Sample

Figure 8-5 Photomicrographs showing partial replacement of A) a disseminated diopside (Diop) crystal by sodic amphibole (richterite - Rich) and B) a pyroxenite veinlet by richterite. C) Photomicrograph of clouded (altered) potassium feldspar (K-fsp) surrounding pyroxenite (pyx) veinlet.



Methodology

In order to determine bulk rock compositions, major elements were analysed by X-ray Fluorescence (XRF), while trace elements and rare earth element concentrations (REE) were determined by Instrumental Neutron Activation (INA). Mineral compositions were obtained by Wave Length Dispersive Spectrometric (WDS) analyses using a JEOL 8900 superprobe equipped with a Tracor Northern energy dispersive system. WDS analyses were performed at 15 kV, with a beam diameter of 10 μ .

Chemistry

Fenite Chemistry

In order to quantify the chemical changes which attended fenitization of country rock, sample profiles of granite (Table 8-1) and granitic gneiss (Table 8-2) were collected and analyzed. Sampling of regional fenites was carried out on successive benches of the open pit towards the contact of the fenitized rocks and the feldspathic pyroxenite. Two samples of granite in close proximity to carbonatite dykes were also included in the set to represent contact fenitization associated with carbonatite (Table 8-1).

In order to represent chemical changes in progressively fenitized felsic rock SiO₂ was used as a reference, with high values representing the lowest grade of fenitization. The silica undersaturated character of both ijolite and carbonatite orthomagmatic fluids has been well documented through other studies of fenitization, and the relationship of decreasing SiO₂ concentrations to increasing intensity of fenitization is well established (Kresten and Morogan, 1986; Morogan, 1994; Palmer and Williams-Jones, 1998a, Chap. 6). Normative mineral calculations for progressively fenitized granite (Fig. 8-4a) and granitic gneiss (Fig. 8-4b) support this conclusion.

Table 8-1 Chemistry of Fentized Granite

Sample	PF-13	PF-12	6c	6	5	PF-7	PF-14	PF-6	PF-8	PF-11	PF-5c	PF-5d
wt. %												
SiO ₂	74.94	74.56	74.40	74.30	74.22	73.71	73.70	73.19	73.13	72.99	60.88	59.93
TiO ₂	0.067	0.065	0.093	0.066	0.072	0.087	0.043	0.071	0.052	0.095	0.077	0.065
Al ₂ O ₃	13.91	14.35	14.44	14.15	13.75	14.04	14.55	13.63	14.27	14.43	16.68	16.58
Fe ₂ O ₃	0.53	0.58	0.63	0.69	0.66	0.69	0.64	0.70	0.44	0.80	1.14	1.07
MnO	0.007	0.008	0.005	0.008	0.008	0.012	0.012	0.012	0.007	0.010	0.020	0.020
MgO	0.02	0.06	0.06	0.06	0.07	0.15	0.05	0.20	0.06	0.16	0.51	0.50
CaO	0.75	0.90	0.67	0.78	0.90	0.90	0.80	0.95	0.71	1.05	3.26	3.54
Na ₂ O	4.56	4.86	4.89	4.70	3.87	4.32	5.10	3.33	3.46	4.54	0.43	0.48
K ₂ O	4.95	4.51	4.84	4.90	5.86	5.36	4.67	6.78	7.10	5.24	14.38	14.24
P ₂ O ₅	0.036	0.049	0.046	0.052	0.050	0.044	0.098	0.045	0.052	0.046	0.236	0.274
CO ₂	0.2	0.25	0.1	0.1	0.23	0.2	0.2	0.88	0.18	n.d.	1.96	1.7
Total	100.06	100.30	100.28	99.92	99.88	99.67	99.96	99.97	99.62	99.62	100.13	98.96
ppm												
BaO	354	317	315	278	696	558	490	763	707	1501	3636	3584
F	210	320	210	190	580	330	200	290	170	200	400	480
Cr ₂ O ₃	26	39	37	28	27	1	45	20	7	25	21	23
Cu	4	n.d.	7	5	3	3	28	88	15	20	77	21
V	7	n.d.	6	3	n.d.	7	3	4	2	n.d.	n.d.	n.d.
Nb	9.9	10.5	11.0	8.4	6.8	10.4	15.1	5.6	7.6	3.9	3.2	2.6
Pb	24.7	20.6	13.7	21.7	18.8	17.2	20.9	16.5	11.7	20.7	2.6	2.9
Rb	203.2	157.4	168.9	178.6	177.0	176.5	126.3	209.2	238.9	159.7	372.0	371.4
Sr	114.2	123.6	133.3	94.1	172.8	221.5	107.1	214.4	313.1	361.0	669.7	727.9
Th	4.3	1.1	5.1	2.7	9.3	4.8	1.3	7.0	3.6	13.2	13.1	13.2
U	11.5	7.3	6.9	7.6	6.1	6.1	8.7	6.2	7.7	3.7	5.1	3.6
Y	15.3	13.5	17.5	18.7	11.8	13.8	15.0	17.9	8.6	13.9	6.3	7.3
Zr	26.3	13.2	31.5	29.5	89.1	60.0	17.3	64.0	6.9	72.6	59.5	64.2
Sc	1.7	2.6	2.5	1.5	2.5	2.7	1.2	1.3	1.3	0.8	2.9	2.8
La	9.1	5.6	15.2	9.6	21	17.6	13.4	16.7	8	32.6	37.5	42
Ce	19	12	32	22	41	34	24	33	14	58	78	84
Nd	8	n.d.	n.d.	n.d.	10	10	10	10	8	17	38	43
Sm	1.3	0.9	1.9	1.5	2.5	2.1	1.5	2.3	1	3.4	5.9	6.6
Eu	0.4	0.3	0.2	0.4	0.6	0.4	0.4	0.6	0.4	0.6	1.3	1.4
Yb	0.9	0.9	1.1	1.2	0.5	0.8	0.7	1	0.6	0.6	0.5	0.3
Lu	0.14	0.14	0.16	0.12	0.07	0.08	0.08	0.1	0.07	0.1	0.06	0.05

n.d. not detected

Table 8-2 Chemistry of Fentized Granitic Gneiss

Sample	PF-1	4	PF-4A	3	PF-10	PF-3	PF-2	2	1	PF-9
wt. %										
SiO ₂	73.48	73.32	73.21	73.17	72.95	72.46	72.11	72.03	71.85	70.84
TiO ₂	0.159	0.161	0.246	0.211	0.170	0.187	0.144	0.193	0.155	0.223
Al ₂ O ₃	14.03	14.10	14.06	14.17	14.32	13.57	14.02	14.07	14.24	13.89
Fe ₂ O ₃	1.32	1.48	1.36	1.35	1.43	1.20	0.80	1.39	1.01	1.29
MnO	0.014	0.015	0.017	0.016	0.015	0.014	0.018	0.020	0.014	0.022
MgO	0.24	0.25	0.26	0.24	0.26	0.25	0.24	0.29	0.18	0.69
CaO	1.21	1.28	1.24	1.13	1.23	1.99	0.78	1.10	0.78	1.62
Na ₂ O	3.99	3.93	3.92	4.11	4.17	3.61	3.15	3.45	3.02	3.26
K ₂ O	4.50	4.51	5.21	4.97	5.08	6.08	7.53	6.45	6.03	7.42
P ₂ O ₅	0.046	0.041	0.105	0.062	0.060	0.054	0.037	0.058	0.039	0.101
CO ₂	0.06	0.3	0.46	0.2	0.7	0.3	0.56	0.33	0.03	0.18
Total	99.30	99.64	100.38	99.85	100.61	99.95	99.65	99.68	99.67	99.87
ppm										
BaO	1170	1305	1225	943	956	1043	1220	1626	2074	1759
F	280	290	480	400	400	360	320	460	140	390
Cr ₂ O ₃	4	31	5	46	41	14	13	26	40	52
Cu	n.d.	n.d.	16	1	15	3	n.d.	8	11	71
V	n.d.	11	9	9	11	9	8	9	n.d.	10
Nb	8.1	6.8	8.6	8.9	5.2	7.9	5.6	7.9	5.3	8.9
Pb	22.7	22.2	22.4	23.3	21.5	13.5	11.0	19.5	5.1	9.4
Rb	163.9	161.7	183.6	185.6	167.4	194.4	230.0	217.5	233.5	217.7
Sr	223.9	251.6	257.3	223.5	220.3	255.6	291.4	255.5	528.4	410.1
Th	22.0	20.1	16.8	12.6	19.8	8.0	6.3	13.8	7.5	14.3
U	4.3	4.6	5.8	5.8	5.5	4.7	4.4	5.7	3.4	4.4
Y	13.9	12.6	13.6	13.2	13.7	9.7	16.7	12.5	11.4	13.5
Zr	142.3	138.8	174.5	119.6	133.3	109.9	48.7	132.0	32.1	71.7
Sc	2.4	1.9	2.3	2	2.8	2.3	2.5	2.2	1.1	2.4
La	48.4	42.5	45.9	36.1	41.6	33	24.4	34.5	18.2	47.2
Ce	78	69	89	60	73	67	53	62	34	96
Nd	22	18	26	19	23	25	23	20	12	33
Sm	4.3	3.5	4.5	3.4	4.1	3.9	3.7	3.6	2.2	6.1
Eu	0.7	0.7	0.7	0.6	0.7	0.7	0.6	0.7	0.4	1
Yb	0.7	0.5	0.7	0.7	0.6	0.5	1	0.7	0.4	0.7
Lu	0.12	0.1	0.12	0.1	0.1	0.05	0.16	0.11	0.07	0.06

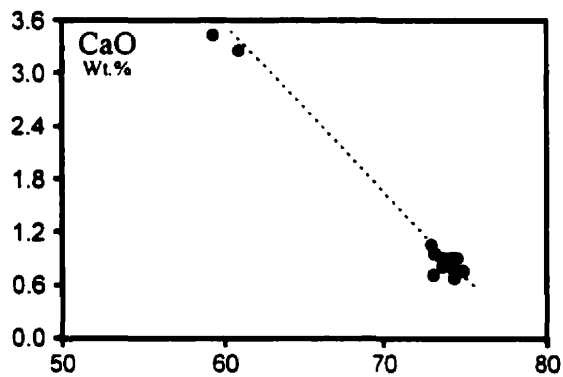
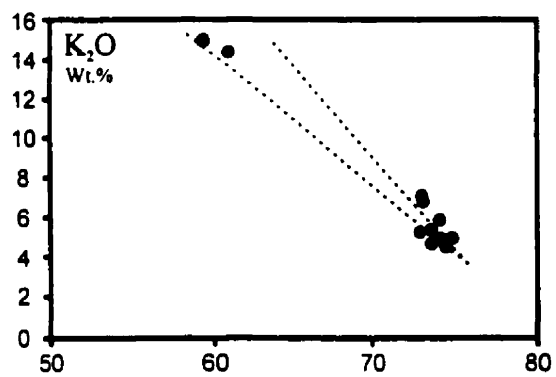
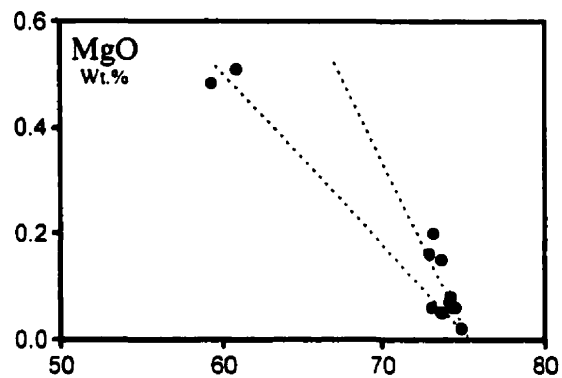
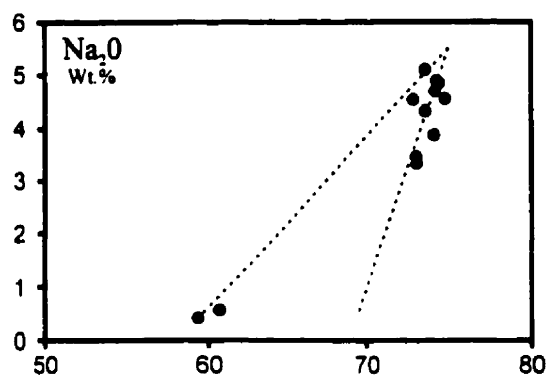
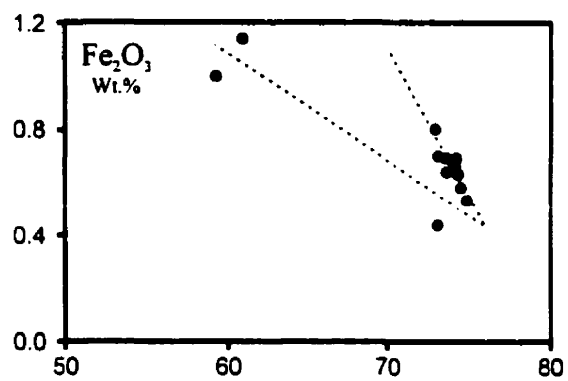
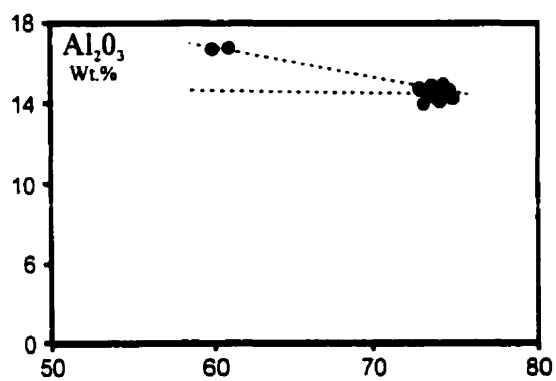
n.d. not detected

Whole Rock Chemistry

Regional fenites derived from both precursors show a narrow range of SiO_2 content from 75 to 71 wt.%, while contact fenites contain only 60 wt.% SiO_2 . Plots of major and minor elements versus SiO_2 are presented in Figures 8-6 and 8-8 and 8-7 and 8-9, for fenitized granites and granitic gneisses, respectively. Among all the oxides analyzed in granite only Na_2O decreases in concentration with decreasing SiO_2 content of the rock, while concentrations of Na_2O and Fe_2O_3 decrease with decreasing SiO_2 content in granitic gneiss, suggesting their removal along with silica (Fig. 8-6, 8-8). MgO shows flat trend with SiO_2 , in granitic gneisses. Progressively fenitized granites show very good negative correlations between K_2O , Fe_2O_3 , MgO and BaO and SiO_2 , consistent with addition of these elements (Fig. 8-6). Although the trends of K, MgO and BaO in granitic gneiss are less well defined, they are also consistent with these elements having been added during fenitization (Fig. 8-8). The behaviour of CaO during fenitization is less obvious, CaO would appear to have been added to granite, while for granitic gneiss no trend is apparent (Fig. 8-6, 8-8). Trace elements patterns show less correlation with SiO_2 than the major element oxides, however, some trends are apparent. Cu concentrations in granite are consistent with its addition during fenitization (Fig. 8-7), while Rb shows a good negative correlation in granitic gneisses (Fig. 8-9). Cu and Rb show no relationship with SiO_2 in granitic gneisses and granites, respectively (Fig. 8-7). Strontium shows a strong negative correlation with silica in both granites and gneisses (Figs. 8-7, 8-9). The behaviour of REE is contrasted between the two lithologies with La correlating positively with silica in granitic gneiss (Fig. 8-9), while the reverse is true for granite (Fig. 8-7). HREE concentrations, represented by Lu and a surrogate in the form of Y, show a strong decrease with decreasing SiO_2 content in granite (Fig. 8-7), while their concentrations in granitic gneiss display a weak positive correlation with SiO_2 contents.

Two samples of granite which represent contact fenitization continue the elemental relationships described above to values as low as 60 wt.% SiO_2 . For all elements the contact fenites conform with the sense of the correlations, either positive or negative, but off the expected linear trend indicated by the regional fenites.

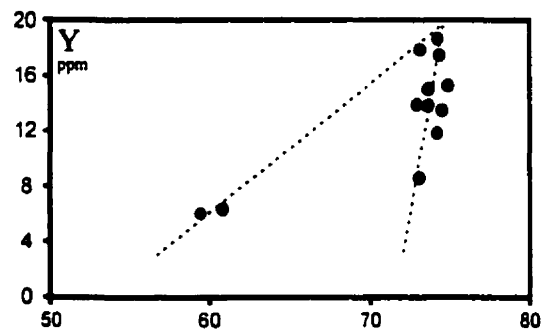
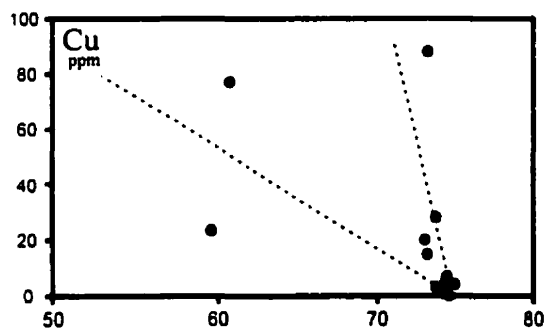
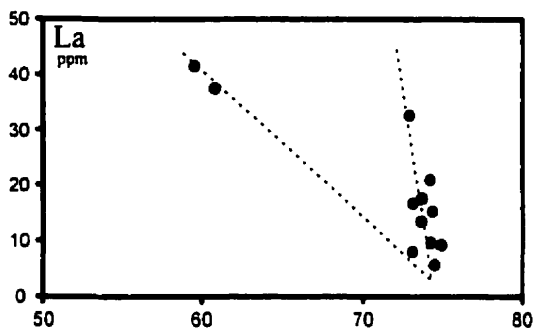
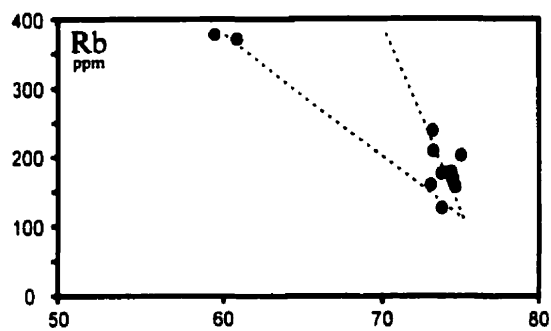
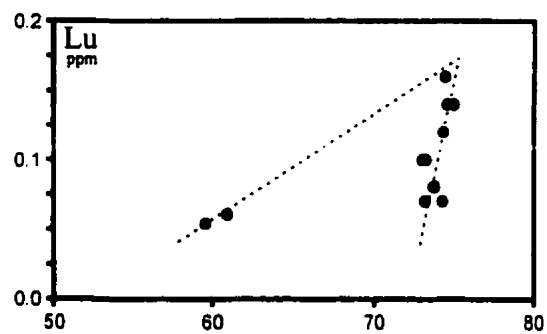
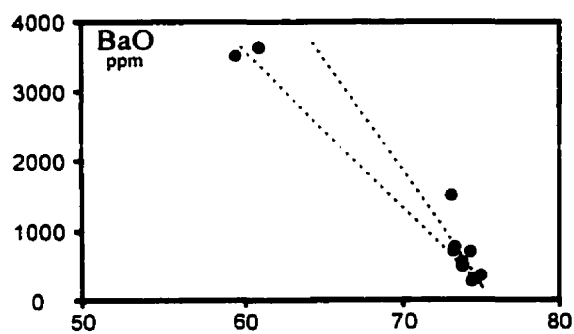
Figure 8-6 Major element plots for progressively fenitized (decreasing SiO₂) granite.



SiO_2 (wt. %)

SiO_2 (wt. %)

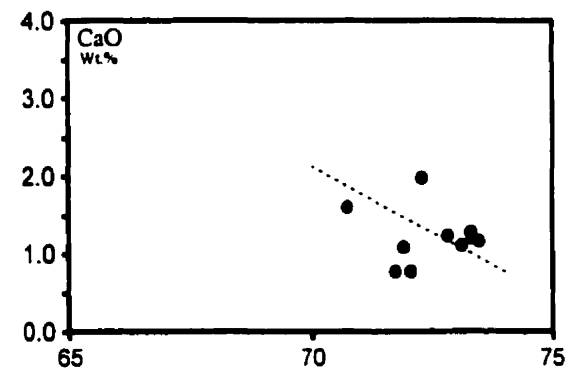
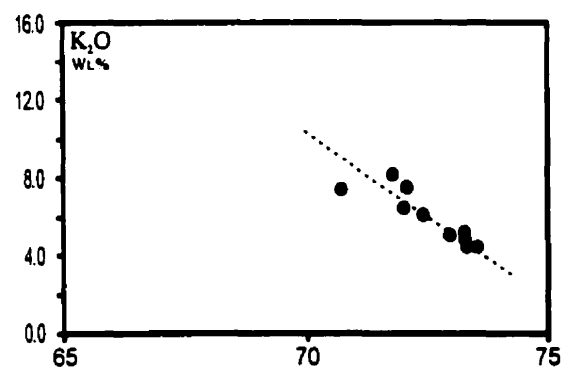
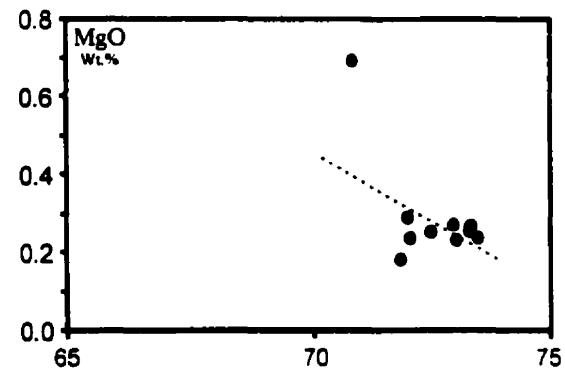
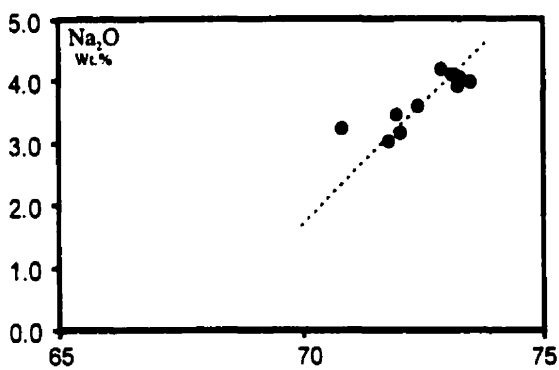
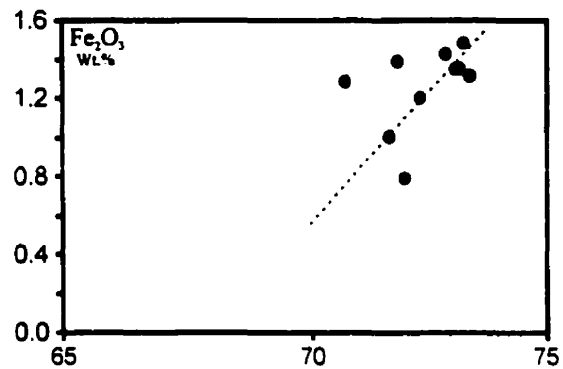
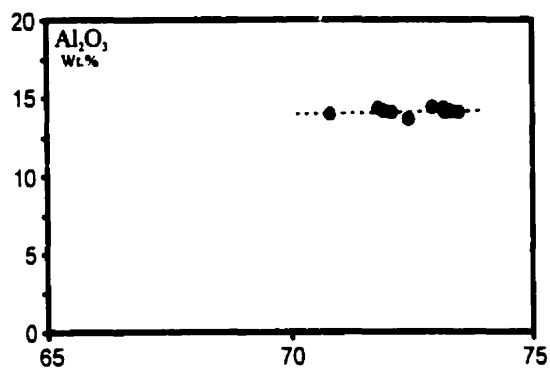
Figure 8-7 Minor element plots for progressively fenitized (decreasing SiO₂) granite.



SiO₂ (wt.%)

SiO₂ (wt.%)

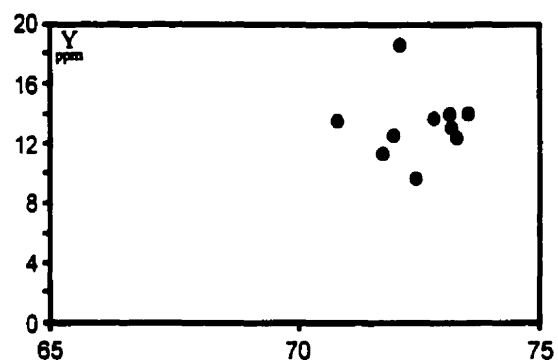
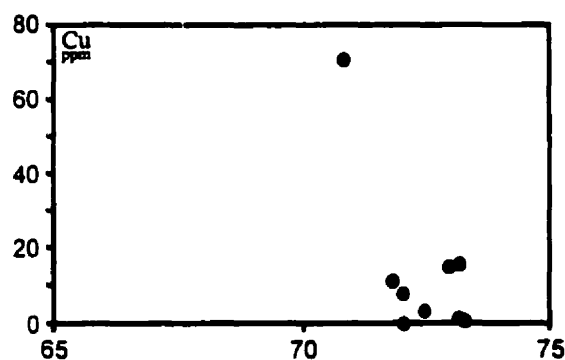
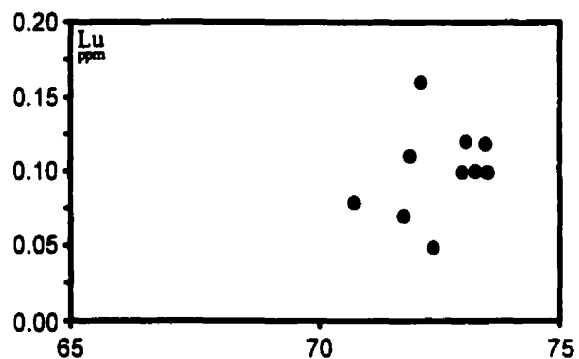
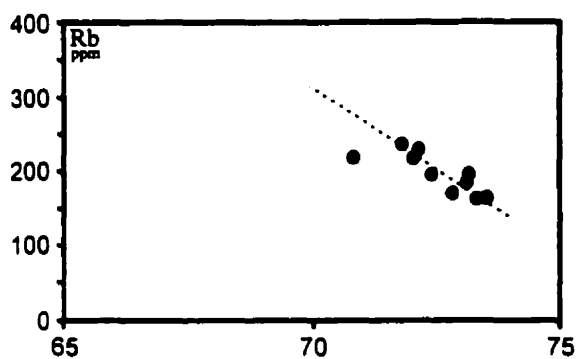
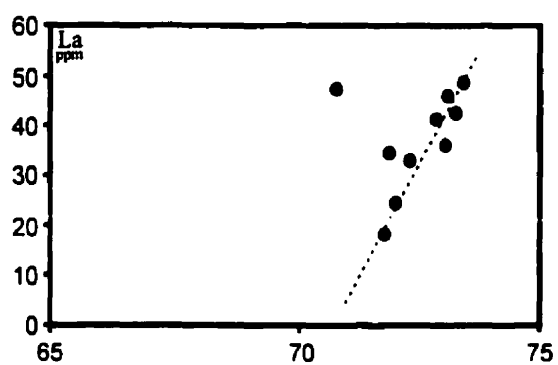
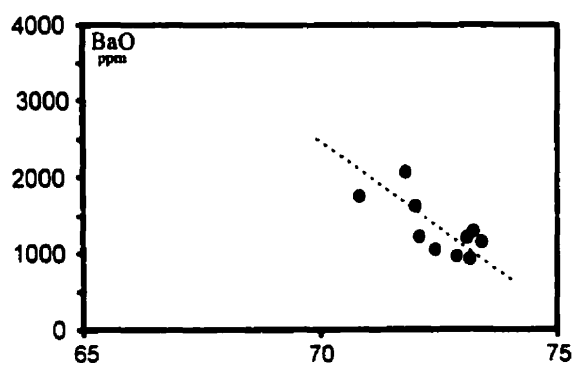
Figure 8-8 Major element plots for progressively fenitized (decreasing SiO₂) granitic gneiss.



SiO_2 (wt.%)

SiO_2 (wt.%)

Figure 8-9 Minor element plots for progressively fenitized (decreasing SiO₂) granitic gneiss.



SiO₂ (wt.%)

SiO₂ (wt.%)

Mineral Chemistry

The replacement of pyroxene by amphibole in fenitized country rocks provides additional constraints on fenitization. Marked chemical differences occur between amphiboles grown in contact fenitised rocks and those in regional fenites (Tables 8-3a,b and 8-4, Fig. 8-10). The most noticeable differences include higher concentrations of Mg, Na and Fe, and significantly lower concentrations of Ca and Al in amphiboles occurring near carbonatite dykes (samples 5c,d; Fig. 8-10a,b). There are also significant chemical differences between the two contact fenites, samples 5c and 5d, which represent average distances from the carbonatite of 5 and 20 cm, respectively (Tables 8-3a,b). With increasing distance from the carbonatite dyke, amphiboles become less magnesian, more calcic and slightly more aluminous, while maintaining an almost constant Fe concentration (Fig. 8-10a,b). Those amphiboles which show no local associations with carbonatite, i.e., in regional fenites, represented by sample PF-7, are separated chemically from contact amphiboles and trend toward lower Mg and Fe, and higher Ca values. By contrast, pyroxenes found in contact fenites are almost indistinguishable, chemically, from those in fenites unrelated to carbonatite dykes.

Alteration of potassium feldspar surrounding pyroxene veinlets was noted in a number of fenites, and feldspar was analyzed in order to determine the chemical changes resulting from its interaction with pyroxenite-derived fluids. The compositions of altered and unaltered potassium feldspar are very similar, with X_{Or} values ranging between 96 and 98 for both regional and contact fenites. However, the behaviour of K and Na displays a marked contrast between regional and contact fenites, and is best described in terms of mass changes.

Aside from the obvious differences in Mg and Ca associated with the dolomitization of calcite surrounding chalcopyrite mineralization, dolomites also differ in minor element concentrations (Table 8-5). Iron is the most significant of the minor elements comprising 0.31 wt. % FeO in calcite and between 0.45 and 1.96 wt. % FeO in magnesian calcite and dolomite. The concentration of Sr is significantly lower in magnesian calcite and dolomite than in calcite, it is between 0.64 and 1.44 wt. % SrO in

Table 8-3a Composition of pyroxenes and amphiboles in contact fente (proximal - PF-5c)

No.	Pyroxene				Amphibole							
SiO ₂	53.71	53.58	53.99	53.66	56.14	55.47	55.74	55.39	56.45	56.57	57.14	55.55
Al ₂ O ₃	0.20	0.34	0.41	0.31	0.28	0.44	0.37	0.42	0.28	0.27	0.21	0.35
TiO ₂	0.08	0.20	0.19	0.12	0.05	0.04	0.07	0.10	0.11	0.06	0.07	0.10
FeO	11.07	10.03	9.63	7.02	13.48	12.26	12.13	11.68	6.38	6.30	6.20	8.20
MgO	12.17	12.71	12.87	14.17	16.46	16.98	17.07	17.13	20.58	20.65	20.86	19.54
MnO	0.13	0.23	0.22	0.15	0.11	0.07	0.08	0.06	0.03	0.04	0.08	0.05
CaO	19.94	21.76	21.81	23.26	5.22	6.96	7.45	7.90	8.35	8.35	8.57	8.95
Na ₂ O	2.94	1.94	1.94	1.20	5.06	3.75	3.52	3.18	3.28	3.32	3.27	2.82
K ₂ O	0.02	0.02	0.03	0.00	0.92	1.53	1.40	1.65	2.46	2.19	2.39	1.67
BaO	0.01	n.d.	0.03	n.d.	0.16	0.01	n.d.	n.d.	0.01	0.04	0.02	0.01
P ₂ O ₅	0.00	0.00	0.01	0.00	n.d.	0.01	n.d.	0.04	n.d.	n.d.	0.04	n.d.
Cr ₂ O ₃	n.d.	n.d.	0.03	0.09	0.00	n.d.	0.01	0.01	n.d.	n.d.	0.01	0.03
Cl	0.00	n.d.	0.00	0.01	0.01	0.01	0.01	0.01	0.05	0.00	0.00	0.01
F	n.d.	0.00	n.d.	n.d.	0.16	0.21	0.19	0.19	0.37	0.36	0.38	0.25
Total	100.28	100.81	101.15	99.99	97.99	97.64	97.95	97.67	98.19	97.99	99.08	97.41
	per 6 oxygen				per 23 oxygen							
Si	2.02	2.00	2.00	2.00	8.05	7.97	7.97	7.95	7.89	7.90	7.91	7.88
Al	0.01	0.01	0.02	0.01	0.05	0.08	0.06	0.07	0.05	0.03	0.04	0.06
Ti	0.00	0.01	0.01	0.00	0.01	0.00	0.01	0.01	0.01	0.01	0.01	0.01
Fe	0.35	0.31	0.30	0.22	1.62	1.47	1.45	1.40	0.75	0.72	0.72	0.97
Mg	0.68	0.71	0.71	0.79	3.52	3.63	3.64	3.66	4.29	4.30	4.30	4.13
Mn	0.00	0.01	0.01	0.00	0.01	0.01	0.01	0.01	0.00	0.01	0.00	0.01
Ca	0.80	0.87	0.87	0.93	0.80	1.07	1.14	1.21	1.25	1.27	1.27	1.36
Na	0.21	0.14	0.14	0.09	1.41	1.04	0.98	0.88	0.89	0.88	0.89	0.78
K	0.00	0.00	0.00	0.00	0.17	0.28	0.26	0.30	0.44	0.42	0.40	0.30
Cl	0.00	0.00	0.00	0.00	0.00	0.00	0.00	0.00	0.01	0.00	0.00	0.00
F	0.00	0.00	0.00	0.00	0.07	0.09	0.09	0.09	0.16	0.17	0.16	0.11
Na/K	263	197	105	454	8.35	3.72	3.81	2.93	2.03	2.08	2.24	2.58
Mg/Fe	1.96	2.26	2.38	3.60	2.18	2.47	2.51	2.62	5.75	6.00	6.02	4.25

n.d. not detected

Table 8-3b Composition of pyroxenes and amphiboles in contact fenite (distal - PF-5d)

	Pyroxene				Amphibole							
SiO ₂	53.34	53.17	53.01	52.63	56.11	55.70	55.46	56.02	56.40	56.42	56.22	56.18
Al ₂ O ₃	0.25	0.31	0.27	0.32	0.43	0.44	0.45	0.42	0.38	0.38	0.36	0.37
TiO ₂	0.13	0.18	0.23	0.18	0.09	0.10	0.10	0.05	0.06	0.06	0.07	0.05
FeO	12.40	12.15	12.56	12.62	12.91	12.45	12.24	12.23	9.28	9.01	9.42	9.41
MgO	10.07	10.04	9.94	10.22	16.62	16.76	16.87	17.10	18.47	19.05	18.67	18.43
MnO	0.30	0.30	0.27	0.36	0.09	0.11	0.08	0.13	0.11	0.09	0.12	0.07
CaO	20.75	21.90	22.06	22.33	6.96	7.74	7.76	7.84	8.86	8.93	8.97	9.19
Na ₂ O	2.59	1.96	1.70	1.48	3.91	3.41	3.28	3.51	3.01	2.95	2.81	2.85
K ₂ O	0.02	0.01	n.d.	0.02	1.46	1.72	1.71	1.71	1.66	1.73	1.67	1.48
BaO	n.d.	n.d.	n.d.	n.d.	0.02	0.03	0.03	n.d.	0.02	0.02	0.03	n.d.
P ₂ O ₅	n.d.	n.d.	n.d.	n.d.	0.03	0.01	n.d.	0.01	0.00	n.d.	0.00	n.d.
Cr ₂ O ₃	n.d.	n.d.	0.01	0.01	0.01	n.d.	n.d.	0.00	0.02	n.d.	n.d.	0.02
Cl	n.d.	0.00	0.00	n.d.	0.01	0.01	0.00	0.01	0.01	0.01	0.00	0.00
F	0.01	n.d.	n.d.	n.d.	0.19	0.21	0.23	0.21	0.23	0.29	0.30	0.26
Total	99.86	100.02	102.06	100.16	98.74	98.60	98.11	99.14	98.41	98.81	98.51	98.21
	per 6 oxygen				per 23 oxygen							
Si	2.01	2.00	2.00	1.99	7.98	7.95	7.94	7.94	7.95	7.91	7.92	7.93
Al	0.01	0.01	0.01	0.01	0.07	0.07	0.08	0.07	0.06	0.06	0.06	0.06
Ti	0.00	0.01	0.01	0.01	0.01	0.01	0.01	0.00	0.01	0.01	0.01	0.01
Fe	0.45	0.44	0.46	0.43	1.54	1.49	1.46	1.45	1.09	1.06	1.11	1.11
Mg	0.57	0.56	0.56	0.58	3.53	3.56	3.60	3.61	3.88	3.98	3.92	3.88
Mn	0.01	0.01	0.01	0.01	0.01	0.01	0.01	0.02	0.01	0.01	0.01	0.01
Ca	0.84	0.88	0.89	0.91	1.06	1.18	1.19	1.19	1.34	1.34	1.35	1.39
Na	0.19	0.14	0.12	0.11	1.08	0.94	0.91	0.96	0.82	0.80	0.77	0.78
K	0.00	0.00	0.00	0.00	0.27	0.31	0.31	0.31	0.30	0.31	0.30	0.27
Cl	0.00	0.00	0.00	0.00	0.00	0.00	0.00	0.00	0.00	0.00	0.00	0.00
F	0.00	0.00	0.00	0.00	0.09	0.09	0.11	0.09	0.10	0.13	0.13	0.12
Na/K	246	212	—	102	4.07	3.02	2.93	3.12	2.75	2.58	2.56	2.92
Mg/Fe	1.26	1.27	1.22	1.33	2.30	2.40	2.46	2.49	3.55	3.77	3.53	3.49

n.d. not detected

Table 8-4 Composition of pyroxenes and amphiboles in regional fenites (PF-7)

	Pyroxene				Amphibole							
SiO ₂	52.03	51.96	52.25	51.92	50.96	50.71	49.89	50.81	51.15	49.77	52.66	52.31
Al ₂ O ₃	0.58	0.57	0.76	0.77	3.15	2.80	3.57	3.11	3.70	3.67	0.89	1.81
TiO ₂	0.13	0.10	0.05	0.07	0.27	0.19	0.32	0.19	0.19	0.27	0.05	0.05
FeO	12.95	12.89	12.95	12.68	13.64	13.87	14.08	13.15	13.65	14.45	13.03	13.34
MgO	11.04	10.97	10.78	10.75	15.32	15.40	15.14	15.77	15.06	14.70	16.06	15.77
MnO	0.47	0.48	0.38	0.41	0.35	0.35	0.31	0.37	0.34	0.38	0.38	0.34
CaO	21.19	21.54	21.93	22.07	9.60	9.75	9.78	9.86	9.90	10.28	10.97	11.16
Na ₂ O	1.73	1.57	1.42	1.41	2.79	2.73	2.82	2.69	2.55	2.66	1.54	1.62
K ₂ O	0.03	0.01	0.02	0.01	1.30	1.37	1.23	1.31	1.34	1.26	0.65	0.81
BaO	n.d.	0.02	n.d.	0.01	0.01	n.d.	n.d.	0.00	n.d.	0.01	n.d.	n.d.
P ₂ O ₅	0.03	n.d.	0.02	0.03	n.d.	n.d.	0.02	n.d.	n.d.	0.02	n.d.	0.02
Cr ₂ O ₃	n.d.	n.d.	n.d.	n.d.	0.01	n.d.	n.d.	0.01	n.d.	n.d.	n.d.	0.01
Cl	0.01	n.d.	0.00	0.01	0.02	0.02	0.02	0.04	0.02	0.04	0.01	0.01
F	n.d.	0.00	n.d.	n.d.	0.52	0.48	0.50	0.57	0.41	0.45	0.36	0.38
Total	100.17	100.10	100.57	100.15	97.70	97.46	97.48	97.63	98.12	97.76	96.43	97.46
	per 6 oxygen				per 23 oxygen							
Si	1.98	1.98	1.98	1.98	7.42	7.43	7.39	7.32	7.42	7.31	7.72	7.61
Al	0.03	0.03	0.03	0.03	0.54	0.48	0.53	0.62	0.63	0.64	0.15	0.31
Ti	0.00	0.00	0.00	0.00	0.03	0.02	0.02	0.04	0.02	0.03	0.01	0.01
Fe	0.41	0.41	0.41	0.40	1.66	1.70	1.60	1.73	1.66	1.77	1.60	1.62
Mg	0.63	0.62	0.61	0.61	3.33	3.36	3.42	3.31	3.26	3.22	3.51	3.42
Mn	0.02	0.02	0.01	0.01	0.04	0.04	0.05	0.04	0.04	0.05	0.05	0.04
Ca	0.87	0.88	0.89	0.90	1.50	1.53	1.54	1.54	1.54	1.62	1.72	1.74
Na	0.13	0.12	0.10	0.10	0.79	0.78	0.76	0.80	0.72	0.76	0.44	0.46
K	0.00	0.00	0.00	0.00	0.24	0.26	0.24	0.23	0.25	0.24	0.12	0.15
Cl	0.00	0.00	0.00	0.00	0.00	0.01	0.01	0.01	0.00	0.01	0.00	0.00
F	0.00	0.00	0.00	0.00	0.24	0.22	0.26	0.23	0.19	0.21	0.17	0.18
Na/K	105	477	102	195	3.27	3.04	3.12	3.47	2.90	3.21	3.61	3.05
Mg/Fe	1.52	1.52	1.48	1.51	2.00	1.98	2.14	1.92	1.97	1.81	2.20	2.11

n.d. not detected

Figure 8-10 Ternary diagrams of A) Ca-Al-Na; B) Ca-Mg+Fe-Na+K; and C) Ca-Mg-Fe for pyroxenes and amphiboles of fenitised granites (PF-5c and d) and granitic gneisses (PF-7).

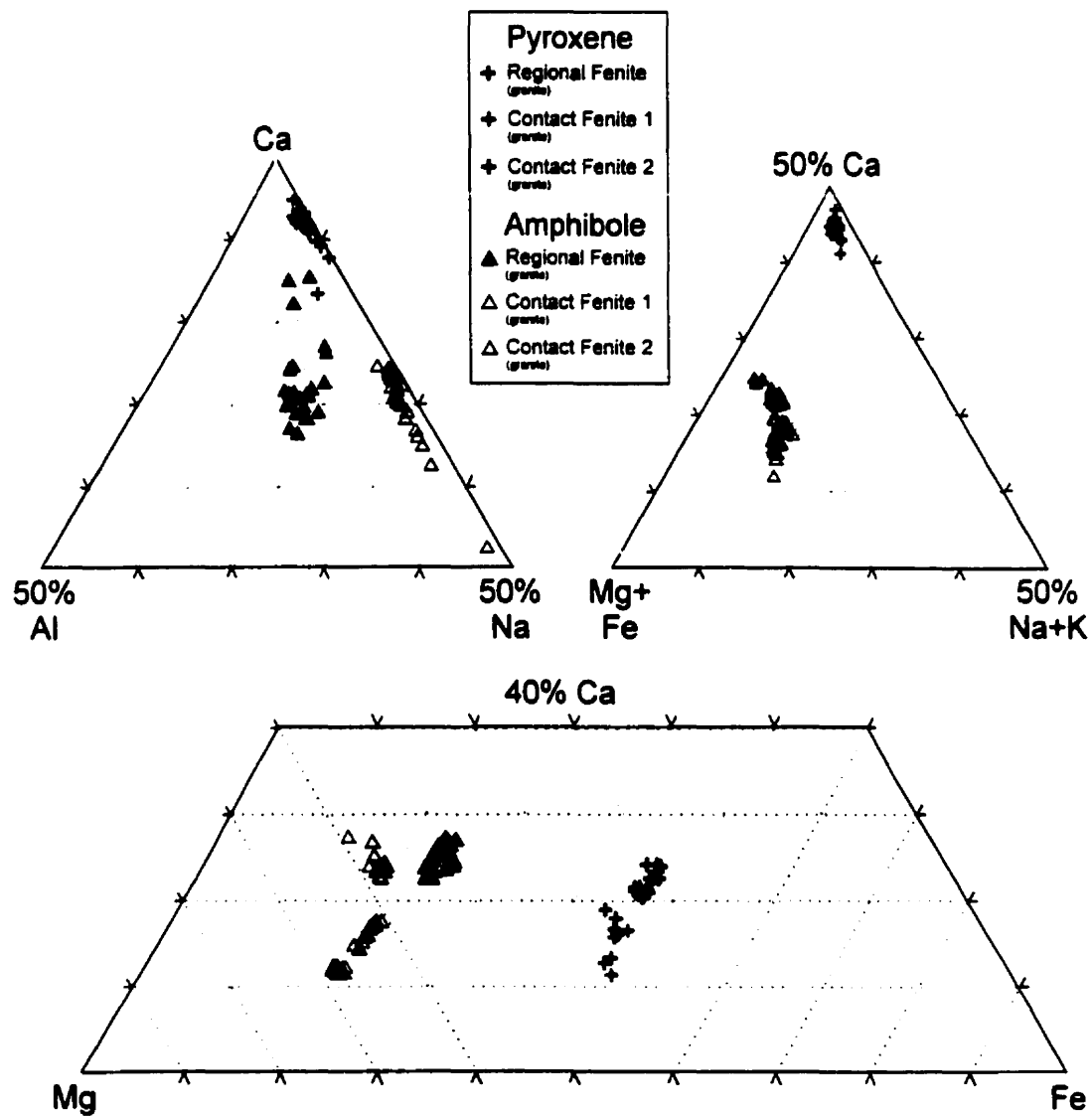


Table 8-5 Mass transfers (MT) associated with dolomitization of calcite surrounding chalcopyrite veinlets

	original calcite	altered Mg-calcite	MT	% Change	altered dolomite	MT	% Change	altered dolomite	MT	% Change
	g/100g									
Wt. %										
CaO	53.73	50.26	-3.47	-6.46	29.69	-24.05	-44.75	29.72	-24.01	-45
SrO	1.51	1.44	-0.07	-4.71	0.71	-0.80	-53.08	0.64	-0.87	-57
FeO	0.31	0.45	0.15	48.20	1.94	1.63	534.75	1.96	1.65	542
MnO	0.31	0.26	-0.04	-13.44	0.25	-0.06	-18.03	0.23	-0.08	-26
MgO	1.26	3.40	2.14	169.28	19.61	18.34	1452.34	20.26	18.99	1504
Na ₂ O	0.03	0.04	0.01	40.00	0.01	-0.02	-76.67	0.01	-0.02	-53
K ₂ O	0.01	0.01	0.01	71.43	0.02	0.01	142.86	0.02	0.01	200
BaO	0.31	0.31	0.00	0.33	0.05	-0.25	-82.41	0.02	-0.29	-94
*CO ₂	42.54	43.82	1.28	3.01	47.73	5.19	12.20	47.14	4.60	11
per 6 Oxygen										
Ca	1.95	1.80	-0.16	-8.04	0.99	-0.97	-49.49	0.99	-0.96	-49
Sr	0.023	0.021	0.00	-6.31	0.010	-0.01	-57.11	0.009	-0.01	-61
Fe	0.01	0.01	0.00	45.70	0.05	0.04	480.30	0.05	0.04	489
Mn	0.01	0.01	0.00	-14.90	0.01	0.00	-25.06	0.01	0.00	-32
Mg	0.06	0.17	0.11	164.75	0.91	0.84	1319.16	0.94	0.88	1371
Ba	0.004	0.004	0.00	-1.36	0.001	0.00	-83.92	0.000	0.00	-94
CO ₃	1.97	1.99	0.03	1.27	2.02	0.05	2.58	2.00	0.03	2

* CO₂ by difference

the former and 1.51 wt.% in the latter. BaO contents, although the same for calcite and Mg-calcite (0.31 wt.%), are much lower in dolomite (0.02-0.05 wt.%).

Mass Changes

The chemical changes described above can be related to quantitative mass changes through the use of mass balance algorithms such as those of Gresens (1967) and Grant (1986). The results of calculations using such algorithms provide a much more accurate representation of fluid-rock interaction by taking into account any volume changes which attended alteration (Gresens, 1967). In order to perform these calculations, the volume change caused by alteration must first be established, typically through the use of immobile elements. If an element is neither gained or lost during metasomatism, its relative abundances in the unaltered and altered rocks can be used to determine the volume change. When dealing with fenitizing fluids, however, many elements which are normally immobile, such as the HFSE, are in fact quite mobile, due to the presence of hard ligands such as F^- and SO_4^{2-} (Palmer and Williams-Jones, 1998a, Chap. 6). The mass factor, which is related to the volume factor (Gresens, 1967), can be calculated however, using the isocon method of Grant (1986)..

Whole rock

Figures 8-11 and 8-12 show a number of isocon diagrams for granite and granitic gneiss fenites, respectively. In each diagram, elements which plot above the isocon are considered to have been added during fenitization, while those below the line have been lost. Elements which plot on the line have been neither lost nor added and are considered to be immobile. The slope of the isocon can then be used to calculate mass and volume changes using a formula developed by Gresens (1967).

Figure 8-11 Isocon diagrams (Grant, 1986) for progressively fenitised granites (PF-11, 5, PF-6 and PF-5c) versus the least altered granite(PF-13). Elements which plot below the solid line (isocon) were removed during fenitization while those above were added.

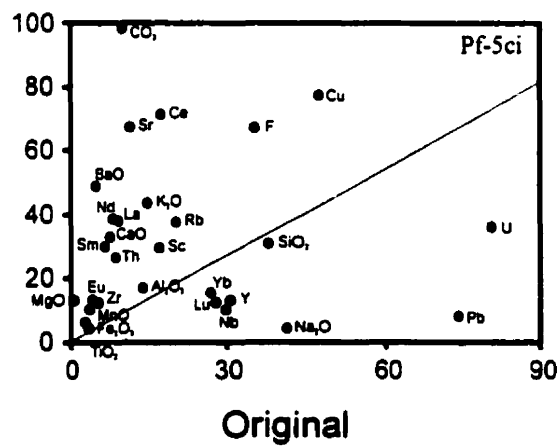
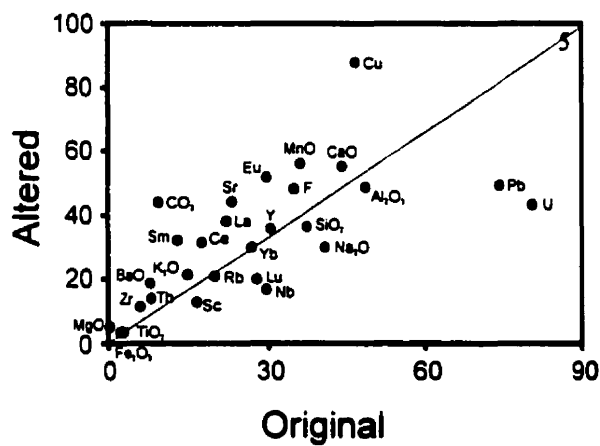
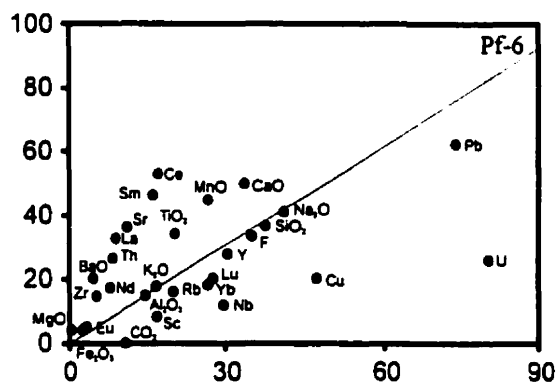
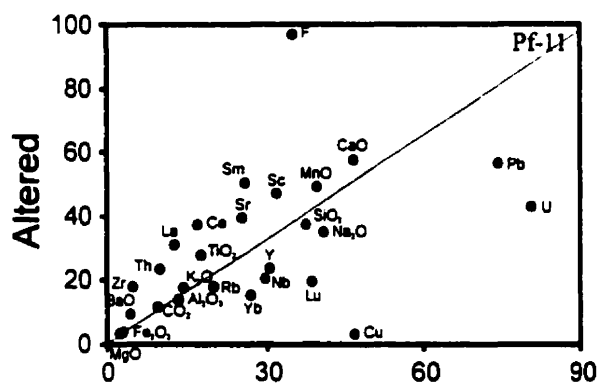
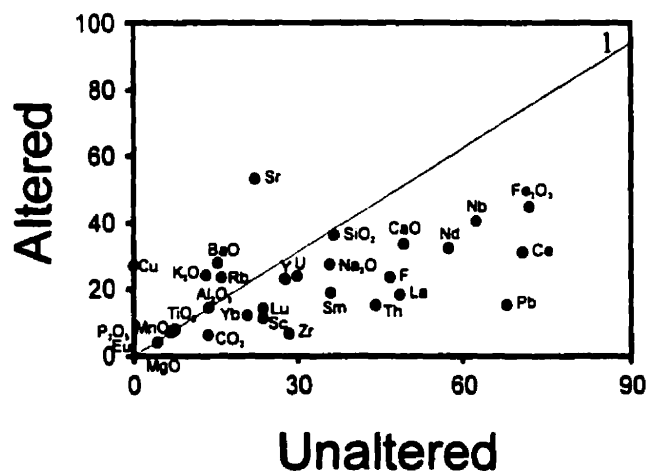
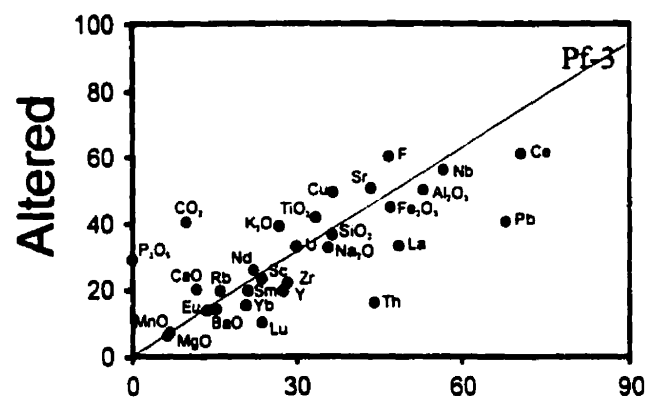
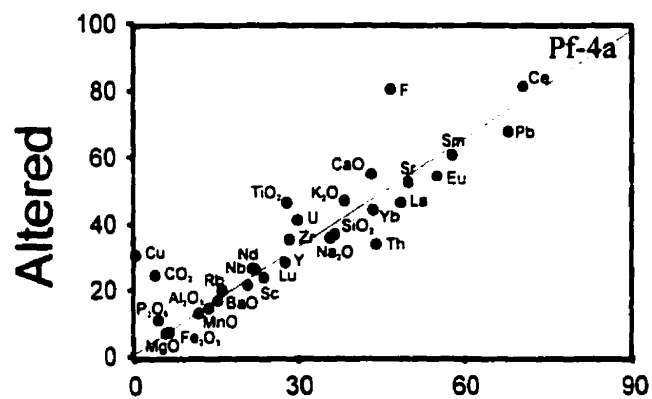


Figure 8-12 Isocon diagrams (Grant, 1986) for progressively fenitised granitic gneisses (PF-4a, PF-3 and 1) versus the least altered granitic gneiss (PF-1). Elements which plot below the solid line (isocon) were removed during fenitization while those above were added.



Mass Transfers

The slope of isocons (and corresponding mass factors) were determined to be 1.09 (0.92), 1.09 (0.92) and 1.00 (1.00) for regionally fenitized granite samples 5, Pf-6, and Pf-11 plotted versus unaltered granite (Pf-13), respectively, corresponding to mass losses of from 8% to 0%. The slope of the isocon for contact fenitized granite Pf-5c is 0.99, corresponding to a mass factor of 1.01 and therefore a mass gain of 1%. Fenitization of granite is characterized by significant, and consistent, losses of the major element oxides SiO_2 and Na_2O , from 2 to 8 g/100g and 1 to 4 g/100g, respectively, and the trace elements V, Nb, Pb and U in amounts of 3-7, 2-5, 4-22 and 5-8 g/1000kg, respectively. Components that experienced significant increases include K_2O (0.29-10g/100g), BaO (280-3318 g/1000kg), Sr (40-570 g/1000 kg), Th (2-9 g/1000kg) and the LREE La (6-29 g/1000kg), Ce (11-60 g/1000kg) and Nd (1-31 g/1000kg) (Table 8-6). Significant additions of copper (16-77 g/1000kg) are estimated for three fenite samples, while one shows no appreciable change and corresponds to the least altered fenite. The HREE, Yb and Lu, although reporting losses, do not change appreciably and can be considered nearly immobile. Y, which closely follows the HREE, shows losses in three samples (1.4 – 8.9g/1000kg) and a slight gain (1.1g/1000kg) in one regional fenite sample. The mass changes in the contact fenite were similar in many respects to those of the regional fenites, with the exception of that for Rb, which involved a large gain in the contact fenite. The greatest gains and losses are typically recorded by the contact fenites, which based on location, can be considered the highest grade fenites.

Isocons for regionally fenitized granitic gneiss samples Pf-4a, Pf-3 and 1, versus unaltered granitic gneiss (Pf-1), were determined to have slopes (and corresponding mass factors) of 1.04 (0.96), 1.04 (0.96) and 0.91 (1.10), respectively, corresponding to mass changes of -6%, -6% and +10%. Mass changes associated with granitic gneiss fenites were grossly similar to those of the granite fenites (Table 8-7), e.g., there were losses of SiO_2 and Na_2O (3.8-6.3 g/100g and 0.4-1.09 g/100g, respectively) and a gain of K_2O (0.28-3.22 g/100g). However, several elements experienced different mass changes in the granitic fenites. Rb was added to all fenites (13-62 g/1000kg), Zr and Th

Table 8-6 Mass transfers (MT) for fenitized granite

Major elements (wt %) for common granite																			
PF-13				S				PF-6				PF-11				PF-Sc			
	original		altered	MT	% change		altered	MT	% change		altered	MT	% change		altered	MT	% change		
g/100g of rock																			
SiO ₂	74.94		74.22	-6.85	-9		73.19	-7.79	-10		72.99	-1.95	-3		60.88	-13.45	-18		
TiO ₂	0.07		0.07	0.00	-1		0.07	0.00	-3		0.10	0.03	42		0.08	0.01	16		
Al ₂ O ₃	13.91		13.75	-1.30	-9		13.63	-1.41	-10		14.43	0.52	4		16.68	2.94	21		
Fe ₂ O ₃	0.53		0.66	0.08	14		0.70	0.11	21		0.80	0.27	51		1.14	0.62	117		
MnO	0.01		0.01	0.00	5		0.01	0.00	57		0.01	0.00	43		0.02	0.01	189		
MgO	0.02		0.07	0.04	221		0.20	0.16	817		0.16	0.14	700		0.51	0.50	2476		
CaO	0.75		0.90	0.08	10		0.95	0.12	16		1.05	0.30	40		3.26	2.54	339		
Na ₂ O	4.56		3.87	-1.01	-22		3.33	-1.50	-33		4.54	-0.02	0		0.43	-4.13	-90		
K ₂ O	4.95		5.86	0.43	9		6.78	1.27	26		5.24	0.29	6		14.38	9.58	193		
P ₂ O ₅	0.04		0.05	0.01	27		0.05	0.01	15		0.05	0.01	28		0.24	0.20	562		
g/1000kg of rock																			
F	210		580	322	153		290	56	27		200	-10	-5		400	194	92		
BaO	354		696	285	80		763	346	98		1501	1147	324		3636	3319	937		
Cr ₂ O ₃	26		27	-1.23	-5		20	-7.65	-29		25	-1.00	-4		21	-4.79	-18		
Cu	4		3	-1.25	-31		88	77	1918		20	16	400		77	74	1844		
V	7		0	-7.00	-100		4	-3.33	-48		0	-7.00	-100		0	-7.00	-100		
Nb	9.9		6.8	-3.66	-37		5.6	-4.76	-48		3.9	-6.00	-61		3.2	-6.67	-67		
Pb	24.7		18.8	-7.45	-30		16.5	-9.56	-39		20.7	-4.00	-16		2.6	-22	-89		
Rb	203.2		177	-41	-20		209.2	-11	-6		159.7	-44	-21		372.0	173	85		
Sr	114.2		173	44	39		214.4	82	72		361.0	247	216		669.7	562	492		
Th	4.3		9.3	4.23	98		7.0	2.12	49		13.2	8.90	207		13.1	8.93	208		
U	11.5		6.1	-5.90	-51		6.2	-5.81	-51		3.7	-7.80	-68		5.1	-6.35	-55		
Y	15.3		12	-4.47	-29		17.9	1.12	7		13.9	-1.40	-9		6.3	-8.94	-58		
Zr	26.3		89	55	211		64.0	32	123		72.6	46	176		59.5	34	129		
Sc	1.7		2.5	0.59	35		1.3	-0.51	-30		0.8	-0.90	-53		2.9	1.23	72		
Trace elements (ppm) for common granite																			
La	9.1		21.0	10	112		16.7	6.22	68		32.6	24	258		37.5	29	316		
Ce	19		41	19	98		33	11	59		58	39	205		78	60	315		
Nd	8		10	1.17	15		10	1.17	15		17	9.00	113		38	30	380		
Sm	1.3		2.5	0.99	76		2.3	0.81	62		3.4	2.10	162		5.9	4.66	358		
Eu	0.4		0.6	0.15	38		0.6	0.15	38		0.6	0.20	50		1.3	0.91	228		
Yb	0.9		0.5	-0.44	-49		1.0	0.02	2		0.6	-0.30	-33		0.5	-0.39	-44		
Lu	0.14		0.07	-0.08	-54		0.10	-0.05	-34		0.10	-0.04	-29		0.06	-0.08	-57		

N/A Not Available

Table 8-7 Mass transfers (MT) for fenitized granitic gneiss

	PF-1	PF-4A			PF-3			I		
	original	altered	MT	% change	altered	MT	% change	altered	MT	% change
g/100g of rock										
SiO ₂	73.48	73.21	-6.31	-9	72.46	-3.81	-5	71.85	-4.39	-6
TiO ₂	0.16	0.25	0.07	42	0.19	0.02	13	0.16	-0.01	-6
Al ₂ O ₃	14.03	14.06	-1.13	-8	13.57	-0.98	-7	14.24	-0.34	-2
Fe ₂ O ₃	1.32	1.36	-0.07	-5	1.20	-0.17	-13	1.01	-0.35	-26
MnO	0.01	0.02	0.00	11	0.01	0.00	-4	0.01	0.00	-4
MgO	0.24	0.26	0.00	-1	0.25	0.00	0	0.18	-0.07	-28
CaO	1.21	1.24	-0.07	-6	1.99	0.70	58	0.78	-0.46	-38
Na ₂ O	3.99	3.92	-0.39	-10	3.61	-0.52	-13	3.02	-1.09	-27
K ₂ O	4.50	5.21	0.28	6	6.08	1.35	30	8.03	3.22	72
P ₂ O ₅	0.05	0.11	0.05	109	0.05	0.01	13	0.04	-0.01	-18
g/1000kg of rock										
F	280	480	160	57	360	66	24	140	-145	-52
BaO	1170	1225	-46	-4	1043	-167	-14	2074	824	70
Cr ₂ O ₃	4	5	0.59	15	14	9.46	237	40	34	862
Cu	0	16	15	N/A	3	2.88	N/A	11	11	N/A
V	0	9	8.26	N/A	9	8.65	N/A	0	0.00	N/A
Nb	8.1	8.6	-0.21	-3	7.9	-0.50	-6	5.3	-3.00	-37
Pb	22.7	22.4	-2.15	-9	13.5	-9.72	-43	5.1	-18	-78
Rb	163.9	193.6	14	8	194.4	23	14	233.5	61	37
Sr	223.9	257.3	12	5	255.6	22	10	528.4	284	127
Th	22.0	16.8	-6.59	-30	8.0	-14	-65	7.5	-15	-67
U	4.3	5.8	1.02	24	4.7	0.22	5	3.4	-1.03	-24
Y	13.9	13.8	-1.24	-9	9.7	-4.57	-33	11.4	-2.94	-21
Zr	142.3	174.5	18	13	109.9	-37	-26	32.1	-111	-78
Sc	2.4	2.3	-0.29	-12	2.3	-0.19	-8	1.1	-1.34	-56
La	48.4	46	-6.29	-13	33.0	-17	-34	18.2	-31	-64
Ce	78	89	3.65	5	67	-14	-17	34	-45	-58
Nd	22	26	1.85	8	25	2.04	9	12	-10	-48
Sm	4.3	4.5	-0.17	-4	3.9	-0.55	-13	2.2	-2.18	-51
Eu	0.7	0.7	-0.06	-8	0.7	-0.03	-4	0.4	-0.32	-45
Yb	0.7	0.7	-0.06	-8	0.5	-0.22	-31	0.4	-0.32	-45
Lu	0.12	0.12	-0.01	-8	0.05	-0.07	-60	0.07	-0.05	-44

N/A Not Available

underwent depletions (36-112 and 7-15 g/1000kg, respectively) and all REE were either depleted or experienced little change.

Mineral Mass Transfers

Pyroxene-Amphibole

The replacement of diopside by richterite can also be quantified chemically (Table 8-8). Mass balance calculations, based on mineral densities, indicate that the conversion of pyroxene to amphibole in contact fenites involved gains of SiO₂, MgO, FeO, Na₂O and K₂O, in amounts ranging between 3.4 and 7.0, 5.4 and 8.4, 0.52 and 2.49, 1.3 and 3.2 and 0.93 and 1.68 g/100g diopside, respectively. The only significant loss was that of CaO, which was depleted by 13.6 to 16.4 g/100g diopside. Al₂O₃ was only slightly affected with gains ranging between 0.07 and 0.23 g/100g diopside. As expected, amphibole in contact fenite amphiboles nearer to carbonatite dykes has less MgO and more Na₂O added per mass of mineral than in contact fenite further out. FeO was added to amphibole in proximal contact fenite (0.6 to 2.5 g/100g diopside) and depleted in distal varieties (-0.7 to -1.5 g/100g diopside). The ranges of K₂O, Na₂O and CaO additions overlapped for proximal and distal varieties.

As was the case for contact fenite, the replacement of pyroxene by amphibole in regional fenites (Table 8-8) was accompanied by the addition of MgO, Na₂O and K₂O and loss of CaO, however, the mass changes were smaller 2.1 to 4.4, 0.14 to 1.7, 0.44 to 1.26 and -10.6 to -12.7 g/100g diopside, respectively. In contrast, SiO₂ was lost (-1.9 to -4.7 g/100g diopside) and Al₂O₃ was added in appreciably higher amounts (0.14 to 3.3 g/100g diopside). Mass changes for FeO were variable ranging from -0.15 to 0.32 g/100g diopside.

Potassium Feldspar

The slight changes in chemistry which accompanied potassium feldspar alteration, caused by fluids exsolved by surrounding pyroxenite veinlets, in contact and regional

Table 8-8 Mass transfer (MT) calculations for replacement of pyroxene by amphibole in regional and contact fenites

	pyroxene			amphibole			amphibole			amphibole			
	A	MT	% change	B	MT	% change	C	MT	% change	D	MT	% change	
g/100g of rock													
Remonal Fenite (PF-7)													
SiO ₂	52.25	52.41	-1.94	-4	52.31	-2.03	-4	49.51	-4.72	-9	51.15	-3.15	-6
Al ₂ O ₃	0.76	0.94	0.14	18	1.81	0.97	127	4.24	3.31	433	3.70	2.78	364
TiO ₂	0.05	0.06	0.01	26	0.05	0.00	4	0.31	0.25	528	0.19	0.13	272
FeO	12.95	13.83	0.32	2	13.34	-0.15	-1	13.30	-0.18	-1	13.65	0.15	1
MgO	10.78	13.45	2.13	20	15.77	4.36	40	14.59	3.23	30	15.06	3.68	34
MnO	0.38	0.46	0.06	15	0.34	-0.06	-15	0.32	-0.08	-20	0.34	-0.05	-14
CaO	21.93	11.84	-10.56	-48	11.16	-11.22	-51	9.59	-12.72	-58	9.90	-12.43	-57
Na ₂ O	1.42	2.00	0.50	36	1.62	0.14	10	3.24	1.70	120	2.55	1.03	73
K ₂ O	0.02	0.48	0.44	2081	0.81	0.75	3594	1.27	1.20	5706	1.34	1.26	6021
BaO	n.d.	n.d.	N/A	N/A	n.d.	N/A	N/A	0.01	N/A	N/A	n.d.	N/A	N/A
P ₂ O ₅	0.02	0.00	-0.02	-100	0.02	0.00	-21	n.d.	N/A	N/A	n.d.	N/A	N/A
Cr ₂ O ₃	n.d.	n.d.	N/A	N/A	0.01	N/A	N/A	n.d.	N/A	N/A	n.d.	N/A	N/A
Cl	0.002	0.03	0.02	1244	0.01	0.01	476	0.03	0.03	1340	0.02	0.02	860
F	n.d.	0.27	N/A	N/A	0.38	N/A	N/A	0.46	N/A	N/A	0.41	N/A	N/A
Proximal Contact Fenite (PF-5c)													
SiO ₂	53.64	55.39	3.41	6	55.74	3.77	7	55.47	3.49	7	56.14	4.18	8
Al ₂ O ₃	0.22	0.42	0.21	96	0.37	0.16	70	0.44	0.23	105	0.28	0.07	31
TiO ₂	0.01	0.10	0.09	724	0.07	0.05	458	0.04	0.03	209	0.05	0.04	303
FeO	11.40	11.68	0.63	6	12.13	1.09	10	12.26	1.23	11	13.48	2.49	22
MgO	11.59	17.13	6.05	52	17.07	5.99	52	16.98	5.90	51	16.46	5.36	46
MnO	0.23	0.06	-0.17	-74	0.08	-0.15	-63	0.07	-0.16	-68	0.11	-0.12	-52
CaO	21.74	7.90	-13.60	-63	7.45	-14.07	-65	6.96	-14.57	-67	5.22	-16.36	-75
Na ₂ O	2.02	3.18	1.25	62	3.52	1.60	79	3.75	1.84	91	5.06	3.19	158
K ₂ O	0.02	1.65	1.68	7988	1.40	1.43	6786	1.53	1.56	7414	0.92	0.93	4422
BaO	0.01	n.d.	N/A	N/A	n.d.	N/A	N/A	0.01	0.00	-44	0.16	0.15	1398
P ₂ O ₅	n.d.	0.04	N/A	N/A	n.d.	N/A	N/A	0.01	N/A	N/A	n.d.	N/A	N/A
Cr ₂ O ₃	0.02	0.01	-0.01	-30	0.01	-0.01	-35	n.d.	N/A	N/A	0.002	-0.02	-89
Cl	0.001	0.01	0.01	518	0.01	0.01	621	0.01	0.01	724	0.01	0.01	930
F	n.d.	0.19	N/A	N/A	0.19	N/A	N/A	0.21	N/A	N/A	0.16	N/A	N/A
Distal Contact Fenite (PF-5d)													
SiO ₂	53.01	55.46	6.32	12	55.70	6.58	12	56.02	6.93	13	56.11	7.02	13
Al ₂ O ₃	0.27	0.45	0.22	81	0.44	0.21	77	0.42	0.18	68	0.43	0.19	71
TiO ₂	0.23	0.10	-0.13	-55	0.10	-0.12	-54	0.05	-0.18	-79	0.09	-0.13	-57
FeO	12.56	12.24	0.53	4	12.45	0.76	6	12.23	0.52	4	12.91	1.25	10
MgO	9.94	16.87	8.11	82	16.76	7.99	80	17.10	8.35	84	16.62	7.84	79
MnO	0.27	0.08	-0.18	-68	0.11	-0.16	-58	0.13	-0.13	-49	0.09	-0.18	-66
CaO	22.06	7.76	-13.76	-62	7.74	-13.78	-62	7.84	-13.68	-62	6.96	-14.62	-66
Na ₂ O	1.70	3.28	1.82	107	3.41	1.96	115	3.51	2.06	121	3.91	2.48	146
K ₂ O	n.d.	1.71	N/A	N/A	1.72	N/A	N/A	1.71	N/A	N/A	1.46	N/A	N/A
BaO	n.d.	0.03	N/A	N/A	0.03	N/A	N/A	n.d.	N/A	N/A	0.02	N/A	N/A
P ₂ O ₅	n.d.	n.d.	N/A	N/A	0.01	N/A	N/A	0.01	N/A	N/A	0.03	N/A	N/A
Cr ₂ O ₃	0.01	n.d.	N/A	N/A	n.d.	N/A	N/A	0.004	0.00	-47	0.01	0.00	-6
Cl	0.001	0.004	0.00	328	0.01	0.01	970	0.01	0.01	649	0.01	0.01	649
F	n.d.	0.23	N/A	N/A	0.21	N/A	N/A	0.21	N/A	N/A	0.19	N/A	N/A

n.d. not detected

N/A Not Available

fenites do not indicate that there was significant volume change. This is supported by the isocons for altered and unaltered feldspar which were calculated as having a slope of 1 and therefore, a mass factor of 1.0. As a result, mass changes can be interpreted directly from chemical analyses (Table 8-9, 10). In contact fenites Al_2O_3 and BaO were consistently lost from feldspar (0.13 to 0.28 and 0.20 to 0.28 g/100g ksp_{par} , respectively), while sodium was added (0.09 to 0.23 g/100g ksp_{par}). Analyses for K_2O record inconsistent changes and overall K_2O concentration probably remained unchanged. By contrast, potassium feldspar proximal to pyroxenite veins in regional fenites shows consistent losses of Na_2O (0.13 to 0.27 g/100g ksp_{par}) and gains of K_2O (0.08 to 0.74 g/100g ksp_{par}) (Table 8-10). Both BaO and Al_2O_3 underwent mass changes similar to those of feldspar in contact fenites.

Calcite-Dolomite

The isocon diagram for the replacement of calcite by Mg-calcite and dolomite is shown in Figure 8-13 and the calculated mass changes in Table 8-5. The isocon for the alteration of calcite to Mg-calcite has a slope of approximately 1 and this value is used throughout the calculations as little volume change should be associated with the transformation of calcite to dolomite (Gresens, 1967).

As was expected, MgO and CaO showed the greatest losses and gains, respectively. Between 2 and 19g/100g calcite of MgO were added and between -3 and -4g/100g calcite of CaO were lost during dolomitization, compared to their original concentrations in calcite of 53 and 1.26 wt.%, respectively. The next largest change was in the concentration of FeO which was added in amounts between 0.15 and 1.96g/100g calcite , compared to the original concentration in calcite of 0.31 wt.%. The minor elements BaO and SrO were lost during dolomitization, in amounts ranging between 0.25 and 0.29g/100g calcite and 0.07 and 0.87g/100g calcite , respectively, compared to their original concentrations of 0.31 and 1.51 wt.%.

Table 8-9 Mass transfers (MT) for altered K-feldspar surrounding pyroxenite veinlet in contact fenite

	original 1-1	altered 1-2	MT	% Change	altered 1-3	MT	% Change	altered 1-4	MT	% Change	altered 1-5	MT	% Change
	g/100g												
SiO ₂	63.21	63.09	-0.12	0	63.44	0.23	0	63.57	0.36	1	63.56	0.35	1
TiO ₂	0.00	0.01	0.01	N/A	0.00	0.00	N/A	0.00	0.00	N/A	0.00	0.00	N/A
Al ₂ O ₃	17.78	17.56	-0.23	-1	17.66	-0.13	-1	17.51	-0.28	-2	17.58	-0.20	-1
FeO	0.46	0.55	0.09	19	0.61	0.15	32	0.63	0.17	36	0.78	0.31	68
MgO	0.01	0.00	0.00	-80	0.00	-0.01	-100	0.01	0.00	20	0.00	-0.01	-100
CaO	0.00	0.00	0.00	-100	0.01	0.00	50	0.00	0.00	-100	0.00	0.00	-100
Na ₂ O	0.20	0.29	0.09	48	0.39	0.20	102	0.42	0.23	117	0.41	0.21	110
K ₂ O	17.21	17.51	0.30	2	17.17	-0.04	0	17.11	-0.10	-1	17.34	0.13	1
BaO	0.54	0.31	-0.23	-43	0.33	-0.20	-38	0.26	-0.28	-51	0.27	-0.27	-50
SrO	0.00	0.00	0.00	N/A	0.00	0.00	N/A	0.00	0.00	N/A	0.00	0.00	N/A
P ₂ O ₅	0.01	0.01	0.00	0	0.00	-0.01	-100	0.00	-0.01	-100	0.00	-0.01	-100
per 32 Oxygens	p.f.u.												
Si	11.92	11.93	0.00	0	11.94	0.01	0	11.96	0.04	0	11.94	0.01	0
Al	3.95	3.91	-0.04	-1	3.91	-0.04	-1	3.88	-0.07	-2	3.89	-0.06	-2
Fe	0.07	0.09	0.01	19	0.10	0.02	32	0.10	0.03	35	0.12	0.05	67
Ca	0.00	0.00	0.00	-100	0.00	0.00	50	0.00	0.00	-100	0.00	0.00	-100
Na	0.04	0.05	0.02	48	0.07	0.04	102	0.08	0.04	116	0.07	0.04	109
K	2.07	2.11	0.04	2	2.06	-0.01	0	2.05	-0.02	-1	2.08	0.01	0
Ba	0.04	0.02	-0.02	-43	0.02	-0.02	-38	0.02	-0.02	-52	0.02	-0.02	-50
Or	98	98			97			96			97		
Ab	2	2			3			4			3		
Na/K	0.017	0.025			0.035			0.038			0.036		

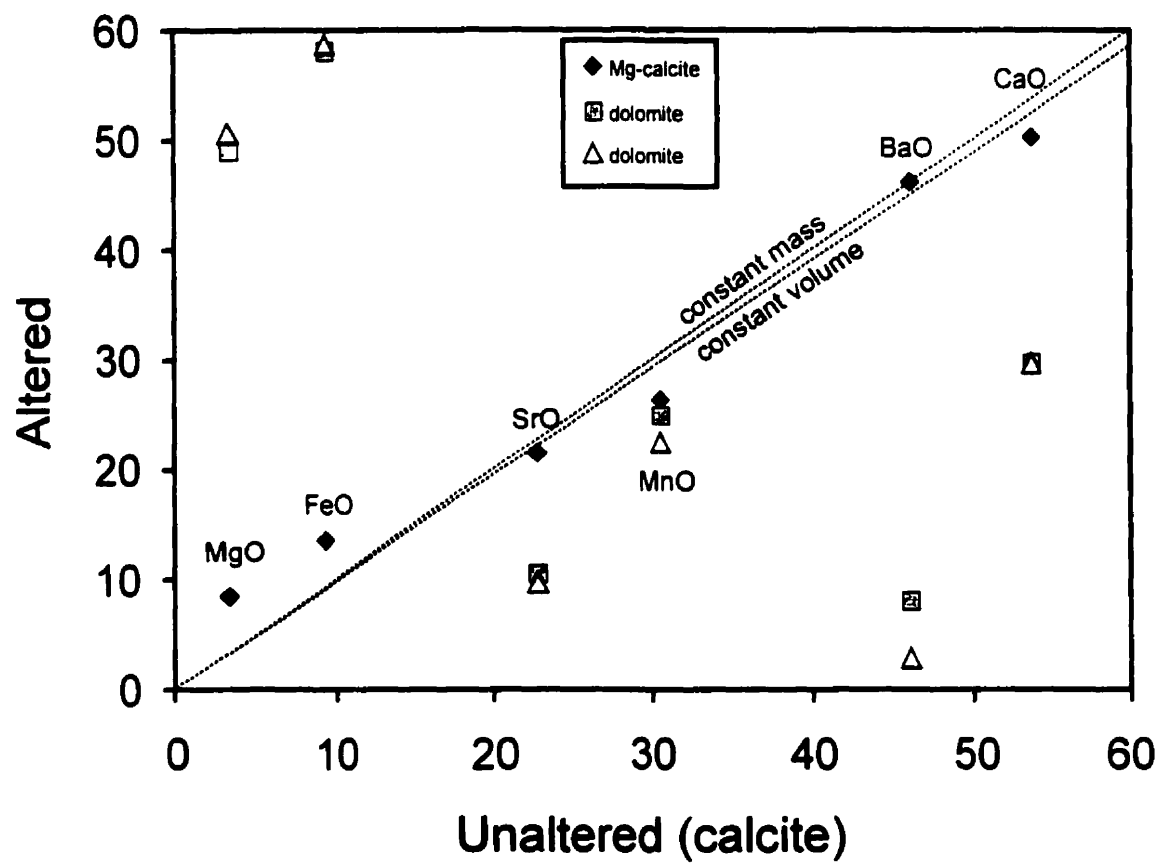
Samples 1-1 to 1-5 represent increasing proximity to vein

N/A Not Available

[illegible]

N/A Not Available

Figure 8-13 Isocon diagrams (Grant, 1986) for the replacement of calcite (unaltered) by Mg-calcite and dolomite (altered). Elements which plot below the solid line (isocon) were removed during fenitization while those above were added.



Discussion

Fenitization at Phalaborwa was more complicated than that originally reported by Frick (1975). The spatial distribution of fenites at Phalaborwa makes it necessary to consider the possibility that fluids derived from either pyroxenite or carbonate melts were involved in the fenitizing process. Numerous studies of fenitization have dispelled earlier theories that carbonatite- and ijolite-derived fluids are responsible for only potassic and sodic fenitization, respectively. They have also shown that both fluid types are silica undersaturated, especially with respect to granitic rocks (Kresten and Morogan, 1986; Morogan, 1994). The mass changes we recorded by whole-rock analyses should be reflected by changes in mineral chemistry. However, minerals may amplify changes for some elements and consequently identify directions of mass change that were not apparent from bulk rock chemistry. They may also provide evidence of sequential changes, i.e., steps in the fenitizing process or the occurrence of more than one fenitizing event.

Regional fenitized rocks are volumetrically the dominant fenite type surrounding the complex, however, numerous examples of contact fenitization associated with carbonatite dykes have been observed. Gross chemical and mineralogical changes of both fenite types indicate that these rocks have undergone predominantly potassic metasomatism. Although sodium showed an overall depletion during fenitization, it was added during the alteration of pyroxene to amphibole in regional and contact fenites and this suggests remobilization of sodium dissolved during the breakdown of plagioclase.

From bulk rock compositions it would appear that fenitization was accomplished either by one fluid or that fluids exsolved from both pyroxenite and carbonatite melts were indistinguishable. Mineralogical changes, however, indicate that two chemically separate fluids may have been present. In regionally fenitised granite, potassium feldspar surrounding pyroxenite veinlets has undergone significant Na losses, however, in contact fenitized rocks, altered potassium feldspar surrounding similar veinlets show an increase in sodium with increasing alteration. This, coupled with the growth of amphibole along the edges of pyroxenite veinlets in contact fenites suggests that carbonatite-derived aqueous fluids, carrying significant Na, exploited fractures associated with pyroxenite

veinlets. In comparing richterite in regional and contact fenites it was noted that, although Na/K ratios are similar, they span a much broader range in the latter, 2.03-8.35 versus 2.90-3.61 in the former. This indicates a higher Na/K ratio in the fluid which metasomatised granites in close proximity to carbonatite intrusions. At first glance this suggests that metasomatism related to intrusion of pyroxenite melts, represented by pyroxenite veinlets, was less sodic than that associated with intrusion of carbonatite and that alteration caused by emplacement of late carbonatite dykes overprinted this earlier metasomatism. However, the different Na concentrations in amphibole from contact and regional fenites can still be explained by a single fluid model owing to the remobilization of Na released during the dissolution/replacement of plagioclase feldspar. Normative mineral calculations (Fig. 8-4) show that contact fenitization was responsible for the removal of much greater quantities of albite than was regional fenitization. Logically, the increased Na in fluids responsible for the former style of fenitization would cause the growth of more sodic amphiboles. However, a single fluid cannot explain the disparity of other elements, such as Mg, Ca, Si and Fe, between richterites in contact and regional fenites and this suggests that the amphiboles in the two settings were precipitated from separate and chemically distinct aqueous fluids.

The dissimilarity in the chemistry of alteration minerals in contact and regional fenites does support the presence of two fluids, one derived from pyroxenite and the other from carbonatite. Mass balance calculations indicate that fluids responsible for the replacement of diopside by richterite during contact fenitization were enriched in Mg, Fe and Si and depleted in Ca, compared to fluids responsible for the replacement of pyroxene by amphibole in regional fenites. The breakdown of minerals during the two types of fenitization cannot be used to explain the differences in their amphibole compositions if only a single fluid were present. Therefore, two separate fluids must have been present, one originating from carbonatite, i.e., contact fenitization, and the other from pyroxenite, i.e., regional fenitization. In considering the relative contributions of the two fluids, mineralogical and mass changes suggest that aqueous fluids exsolved from carbonatite, although more reactive, were volumetrically minor compared to those exsolved from pyroxenite. Only in close proximity to carbonatite, could the contribution of carbonatite-derived fluids be expected to have been significant.

Fluid Compositions from Fenitization Studies

With the identification of two separate fenitising fluids, it is possible to qualify their respective compositions based on mass transfers which must have occurred between aqueous fluid and rock. Hydrothermal fluids exsolved from carbonatite caused significant increases, in the granitic rocks, of K, Ba, Mg, Fe, Sr, Th and the LREE but must have been deficient, with respect to the precursor lithologies, in Si and Nb. Changes in mineral compositions are consistent with these mass transfers, but also show that Na, although not in high concentrations in early fenitising fluids, was acquired by the aqueous fluid through the destruction of albite during alteration. Although Ca appears to have been added to the contact fenites, the replacement of diopside by richterite was accompanied by its loss. The occurrence of small pods of carbonatite as well as thin carbonatite veinlets in contact fenites may explain the large Ca gains obtained from these rock analyses. The absence of Ca in carbonatite derived aqueous fluids is not uncommon and has been reported by Palmer (1994), Vard and Williams-Jones (1993) and Samson *et al.* (1995) for other alkalic complexes.

Mass transfers which occurred between granitic rocks and pyroxenite-derived fluids to produce regional fenites are similar to those for contact fenites. Fenitising fluids added K, Sr, Fe, Mg, Ca and LREE while removing Si and Na. Barium shows contrasting behaviour in granite and granitic gneiss, having been added in the former and removed in the latter. Mineralogical changes, however, indicate that the concentrations of Mg and Fe were smaller, and that the content of Ca was greater, in these aqueous fluids than those exsolved by carbonatite.

Implications for copper mineralization

The evidence presented above for the presence of aqueous fluid phases strengthens the case that copper mineralization in transgressive carbonatite is of a hydrothermal origin. Mass change reconstruction confirms that these aqueous fluids contained Mg, Fe and S, and, together with alteration studies of minerals surrounding ore

veinlets in transgressive carbonatite, indicate that the ore fluids were exsolved from carbonatite.

Chalcopyrite mineralization in carbonatite is typically accompanied by dolomite which replaced the surrounding calcite, and is manifested as dark grey alteration haloes (Fig. 8-3a), which mantle ore minerals, i.e., chalcopyrite and magnetite (Fig. 8-3b). Mass changes which occurred during the replacement of calcite included large gains in MgO and FeO and losses of CaO. The higher Mg concentrations and the presence of Fe in carbonatite-derived aqueous fluids as compared to aqueous fluids exsolved by pyroxenite, inferred from the replacement of diopside by richterite, suggest that these solutions were responsible for the growth of dolomite.

Although the origin of bornite mineralization in banded carbonatite is uncertain, the absence of an identifiable fluid phase and mineral textures supports its being a primary magmatic phase. The presence of copper-bearing sulphides in melt inclusions (Aldous, 1980; Palmer and Williams-Jones, 1998b, Chap. 7) would also indicate a magmatic origin for early copper mineralization.

Copper mineralization is therefore thought to have resulted from early primary crystallization from melts which formed banded carbonatite and later as either hydrothermal remobilization of primary sulphides in transgressive carbonatite or direct precipitation from Cu- and S- bearing orthomagmatic fluids exsolved from transgressive carbonatite melts. The latter is supported by decrepitate studies of Palmer and Williams-Jones (1998b, Chap. 7) who concluded that orthomagmatic fluids associated with transgressive carbonatite were enriched in S. However, a combination of remobilisation and direct precipitation from orthomagmatic fluids remains a possibility.

Conclusions

The emplacement of silicate and carbonate rocks of the Phalaborwa complex was accompanied by finitization of the host granites and granitic gneisses by aqueous fluids exsolved from the respective melts. The greatest fluid flux was associated with pyroxenite and gave rise to widespread potassic finitization. Later carbonatite magmas exsolved aqueous fluids which were also responsible for potassic metasomatism that

locally overprinted the earlier fenitization, and was recognizable due to mineralogical changes which reflected higher concentrations of Na and Mg. The proportions of fluids were highly disproportionate, with much greater volumes of fluids being exsolved from pyroxenite.

Studies of fluid inclusions and fenitization suggest that both fluids contained K, Na, Mg, Fe, Sr and LREE, however, those associated with carbonatite had higher Na/K ratios and greater concentrations of Mg. The higher Mg content of carbonatite-derived aqueous fluids is thought to have been responsible for dolomitization of calcite surrounding chalcopyrite veinlets in transgressive carbonatite. It is therefore proposed that late copper mineralization occurred through remobilization of primary sulphides by a late orthomagmatic fluid exsolved by transgressive carbonatite.

References

- Aldous, R.T., 1980, Ore genesis in copper-bearing carbonatites; a geochemical, fluid inclusion and mineralogical study: Unpublished Ph.D. thesis, Imperial College, London, 365p..
- Briden, J.C., 1976, Application of paleomagnetism to Proterozoic tectonics: *Philosophical Transactions of the Royal Society of London*, v. 280, p. 405-416.
- Eriksson, S.C., 1982, Aspects of the petrochemistry of the Phalaborwa Complex, northeastern Transvaal, South Africa: Unpublished Ph.D. thesis, University of the Witwatersrand, Johannesburg.
- Eriksson, S.C., 1989, Phalaborwa, a saga of magmatism, metasomatism and miscibility: *in* K. Bell (ed.), *Carbonatites: genesis and evolution*: London, Unwin Hyman, p. 221-254.
- Frick, C., 1975, The Phalaborwa syenite intrusions: *Trans.Geol. Soc. S. Afr.*, v. 78, p. 201-213.
- Grant, J.A., 1986, The isocon diagram-A simple solution to Gresens' equation for metasomatic alteration: *Economic Geology*, v. 81, p. 1976-1982.
- Gresens, R.L., 1967, Composition-volume relationships of metasomatism: *Chem. Geol.* v. 2, p. 47-65.
- Hanekom, H.J., van Staden, C.M., Smit, P.J., and Pike, D.R., 1965, The geology of the Palabora Igneous Complex: *South Africa Geological Survey Handbook*, memoir 54.
- Heinrich, E. Wm., 1970, The Palabora carbonatitic complex – a unique copper deposit: *Canadian Mineralogist*, v. 10, p. 585-598.
- Kresten, P., and Morogan, V., 1986, Fenitization at the Fen complex, southern Norway: *Lithos*, v. 19, p. 27-42.
- Morogan, V., 1994, Ijolite versus carbonatite as sources of fenitization: *Terra Nova*, v. 6, p. 166-176.
- Palabora Mining Company, 1976, The geology and the economic deposits of copper, iron and vermiculite in the Palabora Igneous Complex: a brief review: *Economic Geology*, v. 71, p. 177-192.
- Palmer, D.A.S., 1994, Geology and geochemistry of the Amba Dongar carbonatite-hosted fluorite deposit, India: Unpublished M.Sc. thesis, McGill University, Montreal, 110p..

- Palmer, D.A.S., and Williams-Jones, A.E., 1998a, Fenitization associated with the Amba Dongar carbonatite complex, India: Unpublished Ph.D. thesis, McGill University, Montreal, Chapter 6.**
- Palmer, D.A.S., and Williams-Jones, A.E., 1998b. Solid inclusions from the Phalaborwa complex, South Africa: evidence of silicate-carbonate immiscibility: Unpublished Ph.D. thesis, McGill University, Montreal, Chapter 7.**
- Reischmann, T., 1995, Precise U/Pb age determination with baddeleyite (ZrO₂), a case study from the Phalaborwa Igneous Complex, South Africa: S.Afr.J.Geol., v. 98, p. 1-4.**
- Samson, I.M., Weining, L., and Williams-Jones, A.E., 1995, The nature of orthomagmatic hydrothermal fluids in the Oka carbonatite, Quebec: evidence from fluid inclusions: Geochim. Cosmochim. Acta, v. 59, p. 1963-1977.**
- Van Rensburg, W.C., 1965, Copper mineralization in the carbonate members and phoscorite, Phalaborwa, South Africa: Unpublished Ph.D. thesis, University of Wisconsin, Madison.**
- Vard, E., and Williams-Jones, A., 1993, A fluid inclusion study of vug in dawsonite-altered phonolite sills, Montreal, Quebec: implications for HFSE mobility: Contrib. Mineral. Petrol., v. 113, p. 410-423.**

Chapter 9: Conclusions

Conclusions

Carbonatite magmas and their associated fluids follow diverse, and complicated, evolutionary paths before their final emplacement. Two complexes, Amba Dongar, India, and Phalaborwa, South Africa attest to this complexity through observations of solid and fluid inclusions, and fenitization of surrounding host rocks.

Solid inclusions were observed in apatite of calciocarbonatite at Amba Dongar, and comprise ankerite (mottled inclusions); calcite \pm ankerite \pm barite (multiphase inclusions); and monomineralic calcite varieties. Phase relationships observed during heating experiments indicate that the monomineralic calcite inclusions were in fact trapped solids. However, the temperatures of initial and final melting of mottled and multiphase inclusions, 610-660°C and >800°C and 680-740°C and >1100°C, respectively, as well as their consistent compositions, indicate a melt origin.

Based on the close spatial and temporal association of the mottled and multiphase inclusions, it is proposed that carbonate-carbonate liquid immiscibility occurred during ascension of carbonatite magma, with one liquid being of dominantly calciocarbonatitic composition (multiphase inclusions) and the other of ferrocarbonatitic composition (mottled inclusions). Further supporting evidence is found in the formation of small volumes of an immiscible ferrocarbonatitic liquid, within calcitic liquid, during heating of multiphase inclusions.

Solid inclusions in phoscorite- and transgressive carbonatite-hosted apatite from the Phalaborwa complex were similarly shown to represent trapped melts, however, their compositions are distinctly different from those at Amba Dongar. They consist of solid-vapour and solid-liquid-vapour varieties, in which the solids are composed of calcite and olivine. Magnetite \pm Cu-Fe-bearing sulphide are also present in phoscorite-hosted inclusions. The ratios of the volumes of olivine to calcite are variable and are approximately 1, for phoscorite-hosted inclusions, and below 0.2, for inclusions in transgressive carbonatite.

During heating of melt inclusions in phoscorite, two immiscible liquids were produced, at temperatures above 800°C, and were of silicate and carbonate compositions, respectively. Melt inclusions in transgressive carbonatite, however, produced only one

liquid, which began to form at temperatures above 550°C. This is thought to indicate that: 1) liquid immiscibility could not have been responsible for the formation of the earlier pyroxenite; 2) silicate-carbonate immiscibility only acted to remove silica from an already carbonate-rich melt; and 3) although liquid immiscibility took part in the evolution of the carbonate liquid, fractionation was the dominant process acting in the carbonatite magmas.

From melt inclusion studies, it is evident that the processes occurring in carbonatite magmas are diverse, and include silicate-carbonate and carbonate-carbonate immiscibility and fractionation. As well, these processes can work in tandem or alone to produce the relationships of carbonatites seen at surface.

Aqueous fluids in equilibrium with carbonatite and silicate magmas are important in the development of alkaline complexes, and are manifested by fenitization and trapped as fluid inclusions. A complex history of fluid evolution is recorded by fluid inclusions in apatite hosted by calciocarbonatite at the Amba Dongar complex. The first exsolved fluids were, Na- and Fe-bearing and K-rich ($\text{Na/K} < 1$), and were dominated by SO_4^{2-} and HCO_3^- anions, with minor Cl^- . CO_2 and minor CH_4 were also present as dissolved species. These fluids evolved to lower SO_4^{2-} , K, Na, Fe, CO_2 and Cl^- concentrations, and higher concentrations of HCO_3^- and Ca, and higher $f\text{O}_2$ (loss of CH_4). Na/K ratios increased to be greater than 1, in contrast to the earlier fluids. The final, most evolved, fluid, albeit having a lower salinity, was Cl-dominated and possessed an even greater Na/K ratio. Dissolved gas species fell below detection. The pressure-temperature conditions of these fluids spanned a broad range, between 1000°C and 12.5 Kb for early fluids to 300°C and 100 bars for the most evolved fluids.

In contrast to the evidence suggesting large quantities of fluids at Amba Dongar, the carbonatites of Phalaborwa were relatively dry, and primary fluid inclusions were not observed. However, solid-liquid-vapour melt inclusions were present, and can be interpreted similarly to fluid inclusions. Analyses of the aqueous phase of these melt inclusions indicate that it is a concentrated NaCl-KCl brine (≈ 22 wt.% NaCl-KCl), which also contained Mg, Fe and S, and had Na/K ratios around 1.

Fluid inclusions provide an enormous amount of information on the nature of the aqueous fluids in equilibrium with carbonatites, but cannot yet be analysed at the levels

required to determine trace element compositions. Fenitization, however, can be used to this purpose if mass changes can be quantified. At the Amba Dongar complex, the precursor to fenitization, an almost monomineralic quartz sandstone, provided an ideal medium from which to determine fluid composition based on water/rock interactions. Petrographic observations indicate that fenitization was accomplished by the removal of appreciable quantities of quartz and the addition of K and Al in the form of potassium feldspar. The mass changes reflect this alteration but also identify a number of trace elements, Ca, Ba, Fe, F, Rb, Sr, Y and REE, particularly the LREE, which were significant components in the fluid. The water-rock ratio during fenitization, based on the determination of SiO₂ loss from sandstone and the solubility of silica at the conditions of fenitization, was determined to be 722. Based on this water/rock ratio and the estimated mass changes, minimum estimates were made of the concentrations of the above elements in the fenitizing fluids. This method proved to be reasonably accurate for the REE, which are estimated to have had similar concentrations (less than one log unit difference) to those measured in modern hydrothermal waters from the Bitterroot Lobe of the Idaho Batholith, the Salton Sea and the East Pacific Rise vent field (Michard *et al.*, 1983, 1984; Michard, 1989; VanMiddlesworth, 1997).

Fenitization of country rocks surrounding the Phalaborwa complex is more complicated to evaluate due to the close proximity of the fenites to both pyroxenite and carbonatite. However, mass balance calculations involving both bulk rock and mineralogical changes, e.g., replacement of diopside by richterite and alteration of potassium feldspar, were effective in separating fenitizing events associated with emplacement of the two lithologies. Fenitizing fluids derived from pyroxenite magmas were responsible for potassic fenitization, and contained significant concentrations of K, Na, Mg, Fe, Sr and LREE. Although similar to pyroxenite-derived fluids, those associated with carbonatite had higher Na/K ratios and greater concentrations of Mg.

Although magma compositions at Amba Dongar and Phalaborwa differ appreciably, the associated aqueous fluids show little contrast. Salinities of early fluids are slightly higher for Phalaborwa carbonatites than those at Amba Dongar, however, the components that are present in significant concentrations are remarkably similar for both localities, and include Na, K, Ba, Ca, Fe, S, Sr and the REE.

A model involving early primary crystallization of bornite and subsequent hydrothermal remobilization and precipitation of chalcopyrite has been proposed for Phalaborwa. Evidence supporting the crystallization of bornite-dominated mineralization from banded carbonatite magmas can be found in the isolated, blebby, nature of the bornite, which is intimately associated with magmatic layering. The presence of copper-iron sulphide minerals in phoscorite-hosted melt inclusions also indicates that early copper-iron sulphides crystallized directly from magmas. In contrast, chalcopyrite-dominated ores in transgressive carbonatite are localized along fractures and show evidence of dolomitization of calcite surrounding the veinlets, which is suggestive of hydrothermal alteration. It is thought that the source of these aqueous fluids was the transgressive carbonatite, based on the Mg-enrichment of transgressive carbonatite-derived fluids, determined through studies of fenitization, and the observation of a, previously unreported, aqueous-fluid phase in transgressive carbonatite.

Contributions to Knowledge

The following are the most significant contributions made by this thesis:

- 1) This study is the first to propose and provide evidence that ferrocarbonatites may be the product of carbonate-carbonate liquid immiscibility.
- 2) Whereas silicate-carbonate liquid immiscibility is a mechanism that has been invoked to produce carbonatite liquids, the case is made that, at Phalaborwa, the process acted only to rid a carbonate-rich melt of unwanted silica and was not responsible for the pyroxenite-calciocarbonatite association.
- 3) The nature of the aqueous fluids in equilibrium with carbonatite melts, and their evolution, has been characterized in greater detail than in previous studies. This thesis provides the first semi-quantitative data on the compositions of the fluids.
- 4) This study is one of the few that has quantified mass changes associated with fenitization, and is one of an even smaller number that has related mass changes to fluid composition.
- 5) The thesis presents the first evidence that hydrothermal fluids were present during intrusion of carbonatite at Phalaborwa, which supports the hypothesis that hydrothermal fluids were responsible for late-stage chalcopyrite mineralization in transgressive carbonatite.
- 6) Finally, the thesis presents evidence that granite and granitic gneisses surrounding the Phalaborwa complex were fenitized by two separate fluids, one associated with pyroxenite magma and the other from carbonatite magmas.

Recommendations for Future Work

A high priority for future work is in the experimental synthesis of carbonatites in the system CaO-MgO-FeO-CO_2 . The importance of ferrocarbonatites in carbonatite complexes is well established and yet virtually nothing is known about their genesis. It is hoped that the hypothesis presented in this thesis, that ferrocarbonatites are a product of liquid immiscibility, will prompt experimentalists to investigate further the role of this mechanism in carbonatite genesis.

Carbonatite complexes are host to numerous ore deposit types, many of which are hydrothermal in origin (Mariano, 1989). Aqueous fluids exsolved from carbonatite magmas have proved to be important at Amba Dongar, India in the formation of economic fluorite deposits (Palmer, 1994) and at Phalaborwa, in producing the richest of the copper ore zones.

The methods used in this thesis for characterizing aqueous fluids and fenitization, i.e., fluid inclusion analysis and chemical mass balance, are effective and practical, and can be applied to almost all complexes. The greater understanding of fluid compositions and alteration signatures, i.e., fenitization, which would result from new studies could lead to practical exploration models for carbonatite complexes.

References

- Mariano, A.N., 1989, Nature of economic mineralization in carbonatites and related rocks: in Bell, K., ed., *Carbonatites: genesis and evolution*: London, Unwin Hyman, p. 149-176.
- Michard, A., 1989, Rare earth element systematics in hydrothermal fluids: *Geochim. Cosmochim. Acta*, v. 53, p. 745-750.
- Michard, A., Albarede, G., Michard, J.F., Minster, J.L., Charlou, J.L., and Tan, N., 1983, Rare-earth element and uranium in high temperature solutions from the East Pacific Rise hydrothermal vent field (13°N): *Nature*, v. 303, p. 795-797.
- Michard, A., Albarede, G., Michard, J.F., Minster, J.L., Charlou, J.L., and Tan, N., 1983, Chemistry of solutions from the 13°N East Pacific Rise hydrothermal site: *Earth Planet. Sci. Lett.*, v. 67, p. 297-307.
- Palmer, D.A.S., 1994, Geology and geochemistry of the Amba Dongar carbonatite-hosted fluorite deposit, India: Unpublished M.Sc. thesis, McGill University, Montreal, 110p..
- VanMiddlesworth, P.E., 1997, Determination of REE, Th and U concentrations in thermal waters of the Lochsa, Salmon and Stanley regions of the Bitterroot lobe of the Idaho Batholith: Unpublished M.Sc. Thesis, University of Idaho, Moscow, 190p..

**Appendix I: Calculation of Fluid Composition from Decrepitate Residues
and Fluid Inclusion Salinity**

Electron microprobe analyses of the residues of decrepitated fluid inclusions, used in conjunction with salinities estimated microthermometrically, provides a relatively reliable method for estimating the bulk composition of the trapped aqueous fluids. Irrespective of the chemical system, i.e., NaCl, KCl, CaCl₂, salinity estimates can be used to obtain the concentration of the chloride ion in the inclusion fluids. If the ratio of chlorine to other elements (X) can be determined, i.e., from decrepitate analyses, their concentrations can be established by the relationship:

$$[X_{\text{flinc}}] / [X_{\text{decrp}}] = [Cl_{\text{flinc}}] / [Cl_{\text{decrp}}]$$

However, this relationship can lead to spurious interpretations owing to the semi-quantitative nature of decrepitate analyses, e.g., highly variable [Cl_{decrp}] values. This can be overcome if the element in question shows a consistent relationship with Cl. The equation for this relationship can then be substituted for [Cl_{decrp}], providing a control for the concentration of elements from decrepitate analyses.

Example for Sulphur

The simplest example is one in which [Cl_{decrp}] displays a linear relationship with some other element. This occurs between S and Cl (Fig. A-1) in the LV(ap) inclusions from Amba Dongar, and is described by the equation:

$$[S_{\text{decrp}}] = -0.90 \times [Cl_{\text{decrp}}] + 54.37$$

As can be seen in Figure A-1, the linear correlation between S and Cl is quite good ($R^2 = 0.95$), and it must be stressed that only those elements which show such a close relationship can be used by this method. Equation 2 can be used to solve for Cl:

$$[Cl_{\text{decrp}}] = ([S_{\text{decrp}}] - 54.37) / -0.90$$

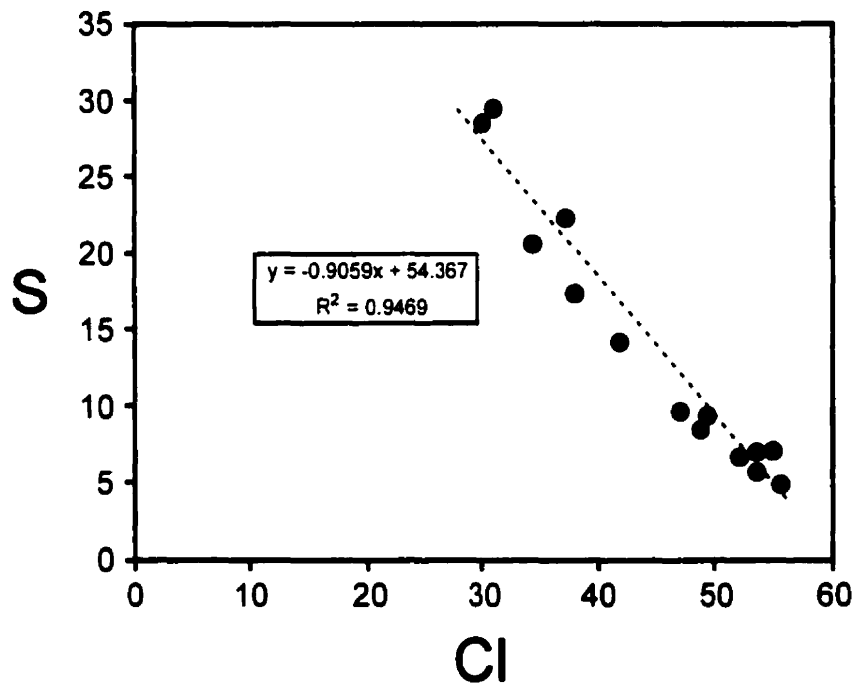


Figure A-1 Diagram showing the linear relationship between S and Cl. The equation for the regression line (dotted line), and correlation coefficient, are given (inset box).

and substituted into equation 1 to produce:

$$[S_{inc}] / [S_{decp}] = [Cl_{inc}] / ([S_{decp}] - 54.37) / -0.90$$

The average concentration of S from the decrepitate residues for LV(ap) inclusions was determined to be 12.76 cat.%, while the concentration of Cl in the inclusion fluids is 1.9m. Solving for $[S_{inc}]$ produces:

$$[S_{inc}] = 12.76 \text{ cat. \%} \times 1.9m / ((12.76 \text{ cat. \%} - 54.37 \text{ cat. \%}) / -0.90)$$

which gives a value of 0.53m for S in inclusion fluids.

**Appendix II: Melt Inclusion Microthermometric Data
(Amba Dongar, India)**

Table A2 Melt Inclusion Microthermometric Data (Amba Dongar)

Sample	Type	L+V °C	T _{melt4} °C	T _{melt3} °C	T _{melt2} °C	T _{melt1} °C
AD061	multiphase	1181		1011		640
AD061	multiphase	1132	1050	1029	873	467
AD061	multiphase	1111			955	742
AD061	multiphase	1157		1036	916	639
AD061	multiphase	1147	1061	1004	888	711
AD061	multiphase	1128		1079	907	691
AD061	multiphase	1128		1033	951	680
AD061	multiphase	1107	1073	1056	735	697
AD061	multiphase	1153	1071	1058	940	744
AD061	multiphase	1143	1089	1047	974	769
AD061	multiphase	1124			937	751
AD061	multiphase	1124		1045	899	755
AD061	multiphase	1103		1020	918	688
AD061	multiphase	1149	1093	1017	962	697
AD061	multiphase	1139	1068		946	712
AD061	multiphase	1118		1046	886	723
AD061	multiphase	1131	1072	1065	985	728
AD061	multiphase	1154			995	745
AD061	multiphase	1135		1042	957	716
AD061	multiphase	1171	1080	1044	895	708
AD061	multiphase	1114	1078	1033	881	699
AD061	multiphase	1147			974	710
AD061	multiphase	1104	1096	1031	900	685
AD061	multiphase	1117		1006	944	733
AD061	multiphase	1168	1100	1003	928	701
AD061	multiphase	1121		-14	868	701
AD061	multiphase	1157		1032	967	758
AD061	multiphase	1100		1051	977	707
AD061	mottled	>800		704	611	438
AD061	mottled	>800		787	655	438
AD061	mottled	>800		668	613	524
AD061	mottled	>800		713	611	432
AD061	mottled	>800		744	631	590
AD061	mottled	>800		753	620	582

Sample	Type	L+V °C	T _{melt4} °C	T _{melt3} °C	T _{melt2} °C	T _{melt1} °C
AD061	mottled	>800		715	641	534
AD061	mottled	>800		697	622	524
AD061	mottled	>800		708		455
AD061	mottled	>800		690	658	455
AD061	mottled	>800		690	616	541
AD061	mottled	>800		773	614	449
AD061	mottled	>800		668	634	607
AD061	mottled	>800		699	623	599
AD061	mottled	>800		697	644	551
AD061	mottled	>800		780	625	541
AD061	mottled	>800		661	3	472
AD061	mottled	>800		684	622	575
AD061	mottled	>800		767	620	483
AD061	mottled	>800		660	640	641
AD061	mottled	>800		693	629	633
AD061	mottled	>800		724	650	585
AD061	mottled	>800		733	631	575
AD061	mottled	>800		682	9	506
AD061	mottled	>800		664		506
AD061	mottled	>800		664	625	592
AD061	mottled	>800		747	623	500
AD061	mottled	>800		677	647	568
AD061	mottled	>800		760	628	558
AD061	mottled	>800		655	6	489
AD061	mottled	>800		686	664	489
AD061	mottled	>800		706	661	472
AD061	mottled	>800		737	619	558
AD061	mottled	>800		746	617	466
AD061	mottled	>800		695	637	624
AD061	mottled	>800		677	626	616

L - Liquid; V - Vapour; T_{melt} - temperature of melting

**Appendix III: Fluid Inclusion Microthermometric Data
(Amba Dongar, India)**

Table A3 Fluid Inclusion Data (Ambe Donger)

Sample	Host	Type	T _{diss} °C	T _{diss} °C	T _{diss} °C	T _{diss} °C	T _{h_{mean}} °C	T _e °C	T _{mice} °C	T _{co-mice} °C
AD061	apette	LVS				>520	271.8	>-27	-4.9	
AD061	apette	LVS				>520	273.6	>-27	-3.3	
AD061	apette	LVS					274	>-27	-6.1	
AD061	apette	LVS				>520	275.5	>-27	-6	-59.1
AD061	apette	LVS				>520	276.8	>-27	-2.9	-56.7
AD061	apette	LVS				>520	280.3	>-27	-7.9	
AD061	apette	LVS				>520	281	>-27	-3.1	
AD061	apette	LVS				>520	281.4	>-27	-7.8	
AD061	apette	LVS				>520	281.6	>-27	-4.5	
AD061	apette	LVS					283.8	>-27	-4.7	-58.2
AD061	apette	LVS				>520	284.1	>-27	-8.1	-57.3
AD061	apette	LVS				>520	284.5	>-27	-7	-58.2
AD061	apette	LVS				>520	287.6	>-27	-9.5	
AD061	apette	LVS				>520	288.2	>-27	-2.6	
AD061	apette	LVS				>520	289.6	>-27	-6.8	
AD061	apette	LVS				>520	290.7	>-27	-4.5	
AD061	apette	LVS				>520	292.7	>-27	-4.6	
AD061	apette	LVS				>520	292.7	>-27	-7.5	
AD061	apette	LVS				>520	296.2	>-27	-4.7	-58.5
AD061	apette	LVS				>520	296.7	>-27	-7.3	-57
AD061	apette	LVS				489.9	297.2	>-27	-5.2	-57
AD061	apette	LVS				>520	297.5	>-27	-4.9	-57
AD061	apette	LVS				511.3	297.6	>-27	-6.7	
AD061	apette	LVS				>520	299	>-27	-5.2	-56.7
AD061	apette	LVS				>520	300.2	>-27	-4.3	
AD061	apette	LVS				496.7	301.2	>-27	-4.6	
AD061	apette	LVS				>520	301.5	>-27	-3.5	
AD061	apette	LVS				>520	302	>-27	-8.1	
AD061	apette	LVS				>520	302.5	>-27	-4.8	-57
AD061	apette	LVS				>520	306.4	>-27	-7	
AD061	apette	LVS				>520	306	>-27	-9	
AD061	apette	LVS				>520	307.6	>-27	-6.8	
AD061	apette	LVS				>520	308.7	>-27	-8.2	
AD061	apette	LVS				>520	310	>-27	-7.3	-58.8
AD061	apette	LVS				>520	311.5	>-27	-9.7	
AD061	apette	LVS				>520	311.8	>-27	-8.4	
AD061	apette	LVS				>520	313.5	>-27	-7	
AD061	apette	LVS				>520	314.6	>-27	-6.5	-56.7
AD061	apette	LVS				>520	314.8	>-27	-9.4	-57
AD061	apette	LVS				>520	316.8	>-27	-7	
AD061	apette	LVS				>520	321.6	>-27	-7.1	-58.8
AD061	apette	LVS				>520	321.8	>-27	-7.7	
AD061	apette	LVS				>520	324.5	>-27	-8	
AD061	apette	LVS				>520	327.6	>-27	-9.2	
AD061	apette	LVS				>520	327.9	>-27	-8.4	-58.2
AD061	apette	LVS				>520	331.8	>-27	-3.1	
AD061	apette	LVS				519.7	332.7	>-27	-9.4	
AD061	apette	LVS				>520	336.1	>-27	-8	
AD061	apette	LVS				>520	336.6	>-27	-6.7	-58.8
AD061	apette	LVS				>520	341.2	>-27	-9.7	
AD061	apette	LVS				>520	451.7	>-27	-7.3	
AD061	apette	LVS				>520	462.8	>-27	-6.7	-59.1
AD061	apette	LVS				>520	474.1	>-27	-8.1	
AD061	apette	LVS				>520	483.2	>-27	-7.1	
AD061	apette	LVS				>520	487	>-27	-8.3	
AD061	apette	LVS				>520	487.4	>-27	-6.8	-57.3
AD061	apette	LVS			434	156	283.4	>-27	-4.9	
AD061	apette	LVS			412	170	285.2	>-27	-3.9	
AD061	apette	LVS			423	178	287.1	>-27	-6	
AD061	apette	LVS			442	183	288.4	>-27	-3.8	
AD061	apette	LVS			411	169	288.6	>-27	-6.1	
AD061	apette	LVS			435	180	289	>-27	-8	
AD061	apette	LVS			420	202	292.1	>-27	-4.7	
AD061	apette	LVS			409	161	295.2	>-27	-7.6	
AD061	apette	LVS			478	153	296.7	>-27	-8.6	
AD061	apette	LVS			436	157	296.9	>-27	-5.1	
AD061	apette	LVS			426	177	297.2	>-27	-5.4	
AD061	apette	LVS					298	>-27	-7.1	
AD061	apette	LVS			433	154	298.3	>-27	-7.7	
AD061	apette	LVS			437	160	298.9	>-27	-5.9	
AD061	apette	LVS			407	190	300.3	>-27	-6.1	
AD061	apette	LVS			432	166	300.4	>-27	-8.5	
AD061	apette	LVS			416	199	306.6	>-27	-8.1	
AD061	apette	LVS			413	164	309.1	>-27	-9	
AD061	apette	LVS			406	214	309.2	>-27	-7.8	
AD061	apette	LVS			424	165	309.6	>-27	-5	
AD061	apette	LVS			438	198	310.1	>-27	-8.5	

L - Liquid; V - Vapour; S - Solid; T_{diss} - Temperature of dissolution; T_h - temperature of homogenization;
T_e - Eutectic temperature; T_{mice} - temperature of final ice melting

Sample	Host	Type	T _{diss} °C	T _{diss} °C	T _{diss} °C	T _{diss} °C	T _{h_{hom}} °C	T _e °C	T _{mce} °C	T _{co-mce} °C
AD061	apette	LVS				481	163	311.6	>-27	-5.1
AD061	apette	LVS				425	196	311.9	>-27	-7.9
AD061	apette	LVS				439	155	312.8	>-27	-8.9
AD061	apette	LVS				440	192	313	>-27	-9
AD061	apette	LVS				408	167	317.6	>-27	-7.5
AD061	apette	LVS				466	158	319.1	>-27	-8.2
AD061	apette	LVS				441	209	319.4	>-27	-9.2
AD061	apette	LVS						320	>-27	-7.4
AD061	apette	LVS						321.3	>-27	-6.4
AD061	apette	LVS				453	197	322.2	>-27	-11.2
AD061	apette	LVS				429	194	326.4	>-27	-9.7
AD061	apette	LVS				444	193	329.2	>-27	-9.4
AD061	apette	LVS					>521	331	>-27	-8.7
AD061	apette	LVS				473	176	331.1	>-27	-10.5
AD061	apette	LVS				428	207	332.1	>-27	-10.7
AD061	apette	LVS				447	173	333.2	>-27	-9.9
AD061	apette	LVS				450	195	335	>-27	-11
AD061	apette	LVS				443	191	336.2	>-27	-11.3
AD061	apette	LVS						337	>-27	-5.3
AD061	apette	LVS						340	>-27	-11.8
AD061	apette	LVS				462	213	340.3	>-27	-9.4
AD061	apette	LVS				471	206	344.2	>-27	-10.9
AD061	apette	LVS						346.8	>-27	-8.4
AD061	apette	LVS				410		556.7	>-27	-9.5
AD061	apette	LVS				479	444	571.3	>-27	-11.1
AD061	apette	LVS				464		576.2	>-27	-10.6
AD061	apette	LVS				406.4	210	579.9	>-27	-3.5
AD061	apette	LVS						584	>-27	-7.3
AD061	apette	LVS						583.3	>-27	-10
AD061	apette	LVS				449	181	583.7	>-27	-10.8
AD061	apette	LVS								-59.1
AD061	apette	LVS								-62.3
AD061	apette	LVS		253	200.5	150				
AD061	apette	LVMS		422	222	151	384	>-27	-6.7	
AD061	apette	LVMS	480		121	417	390	>-27	-5.5	-58
AD061	apette	LVMS		441	258	142	398	>-27	-8.4	
AD061	apette	LVMS		436	232	129	399	>-27	-5.5	
AD061	apette	LVMS	453	345	344	141	420	>-27	-8.2	
AD061	apette	LVMS	451	341	244	133	440	>-27	-5.7	
AD061	apette	LVMS		447	350	136	452	>-27	-6.9	
AD061	apette	LVMS		431	346	146	457	>-27	-5.8	
AD061	apette	LVMS	442	364	218	162	459	>-27	-5.9	
AD061	apette	LVMS	454	353	253	158	464	>-27	-6.9	
AD061	apette	LVMS	428	363	229	143	472	>-27	-4.7	
AD061	apette	LVMS		434	221	140	479	>-27	-6.1	
AD061	apette	LVMS	475	361	238	128	481	>-27	-5.1	
AD061	apette	LVMS	458	418	343	121	506	>-27	-4.3	
AD061	apette	LVMS	487	340	219	120	521	>-27	-6	
AD061	apette	LVMS		485	234	174	523	>-27	-9.1	
AD061	apette	LVMS		430	349	144	527	>-27	-4.8	
AD061	apette	LVMS		435	348	124	528	>-27	-5.2	
AD061	apette	LVMS		463	239	130	530	>-27	-7	
AD061	apette	LVMS	474	362	228	123	533	>-27	-4.9	
AD061	apette	LVMS	427	347	284	163	545	>-27	-7.2	
AD061	apette	LVMS		ddss	444	177	547.2	>-27	-7	-57.6
AD061	apette	LVMS		469	357	164	551	>-27	-7.1	
AD061	apette	LVMS		471	263	134	552	>-27	-8.4	
AD061	apette	LVMS		477	252	163	554	>-27	-8.6	
AD061	apette	LVMS		443	265	160	560	>-27	-7.7	
AD061	apette	LVMS	478	360	248	137	564	>-27	-8.9	
AD061	apette	LVMS		448	354	154	568	>-27	-7.5	
AD061	apette	LVMS		480	358	178	569	>-27	-9.4	
AD061	apette	LVMS		460	245	159	577	>-27	-7.9	
AD061	apette	LVMS		432	231	165	585	>-27	-4.4	
AD061	apette	LVMS		439	355	127	587	>-27	-5	
AD061	apette	LVMS		446	255	147	588	>-27	-7	
AD061	apette	LVMS		470	356	175	591	>-27	-8.9	
AD061	apette	LVMS		466	261	168	595	>-27	-8	
AD061	apette	LVMS	488	342	249	172	600	>-27	-9.3	
AD061	apette	LVMS	462	351	235	170	606	>-27	-8	
AD061	apette	LVMS		465	352	150	614	>-27	-7.9	
AD061	apette	LVMS		456	246	149	628	>-27	-9.4	
AD061	apette	LVMS	ddss	438	357	151	>553	>-27		
AD061	apette	LVMS	668	476.5ppt	266	218	>668	>-27		
AD001	apette	LV					247.9	>-27	-4.2	
AD001	apette	LV					274	>-27	-4.2	
AD001	apette	LV					254.6	>-27	-4.3	

L - Liquid; V - Vapour; S - Solid; T_{diss} - Temperature of dissolution; T_h - temperature of homogenization;
T_e - Ejectic temperature; T_{mce} - temperature of final ice melting

Sample	Host	Type	T _{dss} °C	T _{dss} °C	T _{dss} °C	T _{dss} °C	T _{h_{mean}} °C	T _e °C	T _{mce} °C	T _{co,mce} °C
AD001	spette	LV					268.3	>-27	-4.3	
AD001	spette	LV					249.3	>-27	-4.4	
AD001	spette	LV					260.6	>-27	-4.4	
AD001	spette	LV					273.4	>-27	-4.6	
AD001	spette	LV					253.6	>-27	-4.7	
AD001	spette	LV					261.8	>-27	-4.8	
AD001	spette	LV					274.5	>-27	-4.9	
AD001	spette	LV					276.8	>-27	-4.9	
AD001	spette	LV					262.3	>-27	-5	
AD001	spette	LV					266.3	>-27	-5	
AD001	spette	LV					272.5	>-27	-5.1	
AD001	spette	LV					287.1	>-27	-5.1	
AD001	spette	LV					266.7	>-27	-5.2	
AD001	spette	LV					286.9	>-27	-5.2	
AD001	spette	LV					295.6	>-27	-5.2	
AD001	spette	LV					269.4	>-27	-5.3	
AD001	spette	LV					279.6	>-27	-5.3	
AD001	spette	LV					305.7	>-27	-5.3	
AD001	spette	LV					242.8	>-27	-5.4	
AD001	spette	LV					284.2	>-27	-5.5	
AD001	spette	LV					262.9	>-27	-5.6	
AD001	spette	LV					298.2	>-27	-5.6	
AD001	spette	LV					258.8	>-27	-5.7	
AD001	spette	LV					276.6	>-27	-5.8	
AD001	spette	LV					279.5	>-27	-5.8	
AD001	spette	LV					260.9	>-27	-6.1	
AD001	spette	LV					289.6	>-27	-6.2	
AD001	spette	LV					296.7	>-27	-6.2	
AD001	spette	LV					287.3	>-27	-6.3	
AD001	spette	LV					306.7	>-27	-6.3	
AD001	spette	LV					304.3	>-27	-6.4	
AD001	spette	LV					291.4	>-27	-6.5	
AD001	spette	LV					306.2	>-27	-6.6	
AD001	spette	LV					292.4	>-27	-6.9	
AD001	spette	LV					305.6	>-27	-7.1	
AD001	spette	LV					299.1	>-27	-7.3	
AD002	spette	LV					298.9	>-27	-5.3	
AD002	spette	LV					323.2	>-27	-5.5	
AD002	spette	LV					313.4	>-27	-5.8	
AD002	spette	LV					312.6	>-27	-6.1	
AD002	spette	LV					316.7	>-27	-6.1	
AD002	spette	LV					319.2	>-27	-6.1	
AD002	spette	LV					308.8	>-27	-6.2	
AD002	spette	LV					314.3	>-27	-6.2	
AD002	spette	LV					294.1	>-27	-6.3	
AD002	spette	LV					302.5	>-27	-6.3	
AD002	spette	LV					303.1	>-27	-6.4	
AD002	spette	LV					311.7	>-27	-6.4	
AD002	spette	LV					303.6	>-27	-6.5	
AD002	spette	LV					302.4	>-27	-6.7	
AD002	spette	LV					323.3	>-27	-7	
AD002	spette	LV					323.6	>-27	-7.1	
AD002	spette	LV					331.7	>-27	-7.2	
AD002	spette	LV					312.9	>-27	-7.3	
AD002	spette	LV					313.8	>-27	-7.3	
AD002	spette	LV					332	>-27	-7.8	
AD002	spette	LV					319.8	>-27	-7.9	
AD002	spette	LV					341.9	>-27	-7.9	
AD002	spette	LV					327.7	>-27	-8	
AD002	spette	LV					333.8	>-27	-8.1	
AD002	spette	LV					325.5	>-27	-8.2	
AD002	spette	LV					338.2	>-27	-8.2	
AD003	spette	LV					149.3	>-27	-3.2	
AD003	spette	LV					154.9	>-27	-3.3	
AD003	spette	LV					166.2	>-27	-3.4	
AD003	spette	LV					185.4	>-27	-3.6	
AD003	spette	LV					165	>-27	-3.7	
AD003	spette	LV					175.9	>-27	-3.8	
AD003	spette	LV					156	>-27	-3.9	
AD003	spette	LV					193.6	>-27	-3.9	
AD003	spette	LV					194.8	>-27	-3.9	
AD003	spette	LV					188.2	>-27	-4.1	
AD003	spette	LV					195.6	>-27	-4.1	
AD003	spette	LV					202.7	>-27	-4.2	
AD003	spette	LV					166.1	>-27	-4.3	
AD003	spette	LV					177.1	>-27	-4.3	
AD003	spette	LV					193.5	>-27	-4.5	
AD003	spette	LV					194	>-27	-4.5	
AD003	spette	LV					193.5	>-27	-4.7	
AD003	spette	LV					196.4	>-27	-5	
AD003	spette	LV					207.3	>-27	-5.2	

L - Liquid; V - Vapour; S - Solid; T_{dss} - Temperature of dissolution; T_h - temperature of homogenization;
T_e - Eutectic temperature; T_{mce} - temperature of final ice melting

Sample	Host	Type	T _{dss} °C	T _{dss} °C	T _{dss} °C	T _{dss} °C	T _{hom} °C	T _e °C	T _{mice} °C	T _{co-mice} °C
AD061	spette	LV					232.8	>-27	-5.2	
AD061	spette	LV					236.5	>-27	-5.2	
AD061	spette	LV					237.9	>-27	-4	
AD061	spette	LV					237.9	>-27	-5	
AD061	spette	LV					239.3	>-27	-4.2	
AD061	spette	LV					241.8	>-27	-4.3	
AD061	spette	LV					244.6	>-27	-4.1	
AD061	spette	LV					243.6	>-27	-4.5	
AD061	spette	LV					245.7	>-27	-4	
AD061	spette	LV					246.1	>-27	-4.4	
AD061	spette	LV					248.6	>-27	-4.1	
AD061	spette	LV					248.8	>-27	-5.5	
AD061	spette	LV					249.4	>-27	-4.1	
AD061	spette	LV					250.6	>-27	-4.2	
AD061	spette	LV					250.7	>-27	-5.6	
AD061	spette	LV					250.9	>-27	-5.9	
AD061	spette	LV					251.8	>-27	-4.6	
AD061	spette	LV					252.3	>-27	-4.8	
AD061	spette	LV					252.4	>-27	-4.5	
AD061	spette	LV					252.9	>-27	-5.4	
AD061	spette	LV					253.5	>-27	-4.8	
AD061	spette	LV					254.2	>-27	-5.3	
AD061	spette	LV					254.2	>-27	-4.6	
AD061	spette	LV					256.3	>-27	-4.8	
AD061	spette	LV					256.7	>-27	-5	
AD061	spette	LV					257.6	>-27	-4	
AD061	spette	LV					256.3	>-27	-4.1	
AD061	spette	LV					259.4	>-27	-5.1	
AD061	spette	LV					259.7	>-27	-5.1	
AD061	spette	LV					262.5	>-27	-4.9	
AD061	spette	LV					263.4	>-27	-4.4	
AD061	spette	LV					263.9	>-27	-5.6	
AD061	spette	LV					264	>-27	-4	
AD061	spette	LV					264.5	>-27	-4.7	
AD061	spette	LV					264.8	>-27	-5.7	
AD061	spette	LV					266.6	>-27	-5.5	
AD061	spette	LV					266.8	>-27	-4.5	
AD061	spette	LV					268.1	>-27	-4.7	
AD061	spette	LV					269.5	>-27	-5.4	
AD061	spette	LV					269.6	>-27	-4.9	
AD061	spette	LV					272			
AD061	spette	LV					272.8			
AD061	spette	LV					273.5	>-27	-6	
AD061	spette	LV					276.9	>-27	-4.8	
Adglob	spette	LV					280	>-27	-6.1	
Adglob	spette	LV					281.1	>-27	-6	
Adglob	spette	LV					284.8	>-27	-5.1	
Adglob	spette	LV					286.7	>-27	-6.4	
Adglob	spette	LV					285.9	>-27	-5.3	
Adglob	spette	LV					288.3	>-27	-6.5	
Adglob	spette	LV					288.4	>-27	-6.1	
Adglob	spette	LV					289	>-27	-6.2	
Adglob	spette	LV					289.5	>-27	-6.3	
Adglob	spette	LV					291.4	>-27	-6.3	
Adglob	spette	LV					291.2	>-27	-5.7	
Adglob	spette	LV					293.3	>-27	-6.1	
Adglob	spette	LV					293.8	>-27	-5.2	
Adglob	spette	LV					294.7	>-27	-6	
Adglob	spette	LV					296.7	>-27	-5.6	
Adglob	spette	LV					297.6	>-27	-6.2	
Adglob	spette	LV					298.8	>-27	-7.1	
Adglob	spette	LV					298.5	>-27	-5.9	
Adglob	spette	LV					299.1	>-27	-7.3	
Adglob	spette	LV					299.3	>-27	-5.6	
Adglob	spette	LV					299.7	>-27	-7.1	
Adglob	spette	LV					300.2	>-27	-5.9	
Adglob	spette	LV					302.6	>-27	-5.8	
Adglob	spette	LV					302.7	>-27	-7	
Adglob	spette	LV					304.6	>-27	-5.8	
Adglob	spette	LV					304.8	>-27	-7.3	
Adglob	spette	LV					305.7	>-27	-7.6	
Adglob	spette	LV					305.1	>-27	-6.8	
Adglob	spette	LV					308.4	>-27	-6.8	
Adglob	spette	LV					309.1	>-27	-5.2	
Adglob	spette	LV					309.2	>-27	-6.7	
Adglob	spette	LV					309.5	>-27	-6.8	
Adglob	spette	LV					311.4	>-27	-7.9	
Adglob	spette	LV					313.6	>-27	-7.7	
Adglob	spette	LV					315.4	>-27	-7.5	
Adglob	spette	LV					315.8	>-27	-7.8	
Adglob	spette	LV					317.6	>-27	-6.9	
Adglob	spette	LV					317.9	>-27	-7.5	
Adglob	spette	LV					319.5			
Adglob	spette	LV					319.7	>-27	-7.8	
Adglob	spette	LV					322.6	>-27	-6.9	
Adglob	spette	LV					323			
Adglob	spette	LV					323.5	>-27	-7.2	
Adglob	spette	LV					324.1	>-27	-7.9	

L - Liquid; V - Vapour; S - Solid; T_{dss} - Temperature of dissolution; T_h - temperature of homogenization;
T_e - Ejectic temperature; T_{mice} - temperature of final ice melting

Sample	Host	Type	T _{dss} °C	T _{dss} °C	T _{dss} °C	T _{dss} °C	T _{hom} °C	T _e °C	T _{mce} °C	T _{co-mce} °C
AD021	spette	LV					186	>-27	-5.4	
AD021	spette	LV					185.9	>-27	-4.9	
AD021	spette	LV					186.2	>-27	-4.9	
AD021	spette	LV					192.5	>-27	-4.9	
AD021	spette	LV					170.8	>-27	-4.7	
AD021	spette	LV					188.6	>-27	-4.7	
AD021	spette	LV					185.3	>-27	-4.6	
AD021	spette	LV					152.3	>-27	-4.5	
AD021	spette	LV					179.5	>-27	-4.5	
AD021	spette	LV					180	>-27	-4.5	
AD021	spette	LV					181	>-27	-4.5	
AD021	spette	LV					159.1	>-27	-4.4	
AD021	spette	LV					168.2	>-27	-4.4	
AD021	spette	LV					175.3	>-27	-4.4	
AD021	spette	LV					149	>-27	-4.3	
AD021	spette	LV					188.5	>-27	-4.3	
AD021	spette	LV					145.9	>-27	-4.2	
AD021	spette	LV					159.1	>-27	-4.1	
AD021	spette	LV					165.1	>-27	-4.1	
AD021	spette	LV					179.2	>-27	-4.1	
AD021	spette	LV					181.6	>-27	-4.1	
AD021	spette	LV					188.7	>-27	-4.1	
AD021	spette	LV					157.3	>-27	-4	
AD021	spette	LV					161.8	>-27	-4	
AD021	spette	LV					160.7	>-27	-4	
AD021	spette	LV					179.6	>-27	-3.9	
AD021	spette	LV					184.7	>-27	-3.9	
AD021	spette	LV					158	>-27	-3.8	
AD021	spette	LV					170.9	>-27	-3.8	
AD021	spette	LV					147.9	>-27	-3.7	
AD021	spette	LV					179.5	>-27	-3.7	
AD021	spette	LV					142.3	>-27	-3.6	
AD021	spette	LV					188.9	>-27	-3.6	
AD021	spette	LV					176.4	>-27	-3.6	
AD021	spette	LV					161.2	>-27	-3.5	
AD021	spette	LV					195.8	>-27	-3.5	
AD021	spette	LV					155.4	>-27	-3.4	
AD021	spette	LV					156.3	>-27	-3.3	
AD021	spette	LV					144.6	>-27	-3.1	
AD021	spette	LV					148.5	>-27	-2.6	
AD021	spette	LV					156.8	>-27	-2.4	
AD021	spette	LV					150.1	>-27	-2.2	
AD021	spette	LV					145.7	>-27	-2.1	
AD021	spette	LV					169.4			
AD005	quartz	LV					140	>-23	-2	
AD005	quartz	LV					140	>-23	-3.2	
AD005	quartz	LV					141.6	>-23	-2.2	
AD005	quartz	LV					141.9	>-23	-3	
AD005	quartz	LV					142.6	>-23	-2.4	
AD005	quartz	LV					142.6	>-23	-3.4	
AD005	quartz	LV					143.1	>-23	-3.1	
AD005	quartz	LV					143.8	>-23	-2.4	
AD005	quartz	LV					144.6	>-23	-3.1	
AD005	quartz	LV					145.1	>-23	-2.9	
AD005	quartz	LV					145.7	>-23	-2.3	
AD005	quartz	LV					147.5	>-23	-3.8	
AD005	quartz	LV					147.9	>-23	-3.3	
AD005	quartz	LV					148.1	>-23	-3.8	
AD005	quartz	LV					149	>-23	-2.1	
AD005	quartz	LV					149.1	>-23	-3.2	
AD005	quartz	LV					149.6	>-23	-2.7	
AD005	quartz	LV					150	>-23	-3.4	
AD005	quartz	LV					150	>-23	-3.7	
AD005	quartz	LV					151.9	>-23	-3.7	
AD005	quartz	LV					153.2	>-23	-2.3	
AD005	quartz	LV					153.7	>-23	-3	
AD005	quartz	LV					153.9	>-23	-2.9	
AD005	quartz	LV					154	>-23	-3.6	
AD005	quartz	LV					154.1	>-23	-3.5	
AD005	quartz	LV					154.6	>-23	-2	
AD005	quartz	LV					155.8	>-23	-3.9	
AD005	quartz	LV					156.8	>-23	-2.7	
AD005	quartz	LV					156.9	>-23	-2.3	
AD005	quartz	LV					157	>-23	-3.3	
AD005	quartz	LV					157.4	>-23	-2.8	
AD005	quartz	LV					157.3	>-23	-3.9	
AD005	quartz	LV					157.9	>-23	-4	
AD005	quartz	LV					158.1	>-23	-3.5	
AD005	quartz	LV					158.4	>-23	-3.6	
AD005	quartz	LV					159.1	>-23	-4.1	
AD005	quartz	LV					158.6	>-23	-2.4	
AD005	quartz	LV					158.8	>-23	-4	
AD005	quartz	LV					158.8	>-23	-3.6	
AD005	quartz	LV					161.1	>-23	-2.2	
AD005	quartz	LV					161.2	>-23	-4.2	
AD005	quartz	LV					162.4	>-23	-3.7	
AD005	quartz	LV					162.8	>-23	-3.9	
AD005	quartz	LV					162.9	>-23	-2.1	

L - Liquid; V - Vapour; S - Solid; T_{dss} - Temperature of dissolution; T_h - temperature of homogenization;
T_e - Eutectic temperature; T_{mce} - temperature of final ice melting

Sample	Host	Type	T _{diss} °C	T _{diss} °C	T _{diss} °C	T _{diss} °C	T _{h_{hom}} °C	T _e °C	T _{mce} °C	T _{coymce} °C
AD047	quartz	LV					180	>-23	-2.9	
AD047	quartz	LV					180.1	>-23	-4.2	
AD047	quartz	LV					184.3	>-23	-3.4	
AD047	quartz	LV					185.6	>-23	-4.3	
AD047	quartz	LV					187.9	>-23	-3.2	
AD047	quartz	LV					188.2	>-23	-3.1	
AD047	quartz	LV					188.5	>-23	-3.7	
AD047	quartz	LV					188.9	>-23	-3.2	
AD047	quartz	LV					189.4	>-23	-4.4	
AD047	quartz	LV					191.3	>-23	-3.6	
AD047	quartz	LV					194.3	>-23	-4.7	
AD047	quartz	LV					194.5	>-23	-2	
AD047	quartz	LV					194.6	>-23	-3.1	
AD047	quartz	LV					197	>-23	-3.5	
AD047	quartz	LV					197.1			
AD047	quartz	LV					198.3	>-23	-4.6	
AD047	quartz	LV					198.6	>-23	-3.6	
AD047	quartz	LV					198.7	>-23	-3.3	
AD047	quartz	LV					199	>-23	-4.1	
AD047	quartz	LV					199.1	>-23	-2	
AD047	quartz	LV					199.1	>-23	-3.5	
AD047	quartz	LV					200.4	>-23	-4.2	
AD047	quartz	LV					202.3	>-23	-3.9	
AD047	quartz	LV					205.9	>-23	-4	
AD047	quartz	LV					205.9	>-23	-4.2	
AD047	quartz	LV					207	>-23	-4.6	
AD047	quartz	LV					207.8	>-23	-4	
AD047	quartz	LV					208.1	>-23	-4.7	
AD047	quartz	LV					208.7	>-23	-4.6	
AD047	quartz	LV					211	>-23	-3	
AD047	quartz	LV					211.1	>-23	-4.2	
AD047	quartz	LV					214.6	>-23	-4.6	
AD047	quartz	LV					214.9	>-23	-4.4	
AD047	quartz	LV					215.1	>-23	-3.4	
AD047	quartz	LV					216.9	>-23	-3.5	
AD047	quartz	LV					216.7	>-23	-4	
AD047	quartz	LV					217.5	>-23	-4.3	
AD047	quartz	LV					217.6	>-23	-3.8	
AD047	quartz	LV					218.1	>-23	-4.1	
AD047	quartz	LV					218	>-23	-3.6	
AD047	quartz	LV					218.5	>-23	-2.3	
AD047	quartz	LV					219.3	>-23	-4.7	
AD047	quartz	LV					219.9	>-23	-4.6	
AD047	quartz	LV					223.6	>-23	-2.3	
AD047	K-Feld	LV					183.2	>-23	-4.1	
AD047	K-Feld	LV					184.4	>-23	-4	
AD047	K-Feld	LV					185.5	>-23	-3.1	
AD047	K-Feld	LV					185.8	>-23	-3.4	
AD047	K-Feld	LV					186.3	>-23	-3.5	
AD047	K-Feld	LV					190	>-23	-4.2	
AD047	K-Feld	LV					190.1	>-23	-3.1	
AD047	K-Feld	LV					192.6	>-23	-4	
AD047	K-Feld	LV					192.5	>-23		
AD047	K-Feld	LV					195.9	>-23	-3.6	
AD047	K-Feld	LV					196.7	>-23	-3.1	
AD047	K-Feld	LV					197.1	>-23	-4.3	
AD047	K-Feld	LV					198	>-23	-4.1	
AD047	K-Feld	LV					198.2	>-23	-4.4	
AD047	K-Feld	LV					199.7	>-23		
AD047	K-Feld	LV					199.7	>-23	-4.7	
AD047	K-Feld	LV					201.1	>-23	-4.2	
AD047	K-Feld	LV					201.3	>-23	-3.3	
AD047	K-Feld	LV					203.7	>-23		
AD047	K-Feld	LV					204.1	>-23	-4.6	
AD047	K-Feld	LV					204.8	>-23		
AD047	K-Feld	LV					205.5	>-23	-3.6	
AD047	K-Feld	LV					208.4	>-23	-3.2	
AD047	K-Feld	LV					206.3	>-23		
AD047	K-Feld	LV					209.1	>-23	-3.7	
AD047	K-Feld	LV					208.8	>-23	-4.6	
AD047	K-Feld	LV					211.9	>-23	-4.9	
AD047	K-Feld	LV					213.5	>-23	-4.6	
AD047	K-Feld	LV					214	>-23	-4.9	
AD047	K-Feld	LV					218.1	>-23	-3.5	
AD047	K-Feld	LV					224.6	>-23	-3.9	
AD047	K-Feld	LV					227.5	>-23	-4.4	
AD049	quartz	LV					142.6	>-23	-2.4	
AD049	quartz	LV					143.2	>-23	-2.2	
AD049	quartz	LV					143.9	>-23	-1.2	
AD049	quartz	LV					144.9	>-23	-3.5	
AD049	quartz	LV					145.2	>-23	-1	
AD049	quartz	LV					145.6	>-23	-2.1	
AD049	quartz	LV					147.9	>-23	-2.3	
AD049	quartz	LV					148.3	>-23	-1.3	
AD049	quartz	LV					148.6	>-23	-3.4	
AD049	quartz	LV					149	>-23	-2	
AD049	quartz	LV					149.5	>-23	-1.9	

L - Liquid; V - Vapour; S - Solid; T_{diss} - Temperature of dissolution; T_h - temperature of homogenization; T_e - Eutectic temperature; T_{mce} - temperature of final ice melting

Sample	Host	Type	T _{dss} °C	T _{dss} °C	T _{dss} °C	T _{dss} °C	T _{hom} °C	T _e °C	T _{mce} °C	T _{co-mce} °C
AD049	quartz	LV					149.9	>-23	-2.6	
AD049	quartz	LV					153.6	>-23	-2.1	
AD049	quartz	LV					154.1	>-23	-1.6	
AD049	quartz	LV					154.7	>-23	-2	
AD049	quartz	LV					156.1	>-23	-3	
AD049	quartz	LV					156.9	>-23	-3.1	
AD049	quartz	LV					157.4	>-23	-1.5	
AD049	quartz	LV					159.2	>-23	-3.2	
AD049	quartz	LV					160.1	>-23	-2.4	
AD049	quartz	LV					162.5	>-23	-3.1	
AD049	quartz	LV					162.6	>-23	-2.7	
AD049	quartz	LV					164.8	>-23	-2.5	
AD049	quartz	LV					165.8	>-23	-3	
AD049	quartz	LV					166.3	>-23	-2	
AD049	quartz	LV					166.4	>-23	-3.3	
AD049	quartz	LV					167.5	>-23	-2.9	
AD049	quartz	LV					168.2	>-23	-2.1	
AD049	quartz	LV					168.6	>-23		
AD049	quartz	LV					169	>-23	-1.8	
AD049	quartz	LV					169.1	>-23		
AD049	quartz	LV					169.1	>-23	-1.8	
AD049	quartz	LV					169.6	>-23	-2.3	
AD049	quartz	LV					170.8	>-23	-3.3	
AD049	quartz	LV					171.1	>-23	-3.6	
AD049	quartz	LV					171.5	>-23		
AD049	quartz	LV					171.6	>-23	-3.9	
AD049	quartz	LV					175.3	>-23	-2.5	
AD049	quartz	LV					175.8	>-23	-3.8	
AD049	quartz	LV					176	>-23	-2.2	
AD049	quartz	LV					176.1	>-23	-2.3	
AD049	quartz	LV					177.7	>-23	-3.7	
AD049	quartz	LV					182.5	>-23	-3	
AD049	quartz	LV					183.5			
AD031	quartz	LV					122.3	>-23	-0.8	
AD031	quartz	LV					124.5	>-23	-1.3	
AD031	quartz	LV					126.8	>-23	-2.3	
AD031	quartz	LV					127.1	>-23	-0.7	
AD031	quartz	LV					127.4	>-23	-2.1	
AD031	quartz	LV					128.8	>-23	-1.2	
AD031	quartz	LV					129	>-23	-1.3	
AD031	quartz	LV					131	>-23	-1	
AD031	quartz	LV					131.1	>-23	-0.9	
AD031	quartz	LV					133.9	>-23	-1.1	
AD031	quartz	LV					134.2	>-23	-2.4	
AD031	quartz	LV					134.9	>-23	-0.9	
AD031	quartz	LV					135.5	>-23	-2.7	
AD031	quartz	LV					135.6	>-23	-2.3	
AD031	quartz	LV					137	>-23	-1.1	
AD031	quartz	LV					137.7	>-23	-0.8	
AD031	quartz	LV					138.4	>-23	-1.6	
AD031	quartz	LV					138.6	>-23	-1.4	
AD031	quartz	LV					138.9	>-23	-2.3	
AD031	quartz	LV					139.1	>-23	-2	
AD031	quartz	LV					139.1	>-23	-2.5	
AD031	quartz	LV					139.2	>-23	-2.2	
AD031	quartz	LV					139.9	>-23	-2.4	
AD031	quartz	LV					140.9	>-23	-1.9	
AD031	quartz	LV					140.6	>-23	-1.2	
AD031	quartz	LV					141.1	>-23		
AD031	quartz	LV					143.5	>-23	-2.7	
AD031	quartz	LV					143.6	>-23		
AD031	quartz	LV					144.4	>-23	-2.8	
AD031	quartz	LV					144.8	>-23	-1.8	
AD031	quartz	LV					146.8	>-23	-1.8	
AD031	quartz	LV					147.3	>-23	-1.9	
AD031	quartz	LV					147.8	>-23	-1.1	
AD031	quartz	LV					148	>-23	-2	
AD031	quartz	LV					148.1	>-23	-2.4	
AD031	quartz	LV					149.5	>-23	-2.2	
AD031	quartz	LV					151.3	>-23	-1.7	
AD031	quartz	LV					152	>-23	-2.5	
AD031	quartz	LV					154.6	>-23	-1	
AD031	quartz	LV					156.6	>-23	-2.8	
AD031	quartz	LV					157.6	>-23	-2.9	
AD031	quartz	LV					158.1	>-23	-1	
AD031	quartz	LV					158.9	>-23	-2.9	
Adglob	calcite	LV					166	>-27	-9.2	
Adglob	calcite	LV					173	>-27	-9.2	
Adglob	calcite	LV					186	>-27	-9.2	
Adglob	calcite	LV					182	>-27	-9.1	
Adglob	calcite	LV					175	>-27	-9	
Adglob	calcite	LV					169	>-27	-8.9	
Adglob	calcite	LV					171	>-27	-8.9	
Adglob	calcite	LV					161	>-27	-8.8	
Adglob	calcite	LV					175	>-27	-8.8	
Adglob	calcite	LV					165	>-27	-8.8	
Adglob	calcite	LV					157	>-27	-8.7	

L - Liquid; V - Vapour; S - Solid; T_{dss} - Temperature of dissolution; T_h - temperature of homogenization;
T_e - Eutectic temperature; T_{mce} - temperature of final ice melting

Sample	Host	Type	T _{diss} °C	T _{diss} °C	T _{diss} °C	T _{diss} °C	T _{hom} °C	T _e °C	T _{mce} °C	T _{co-mce} °C
Adglob	calcite	LV					163	>-27	-8.6	
Adglob	calcite	LV					167	>-27	-8.4	
Adglob	calcite	LV					148	>-27	-8.3	
Adglob	calcite	LV					191.5	>-27	-8.3	
Adglob	calcite	LV					169	>-27	-8.2	
Adglob	calcite	LV					154	>-27	-8.1	
Adglob	calcite	LV					165	>-27	-8.1	
Adglob	calcite	LV					168	>-27	-8	
Adglob	calcite	LV					168	>-27	-7.9	
Adglob	calcite	LV					163	>-27	-7.8	
Adglob	calcite	LV					165	>-27	-7.7	
Adglob	calcite	LV					163	>-27	-7.7	
Adglob	calcite	LV					164	>-27	-7.2	
Adglob	calcite	LV					167	>-27	-7.1	
Adglob	calcite	LV					174	>-27	-7.1	
Adglob	calcite	LV					168	>-27	-7	
Adglob	calcite	LV					168	>-27	-7	
Adglob	calcite	LV					162	>-27	-6.9	
Adglob	calcite	LV					169	>-27	-6.9	
Adglob	calcite	LV					156	>-27	-6.8	
Adglob	calcite	LV					163	>-27	-6.8	
Adglob	calcite	LV					147.4	>-27	-6.7	
Adglob	calcite	LV					174	>-27	-6.6	
Adglob	calcite	LV					164	>-27	-6.5	
Adglob	calcite	LV					168	>-27	-6.4	
Adglob	calcite	LV					169	>-27	-6.4	
Adglob	calcite	LV					153	>-27	-6.3	
Adglob	calcite	LV					167	>-27	-6.3	
AD061	calcite	LV					136	>-27	-6.3	
AD061	calcite	LV					138	>-27	-5.9	
AD061	calcite	LV					138	>-27	-6.8	
AD061	calcite	LV					139	>-27	-7.7	
AD061	calcite	LV					140	>-27	-6.4	
AD061	calcite	LV					141	>-27	-7.1	
AD061	calcite	LV					142	>-27	-6.6	
AD061	calcite	LV					142	>-27	-6.2	
AD061	calcite	LV					144	>-27	-6.6	
AD061	calcite	LV					144	>-27	-6.5	
AD061	calcite	LV					145	>-27	-7.1	
AD061	calcite	LV					145	>-27	-7.8	
AD061	calcite	LV					145	>-27	-6.5	
AD061	calcite	LV					146	>-27	-7.2	
AD061	calcite	LV					146	>-27	-6.9	
AD061	calcite	LV					147	>-27	-6.8	
AD061	calcite	LV					147	>-27	-6.3	
AD061	calcite	LV					147	>-27	-6.4	
AD061	calcite	LV					148	>-27	-6.5	
AD061	calcite	LV					148	>-27	-6.1	
AD061	calcite	LV					148	>-27	-6.9	
AD061	calcite	LV					149	>-27	-6.1	
AD061	calcite	LV					149	>-27	-7	
AD061	calcite	LV					150	>-27	-7.5	
AD061	calcite	LV					151	>-27	-5.8	
AD061	calcite	LV					152	>-27	-6.8	
AD061	calcite	LV					152	>-27	-6.1	
AD061	calcite	LV					153	>-27	-6.3	
AD061	calcite	LV					154	>-27	-5.8	
AD021	calcite	LV					120.6	>-27	-1.2	
AD021	calcite	LV					122.6	>-27	-2.8	
AD021	calcite	LV					125	>-27	-6	
AD021	calcite	LV					128.9	>-27	-1.8	
AD021	calcite	LV					129.1	>-27	-4.1	
AD021	calcite	LV					129.7	>-27	-3.4	
AD021	calcite	LV					132.4	>-27	-2.3	
AD021	calcite	LV					132.5	>-27	-3.1	
AD021	calcite	LV					136.8	>-27	-3.2	
AD021	calcite	LV					139	>-27	-1.7	
AD021	calcite	LV					139.5	>-27	-3.7	
AD021	calcite	LV					139.5	>-27		
AD021	calcite	LV					139.6	>-27	-4.8	
AD021	calcite	LV					139.9	>-27	-4.4	
AD021	calcite	LV					140	>-27	-2.8	
AD021	calcite	LV					140.2	>-27	-4.5	
AD021	calcite	LV					145.4	>-27	-5.1	
AD021	calcite	LV					148.8	>-27	-5	
AD021	calcite	LV					147.5	>-27	-4.6	
AD021	calcite	LV					147.4	>-27	-6	
AD021	calcite	LV					148.5	>-27	-5.9	
AD021	calcite	LV					155.6	>-27	-5.5	
AD021	calcite	LV					156.1	>-27	-6.3	
AD021	calcite	LV					156.4	>-27	-3.8	
AD021	calcite	LV					157.9	>-27	-4.7	
AD021	calcite	LV					157.8	>-27	-5.6	
AD021	calcite	LV					157.2	>-27		
AD021	calcite	LV					157.4	>-27	-5.8	
AD021	calcite	LV					159.2	>-27	-3.1	
AD021	calcite	LV					159.5	>-27	-4.2	

L - Liquid; V - Vapour; S - Solid; T_{diss} - Temperature of dissolution; T_h - temperature of homogenization;
T_e - Eutectic temperature; T_{mce} - temperature of final ice melting

Sample	Host	Type	T _{diss}	T _{diss}	T _{diss}	T _{diss}	T _{h_{liquid}}	T _e	T _{mice}	T _{co,mice}
			°C	°C	°C	°C	°C	°C	°C	°C
AD021	calcite	LV					166.4	>-27	-6.6	
AD021	calcite	LV					166.9	>-27	-4.3	
AD021	calcite	LV					168	>-27	-6.7	
AD021	calcite	LV					168.7	>-27	-4.9	
AD021	calcite	LV					169.5	>-27	-3.6	
AD021	calcite	LV					170.1	>-27	-5.7	
AD021	calcite	LV					170.6	>-27	-4.3	
AD021	calcite	LV					171.9	>-27	-4.9	
AD021	calcite	LV					173.2	>-27	-5.3	
AD021	calcite	LV					173.4	>-27	-4.5	

L - Liquid; V - Vapour; S - Solid; T_{diss} - Temperature of dissolution; T_h - temperature of homogenization;
T_e - Eutectic temperature; T_{mice} - temperature of final ice melting

**Appendix IV: Melt Inclusion Microthermometric Data
(Phalaborwa, South Africa)**

Table A4 Melt Inclusion Microthermometric Data (Phalaborwa)

Sample	Host Rock	Type	L+V °C	L+L+V °C	T _{melt2} °C	T _{melt1} °C	V _{change} °C	T _{D2} °C	T _{D1} °C	T _{H₂O}	T _{mice} °C
39-3	phosc	S+V	893	794	756	668	472				
39-3	phosc	S+V	888	779	731	658	457				
39-3	phosc	S+V	856	797	740	664	448				
39-3	phosc	S+V	907	761		658	429				
39-3	phosc	S+V	804	791	758	649	434				
39-3	phosc	S+V	925	790	759	635	429				
39-3	phosc	S+V	933	773	782	649	448				
39-3	phosc	S+V	817	796	757	679	477				
39-3	phosc	S+V	938	781	766	669	462				
39-3	phosc	S+V	946	799		675	453				
39-3	phosc	S+V	919	763	745	669	434				
39-3	phosc	S+V	906	793	746	660	439				
39-3	phosc	S+V	901	792	769	646	434				
39-3	phosc	S+V	869	775	744	680	453				
39-3	phosc	S+V	920	798	753	690	482				
39-3	phosc	S+V	931	794		683	440				
39-3	phosc	S+V	942	790		677	445				
39-3	phosc	S+V	963	786	772	668	440				
39-3	phosc	S+V	964	782	747	654	459				
39-3	phosc	S+V	975	778	756	668	488				
39-3	phosc	S+V	986	774	3	672	446				
39-6	T Carb	S+V	766		713	639					
39-6	T Carb	S+V	840		755	613					
39-6	T Carb	S+V	803		763	551					
39-6	T Carb	S+L+V	781			652			218	429	
39-6	T Carb	S+L+V	840		678	615	304	228			
39-6	T Carb	S+L+V	735		733	639	333	256			
39-6	T Carb	S+L+V	803		714	608	333			496	
41-17	T Carb	S+V	787		761	667					
41-17	T Carb	S+V	814		759	628					
41-17	T Carb	S+V	836		739	604					
41-17	T Carb	S+L+V	752		741	627	292	244		500	
41-17	T Carb	S+L+V	706		681	611	304			406	
20-44	T Carb	S+V	844		746	600					
20-44	T Carb	S+V	831		742	611					
20-44	T Carb	S+V	849		760	667					
20-44	T Carb	S+V	811		764	551					
20-44	T Carb	S+L+V	799		713	614		229		491	
20-44	T Carb	S+L+V	812		691	622	366			496	
20-44	T Carb	S+L+V	826		689	652				452	
20-22b	T Carb	S+V	752		706	601					
20-22b	T Carb	S+V	768		764	563					
20-22b	T Carb	S+V	799		721	661					
20-22b	T Carb	S+V	824		701	578					
20-22b	T Carb	S+V	819		764	618					
20-22b	T Carb	S+V	772		707	577					
20-22b	T Carb	S+L+V	847		703	604					-22.8
20-22b	T Carb	S+L+V	773		677	668					-21.3
20-22b	T Carb	S+L+V	810		731	661	333			431	-22.8
20-22b	T Carb	S+L+V	825			648	381			453	-22.2

Pile 5	T Carb	S+V	830	734	638	429	
Pile 5	T Carb	S+V	811	749	610		
Pile 5	T Carb	S+V	805	737	584		
Pile 5	T Carb	S+L+V				274	536
Pile 5	T Carb	S+L+V				343	
Pile 5	T Carb	S+L+V				305	
40-2	T Carb	S+L+V					-23
40-2	T Carb	S+L+V					-23.3
20-22b	T Carb	S+L+V				209	-22.4
20-22b	T Carb	S+L+V				260	-23.3
20-22b	T Carb	S+L+V					-23.6
20-22b	T Carb	S+L+V					-22.8
20-22b	T Carb	S+L+V					-23
20-22b	T Carb	S+L+V				188	
39-9c	T Carb	S+L+V				361	272
39-9c	T Carb	S+L+V				300	251
39-9c	T Carb	S+L+V				343	289
39-9c	T Carb	S+L+V				377	256
39-9c	T Carb	S+L+V				388	266
39-9c	T Carb	S+L+V				364	269

S - Solid; L - Liquid; V - Vapour; phosc - phoscorite, T carb - transgressive carbonatite

Appendix V: Electron Microprobe Mineral Analyses

Electron-microprobe analyses of diopside in regional fenite (sample PF-7)

Sample	PF-7	PF-7	PF-7	PF-7	PF-7	PF-7	PF-7	PF-7	PF-7	PF-7	PF-7	PF-7	PF-7	PF-7
wt. %														
SiO₂	52.22	52.03	51.93	52.01	51.71	52.12	52.18	51.86	51.96	51.50	51.80	51.99	52.25	51.92
Al₂O₃	0.48	0.58	0.54	0.54	0.76	0.51	0.52	0.66	0.57	0.68	0.65	0.75	0.76	0.77
TiO₂	0.05	0.13	0.16	0.14	0.11	0.15	0.16	0.11	0.10	0.07	0.08	0.10	0.05	0.07
FeO	14.18	12.95	12.85	12.76	12.75	12.88	12.79	12.46	12.89	12.67	12.18	12.43	12.95	12.68
MgO	9.88	11.04	10.77	11.12	10.87	10.89	11.05	11.05	10.97	10.98	11.04	11.02	10.78	10.75
MnO	0.46	0.47	0.51	0.45	0.41	0.49	0.44	0.43	0.48	0.39	0.44	0.46	0.38	0.41
CaO	20.43	21.19	21.27	21.30	21.34	21.42	21.49	21.51	21.54	21.59	21.71	21.92	21.93	22.07
Na₂O	2.54	1.73	1.72	1.82	1.58	1.77	1.77	1.42	1.57	1.44	1.50	1.53	1.42	1.41
K₂O	0.02	0.03	0.01	0.02	0.05	0.02	0.02	0.01	0.01	0.02	0.01	0.02	0.02	0.01
BaO	0.00	0.00	0.01	0.00	0.00	0.02	0.01	0.00	0.02	0.02	0.01	0.02	0.00	0.01
P₂O₅	0.02	0.03	0.00	0.00	0.02	0.00	0.00	0.00	0.00	0.05	0.02	0.00	0.02	0.03
Cr₂O₃	0.00	0.00	0.00	0.00	0.00	0.00	0.00	0.03	0.00	0.02	0.00	0.00	0.00	0.00
Cl	0.00	0.01	0.00	0.01	0.00	0.00	0.00	0.00	0.00	0.01	0.00	0.01	0.00	0.01
F	0.00	0.00	0.00	0.01	0.00	0.00	0.00	0.00	0.00	0.00	0.00	0.00	0.00	0.00
Total	100.28	100.17	99.78	100.17	99.57	100.28	100.43	99.55	100.10	99.44	99.44	100.24	100.57	100.15

Electron-microprobe analyses of diopside in contact fenites (samples PF-5c,d)

Sample	PF-5c	PF-5c	PF-5c	PF-5c	PF-5c	PF-5c	PF-5c	PF-5d	PF-5d	PF-5d	PF-5d	PF-5d	PF-5d	PF-5d
wt. %														
SiO₂	53.99	53.32	53.85	53.08	53.14	53.66	53.66	53.04	53.30	52.90	53.18	53.36	52.63	53.61
Al₂O₃	0.41	0.46	0.23	0.42	0.42	0.33	0.31	0.25	0.18	0.32	0.25	0.25	0.32	0.33
TiO₂	0.19	0.18	0.09	0.23	0.17	0.04	0.12	0.17	0.09	0.18	0.15	0.16	0.18	0.22
FeO	9.63	9.77	7.80	10.15	11.63	8.24	7.02	14.57	13.67	13.69	12.53	12.53	13.72	11.38
MgO	12.87	12.68	13.84	12.29	11.64	13.82	14.17	9.89	10.48	10.36	10.98	11.30	10.22	11.92
MnO	0.22	0.21	0.16	0.17	0.28	0.20	0.15	0.35	0.28	0.30	0.30	0.31	0.36	0.26
CaO	21.81	21.90	22.23	22.26	22.66	22.79	23.26	21.68	21.91	21.98	22.21	22.28	22.33	23.02
Na₂O	1.94	2.03	1.70	1.52	1.40	1.47	1.20	2.00	1.67	1.88	1.60	1.50	1.48	1.11
K₂O	0.03	0.03	0.03	0.02	0.02	0.03	0.00	0.02	0.01	0.02	0.03	0.01	0.02	0.03
BaO	0.03	0.01	0.03	0.00	0.01	0.01	0.00	0.01	0.00	0.02	0.02	0.00	0.00	0.00
P₂O₅	0.01	0.00	0.01	0.02	0.00	0.04	0.00	0.00	0.02	0.03	0.00	0.01	0.00	0.00
Cr₂O₃	0.03	0.01	0.13	0.04	0.00	0.04	0.09	0.00	0.01	0.00	0.00	0.00	0.01	0.02
Cl	0.00	0.01	0.01	0.01	0.00	0.01	0.01	0.00	0.00	0.01	0.01	0.00	0.00	0.00
F	0.00	0.00	0.00	0.00	0.00	0.00	0.00	0.00	0.01	0.00	0.00	0.00	0.00	0.00
Total	101.15	100.59	100.09	100.19	101.37	100.69	99.99	101.98	101.61	101.67	101.24	101.71	101.26	101.91

Electron-microprobe analyses of richterite in regional fenite (sample PF-7)

Sample	PF-7	PF-7	PF-7	PF-7	PF-7	PF-7	PF-7	PF-7	PF-7	PF-7	PF-7	PF-7	PF-7	PF-7
wt. %														
SiO₂	49.51	50.96	52.56	50.49	50.23	51.58	50.71	50.86	53.05	50.79	52.66	52.31	52.54	52.41
Al₂O₃	4.24	3.15	2.11	3.31	3.37	2.84	2.80	2.83	1.60	3.03	0.89	1.81	1.52	0.94
TiO₂	0.31	0.27	0.12	0.21	0.15	0.26	0.19	0.23	0.03	0.19	0.05	0.05	0.07	0.06
FeO	14.68	13.64	12.79	13.80	14.09	13.10	13.87	13.83	12.34	13.47	13.03	13.34	13.65	16.83
MgO	14.59	15.32	16.14	15.29	15.18	15.77	15.40	15.20	16.45	15.24	16.06	15.77	15.87	13.45
MnO	0.32	0.35	0.35	0.31	0.34	0.33	0.35	0.31	0.36	0.34	0.38	0.34	0.34	0.46
CaO	9.59	9.60	9.83	9.64	9.65	9.69	9.75	10.37	10.42	10.53	10.97	11.16	11.33	11.84
Na₂O	3.24	2.79	2.79	3.04	3.00	3.12	2.73	2.24	2.50	2.25	1.54	1.62	1.31	1.19
K₂O	1.27	1.30	1.32	1.22	1.26	1.19	1.37	1.16	0.98	1.01	0.65	0.81	0.66	0.48
BaO	0.01	0.01	0.01	0.04	0.01	0.01	0.00	0.01	0.01	0.01	0.00	0.00	0.01	0.00
P₂O₅	0.00	0.00	0.03	0.00	0.00	0.00	0.00	0.00	0.00	0.00	0.00	0.02	0.02	0.00
Cr₂O₃	0.00	0.01	0.00	0.00	0.00	0.00	0.00	0.02	0.00	0.00	0.00	0.01	0.00	0.00
Cl	0.03	0.02	0.01	0.03	0.02	0.01	0.02	0.03	0.01	0.04	0.01	0.01	0.01	0.03
F	0.46	0.52	0.49	0.47	0.51	0.53	0.48	0.45	0.45	0.40	0.36	0.38	0.32	0.27
Total	98.06	97.70	98.12	97.64	97.58	98.20	97.46	97.35	98.01	97.13	96.43	97.46	97.51	97.83

Electron-microprobe analyses of richterite in contact fenites (samples PF-5c,d)

Sample	PF-5c	PF-5c	PF-5c	PF-5c	PF-5c	PF-5c	PF-5c	PF-5d	PF-5d	PF-5d	PF-5d	PF-5d	PF-5d	PF-5d
wt. %														
SiO₂	56.50	57.14	56.57	56.94	56.63	57.02	57.09	56.24	56.21	56.42	56.60	56.22	56.17	56.18
Al₂O₃	0.24	0.21	0.24	0.22	0.28	0.23	0.22	0.37	0.36	0.38	0.33	0.36	0.33	0.37
TiO₂	0.11	0.07	0.10	0.05	0.06	0.06	0.08	0.08	0.06	0.06	0.09	0.07	0.10	0.05
FeO	6.25	6.20	6.15	6.19	6.45	6.34	6.20	9.36	9.16	9.01	7.67	9.42	8.67	9.41
MgO	20.56	20.86	20.39	20.53	20.29	20.65	20.57	18.70	18.58	19.05	19.69	18.67	19.19	18.43
MnO	0.04	0.08	0.05	0.05	0.03	0.03	0.05	0.09	0.10	0.09	0.07	0.12	0.10	0.07
CaO	8.56	8.57	8.61	8.61	8.72	8.75	8.87	8.89	8.91	8.93	8.94	8.97	8.99	9.19
Na₂O	3.26	3.27	3.26	3.20	3.28	3.25	3.07	2.96	2.97	2.95	2.96	2.81	2.92	2.85
K₂O	2.20	2.39	2.15	2.24	2.16	2.15	2.16	1.69	1.58	1.73	2.14	1.67	1.78	1.48
BaO	0.00	0.02	0.00	0.01	0.00	0.02	0.03	0.00	0.00	0.02	0.00	0.03	0.02	0.00
P₂O₅	0.00	0.04	0.01	0.00	0.02	0.00	0.00	0.04	0.00	0.00	0.01	0.00	0.00	0.00
Cr₂O₃	0.00	0.01	0.04	0.00	0.00	0.00	0.00	0.00	0.00	0.00	0.00	0.00	0.01	0.02
Cl	0.00	0.00	0.00	0.00	0.04	0.01	0.01	0.01	0.00	0.01	0.01	0.00	0.00	0.00
F	0.37	0.38	0.35	0.37	0.31	0.36	0.35	0.25	0.27	0.29	0.31	0.30	0.28	0.26
Total	97.94	99.08	97.77	98.25	98.13	98.71	98.53	98.57	98.09	98.81	98.69	98.51	98.45	98.21

Electron-microprobe analyses of calcite surrounding chalcopyrite in transgressive carbonatite

Sample	Pile 9-16	Pile 9-9	Pile 9-15	22-55 1-18	22-55 1-19	22-55 1-10	22-55 1-9	22-55 1-11	22-55 1-12	22-55 1-17
CaO	53.73	52.43	51.77	56.99	56.34	53.85	54.96	54.56	54.57	53.94
SrO	1.51	1.37	1.34	0.31	0.54	0.85	0.80	0.85	0.82	0.54
FeO	0.31	0.36	0.41	0.04	0.02	0.13	0.13	0.15	0.18	0.26
MnO	0.31	0.22	0.29	0.10	0.08	0.13	0.10	0.12	0.09	0.11
MgO	1.26	1.97	1.98	0.40	0.43	1.77	2.09	2.17	2.17	2.53
Na ₂ O	0.03	0.02	0.03	0.00	0.00	0.00	0.00	0.02	0.00	0.00
K ₂ O	0.01	0.02	0.02	0.20	0.15	0.04	0.02	0.01	0.02	0.53
BaO	0.31	0.00	0.18	0.08	0.02	0.00	0.00	0.00	0.00	0.00
*CO ₂	42.54	43.60	43.99	41.88	42.42	43.23	41.90	42.12	42.15	42.09
Total	100.00	100.00	100.00	100.00	100.00	100.00	100.00	100.00	100.00	100.00

* CO₂ by difference

Electron-microprobe analyses of Mg-calcite surrounding chalcopyrite in transgressive carbonatite

Sample	Pile 9-7	Pile 9-4	Pile 9-11	Pile 9-14	Pile 9-6	Pile 9-2	Pile 9-18	Pile 9-3	Pile 9-22	Pile 9-17
CaO	50.19	51.78	52.02	51.22	50.56	50.82	50.26	50.39	50.33	45.00
SrO	1.42	1.41	1.50	1.46	1.37	1.35	1.44	1.23	1.46	1.18
FeO	0.68	0.63	0.38	0.40	0.74	0.67	0.45	0.73	0.33	0.58
MnO	0.20	0.18	0.21	0.28	0.21	0.19	0.26	0.18	0.20	0.35
MgO	2.89	2.92	2.96	3.00	3.02	3.14	3.40	3.42	4.04	8.42
Na ₂ O	0.09	0.04	0.06	0.08	0.06	0.11	0.04	0.06	0.04	0.03
K ₂ O	0.02	0.03	0.02	0.02	0.01	0.03	0.01	0.02	0.01	0.02
BaO	0.29	0.27	0.21	0.36	0.25	0.24	0.31	0.20	0.41	0.29
*CO ₂	44.22	42.74	42.65	43.18	43.77	43.47	43.82	43.78	43.19	44.12
Total	100.00	100.00	100.00	100.00	100.00	100.00	100.00	100.00	100.00	100.00

* CO₂ by difference

Electron-microprobe analyses of dolomite surrounding chalcopyrite in transgressive carbonatite

Sample	Pile 9-20	Pile 9-13	Pile 9-21	Pile 9-12	22-55 1-15	22-55 1-8	22-55 1-13	22-55 1-7	22-55 1-5	22-55 1-6
CaO	29.13	29.40	29.34	29.72	30.02	30.08	30.23	30.23	30.26	29.82
SrO	0.65	0.58	0.54	0.64	0.34	0.27	0.28	0.36	0.30	0.31
FeO	2.09	2.43	2.20	1.96	1.15	0.72	0.79	0.79	0.74	0.77
MnO	0.29	0.30	0.27	0.23	0.15	0.14	0.09	0.12	0.12	0.15
MgO	20.04	20.10	20.13	20.26	21.10	21.14	21.23	21.25	21.29	21.32
Na ₂ O	0.00	0.01	0.02	0.01	0.01	0.00	0.00	0.00	0.01	0.01
K ₂ O	0.01	0.01	0.02	0.02	0.02	0.01	0.02	0.02	0.02	0.03
BaO	0.03	0.03	0.02	0.02	0.00	0.00	0.00	0.00	0.03	0.03
*CO ₂	47.76	47.13	47.47	47.14	47.21	47.65	47.35	47.23	47.23	47.58
Total	100.00	100.00	100.00	100.00	100.00	100.00	100.00	100.00	100.00	100.00

* CO₂ by difference